SYNTHESIS, CHARACTERIZATION AND TESTING OF POTENTIAL ENERGETIC MATERIALS

TOMASZ GRZEGORZ WITKOWSKI

aus

Zawiercie, POLEN

2017

Erklärung:

Diese Dissertation wurde im Sinne von § 7 der Promotionsordnung vom 28. November 2011 von Herrn Professor Dr. Thomas M. Klapötke betreut.

Eidesstattliche Versicherung:

Diese Dissertation wurde eigenständig und ohne unerlaubte Hilfe erarbeitet.

München, den 09. Januar 2017

Witkowski Tomasz

Dissertation eingereicht am: 09. Januar 2017

1. Gutachter: Prof. Dr. Thomas M. Klapötke

2. Gutachter: Prof. Dr. Konstantin Karaghiosoff

Mündliche Prüfung am: 24.04.2017

Acknowledgement

Contents

1. Introduction

1.1 Definition and Classification

Research into new energetic materials (EMs) with improved properties is an ongoing project in many research groups. Depending on the purpose the EMs should fulfill, research is focused on improving different key characteristics of the materials. EMs are usually subdivided into following classes:[1]

Primary explosives (*"primers"*) are substances which are principally used to detonate secondary explosives.[1a, 1b, 1d-f] Primary explosives undergo very rapid combustion (or deflagration) to detonation transfer and are significantly more sensitive towards external stimuli (*e.g.*: heat, impact, friction, electrostatic discharge) than secondary explosives.[1a, 1b, 1d-f] More details on primary explosives are given in the introduction to chapter nine.

Secondary explosives (*"high explosives"*) are less sensitive to external stimuli but higher performing than primary explosives.[1a, 1b, 1e, 1f] Modern trends in the research of high explosives can be divided into following key areas: high performance explosives, heat resistant explosives, and low sensitivity explosives.[1e, 1f]

Tertiary explosives (*"blasting agents"*) – are highly insensitive to external stimuli (*e.g.*: impact, friction, heat, shock) and consequently must be initiated using an intermediate charge of a secondary explosive (*"booster"*).[1a, 1c, 1d, 1f] Moreover these explosives posses a relatively large critical diameter and are therefore not used in small charges.[1a] Tertiary explosives are predominantly used in large-scale mining and construction operations. Examples of tertiary explosives include ammonia nitrate fuel mixtures (ANFO) and slurry explosives.[1f]

The destructive action of explosives is caused by two factors: expansion of the gaseous detonation products and the shock wave. In the assessment of destructive action of explosive can be distinguished:[1b, 1e, 1f, 2]

Brisance – this is the destructive fragmentation effect of an explosive on its direct vicinity, and which depends mainly on the pressure of the shock wave front of the detonation products (important parameters are: detonation velocity, loading density of the explosive, volume of gas released, and heat of explosion).[1b, 1e, 1f, 2] Assessment of this property can be achieved using for example aballistic mortar test,[1b, 1f, 2] cylinder test,[1b, 1f, 2] Hess test,[1b, 1f, 2] Kast

test,[1f, 2] lead block test,[1b, 1e, 1f, 2] plate dent test,[1b, 1f, 2] or underwater explosion test[1e, 2-3] (more details on underwater explosion phenomena are given in chapter four).

Heaving effect – this is the destructive action of the detonation gaseous products at larger distances from the point of initiation, and can be estimated using the Held test[4] or underwater explosion test amongst others.[1e, 2-3]

Propellants are used to either accelerate munition (gun propellants) or to produce thrust in rockets (rocket propellants).[1a, 1b, 1e, 1f] Their foremost function is to combust in a controlled way and not to detonate.[1a, 1b, 1e, 1f]

Pyrotechnics are compositions which are used to produce different effects such as heat, light, sound, gas or smoke.[1a, 1b, 1e, 1f] Generally, they undergo non-detonative exothermic reactions, however, under certain conditions they can detonate.[1a, 1b, 1e, 1f]

More details on the classification and requirements of EMs, as well as on promising research areas for the discovery of novel EMs with tailored physico-chemical properties, as well as the different strategies which are used in order to obtain novel EMs are briefly described in the following chapters of this thesis:

- chapter 10: Nitrogen-Rich Energetic 1,2,5-Oxadiazole-Tetrazole – Based Energetic Materials;[5]
- chapter 11: Covalent and Ionic Insensitive High-Explosives.[6]

1.2   Motivation and Objectives

The objectives of this thesis are to synthesize, characterize, and investigate different EMs which could be used as replacements for EMs which are currently used. It is of great importance to synthesize EMs which not only have the desired properties, but which can also be prepared using cheap reagents and facile synthetic routes with high selectivities and yields. Moreover, since there is a great need for methods which can be used for the preliminary testing of promising EMs on a small scale for both safety and cost reasons, two suitable methods for characterizing the performance of EMs are discussed: small scale underwater test and laser-induced air shock from energetic materials (LASEM) method.

1.3   References

[1]   a) J. P. Agrawal, *High Energy Materials*, Wiley, Weinheim, Germany, **2010**; b) E. Włodarczyk, *Podstawy Fizyki Wybuchu*, Military University of Technology in Warsaw, Warsaw, Poland, **2012**; c) E. G. Mahadevan, *Ammonium Nitrate*

Explosives for Civil Applications: Slurries, Emulsions and Ammonium Nitrate Fuel Oils, Wiley, Weinheim, Germany, **2013**; d) R. Matyáš, J. Pachmáň, *Primary Explosives*, Springer, Berlin, Germany, **2013**; e) T. M. Klapötke, *Chemistry of High-Energy Materials, 3rd edn.*, Walter de Gruyter, Berlin, Germany, **2015**; f) R. Meyer, J. Köhler, A. Homburg, *Explosives, 7th edn.*, Wiley, Weinheim, Germany, **2016**.

[2]   M. Sućeska, *Test Methods for Explosives*, New York, USA, **1995**.

[3]   T. M. Klapötke, T. G. Witkowski, Z. Wilk, J. Hadzik, *Propellants, Explos., Pyrotech.* **2016**, *41*, 92–97.

[4]   M. Held, *New Diagnostic Techniques in Blast Waves*, Proceedings of Seminar on New Trends in Research of Energetic Materials, Pardubice, Czech Republic, April 19–21, **2006**, 16–41.

[5]   T. M. Klapötke, T. G. Witkowski, *Propellants, Explos., Pyrotech.* **2015**, *40*, 366–373.

[6]   T. M. Klapötke, T. G. Witkowski, *Propellants, Explos., Pyrotech.* **2016**, *41*, 470–483.

2.   Summary and Conclusion

Chapters 3–11 have been published in peer-reviewed scientific journals.[1-9] The content of these chapters is consistent with the publications; however, the layout of the articles has been modified in order to fit this thesis. A brief summary of the results presented in this thesis is given in this chapter.

2.1   Chapter 3: Synthesis, Characterization and Crystal Structures of Two Bi-oxadiazole Derivatives Featuring the Trifluoromethyl Group[1]

The synthesis and characterization of two oxadiazoles (3,3′-bi-(5-trifluoromethyl-1,2,4-oxadiazole), **1**; 5,5′-bi-(2-trifluoromethyl-1,3,4-oxadiazole), **2**; Figure 1) is presented.
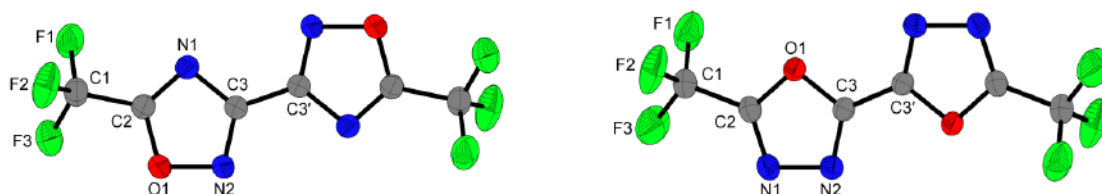
Figure 1. Molecular structures of 3,3′-bi-(5-trifluoromethyl-1,2,4-oxadiazole) (**1**, left) and 5,5′-bi-(2-trifluoromethyl-1,3,4-oxadiazole) (**2**, right) in the crystals.

The compounds were synthesized by the reaction of either diaminoglyoxime (**1**) or 5,5′-bitetrazole (**2**) with trifluoroacetic anhydride. The latter acts as both the solvent and the reactant.[1] The oxadiazoles which obtained showed similar densities and calculated standard molar enthalpies of formation, and therefore the calculated detonation and combustion parameters are comparable. Nevertheless, **2** has both a higher melting and boiling point than **1**.

Oxadiazoles **1** and **2** were used as model compounds for further theoretical studies of energetic materials which are derived from them in which the fluorine atoms in the CF_3 moiety are substituted successively by the nitro functionality (Figure 2).

Figure 2. Molecular structures of 5,5′-bi-(2-difluoronitromethyl-1,3,4-oxadiazole) (**3**), 5,5′-bi-(2-fluorodinitromethyl-1,3,4-oxadiazole) (**4**) and 5,5′-bi-(2-trinitromethyl-1,3,4-oxadiazole) (**5**).

From the investigations presented in this chapter, it can be concluded that among the compounds that were considered, compound **5** would be the most suitable candidate to be used as an oxidizer ($\Omega = 7.3\%$) in solid rocket propellants.

2.2 Chapter 4: Determination of the Initiating Capability of Detonators Containing TKX 50, MAD-X1, PETNC, DAAF, RDX, HMX or PETN as a Base Charge, by Underwater Explosion Test[2]

A comprehensive study of the candidates which show the most promise for application out of recently developed explosives is presented. The explosives which were studied are shown in Figure 3 and are the following: dihydroxylammonium 5,5′-bis(tetrazolate-1*N*-oxide – TKX-50, dihydroxylammonium 5,5′-bis(3-nitro-1,2,4-triazolate-1*N*-oxide) – MAD-X1, pentaerythritol tetranitrocarbamate – PETNC and 3,3′-diamino-4,4′-azoxyfurazan – DAAF.

Figure 3. Chemical structures of TKX-50, MAD-X1, PETNC and DAAF.

The explosives shown in Figure 3 were synthesized and characterized and the initiating capability of detonators which contained one of them as a base charge was determined using an underwater explosion test. The results of the initiating capabilities were compared to those of detonators containing RDX, HMX or PETN.

Novel explosives (TKX-50, MAD-X1, PETNC and DAAF) show slightly lower values for the recorded maximum overpressure than reference explosives (RDX, HMX and PETN). A similar observation can be made for the time necessary for the overpressure to decrease to $P_{max} \cdot e^{-1}$ - *which is* shorter for the new explosives. These two factors show that the primary shock waves generated by explosives investigated in this work have similar behavior. The highest values for the time of the first bubble collapse are obtained for well-known explosives such as RDX, however, the new explosives differ in value from RDX by not more

than 6%. This indicates that the explosives investigated in this chapter show good action also at longer distances from the point of initiation.

2.3 Chapter 5: 5,5′-Bis(2,4,6-trinitrophenyl)-2,2′-bi(1,3,4-oxadiazole) (TKX-55): a Thermally Stable Explosive with Outstanding Properties[3]

This study presents the synthesis and investigation of one of the most thermally stable explosives, 5,5′-bis(2,4,6-trinitrophenyl)-2,2′-bi(1,3,4-oxadiazole) (TKX-55, Figure 4).

T_{dec} = 335 °C

FS > 360 N

IS = 5 J

ESD = 1.0 J

$\Delta_f H°$ = 197.6 kJ·mol^{-1}

ρ = 1.837 g·cm^{-3}

p_{C-J} = 27.3 GPa

V_{C-J} = 8030 m·s^{-1}
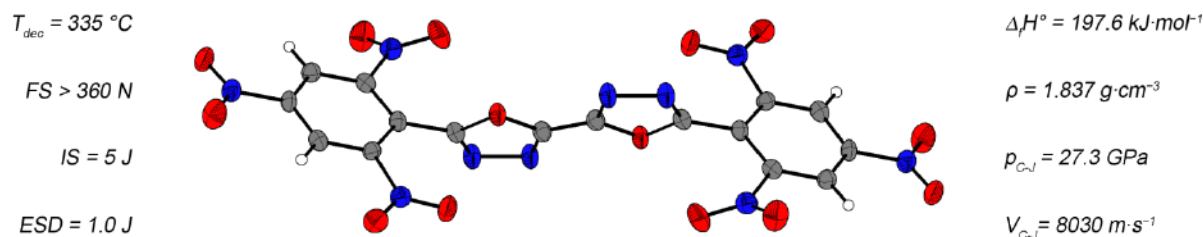
Figure 4. Molecular structure of 5,5′-bis(2,4,6-trinitrophenyl)-2,2′-bi(1,3,4-oxadiazole) - TKX-55 in the crystal and its selected properties.

The density, standard molar enthalpy of formation, nitrogen content, detonation velocity, and detonation pressure of TKX-55 are higher than those of the currently used heat-resistant explosives HNS and PYX. Moreover, TKX-55 is insensitive to friction, and its sensitivity to impact and electrostatic discharge are comparable with those of HNS. Furthermore, TKX-55 is practically insoluble in water and can be prepared using a facile synthetic route with high yield and selectivity. The combination of these properties makes TKX-55 unique among thermally stable explosives.

2.4 Chapter 6: Experimental Study on the Heat Resistant Explosive 5,5′-Bis(2,4,6-trinitrophenyl)-2,2′-bi(1,3,4-oxadiazole) (TKX-55): the Jet Penetration Capability and Underwater Explosion Performance[4]

5,5'-Bis(2,4,6-trinitrophenyl)-2,2'-bi(1,3,4-oxadiazole) (TKX-55) is one of the most promising candidates for use in practical applications because of its physico-chemical properties as well as its convenient synthesis. Therefore, further investigations into the performance of TKX-55 were performed. This study is focused on the investigation of both the jet penetration capability of shaped charges and the initiating capability of detonators containing TKX-55 as a base charge.

The jet penetration capability of conical shaped charges containing 16.00 g of TKX-55 as a base charge is relatively high (the depth of penetration, h = 91.2 mm; inlet diameter, φ_i = 13.4 mm, and volume of the crater, V = 3200mm^3). The results of the action of the shaped charge filled with TKX-55 as a base charge is shown in Figure 5.

Figure 5. Steel witness plates after firing of the shaped charge filled with TKX-55.

The primary shock waves (and therefore the brisance) generated by TKX-55 and PYX are comparable in nature. The first bubble collapses obtained for TKX-55 and PYX are also comparable. This indicates that TKX-55 and PYX show similar action (heaving power) at longer distances from the point of initiation. The calculated total energies as the sum of the primary shock wave energy and the bubble gas energy of TKX-55 for 0.5 g and 0.7 g base charges are similar to those obtained for PYX, while for the 0.2 g base charges, TKX-55 generates a larger bubble energy and therefore the total energy released by TKX-55 is higher than the total energy of PYX (Figure 6).
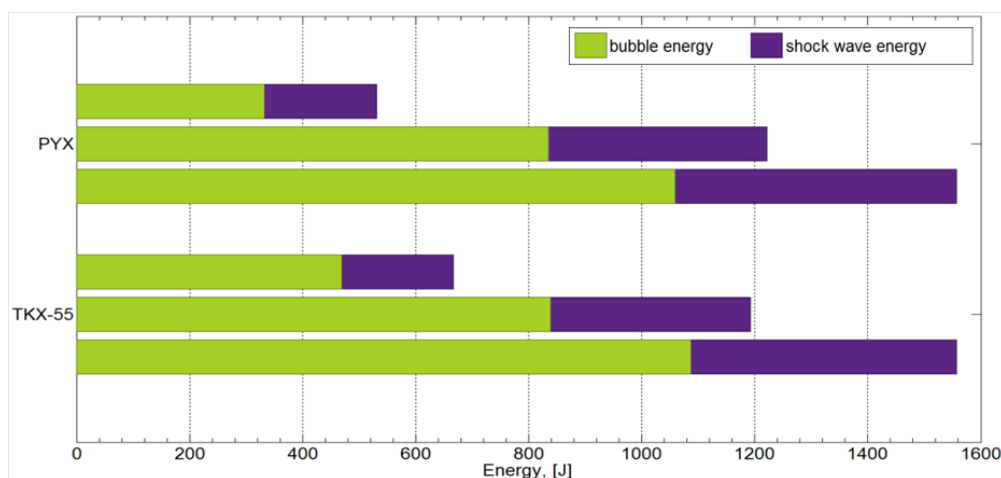
Figure 6. Total energies (E) generated in water by PYX and TKX-55 (0.2, 0.5, 0.7 g).

2.5 Chapter 7: Synthesis and Investigation of Advanced Energetic Materials Based on Bispyrazolylmethanes[5]

The preparation and comprehensive characterization of new energetic materials containing the *N,N′*-methylene bridged bis(nitropyrazoles) moiety are reported (Figure 7). The reaction of sodium 4-amino-3,5-dinitropyrazolate with dimethyliodide afforded bis(4-amino-3,5-di-nitropyrazolyl)methane which can be classified as a thermally stable explosive. The subsequent oxidation of the amino groups using a mixture of sulfuric acid and hydrogen

8

peroxide yielded bis(3,4,5-trinitropyrazolyl)methane – a secondary explosive with a high nitrogen content, good oxygen balance and exceptionally high theoretical detonation performance. The remarkably high value for the calculated detonation velocity was corroborated using the Laser-induced Air Shock from Energetic Materials (LASEM) technique. The reaction of bis(4-amino-3,5-dinitropyrazolyl)methane with nitrite acid - which was generated *in situ* - yielded the primary explosive bis(4-diazo-5-nitro-3-oxopyrazolyl)methane which shows superior properties to those of the currently used explosive DDNP.
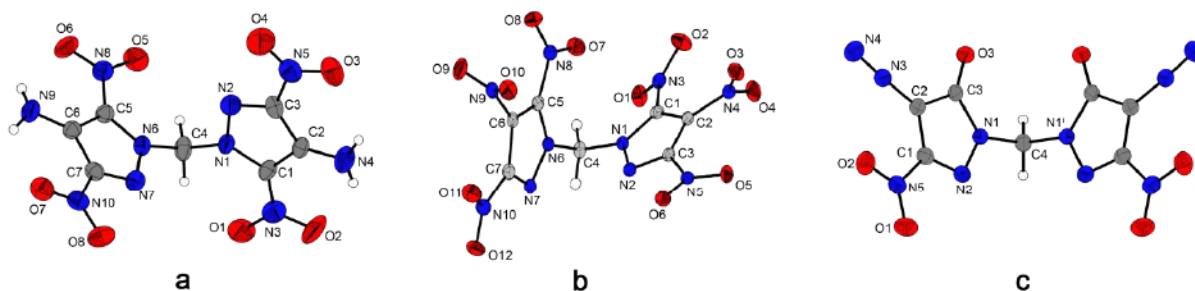
Figure 7. Molecular structures of bis(4-amino-3,5-dinitropyrazolyl)methane (a), bis(3,4,5-trinitropyrazolyl)methane (b), and bis(4-diazo-5-nitro-3-oxopyrazolyl)methane (c) in the crystals.

2.6 Chapter 8: Estimated Detonation Velocities for TKX-50, MAD-X1, BDNAPM, BTNPM, TKX-55 and DAAF using the Laser-induced Air Shock from Energetic Materials Technique[6]

This study presents the synthesis and investigation of the detonation velocities of the following explosives: dihydroxylammonium 5,5′-bistetrazole-1,1′-diolate (TKX-50), dihydroxylammonium 5,5′-bis(3-nitro-1,2,4-triazolate-1*N*-oxide) (MAD-X1), bis(4-amino-3,5-dinitropyrazol-1-yl)methane (BDNAPM), bis(3,4,5-trinitropyrazol-1-yl)methane (BTNPM), 5,5′-bis(2,4,6-trinitrophenyl)-2,2′-bi(1,3,4-oxadiazole) (TKX-55), and 3,3′-diamino-4,4′-azoxyfurazan (DAAF), which are shown in Figure 8.

The estimated detonation velocities of these explosives based on the measured characteristic laser-induced air shock velocities, are in very good agreement with the detonation velocities calculated using the EXPLO5 V6.01 and CHEETAH V8.0 thermochemical codes.
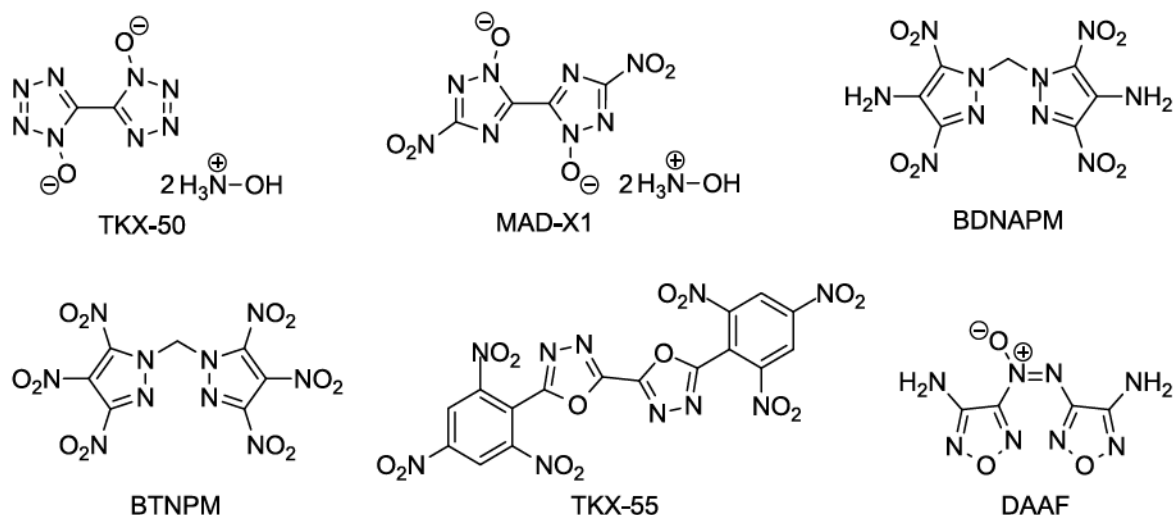
Figure 8. Chemical structures of TKX-50, MAD-X1, BDNAPM, BTNPM, TKX-55 and DAAF.

2.7   Chapter 9: Synthesis and Characterization of 5-methyl-2,4,6-trinitrobenze-ne-1,3-diol and its Energetic Cesium Salt[7]

The synthesis and characterization of the primary explosive cesium 5-methyl-2,4,6-trinitrobenzene-1,3-diolate (**3**, Scheme 1) as well as its precursor compound (**2**) is described.
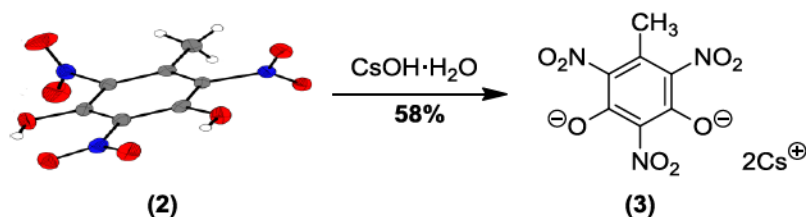
Scheme 1. Synthesis of cesium 5-methyl-2,4,6-trinitrobenzene-1,3-diolate (**3**).

The cesium salt (**3**) has a high decomposition temperature (255 °C, onset). Sensitivity investigations show that **3** is more sensitive to impact than lead azide (LA). The electrostatic sensitivity of **3** is in the range of LA, whereas **3** shows a much lower sensitivity to friction than that determined for LA. The preliminary flame test and measurements of the sensitivity to external stimuli show that **3** has the properties of a primary explosive.

2.8   Chapter 10: Nitrogen-Rich Energetic 1,2,5-Oxadiazole-Tetrazole – Based Energetic Materials[8]

The combination of nitrogen-rich tetrazole and tetrazole oxides with oxygen-containing furazan and furoxan rings is a new trend in the synthesis of energetic materials (EMs) resulting in compounds which have appropriate oxygen balances, a high density, and good

thermal stability. In this paper, the results of recent research in nitrogen-rich compounds containing 1,2,5-oxadiazole–tetrazole moieties are presented (Figure 9).
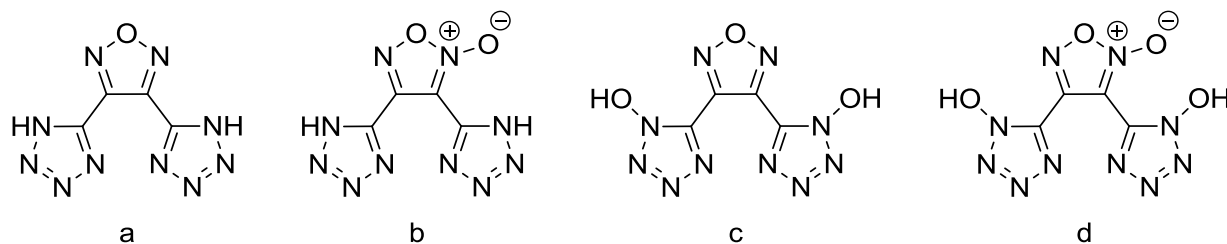
Figure 9. Chemical structures of 3,4-bis(1*H*-tetrazol-5-yl)-1,2,5-oxadiazole (a), 3,4-bis(1*H*-5-tetrazolyl)furoxan (b), 3,4-bis(1-hydroxytetrazolyl)furazan (c), and 3,4-bis(1-hydroxytetrazolyl)furoxan (d).

Energetic materials in which tetrazole rings are connected through the 1,2,5-oxadiazole moiety are a new and promising area of research for finding replacements for currently used energetic materials (including commonly used explosives). Most of the compounds which were investigated in this work have a high density and range from 1.59 g·cm^{-3} for bis(1-amino-3-methyl-1,2,3-triazolium) 3,4-bis(1*H*-5-tetrazolyl)furoxan to 1.82 g·cm^{-3} for hydrazinium hydrogen 3,4-bis(1*H*-5-tetrazolyl)furoxan. The heats of formation range from 471.6 kJ·mol^{-1} for bis(*N*-carbamoylguanidinium) 3,4-bis(1*H*-tetrazol-5-yl)furoxan to 1762.0 kJ·mol^{-1} for bis(1-amino-3-methyl-1,2,3-triazolium) 3,4-bis(1*H*-5-tetrazolyl)furoxan. The values of the densities and heats of formation are reflected in the good detonation properties of those compounds. Out of the EMs which were investigated, the most insensitive towards friction and impact are 3,4-bis(1-hydroxytetrazolyl)furazan and the furoxan-based EMs. The EMs which are presented in this section mostly possess a good oxygen balance, high density, and high thermal stability. Therefore, it can be concluded that the 1,2,5-oxadiazole–tetrazole moiety provides a highly useful skeleton for the synthesis of novel EMs.

2.9   Chapter 11: Covalent and Ionic Insensitive High-Explosives[9]

In this work, the synthesis and properties of both covalent (3-nitro-1,2,4-triazol-5-one, NTO; 4,10-dinitro-2,6,8,12-tetraoxa-4,10-diazaisowurtzitane, TEX; 1,1-diamino-2,2-dinitroethylene, FOX-7; 4-amino-3,5-dinitropyrazole, ADNP; 3,6-dinitropyrazolo[4,3-*c*]pyrazole, DNPP) and ionic (salts of ANDP and DNPP) insensitive explosives are presented. The compounds which are discussed are of great interest to this field of research (Figure 1).
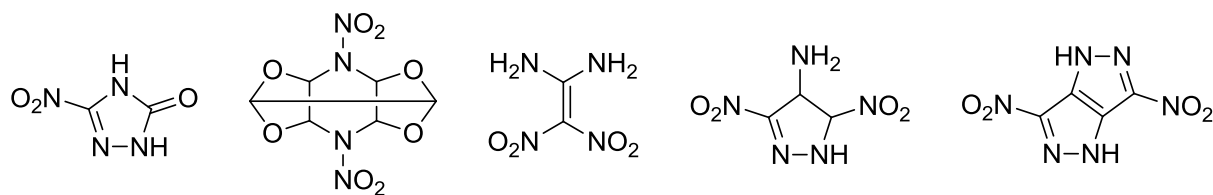
Figure 10. 3-Nitro-1,2,4-triazol-5-one (NTO), 4,10-dinitro-2,6,8,12-tetraoxa-4,10-diazaisowurtzitane (TEX), 1,1-diamino-2,2-dinitroethylene (FOX-7), 4-amino-3,5-dinitropyrazole (ADNP), and 3,6-dinitropyrazolo[4,3-*c*]pyrazole (DNPP).

Recently, different pyrazole-based ionic compounds were synthesized which show promise as insensitive explosives. Such energetic materials are characterized by a low sensitivity towards external stimuli and generally show high values for the detonation velocity and detonation pressure. Most of the compounds which are discussed possess high densities and are endothermic. The high densities and heats of formation are reflected in the high detonation parameters, which are reported for these compounds.

2.10 References

[1]   M. A. Kettner, T. M. Klapötke, T. G. Witkowski, F. von Hundling, *Chem. Eur. J.* **2015**, *21*, 4238–4241.

[2]   T. M. Klapötke, T. G. Witkowski, Z. Wilk, J. Hadzik, *Propellants, Explos., Pyrotech.* **2016**, *41*, 92–97.

[3]   T. M. Klapötke, T. G. Witkowski, *ChemPlusChem* **2016**, *81*, 357–360.

[4]   T. M. Klapötke, T. G. Witkowski, Z. Wilk, J. Hadzik, *Cent. Eur. J. Energ. Mater.* **2016**, *13*, 821–837.

[5]   D. Fischer, J. L. Gottfried, T. M. Klapötke, K. Karaghiosoff, J. Stierstorfer, T. G. Witkowski, *Angew. Chem., Int. Ed.* **2016** , *55*, 16132–16135.

[6]   J. L. Gottfried, T. M. Klapötke, T. G. Witkowski, *Propellants, Explos., Pyrotech.* **2017**, *42*, 353–359.

[7]   A. Drechsel, T. M. Klapötke, T. G. Witkowski, *J. J. Inorg. Chem.* **2016**, *1*, 008(1–8).

[8]   T. M. Klapötke, T. G. Witkowski, *Propellants, Explos., Pyrotech.* **2015**, *40*, 366–373.

[9]   T. M. Klapötke, T. G. Witkowski, *Propellants, Explos., Pyrotech.* **2016**, *41*, 470–483.

Synthesis, Characterization and Crystal Structures of Two Bi-oxadiazole Derivatives Featuring the Trifluoromethyl Group
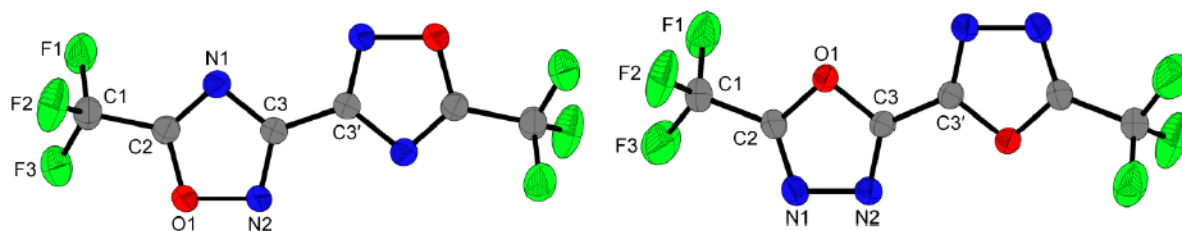
Abstract: The synthesis, characterisation, and crystal structure determination of the closely related compounds 3,3′-bi-(5-trifluoromethyl-1,2,4-oxadiazole) and 5,5′-bi-(2-trifluoromethyl-1,3,4-oxadiazole) are reported. These two compounds are known for their bioactivity; however, in this study they serve as model compounds to evaluate the suitability of the heterocyclic oxadiazole ring system for energetic materials when the fluorine atoms in the exocyclic CF_3 groups are substituted successively by nitro groups. Quantum chemical calculations for the bi-1,3,4-oxadiazole derivatives with difluoronitromethyl, fluorodinitromethyl, and trinitromethyl groups have been carried out and predict promising energetic performances for both explosive and propulsive applications.

3.1   Introduction

The heterocyclic class of oxadiazoles includes four different isomers. They find application as ingredients for drugs,[1] dyestuffs,[2] ionic liquids,[3] and scintillators.[4] The bi-oxadiazoles form two further isomers, owing to the asymmetry of the 1,2,3- and 1,2,4-oxadiazoles, which can be linked at two different carbon atoms. In the area of energetic materials, largely only 1,2,5-oxadiazole (furazane) derivatives have been exhaustively investigated.[5] In contrast 1,2,3-, 1,2,4-, and 1,3,4-oxadiazoles have only been explored sparsely with respect to derivatives in which energetic moieties such as polynitro groups or azides are attached.[6] Furazanes or furoxanes are not necessarily the thermally and chemically most stable derivatives of this class, but are favored due to their positive heats of formation and high densities.[5h]

3.2   Results and Discussion

Herein we summarise the synthetic pathways for 3,3′-bi-(5-trifluoromethyl-1,2,4-oxadiazole) (TFM$_2$-^{1,2,4}BOD, **1**) and the analogous 5,5′-bi-(2-trifluoromethyl-1,3,4-oxadiazole) (TFM$_2$-^{1,3,4}BOD, **2**) and compare the density and thermal behaviour of the two compounds. The trifluoromethyl group serves as a non-energetic moiety, in which fluorine atoms can be substituted stepwise by nitro groups, as reported previously for several 3,3′-bi-(5-polynitro-methyl-1,2,4-oxadiazole) derivatives.[6b,c, 7]

The synthetic routes used are depicted in Scheme 1. Compound **1** was synthesised according to a slightly modified literature procedure in which trifluoromethyl acetic acid anhydride acts as both the solvent and reactant, resulting in an increase in the yield by 11% in comparison with the previously reported yield.[8] Compound **2**[9] was synthesised using a convenient literature method for the formation of bi-1,3,4-oxadiazoles. The conversion of bi-5,5′-tetrazoles into the oxadiazoles with formation of N$_2$ results in very high yields (93%) and a high purity of the target compound.[10]
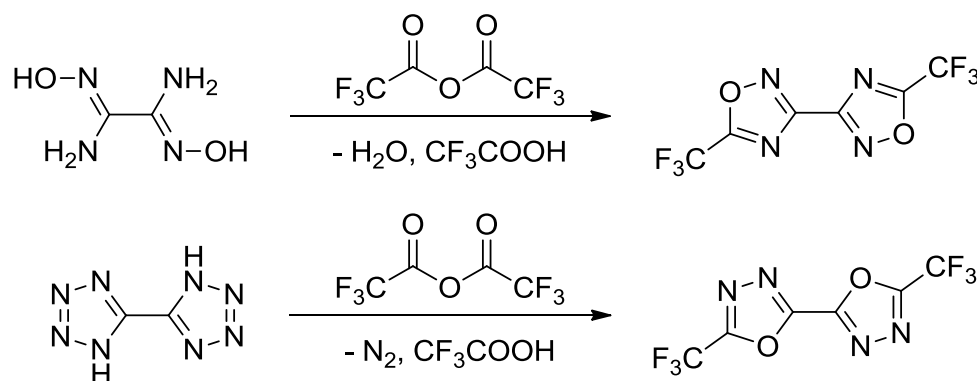
Scheme 1. Syntheses of compounds **1**[8] and **2**.[9, 10]

14

IR and Raman spectra show the expected bands for the two title molecules.[11, 12] The characteristic stretching modes (sym. and asym.) of the CF_3 groups are observed in the IR spectra at 1212 and 1171 cm^{-1} (**1**), and at 1227 and 1169 cm^{-1} (**2**), respectively. Additionally, some characteristic vibrations of the ring systems could be assigned according to the literature (see Experimental Section).[12] The ^{13}C NMR spectra show the expected $^1J(C,F)$ and $^2J(C,F)$ coupling constants.[12,13] In addition, ^{19}F and ^{15}N NMR spectra were obtained showing the chemical shifts for the ring nitrogen atoms of the 1,2,4- and 1,3,4-oxadiazole derivatives as well as their $^3J(^{15}N,^{19}F)$ coupling constants (Table 1).

Table 1. ^{13}C, ^{15}N, and ^{19}F NMR chemical shifts of compounds **1** and **2** in DMSO-d_6.

Nucleus	Assignment	1	2
^{13}C	$C_{oxadiazole}$	166.5 (q)	155.3 (q)
	CC	159.3 (s)	153.8 (s)
	CF_3	115.4 (q)	115.7 (q)
^{15}N	CNC/3-N	−134.8 (q)	−64.2 (q)
	ONC/4-N	−9.3 (s)	−64.6 (s)
^{19}F	CF_3	−65.1 (s)	−64.7 (s)

According to differential scanning calorimetry (DSC) measurements, compound **1** melts at 98 °C and boils at 142 °C, whereas compound **2** melts at 169 °C and boils at 199 °C. Both compounds showed no decomposition until a temperature of 400 °C in a closed aluminium vessel in the DSC measurements.

Compounds **1** and **2** crystallised from ethanol as very thin colourless plates, or by sublimation as thin needles (**1**) or blocks (**2**). Both compounds crystallise in the monoclinic space group $P2_1/c$ with two molecules per unit cell and show remarkably high densities of 2.01 $g \cdot cm^{-3}$ (**1**) and 1.98 $g \cdot cm^{-3}$ (**2**) at 173 K. Figure 1 depicts the molecular structures of both TFM$_2$-BODs viewed perpendicular to the ring systems, which are planar in both molecules. Table 2 lists the crystallographic data.
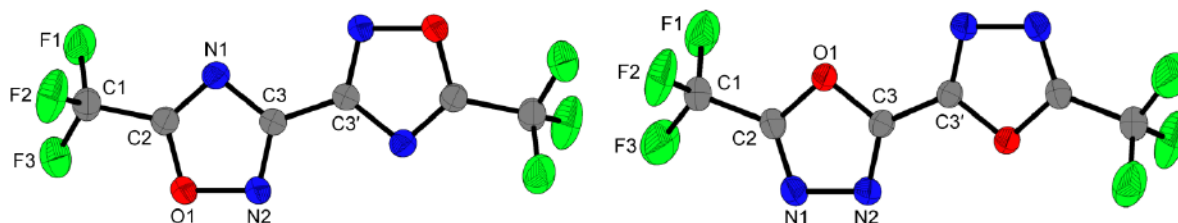
Figure 1. Molecular structures of 3,3′-bi-(5-trifluoromethyl-1,2,4-oxadiazole) (**1**, left) and 5,5′-bi-(2-trifluoromethyl-1,3,4-oxadiazole) (**2**, right) in the crystals; bond lengths [Å] and angles [°]: **1**) O1−C2 1.332(2), O1−N2 1.405(2), N1−C2 1.285(2), N1−C3 1.380(2), N2−C3 1.301(2), average F−C1 1.315(2), C3−C3′ 1.458(3), C2−C1 1.510(2); average F−C1−F 108.2(2), C2−C1−F 110.8(3), N2−C3−N1 115.7(1), O1−N2−C3−C3′ 178.6(2), N2−O1−C2−C1 178.7(1); **2**) O1−C2 1.350(2), O1−C3 1.353(2), N2−C3 1.288(2), N2−N1 1.405(2), N1−C2 1.278(2), average F−C1 1.306(2), C3−C3′ 1.446(3), C2−C1 1.504(2); average F−C1−F 107.9(2), C2−C1−F 111.0(2), N2−C3−O1 114.1(1), C2−O1−C3 100.8(1), N1−N2−C3−C3′ −179.1(2), N2−N1−C2−C1 −178.3(2).

Table 2. Crystallographic data for compounds **1** and **2**.

Compound	1	2
Formula	$C_6N_4O_2F_6$	
Molecular weight [g·mol^{-1}]	274.10	
Crystal dimensions [mm]	0.404×0.291×0.067	0.550×0.338×0.188
Crystal description	colourless platelet	colourless block
Crystal system	monoclinic	
Space group	$P2_1/c$	
a [Å]	11.1575(8)	10.9970(5)
b [Å]	4.7619(2)	5.1570(3)
c [Å]	8.7461(6)	8.2190(5)
α, γ [°]	90.0	
β [°]	103.142(7)	99.428(5)
V [Å^3]	452.52(5)	459.82(4)
Z	2	
ρ_{calc} [g·cm^{-3}]	2.012	1.980
μ [mm^{-1}]	0.230	0.227
$F(000)$	268	268
Temperature [K]	173(2)	
θ range [°]	4.67–28.27	4.38–28.27
Index ranges	$-14 \leq h \leq 14$	$-14 \leq h \leq 14$
	$-3 \leq k \leq 6$	$-6 \leq k \leq 6$
	$-11 \leq l \leq 10$	$-10 \leq l \leq 10$
Reflections measured	3724	4399
Reflections independent	1104	1133
Reflections unique	876	922
R(int)	0.0245	0.0206
$R1$, $wR2$ (2σ data)	0.0390, 0.0977	0.0437, 0.1107
$R1$, $wR2$ (all data)	0.0530, 0.1097	0.0544, 0.1201
Data/restraints/parameters	1104/0/82	1133/0/82
GoF on F^2	1.026	1.074
Residual electron density [e·Å^{-3}]	−0.298/0.261	−0.421/0.377

The structures exhibit some short intermolecular contacts that are well below the sum of van der Waals radii. For example, in the structure of compound **1**, N2···C3^i 3.105(2) and O1···C3^i 3.122(2) Å [symmetry operator i) −x, 1/2+y, 1/2−z], and in the structure of compound **2**, N1···C3^i 3.062(2) and N2···C3$^{i\prime}$ 2.984(2) Å [symmetry operator i) 1−x, −1/2+y, 1 1/2−z; ∑(van der Waals radii): N,C = 3.25 Å; O,C = 3.22 Å].[14] These short contacts may be responsible for the high densities observed for compounds **1** and **2**.

The bi-1,2,4-oxadiazole derivatives featuring the trinitromethyl and fluorodinitromethyl moieties have been reported previously and revealed good detonation and combustion properties, whereas the trinitromethyl compound shows a relatively low thermal stability, decomposing at 124 °C.[6c, 7] For the bi-1,3,4-oxadiazole derivatives that are assumed to be thermally more stable, the heats of formation for compounds containing

the difluoronitromethyl (**3**), fluorodinitromethyl (**4**), and trinitromethyl (**5**) groups attached were computed by ab initio calculations using the GAUSSIAN 09 program package[15] at the CBS-4M level of theory (Figure 2).[16] The heat of formation of compound **2** ($\Delta_f H° = -1191$ kJ·mol^{-1}) was calculated to be slightly more negative than that of compound **1** ($\Delta_f H° = -1135$ kJ·mol^{-1}). The effect of C−F bonds on the heat of formation can clearly be observed in this series of polyfluoro/polynitro compounds. Using these values and an estimated density of 1.90 g·cm^{-3} (minimum estimation supported by previous work)[6c, 7] the detonation and combustion parameters were calculated using the EXPLO5 (V6.02) computer code (Table 3)[17] and the ICT-THERMODYNAMIC CODE (see the Supporting Information).[20] Providing the thermal stability of the non-fused heterocyclic system is not decreased too much by the trinitromethyl moiety, compound **5** would be a suitable candidate as oxidiser in solid rocket propellants.[18]

Table 3. Calculated detonation and combustion parameters for predicted energetic compounds **3**, **4** and **5** depicted in Figure 2.

	3	**4**	**5**
Formula	$C_6N_6O_6F_4$	$C_6N_8O_{10}F_2$	$C_6N_{10}O_{14}$
Molecular weight [g·mol^{-1}]	328.09	382.11	436.12
$N+O$[a] [%]	54.87	71.20	83.48
Ω_{CO}[b] [%]	0.0	16.8	29.3
Ω[c] [%]	−29.3	−8.4	7.3
ρ_{est}[d] [g·cm^{-3}]	1.90	1.90	1.90
$\Delta_f H°$[e] [kJ·mol^{-1}]	−685	−212	231
Detonation parameters			
$-\Delta_E U°$[f] [kJ·kg^{-1}]	1606	4316	5893
T_{C-J}[g] [K]	2220	3647	4633
V_{C-J}[h] [m·s^{-1}]	6898	8440	8764
p_{C-J}[i] [GPa]	24.8	29.7	33.2
Gas vol.[j] [dm^3·kg^{-1}]	597	677	677
Combustion parameters, chamber pressure 70 bar *vs.* atmosphere[40-43]			
I_{sp} (neat) [s][k]	203 (2894 K)	244 (3581 K)	252 (3562 K)
I_{sp} (15% Al) [s][l]	236 (3750 K)	260 (4455 K)	260 (4447 K)
I_{sp} (16% Al, 14% PBAN) [s][m]	221 (2908 K)	238 (2952 K)	253 (2957 K)
I_{sp} (10% Al, 10% PBAN) [s][n]	225 (2908 K)	248 (3220 K)	267 (3867 K)

[a] Combined nitrogen and oxygen content; [b] oxygen balance assuming the formation of CO; [c] oxygen balance assuming the formation of CO_2; [d] estimated density; [e] heat of formation calculated at the CBS-4M level of theory; [f] heat of detonation; [g] temperature of the explosion gases; [h] detonation velocity; [i] detonation pressure; [j] volume of detonation gases at standard temperature and pressure conditions; [k] specific impulse of the neat compound; [l] specific impulse of a mixture with 15% aluminium; [m] the specific impulse for the composition with 16% aluminium, 6% polybutadiene acrylic acid, 6% polybutadiene acrylonitrile, and 2% bisphenol A ether; the according mixture with 70% ammonium perchlorate as the NASA Space Shuttle used was calculated to $I_{sp} = 260$ s;[46] [n] specific impulse for the composition with 10% aluminium, 4% polybutadiene acrylic acid, 4% polybutadiene acrylonitrile, and 2% bisphenol A ether; [k–n] isobaric combustion temperature in parenthesis.
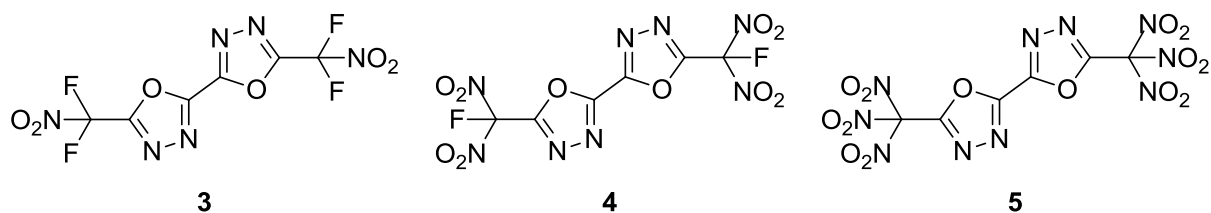
Figure 2. Chemical structures of 5,5′-bi-(2-difluoronitromethyl-1,3,4-oxadiazole) (**3**), 5,5′-bi-(2-fluorodinitromethyl-1,3,4-oxadiazole) (**4**) and 5,5′-bi-(2-trinitromethyl-1,3,4-oxadiazole) (**5**) with successive substitution of the fluorine atoms by nitro groups.

From this comparative study on CF_3-substituted bi-1,2,4- and bi-1,3,4-oxadiazoles the following conclusions can be drawn:

- Bi-1,2,4-oxadiazole **1** has only a slightly higher density than bi-1,3,4-oxadiazole **2**.

- In comparing the bi-1,2,4-oxadiazole with the bi-1,3,4-oxadiazole ring system, the heats of formation are barely affected by the position of the oxygen atom in the oxadiazole rings.

- The calculations on bi-1,3,4-oxadiazoles with difluoronitromethyl, fluorodinitromethyl, and trinitromethyl groups predict promising properties for these compounds for both explosive and propulsive applications. Work on the syntheses of these and various related compounds is already in progress within our group.

3.3 Experimental Section

3,3′-Bi-(5-trifluoromethyl-1,2,4-oxadiazole) (1):[8] Diaminoglyoxime (1.00 g, 8.47 mmol) was added to trifluoroacetic anhydride (10 mL) and stirred at 35 °C for 3 h. The solution was kept under reduced pressure and the acid was collected into an external cooling trap (−78 °C). On cooling, the crude product precipitated and was removed by filtration using a glass frit (porosity 4). The white precipitate was recrystallised from hot ethanol yielding compound **1** (1.72 g, 6.27 mmol, 75%) as colourless crystals. Alternatively, the crude compound can be purified by sublimation. **DSC** (5 °C min^{-1}, onset): 98 °C (melt.) ; 142 °C (boil.); **^{13}C NMR** (101 MHz, DMSO-d_6, ppm) δ: 166.5 (q, ^2J(C,F) = 44.8 Hz, OCN), 159.3 (CC), 115.4 ppm (q, J(C,F) = 273.4 Hz, CF$_3$); **^{15}N NMR** (40.6 MHz, DMSO-d_6, ppm) δ: −9.3 (ONC), −134.8 ppm (q, ^3J(^{15}N,^{19}F) = 1.9 Hz, CNC); **^{19}F NMR** (377 MHz, DMSO-d_6, ppm) δ: −65.1 ppm (s, CF$_3$); **IR** (ATR, 25 °C, cm^{-1}) $\tilde{v}$:1605 (w, $v_{C=N}$), 1453 (vw), 1431 (w), 1334 (m), 1276 (vw), 1212 (s, $v_{sym\,C-F}$), 1171 (vs, $v_{asym\,C-F}$), 1138 (vs), 996 (m), 951 (w), 911 (m, v_{2N-O}), 758 (s), 668 (m); **Raman** (1064 nm, 200 mW, 25 °C, cm^{-1}) $\tilde{v}$: 1615 (17), 1601 (100), 1432 (12), 1329 (4), 1185 (5, $v_{asym\,C-F}$), 1150 (4), 1022 (9), 994 (38),

923 (8, v_{2N-O}), 766 (22), 737 (10); **MS** (DCI+): $m/z = 275.2$ [M+H]$^{+}$; **MS** (DEI+): $m/z = 274.2$ [M]$^{+}$; **EA** ($C_6F_6N_4O_2$, 274.08) calc.: C 26.29, N 20.44 %; found: C 26.29, N 20.60 %.

5,5′-Bi-(2-trifluoromethyl-1,3,4-oxadiazole) (2): To a stirred suspension of 5,5′-bi-1*H*-tetra-zole (2.15 g, 15.56 mmol) in *p*-xylene (30 mL), a solution of trifluoroacetic acid anhydride (5.56 mL, 8.40 g, 40 mmol) in *p*-xylene (12 mL) was added dropwise. The reaction mixture was stirred at 100 °C until N_2 no longer evolved. The mixture was allowed to cool to room temperature and was then adjusted to pH = 9 using a saturated $NaHCO_3$ solution. The white precipitate was filtered off, washed with water (200 mL), and dried under reduced pressure yielding pure product **2** (3.97 g, 14.48 mmol, 93%). The compound could be further purified by sublimation. **DSC** (5 °C·min^{-1}, onset): 169 °C (melt.), 199 °C (boil.); **^{13}C NMR** (101 MHz, DMSO-d_6, ppm) δ: 155.3 (q, ^2J(C,F) = 44.7 Hz, OCN), 153.8 (CC), 115.7 ppm (q, J(C,F) = 271.9 Hz, CF$_3$); **^{15}N NMR** (40.6 MHz, DMSO-d_6, ppm) δ: −64.2 (q, ^3J(^{15}N,^{19}F) = 1.5 Hz, 3-N), −64.6 ppm (4-N); **^{19}F NMR** (377 MHz, DMSO-d_6, ppm) δ: −64.7 ppm (br, CF$_3$); **IR** (ATR, 25 °C, cm^{-1}) $\tilde{v}$: 1579 (w, $v_{C=N}$), 1476 (s, $v_{C=N}$), 1378 (s), 1227 (w, $v_{sym\,C-F}$), 1169 (vs, $v_{asym\,C-F}$), 1118 (vs, v_{C-O}), 1005 (vs), 974 (s, v_{C-O}), 950 (s), 755 (s), 735 (s), 674 (s); **Raman** (1064 nm, 200 mW, 25 °C, cm^{-1}) $\tilde{v}$: 1651 (64), 1580 (4, $v_{C=N}$), 1037 (11), 973 (7), 764 (5), 721 (4); **MS** (DCI+): $m/z = 274.1$ [M]$^{+}$; **EA** ($C_6F_6N_4O_2$, 274.08) calc.: C 26.29, N 20.44 %; found: C 26.21, N 20.33 %.

3.4   References

[1]   a) M. Heitzmann, *Pat. CH 661270*, Sandoz AG, **1987**; b) T. Kim, J. W. Suh, J. C. Ryu, B. C. Chung, J. Park, *J. Chromatogr. B* **1996**, *687*, 79–83.

[2]   a) D. V. Nightingale, R. M. Brooker, *J. Am. Chem. Soc.* **1950**, *72*, 5539–5543; b) K. H. Kim, H. J. Lee, *Pat. US 8970108*, Samsung Display Co., Ltd, **2015**.

[3]   a) A. Pace, P. Pierro, *Org. Biomol. Chem.* **2009**, *7*, 4337–4348; b) J. A. Pedro, J. R. Mora, E. Westphal, H. Gallardo, H. D. Fiedler, F. Nome, *J. Mol. Struct.* **2012**, *1016*, 76–81; c) E. Westphal, D. Henrique da Silva, F. Molin, H. Gallardo, *RSC Adv.* **2013**, *3*, 6442–6454.

[4]   a) J. B. Birks, *Pat. GB 1286622 19720823*, **1972**; b) M. Hyman, Jr., *Pat. U.S. 4017738 A 19770412*, **1977**; c) V. Rimbau Barreras, *Pat. ES 551136 A1 19870316*, **1987**; d) F. Dubois, R. Knochenmuss, R. Zenobi, *Int. J. Mass Spectrom. Ion Processes* **1997**, *169/170*, 89–98.

[5]   a) D. Chavez, L. Hill, M. Hiskey, S. Kinkead, *J. Energ. Mater.* **2000**, *18*, 219–236; b) D. Fischer, T. M. Klapötke, M. Reymann, J. Stierstorfer, *Chem. Eur. J.* **2014**, *20*,

6401–6411; c) A. B. Sheremetev, *J. Heterocycl. Chem.* **1995**, *32*, 371–385; d) P. W. Leonard, D. E. Chavez, P. F. Pagoria, D. L. Parrish, *Propellants Explos. Pyrotech.* **2011**, *36*, 233–239; e) R. Wang, Y. Guo, Z. Zeng, B. Twamley, J. M. Shreeve, *Chem. Eur. J.* 2009, *15*, 2625–2634; f) V. Zelenov, A. Lobanova, S. Sysolyatin, N. Sevodina, *Russ. J. Org. Chem.* **2013**, *49*, 455–465; g) A. M. Churakov, S. L. Ioffe, V. A. Tartakovsky, *Mendeleev Commun.* **1995**, *5*, 227–228; h) N. N. Makhova, Proceedings of Seminar on New Trends in Research of Energetic Materials, Part 2, Pardubice, Czech Republic, April 9–11, **2014**, 647–652.

[6]   a) L. Zhanxiong, O. Yuxiang, C. Boren, *Chem. J. Internet* **2001**, *3*, 13; b) T. M. Klapötke, N. Mayr, J. Stierstorfer, M. Weyrauther, *Chem. Eur. J.* **2014**, *20*, 1410–1417; c) M. A. Kettner, K. Karaghiosoff, T. M. Klapötke, M. Sućeska, S. Wunder, *Chem. Eur. J.* **2014**, *20*, 7622–7631; d) V. Thottempudi, J. Zhang, C. He, J. M. Shreeve, *RSC Adv.* **2014**, *4*, 50361–50364.

[7]   M. A. Kettner, T. M. Klapötke, *Chem. Commun.* **2014**, *50*, 2268–2270.

[8]   V. G. Andrianov, V. G. Semenikhina, A. V. Eremeev, *Chem. Heterocycl. Compd.* **1994**, *30*, 475–477.

[9]   G. Seitz, C. H. Gerninghaus, *Pharmazie* **1994**, *49*, 102–106.

[10]   L. I. Vereshchagin, A. V. Petrov, V. N. Kizhnyaev, F. A. Pokatilov, A. I. Smirnov, *Russ. J. Org. Chem.* **2006**, *42*, 1049–1055.

[11]   G. Socrates, *Infrared and Raman Characteristic Group Frequencies: Tables and Charts*, 3rd edition, Wiley, Chichester, **2004**.

[12]   a) K. Hemming in *Comprehensive Heterocyclic Chemistry III, Vol. 5* (Eds.: A. R. Katritzky, C. A. Ramsden, E. F. V. Scriven, R J. K. Taylor) Elsevier, Amsterdam, **2008**, 243–314; b) J. Suwiński, W. Szczepankiewicz in *Comprehensive Heterocyclic Chemistry III, Vol. 5* (Eds.: A. R. Katritzky, C. A. Ramsden, E. F. V. Scriven, R J. K. Taylor) Elsevier, Amsterdam, **2008**, 397–466.

[13]   H.-O. Kalinowski, S. Berger, S. Braun, *13C NMR Spektroskopie*, Thieme, Stuttgart, **1984**.

[14]   A. Bondi, *J. Phys. Chem.* **1964**, *68*, 441–451.

[15]   a) *Gaussian 09, Revision C.01*, M. J. Frisch, G. W. Trucks, H. B. Schlegel, G. E. Scuseria, M. A. Robb, J. R. Cheeseman, G. Scalmani, V. Barone, B. Mennucci, G. A. Petersson, H. Nakatsuji, M. Caricato, X. Li, H. P. Hratchian, A. F. Izmaylov, J. Bloino, G. Zheng, J. L. Sonnenberg, M. Hada, M. Ehara, K. Toyota, R. Fukuda, J. Hasegawa, M. Ishida, T. Nakajima, Y. Honda, O. Kitao, H. Nakai, T. Vreven,

J. A. Montgomery, Jr., J. E. Peralta, F. Ogliaro, M. Bearpark, J. J. Heyd, E. Brothers, K. N. Kudin, V. N. Staroverov, R. Kobayashi, J. Normand, K. Raghavachari, A. Rendell, J. C. Burant, S. S. Iyengar, J. Tomasi, M. Cossi, N. Rega, J. M. Millam, M. Klene, J. E. Knox, J. B. Cross, V. Bakken, C. Adamo, J. Jaramillo, R. Gomperts, R. E. Stratmann, O. Yazyev, A. J. Austin, R. Cammi, C. Pomelli, J. W. Ochterski, R. L. Martin, K. Morokuma, V. G. Zakrzewski, G. A. Voth, P. Salvador, J. J. Dannenberg, S. Dapprich, A. D. Daniels, Ö. Farkas, J. B. Foresman, J. V. Ortiz, J. Cioslowski, D. J. Fox, Gaussian, Inc., Wallingford, CT, **2009**; b) *Gauss-View 5*, V5.0.8, T. K. R. Dennington, J. Millam, Semichem Inc., Shawnee Mission, **2009**.

[16]   a) J. J. A. Montgomery, M. J. Frisch, J. W. Ochterski, G. A. Petersson, *J. Chem. Phys.* **2000**, *112*, 6532–6542; b) J. W. Ochterski, G. A. Petersson, J. J. A. Montgomery, *J. Chem. Phys.* **1996**, *104*, 2598–2619.

[17]   a) M. Sućeska, Version 6.02, Zagreb, Croatia, **2014**; b) M. Sućeska, *Propellants Explos. Pyrotech.* **1991**, *16*, 197–202; c) M. Sućeska, *Propellants Explos. Pyrotech.* **1999**, *24*, 280–285; d) M. Sućeska, H. G. Ang, H. Y. Chan, *Mater. Sci. Forum* **2011**, *673*, 47–52.

[18]   a) T. M. Klapötke, *Chemie der Hochenergetischen Materialien*, de Gruyter, Berlin, **2009**; b) T. M. Klapötke, *Chemistry of High-Energy Materials*, de Gruyter, Berlin, New York, **2011**.

[19]   a)   *NASA,   Space   Shuttle   News   Reference,   2–20–22–21, http://de.scribd.com/doc/17005716/NASA-Space-Shuttle-News-Reference-1981 (accessed: 13.11.2014);* b) NASA, press release: STS-122 The Voyage of Columbus, **2008**, 82–84, *http://www.nasa.gov/pdf/203212mainsts122presskit2.pdf* (accessed: 13.11.2014).

[20]   F. Volk, H. Balthet, *The ICT-Thermodynamic Code (ICT-Code)*, 27th International Annual Conference of ICT, Karlsruhe, Germany, 92/1–16, **1996**.

3.5 Supplementary information

The analytical methods, general procedures and computational details are described in the appendix of this thesis.

3.5.1 The performance parameters (ICT-Thermodynamic Code)

Table 1. The performance parameters of **3**, **4** and **5** computed using the ICT-Thermodynamic Code.[1]

	3	4	5
Detonation parameters[6]			
$-\Delta_E U°$ [kJ·kg^{-1}]	4094	5635	5940
$T_{C\text{-}J}$ [K]	3437	4819	4882
Gas vol. [dm^3·kg^{-1}]	537	625	673
Combustion parameters, chamber pressure 70 bar *vs.* atmosphere[6]			
I_{sp} (neat) [s]	205 (2767 K)	240 (3232 K)	252 (3570 K)
I_{sp} (15% Al) [s]	227 (3485 K)	259 (3801 K)	270 (3801 K)
I_{sp} (16% Al, 14% PBAN) [s]	218 (2466 K)	238 (2699 K)	255 (3132 K)
I_{sp} (10% Al, 10% PBAN) [s]	224 (2831 K)	248 (3255 K)	271 (3801 K)

3.5.2 References

[1] a) F. Volk, H. Balthelt, R. Kuthe, Thermodynamic Data of rocket fuels, propellants and there components, ICT-Bericht, 1/81, Pfinztal **1971**; b) F. Volk, H. Balthet, The ICT-Thermodynamic Code (ICT-Code), 27th International Annual Conference of ICT, Karlsruhe, Germany, 92/1-16, **1996**; c) P. B. Kempa, H. Bathelt, F. Volk, M. Weidel; ICT-Database of Thermochemical Values, 8th Update; Pfinztal, **2008**.

Determination of the Initiating Capability of Detonators Containing TKX-50, MAD-X1, PETNC, DAAF, RDX, HMX or PETN as a Base Charge, by Underwater Explosion Test
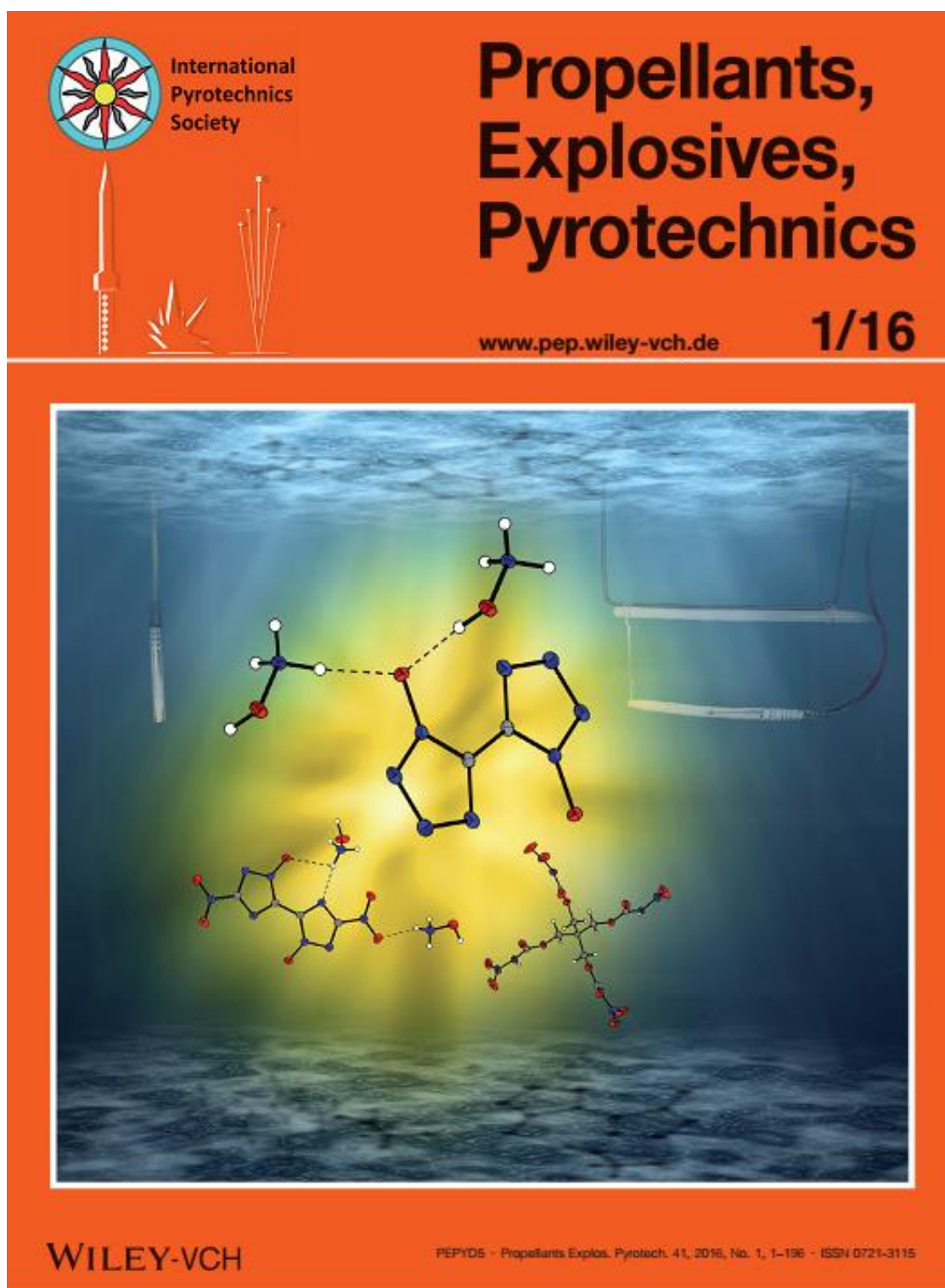
Abstract: A comprehensive investigation to determine the initiation power of detonators containing as a base charge the novel explosives: dihydroxylammonium 5,5′-bis(tetrazo-late-1*N*-oxide) – TKX-50, dihydroxylammonium 5,5′-bis(3-nitro-1,2,4-triazolate-1*N*-oxide) – MAD-X1, pentaerythritol tetranitrocarbamate – PETNC and 3,3′-diamino-4,4′-azoxyfurazan – DAAF in comparison with RDX, HMX and PETN was undertaken. In order to estimate the initiation power of the detonators, the underwater initiating capability test was used. The total energy as a sum of the primary shock wave energy and the bubble gas energy was determined for each of these explosives, by measuring the overpressure of the shock waves generated in water. Moreover, the complete synthesis for novel explosives is presented. The thermal behavior of the explosives was investigated using DSC (differential scanning calorimetry). The gas phase absolute molar enthalpies at 298 K and 10^5 Pa were calculated theoretically using the modified complete basis set method (CBS-4M; M referring to the use of minimal population localization) with the GAUSSIAN 09 software. Gas phase standard molar enthalpies of formation ($\Delta_f H_{(g)}°$) at 298 K were computed using the atomization energy method. Standard molar enthalpies of formation ($\Delta_f H°$), for the prepared covalent compounds, were calculated using $\Delta_f H_{(g)}°$ and the standard molar enthalpies of sublimation by applying Trouton's rule. In the case of salts, $\Delta_f H_{(g)}°$ of ions as well as the calculated standard molar lattice enthalpies were used to calculate $\Delta_f H°$. The Chapman-Jouguet (C-J) characteristics based on calculated $\Delta_f H°$ values were computed using the EXPLO5 V6.01 thermochemical computer code. For the calculations the theoretical maximum densities and densities obtained during the experiments presented in this work were used.

Keywords: DAAF · TKX-50 · MAD-X1 · PETNC · Underwater explosion

4.1   Introduction

Recently, many new types of detonators have been developed and implemented for production. The continuous research for new types of detonators is driven by increasingly strict safety requirements and environmental concerns, protection against unauthorized use, as well as specific requirements set by users. In order to fulfil these requirements, novel explosives with tailored properties which have been recently synthesized, could be used as the base charge in detonators.[1] Nevertheless, the shock wave generated during the action of the detonator has to be higher than the initiation pressure of the acceptor explosive charge. If the generated shock wave is not sufficient to initiate the detonation of the explosive, it can result in low-order detonation or misfire.[2] Therefore, the energy output of detonators containing new explosives as a base charge has to be determined and compared with currently used ones.

Various new strategies were developed in order to obtain novel explosives. Most of them can be classified into one of the following groups:

− Explosives which contain the oxidizer and fuel within one molecule (e.g. PETN, RDX, HMX). Heat is released due to the oxidation of the carbon backbone during detonation;

− Compounds containing a strained ring or cage assembly in their structure (TEX, CL-20, ONC, TNAZ) which increases the energy of the explosive in comparison with an unstrained system. Strain causes more energy to be released during decomposition than in an unstrained system;

− Compounds with high nitrogen contents. Due to difference in the bond energies for single, double, and triple NN bonds, nitrogen-rich compounds decompose releasing a large amount of heat.

Useful explosives not only have to undergo a self-contained and self-sustained decomposition reaction in which an enormous amount of heat and gas is released in a short space of time, but also have to meet following demands: tailored performance, sensitivity, stability, vulnerability, environmental safety, low solubility in water, hydrolytic stability, longevity and compatibility.[3] Furthermore, if application of these explosives as a base charge in detonators is being considered, they have to possess a low critical diameter.

4.2   Materials and Methods

Among the recently developed explosives, the most promising candidates for application based on their performance as well as convenient synthetic method are TKX-50, MAD-X1, PETNC and DAAF (Figure 1).
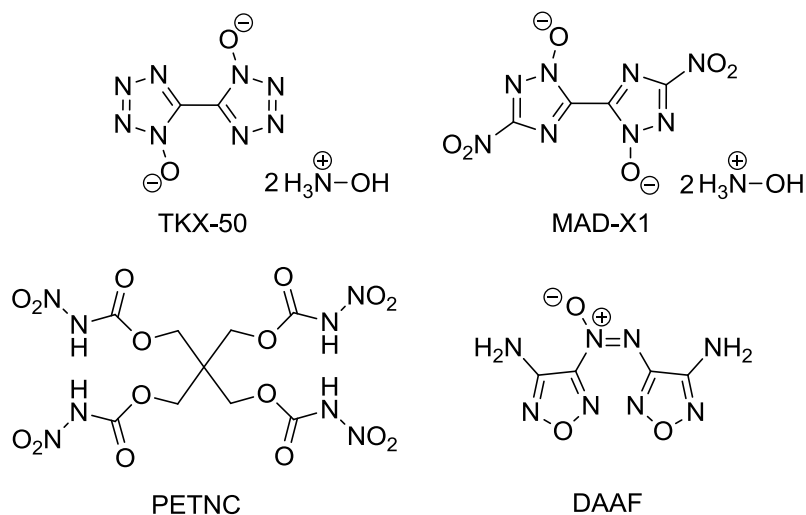
Figure 1. Chemical structures of TKX-50, MAD-X1, PETNC and DAAF.

The explosives (shown in Figure 1) have high decomposition temperatures ($\geq 196\,°C$) and the theoretical maximum densities are between 1.76 and 1.90 $g \cdot cm^{-3}$. TKX-50, MAD-X1 and DAAF are endothermic compounds, while PETNC (similar to its analog PETN) is an exothermic compound, which contains four explosophore nitro functionalities. Theoretically calculated Chapman-Jouguet (C-J) characteristics of these explosives (detonation pressure, 24.8–40.2 GPa; detonation velocities, 7742–9766 $m \cdot s^{-1}$), as well as their sensitivity to external stimuli ($FS > 120$ N, $IS > 7$ J) also make these species interesting for possible application (see Supporting Information). DAAF – which was first synthesized by Solodyuk et al.[1a] – and its detonation parameters were also experimentally investigated.[4] The critical diameter which was determined for DAAF is lower than 2 mm (at density 1.69 $g \cdot cm^{-3}$)[4a] and possesses a high measured detonation velocity (7.98 $km \cdot s^{-1}$ at a diameter of charge of 16.00 mm and density 1.69 $g \cdot cm^{-3}$; 7.93 $km \cdot s^{-1}$ at 1.685 $g \cdot cm^{-3}$)[4] and pressure (30.6 GPa at a density of 1.685 $g \cdot cm^{-3}$)[4b]. Moreover these explosives can be obtained from cheap starting materials, in high yields and good purities. As a result of these advantages, these explosives can be considered for use as secondary explosives in detonators. This means that their energy outputs have to be determined and compared with those of currently used secondary explosives.

In order to estimate the initiation power of the detonators, the underwater initiating capability test was applied. The primary shock wave energies and the bubble gas energies were

determined by measuring the overpressures of the shock waves generated in water. Measurement of the shock wave and the time between the primary shock wave and first pulsation of the gas bubble, allows the energies of the shock wave and gas bubble to be determined. These parameters allow a comparison to be made between the investigated explosives with currently used explosives (RDX, HMX, PETN).[2, 5]

4.2.1   Underwater Explosion – Test Arrangement

The initiating capability of detonators containing TKX-50, MAD-X1, PETNC and DAAF as a base charge was measured in underwater explosion test according to the methodology described in European Standard (EN 13763-15: 2004, Determination of equivalent initiating capability).[5a] Additionally, commercial available explosives (RDX, HMX, PETN) were used as reference materials.

Theoretical background of the underwater explosion and methodology used for calculation of the primary shock-wave energy (E_{SW}), shock energy equivalent (E_s), the bubble gas energy (E_{BW}) and the bubble energy equivalent (E_B) are briefly described in the Supporting Information.

The explosives which were tested were pressed into aluminum shells under a pressure of 4.40 MPa. For each explosive, the following masses were used: 0.2 g, 0.5 g and 0.7 g. The tests with different detonator masses were carried out five times. For the 0.5 g and 0.7 g explosive samples, two equal loading operations were applied (2×0.25 g and 2×0.35 g, respectively). The priming charge (lead azide, 0.3 g) was compressed at 4.40 MPa into an inner cup, and placed onto the base charge by applying a pressure of 4.40 MPa. Subsequently, an electric fuse-head with sealing plug and leading wires was fixed to the loaded detonator shell (containing the explosive to be tested) and an inner cup filled with the initiation charge.

In order to perform the underwater explosion tests, a water tank made from non-reflecting and energy-absorbing material with a positioning system for the sensor and detonator was used (Figure 2).
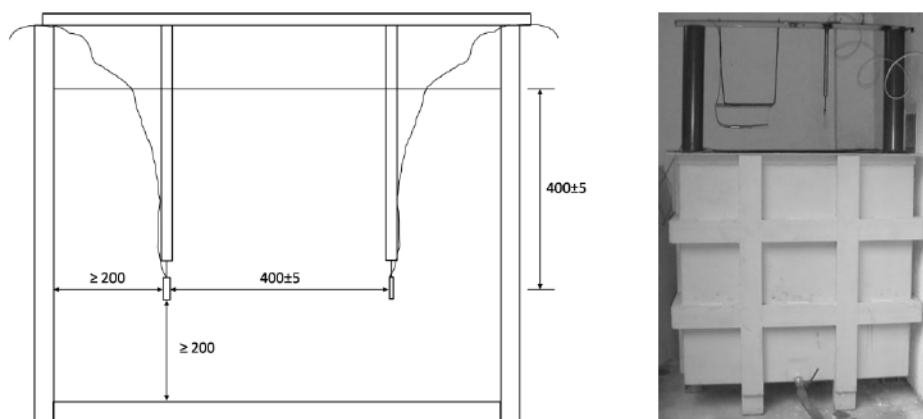
Figure 2. Model of the water tank showing the location of the detonator and the location of the pressure sensor (left) and the arrangement for testing (right).

The voltage mode tourmaline pressure sensor (PCB Piezotronics, Inc, model 138A05) and oscilloscope (Agilent, model 54622A) were used to collect data. The testing conditions during measurements were constant and as follows: water temperature: 10 °C, atmospheric pressure 980 hPa.

4.3 Results and Discussion

4.3.1 Synthesis

Explosives: TKX-50, MAD-X1, PETNC, DAAF were synthesized according to the methods given in the literature,[1b–d, 6] but with some improvements (see Supporting Information). Industrially produced explosives were supplied by Chemical Works "NITRO-CHEM" S.A. (RDX, HMX), Nitroerg S.A. (PETN).

4.3.2 The Initiating Capability of Detonators

The detonators being tested were placed in the positioning system. Detonation of the explosives generates overpressures in water which were recorded by a piezoelectric transducer. The amplified signal was collected using a digital oscilloscope, since current changes as a function of time ($I = f(t)$). Subsequently, by using the characteristics of the pressure sensor, the $I = f(t)$ was transferred into $P = f(t)$ relationship. The collected data are presented in two time scales. First one takes into account the presentation of the primary shock wave generated in water (*c.a.* 0–50 µs) which is used to determine maximum of overpressure (P_{max}), time at which the sensor output has decreased to $P_{\Theta} = P_{max} \cdot e^{-1}$ (Θ) (see Supporting Information). The second time frame (*c.a.* 0–30 ms) is used to determine the time interval between the shock-wave pressure peak and the first collapse of the gas bubble (t_b). Based on the obtained data, P_{max}, P_{Θ}, Θ, t_b, were determined (Table 1) then E_S, E_{SW}, E_B, E_{BW} and the total energies as a sum of the shock wave and bubble energies

generated in water (E) were calculated for the detonators being investigated (Table 2) are summarized graphically (Figure 3).

Table 1. Values of the experimental shock wave parameters: P_{max}, P_Θ, Θ, t_b, for investigated explosives.

	m [g]	ρ [g·cm^{-3}]	P_{max} [MPa]	P_Θ [MPa]	Θ [µs]	t_b [ms]
RDX	0.2	1.24 (4.20)	5.07 (2.53)	1.86	19.77 (3.09)	18.58 (0.45)
	0.5	1.37 (0.84)	7.04 (1.35)	2.59	21.44 (2.78)	22.63 (0.15)
	0.7	1.43 (2.37)	8.00 (0.64)	2.94	21.69 (3.75)	24.79 (0.70)
HMX	0.2	1.34 (2.10)	5.16 (1.95)	1.90	19.94 (3.76)	18.50 (0.37)
	0.5	1.61 (1.20)	7.04 (1.31)	2.59	22.06 (3.28)	22.53 (0.38)
	0.7	1.58 (1.14)	7.97 (0.43)	2.93	21.55 (3.03)	24.58 (0.23)
PETN	0.2	1.25 (3.23)	5.12 (1.15)	1.88	19.01 (1.16)	18.68 (0.12)
	0.5	1.51 (2.38)	7.12 (1.37)	2.62	21.56 (3.69)	22.84 (0.55)
	0.7	1.50 (1.68)	8.06 (0.45)	2.97	23.91 (3.02)	25.05 (0.04)
TKX-50	0.2	1.22 (2.35)	4.41 (1.31)	1.62	19.77 (2.00)	17.66 (0.25)
	0.5	1.44 (1.55)	6.31 (1.88)	2.32	22.37 (4.37)	21.57 (0.59)
	0.7	1.45 (2.03)	7.39 (1.16)	2.72	21.23 (2.98)	23.57 (0.34)
MAD-X1	0.2	0.97 (1.41)	4.56 (0.66)	1.68	20.90 (4.49)	18.35 (1.06)
	0.5	1.15 (3.76)	6.41 (0.48)	2.36	21.82 (2.39)	22.25 (0.33)
	0.7	1.07 (2.04)	7.52 (1.14)	2.77	21.96 (1.65)	24.58 (0.83)
PETNC	0.2	1.03 (2.19)	4.20 (0.63)	1.54	21.63 (3.11)	17.65 (1.23)
	0.5	1.18 (2.15)	5.76 (1.81)	2.12	21.55 (3.38)	21.22 (0.84)
	0.7	1.08 (1.35)	6.83 (1.39)	2.51	21.06 (3.21)	23.35 (0.44)
DAAF	0.2	1.40 (1.23)	4.71 (1.78)	1.73	21.34 (1.88)	18.28 (0.80)
	0.5	1.45 (0.93)	6.56 (1.24)	2.41	22.07 (2.56)	22.06 (0.59)
	0.7	1.45 (1.17)	7.53 (0.93)	2.77	21.71 (1.91)	24.24 (0.62)

Coefficient of variation (C_V, %) is given in brackets.

Table 2. Values of the calculated E_S, E_{SW}, E_B, E_{BW}, E for investigated explosives.

	m [g]	$E_S \cdot 10^8$ [Pa$^2\cdot$s]	E_{SW} [J]	$E_B \cdot 10^{-6}$ [s^3]	E_{BW} [J]	E [J]
RDX	0.2	1.60 (3.05)	217.47	6.41 (1.36)	498.61	716.08 (1.73)
	0.5	3.29 (1.89)	446.45	11.59 (0.44)	901.27	1347.72 (0.40)
	0.7	4.35 (1.95)	590.53	15.24 (2.09)	1184.82	1775.35 (0.99)
HMX	0.2	1.63 (3.03)	221.35	6.33 (1.12)	492.42	713.78 (1.64)
	0.5	3.31 (2.93)	449.55	11.44 (1.13)	889.63	1339.18 (1.61)
	0.7	4.37 (1.63)	593.87	14.85 (0.70)	1154.34	1748.21 (0.76)
PETN	0.2	1.65 (1.52)	224.60	6.52 (0.36)	506.94	731.54 (0.37)
	0.5	3.39 (1.86)	459.75	11.91 (1.65)	926.22	1385.97 (1.69)
	0.7	4.63 (1.11)	629.15	15.73 (0.12)	1222.87	1852.02 (0.41)
TKX-50	0.2	1.23 (1.75)	167.08	5.51 (0.74)	428.41	595.49 (0.76)
	0.5	2.70 (3.00)	366.73	10.03 (1.76)	779.95	1146.68 (1.99)
	0.7	3.59 (1.63)	488.14	13.12 (1.38)	1020.34	1508.48 (1.38)
MAD-X1	0.2	1.31 (3.31)	177.73	6.18 (3.17)	480.82	658.54 (2.95)
	0.5	2.76 (0.87)	375.13	11.01 (0.98)	856.33	1231.46 (0.81)
	0.7	3.66 (1.43)	496.74	14.86 (0.98)	1155.13	1651.87 (1.84)
PETNC	0.2	1.12 (1.37)	151.61	5.50 (3.74)	427.48	579.09 (2.91)
	0.5	2.16 (3.25)	292.92	9.55 (2.49)	742.79	1035.71 (2.61)
	0.7	2.93 (2.72)	398.48	12.73 (1.31)	990.22	1388.70 (1.51)
DAAF	0.2	1.43 (2.09)	194.42	6.11 (2.41)	475.08	669.50 (2.24)
	0.5	2.85 (2.40)	387.27	10.79 (1.45)	839.23	1226.50 (1.51)
	0.7	3.76 (1.80)	511.26	14.25 (1.85)	1107.72	1618.98 (1.54)

Coefficient of variation (C_V, %) is given in brackets.
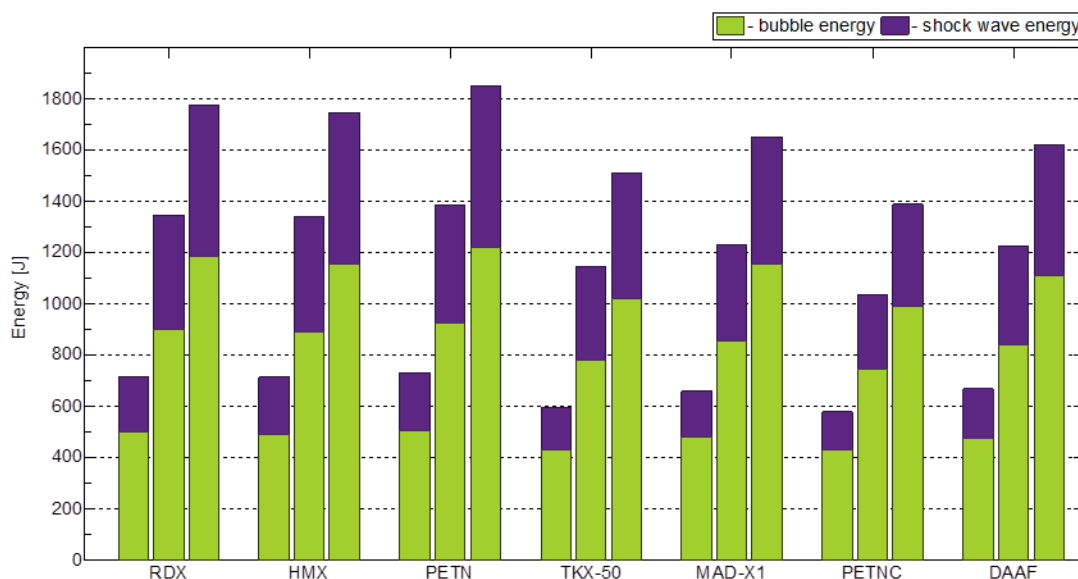
Figure 3. Total energy (E) generated in water for the explosives being investigated (0.2, 0.5, 0.7 g).

4.3.3 Detonation Parameters

The gas phase absolute molar enthalpies at 298 K and 10^5 Pa for the compounds in Table 3 were calculated theoretically using the modified complete basis set method (CBS-4M; M refers to the use of minimal population localization) with the GAUSSIAN 09 software.[7] The atomization energies method was applied in order to calculate the gas phase standard molar enthalpies of formation ($\Delta_f H_{(g)}°$) at 298.15 K. In order to obtain the standard molar enthalpy of formation ($\Delta_f H°$) for the prepared covalent compounds, the values of the standard molar enthalpies of sublimation (estimated using Trouton's rule using temperature of decomposition determined *via* differential scanning calorimetry measurements) were subtracted from $\Delta_f H_{(g)}°$. In the case of salts, $\Delta_f H_{(g)}°$ of ions as well as the calculated standard molar lattice enthalpies were used to calculate $\Delta_f H°$ (see Supporting Information).

The Chapman-Jouguet (C-J) characteristics, (*i.e.* heat of detonation, $\Delta_E U°$; detonation temperature, T_{C-J}; detonation pressure, p_{C-J}; detonation velocity V_{C-J}) based on the calculated $\Delta_f H°$ value, and both the theoretical maximum densities (obtained either from X-ray diffraction measurements at 298 K or from recalculation from the values obtained at 173 K using following equation:[8] $\rho_{298} = \rho_T[1 + \alpha_v(298 - T)]^{-1}$; $\alpha_v = 1.5 \times 10^{-4}$; $T = 173$ K) – see Supporting Information – and the densities obtained during the experiments described in this work (Table 3) were computed using the EXPLO5 V6.01 thermochemical computer code.[9] The Becker-Kistiakowsky-Wilson equation of state (BKW EOS) with the following sets of constants: $\alpha = 0.5$, $\beta = 0.29$, $\kappa = 10.45$, and $\Theta = 4120$ for gaseous detonation products and the Murnaghan equation of state for condensed products were applied.

Table 3. Calculated values of $\Delta_E U°$, $T_{C\text{-}J}$, $p_{C\text{-}J}$, $V_{C\text{-}J}$, of the explosives being investigated using densities obtained during tests.

	ρ [g·cm^{-3}]	$\rho \cdot \rho_{TMD}^{-1}$ ·100 [%]	$-\Delta_E U°$ [kg·kJ^{-1}]	$T_{C\text{-}J}$ [K]	$p_{C\text{-}J}$ [GPa]	$V_{C\text{-}J}$ [m·s^{-1}]
RDX	1.24	68.66	5392	4137	15.8	6946
	1.37	75.86	5450	4067	19.7	7389
	1.43	79.18	5522	4046	21.4	7582
HMX	1.34	70.38	5425	4078	18.8	7297
	1.58	82.98	5683	3989	26.5	8076
	1.61	84.56	5707	3972	27.6	8176
PETN	1.25	71.43	6017	4463	15.0	6718
	1.50	85.71	6085	4295	22.5	7598
	1.51	86.29	6087	4287	22.8	7632
TKX-50	1.22	65.00	5410	3936	16.1	7087
	1.44	76.72	5655	3878	22.1	7889
	1.45	77.25	5664	3876	22.5	7928
MAD-X1	0.97	51.05	5205	4303	9.56	5953
	1.07	56.32	5214	4236	11.5	6310
	1.15	60.53	5222	4180	13.3	6596
PETNC	1.03	58.52	3194	2946	7.6	5335
	1.08	61.36	3270	2964	8.5	5493
	1.18	67.05	3416	2993	10.2	5811
DAAF	1.40	80.14	4863	3730	16.7	6957
	1.45	83.00	4905	3718	18.0	7143

4.4 Conclusion

The novel explosives: TKX-50, MAD-X1, PETNC, DAAF have been synthesized and characterized. Syntheses of those explosives are characterized by high yields and selectivity as well as good purities. The Chapman-Jouguet (C-J) characteristics, energy of detonation (which for ideal explosives relates to calorimetrically measured heat of detonation) for theoretically maximum densities (TMD) as well as for those obtained during underwater explosion tests for all studied explosives were calculated using EXPLO5 computer code. All investigated explosives show high values of detonation parameters at TMD as well as high temperature of decomposition. Therefore, they were chosen for experimental investigation of their initiating capability.

The initiating capability of detonators containing as base charge TKX-50, MAD-X1, PETNC, DAAF in comparison to RDX, HMX or PETN using an underwater explosion test was determined. Densities obtained during the experiments are lower than TMD. The lowest values of densities in comparison to TMD are obtained for base charges equal 0.2 g of studied explosives (between 51.05% TMD for MAD-X1 and 80.14% TMD for DAAF). The highest values of densities obtained among investigated explosives were those of commercially

available explosives PETN, HMX and DAAF (86.29, 84.56, 83.00 % TMD, respectively). The differences in the densities obtained are due to the methodology used, which is described in the European Standard,[5a] *i.e.* the same pressing pressure (4.40 MPa) for all investigated explosives. That has direct impact on the primary shock wave generated in water, maximum of overpressure, the time interval between the shock-wave pressure peak and the first collapse of the gas bubble as well as calculated on those data values *i.e.* the shock wave and bubble energies generated in water. Nevertheless a constant value of pressing pressure was used for comparative reasons. Therefore additionally, underwater test results are supported by calculated detonation parameters at obtained densities.

Reference explosives (RDX, HMX and PETN) possess the highest values of the peak overpressure. Nevertheless novel explosives are characterized by slightly lower values of the recorded maximum overpressure (DAAF > 92.89%, MAD-X1 > 89.93%, TKX-50 > 86.97%, PETNC > 81.81%, of RDX). Similar tendency appears for the time of decreasing of the overpressure to $P_{max} \cdot e^{-1}$. Those factors show that primary shock waves generated by investigated explosives possess similar nature.

The highest values of time of the first bubble collapse are also obtained for reference explosives; however, new explosives differs from RDX not more than 7% of t_b (MAD-X1 > 98.31%, DAAF > 97.47%, TKX-50 > 95.04%, PETNC > 93.76% of RDX). That indicates also good action of mentioned explosives at longer distance from the point of initiation.

The total energies as sum of primary shock wave energies and the bubble gas energies were determined. The highest value of the total energy acquired for 0.7 g base charge mass was for PETN (104.32% RDX), the lowest for PETNC (78.82% of RDX). MAD-X1, DAAF and TKX-50 possess also high values of the total energy (93.04%, 91.19%, 84.97% of RDX, respectively). The primary shock wave energy (which corresponds to brisance of explosive) for investigated explosives is between 26.18% (PETNC, 0.2 g of base charge) and 33.97% (HMX, 0.7 g of base charge) of the total energy. Endothermal explosives show following contribution of shock wave energy to the total energy: TKX-50 > 28.05%; MAD-X1 > 26.98%, DAAF > 29.03%. The second part of the total energy namely bubble energy, which correlates with heaving power of explosive, is for investigated species higher than 66.01% of the total energy.

Moreover, presented technique can be also used as a comparative method; therefore the shock wave and bubble energies equivalents are also given. Thus the small scale underwater test can be useful tool for determining and comparing blast parameters (brisance, heaving power)

of different explosives. It is characterized by using small amount of tested species, and a great amount of information which can be obtained from the tests.

Therefore we can conclude that the data obtained are consistent and show that the explosives presented can be used as based charges in detonators. They meet requirements which are demanded from energetic materials intended for use in detonators. In order to maximize performance parameters pressing pressure should be optimized for every explosive.

4.5 References

[1] a) G. D. Solodyuk, M. D. Boldyrev, B. V. Gidaspov, V. D. Nikolaev, *Zh. Org. Khim.* **1981**, *17*, 861−865; b) Q. J. Axthammer, B. Krumm, T. M. Klapötke, *Eur. J. Org. Chem.* **2015**, *2015*, 723−729; c) N. Fischer, D. Fischer, T. M. Klapötke, D. G. Piercey, J. Stierstorfer, *J. Mater. Chem.* **2012**, *22*, 20418−20422; d) A. A. Dippold, T. M. Klapötke, *J. Am. Chem. Soc.* **2013**, *135*, 9931−9938.

[2] M. H. Lefebvre, *6th Seminar "New Trends in Research of Energetic Materials"*, Pardubice, Czech Republic, April 23−25, **2003**, 198−204.

[3] a) H. Gao, J. M. Shreeve, *Chem. Rev.* **2011**, *111*, 7377−7436; b) T. M. Klapötke, Chemistry of High-Energy Materials, De Gruyter, Berlin, **2011**; c) U. R. Nair, G. M. Gore, R. Sivabalan, S. J. Pawar, S. N. Asthana, S. Venugopalan, *J. Hazard. Mater.* **2007**, *143*, 500−505; d) A. K. Sikder, N. Sikder, *J. Hazard. Mater.* **2004**, *112*, 1−15; e) D. M. Badgujar, M. B. Talawar, S. N. Asthana, P. P. Mahulikar, *J. Hazard. Mater.* **2008**, *151*, 289−305.

[4] a) E. G. Francois, D. E. Chavez, M. M. Sandstrom, *Propellants, Explos., Pyrotech.* **2010**, *35*, 529−534; b) M. Szala, A. Kruzel, L. Szymańczyk, *High-Energetic Materials* **2012**, *4*, 27−35.

[5] a) EN 13763-15: 2004 *Explosives for Civil Uses – Detonators and Relays – Part 15: Determination of Equivalent Initiating Capability*, **2004**; b) J. Paszula, A. Maranda, T. Szydłowska, *Cent. Eur. J. Energ. Mater.* **2006**, *3*, 73−82; c) P. Koślik, J. Staś, Z. Wilk, A. Zakrzewski, *Cent. Eur. J. Energ. Mater.* **2007**, *4*, 3−13; d) S. Cudziło, W. A. Trzciński, J. Paszula, M. Nita, *Cent. Eur. J. Energ. Mater.* **2014**, *11*, 539−552.

[6] A. A. Dippold, T. M. Klapötke, *Chem. Eur. J.* **2012**, *18*, 16742−16753.

[7] M. J. Frisch, G. W. Trucks, H. B. Schlegel, G. E. Scuseria, M. A. Robb, J. R. Cheeseman, G. Scalmani, V. Barone, B. Mennucci, G. A. Petersson, H. Nakatsuji, M. Caricato, X. Li, H. P. Hratchian, A. F. Izmaylov, J. Bloino, G. Zheng, J. L. Sonnenberg, M. Hada, M. Ehara, K. Toyota, R. Fukuda, J. Hasegawa, M. Ishida,

T. Nakajima, Y. Honda, O. Kitao, H. Nakai, T. Vreven, J. A. Montgomery Jr., J. E. Peralta, F. Ogliaro, M. J. Bearpark, J. Heyd, E. N. Brothers, K. N. Kudin, V. N. Staroverov, R. Kobayashi, J. Normand, K. Raghavachari, A. P. Rendell, J. C. Burant, S. S. Iyengar, J. Tomasi, M. Cossi, N. Rega, N. J. Millam, M. Klene, J. E. Knox, J. B. Cross, V. Bakken, C. Adamo, J. Jaramillo, R. Gomperts, R. E. Stratmann, O. Yazyev, A. J. Austin, R. Cammi, C. Pomelli, J. W. Ochterski, R. L. Martin, K. Morokuma, V. G. Zakrzewski, G. A. Voth, P. Salvador, J. J. Dannenberg, S. Dapprich, A. D. Daniels, Ö. Farkas, J. B. Foresman, J. V. Ortiz, J. Cioslowski, D. J. Fox, *Gaussian 09*, Gaussian, Inc. Wallingford, CT, USA, **2009**.

[8] C. Xue, J. Sun, B. Kang, Y. Liu, X. Liu, G. Song, Q. Xue, *Propellants, Explos., Pyrotech.* **2010**, *35*, 333−338.

[9] M. Sućeska, *EXPLO5 6.01*, Brodarski Institute, Zagreb, Croatia, **2013**.

4.6 Supplementary Information

The analytical methods, general procedures and computational details are described in the appendix of this thesis. In addition, oscillograms showing the primary shock wave and the period of the first bubble pulsation, along with graphical comparisons of the shock wave energy, the bubble energy, and the total energy generated in water for all of the investigated explosives are also given in the appendix of this thesis.

4.6.1 Physico-chemical properties of the investigated explosives

Table 1. Physico-chemical properties of TKX-50, MAD-X1, PETNC and DAAF in comparison with PETN, RDX, HMX.

	PETN[1]	RDX[2]	HMX[2a, c), f)]	TKX-50[3]	MAD-X1[2a]	PETNC[4]	DAAF[5]
Formula	$C_5H_8N_4O_{12}$	$C_3H_6N_6O_6$	$C_4H_8N_8O_8$	$C_2H_8N_{10}O_4$	$C_4H_8N_{10}O_8$	$C_9H_{12}N_8O_{16}$	$C_4H_4N_8O_3$
MW [g·mol^{-1}]	316.13	222.12	296.16	236.16	324.2	488.23	212.13
IS[a] [J]	3.0	7.5	7	20	> 40	8	7
FS[b] [N]	60	120	112	120	> 360	360	> 360
ESD[c] [J]	0.19	0.20	0.20	0.10	0.50	0.75	0.15
N[d] [%]	17.72	37.84	37.84	59.3	43.2	23.0	52.75
Ω[e] [%]	−10.12	−21.61	−21.61	−27.10	−19.74	−26.22	−52.79
T_m[f] [°C]	142.6	205	275	–	–	–	–
T_{dec}[g] [°C]	208	210	279	221	217	196	239
ρ[h] [g·cm^{-3}]	1.75	1.806	1.904	1.877	1.90	1.76	1.747
$\Delta_f H°$[i] [kJ·mol^{-1}]	−479.7	86.3	118.8	446.6	213	−1311	443[i1)]
EXPLO5 V6.01							
$-\Delta_E U°$[j] [kJ·kg^{-1}]	6140	5799	5828	5890	5632	3928	5082
T_{C-J}[k] [K]	4083	3833	3753	3626	3722	2951	3590
p_{C-J}[l] [GPa]	31.4	35.4	39.8	40.2	39.2	25.8	27.7
V_{C-J}[m] [m·s^{-1}]	8448	8834	9177	9766	9195	7743	8325
Gas vol.[n] [dm^3·kg^{-1}]	752	792	769	913	786	728	758

[a] Impact sensitivity (BAM drophammer); [b] Friction sensitivity (BAM friction tester); [c] Electrostatic discharge device (OZM research); [d] Nitrogen content; [e] Oxygen balance; [f] Melting temperature; [g] Temperature of decomposition (DSC, β = 5 [°C], onset values); [h] Density at 298 K; [i] Standard molar enthalpy of formation (calculated, CBS-4M method); [i1] measured; [j] Heat of detonation; [k] Detonation temperature; [l] Detonation pressure; [m] Detonation velocity; [n] Volume of detonation gases at standard temperature and pressure conditions (assuming only gaseous products).

4.6.2 Underwater explosion - Theoretical background[6]

A detonating explosive undergoes prompt transformation into gaseous products under high temperature and pressure. If this process takes place in underwater conditions, complex physicochemical processes occur. Nonetheless, considering the damage, which a detonation causes, an underwater explosion can be considered as a shock wave and subsequent gas bubble pulsations of the detonation products. The shock wave which is created moves radially outward, acting on the surrounding water. In the front of the shock wave, the pressure increases sharply to the peak pressure and consequently decreases exponentially to hydrostatic pressure. Subsequently, pulsations of the gaseous detonation products take place which is a slower process. Initially, the gases which are compacted to high pressures

effect rapid expansion of the detonation products. The bubble expands to pressures which are lower than hydrostatic equilibrium pressure of the surrounded water because of the inertia of outwardly moving water. This continues until the pressure difference becomes high enough to discontinue the outer flow of water. Consequently, higher pressures in the surrounding water inverts this process causing contraction of the detonation gas bubble. Correspondingly, this process does not end at pressure equilibrium but recompresses the gasses to higher pressure. This expansion-contraction process of the gaseous products takes place several times. However, because of energy losses, the consequent oscillations get weaker and weaker. Phenomena caused by underwater explosions can be used to determine the following performance characteristics:

- the shock energy generated during the underwater explosion corresponds to the shattering action of the detonation products on other materials;
- the bubble energy produced during the underwater explosion corresponds to the heaving action of the detonation products.

The full description of shock wave energy generated in water

The primary shock-wave energy (E_{SW}) is determined from the following equation:[7]

$$E_{SW} = \frac{4\pi R^2}{\rho_w c_w} \int_{t_0}^{t_0+\theta} P^2(t)\, dt \tag{1}$$

where:

R – distance between detonator and pressure sensor;

ρ_w – water density;

c_w – sound velocity in water;

t_0 – moment of starting of shock wave;

θ – time at which the sensor output has decreased to $P_\Theta = P_{max} \cdot e^{-1}$;

P_{max} – maximum value of the overpressure.

The full description of bubble energy generated in water

The bubble gas energy (E_{BW}) can be determined by applying the following equation:

$$E_{BW} = \frac{A \cdot \sqrt{(Bh + C)^5}}{m_{Ex}} t_b^3 \tag{2}$$

where:

A, B, C – constants depending on arrangement system;

h – depth of immersion of detonator;

m_{Ex} – mass of explosive;

t_b – time interval between the shock-wave pressure peak and the first collapse of the gas bubble.

Assuming no boundary effects, the so-called Willis formula is used to calculate the bubble energy from the first period of pulsation of the gas bubble (t_b):[7]

$$t_b = \frac{1.135 \cdot \sqrt[3]{E_{BW}} \cdot \sqrt{\rho_w}}{\sqrt[6]{p_h{}^5}} = \frac{1.135 \cdot \sqrt[3]{E_{BW}} \cdot \sqrt{\rho_w}}{\sqrt[6]{(\rho_w \cdot g \cdot h + 101325)^5}} \tag{3}$$

where:

p_h – total hydrostatic pressure at the charge depth;

g – gravitational acceleration.

The total explosive energy (E) is assumed to be the sum of the shock wave and bubble energies.

$$E = E_{SW} + E_{BW} \tag{4}$$

However, if the test is standardized, it can be used as a comparative one which is based on so-called equivalents given by following equations:

- Shock energy equivalent, E_s (Figure 1):

$$E_S = \int_{t_0}^{t_0+\theta} P^2(t)\, dt \tag{5}$$
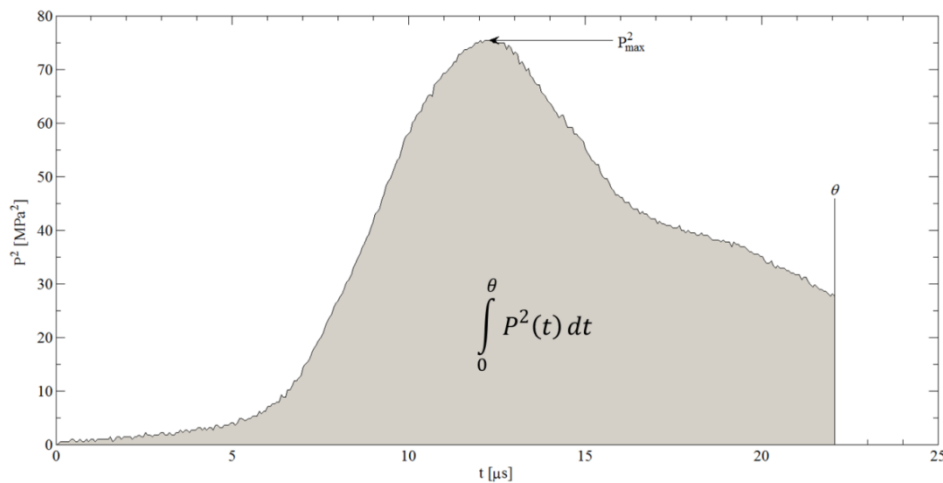
Figure 1. Calculation of the shock energy equivalent.

- Bubble energy equivalent, E_B (Figure 2):

$$E_B = t_b^3 \tag{6}$$
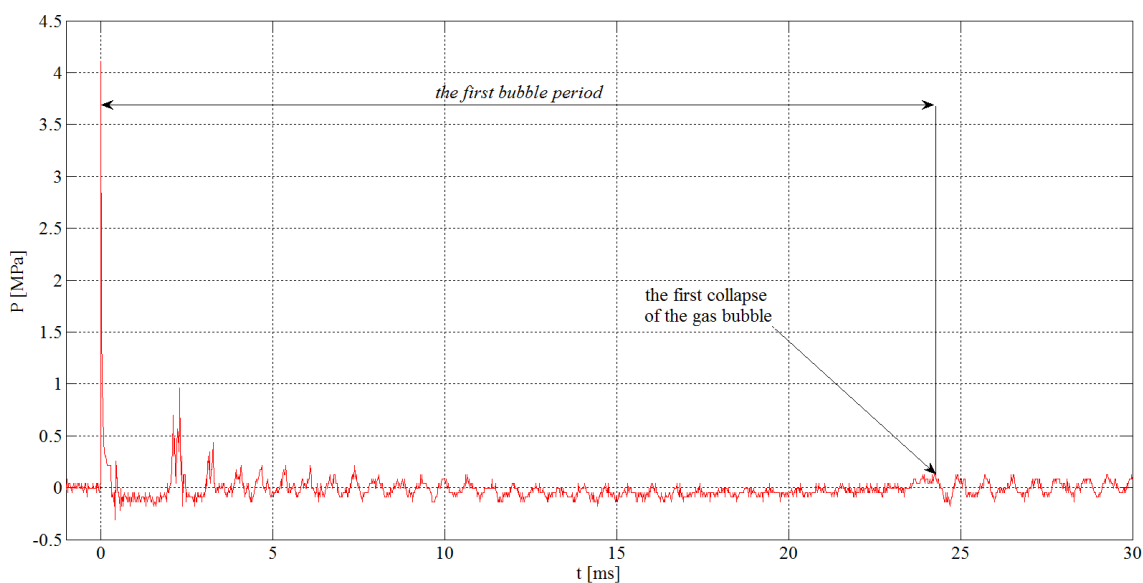
Figure 2. Plot of the bubble energy equivalent.

4.6.3   Synthesis of TKX-50, MAD-X1, PETNC and DAAF

TKX-50

5,5′-Bistetrazole-1,1′-diol dihydrate

Diazidoglyoxime (10 mmol, 1.70 g, obtained accordingly to Tselinskii et al.[8]) was suspended in 80 mL of diethyl ether. Subsequently, hydrogen chloride was bubbled for 2 hours through the reaction mixture at 0−5 °C while stirring. After that the flask was sealed and stirred at ambient temperature for 16 hours. The solution was allowed to stand for crystallization yielding 1.52 g (73%) of pale yellow crystals of 5,5′-bistetrazole-1,1′-diol dehydrate. **^{1}H NMR** (270.17 MHz, DMSO-d_6, ppm) δ: 6.80 (s, 2H, OH); **^{13}C{^{1}H} NMR** (67.9 MHz, DMSO-d_6, ppm) δ: 135.8; **EA** ($C_2H_6N_8O_4$, 206.12) calc.: C 12.01, H 2.81, N 54.12 %; found: C 11.64, H 2.91, N 54.29 %.

Dihydroxylammonium 5,5′-bistetrazole-1,1′-diolate (TKX-50)[3a]

5,5′-Bistetrazole-1,1′-diol dihydrate (2.06 g, 10 mmol) was dissolved in 50 mL of water at 65 °C. Subsequently, hydroxylamine solution (1.32 g, 20 mmol, 50% wt. in water) was dropwise added while stirring. Upon cooling of the solution to the ambient temperature TKX-50 crystallized. (Yield: 82%). **^{1}H NMR** (400.13 MHz, DMSO-d_6, ppm) δ: 9.66 (s, 8H, NH_3OH^+); **^{13}C{^{1}H} NMR** (100.6 MHz, DMSO-d_6, ppm) δ: 135.1; **EA** ($C_2H_8N_{10}O_4$, 236.15) calc.: C 10.50, H 3.63, N 59.31 %; found: C 10.21, H 3.46, N 59.21 %.

MAD-X1

3,3'-Dinitro-5,5'-bis-1H-1,2,4-triazole-1,1'-diol (DNBTO) [2a]

To the solution of potassium acetate (66 mmol, 6.46 g) in 33 mL of water 3,3'-di-nitro 5,5'-bis(1H-1,2,4-triazole) (50 mmol, 11.31 g; DNBT, obtained accordingly to literature[9]) was added and heated to 40 °C. Afterward potassium peroxymonosulfate (36 mmol, 10.92 g) was slowly added to the reaction mixture at pH 4−5 (tuned by adding a solution of potassium acetate − 50 mmol, 4.91 g − in 20 mL of water). After addition of potassium peroxymonosulfate the reaction mixture was stirred at 40 °C for 48 h followed by acidification using sulfuric acid solution (50% wt., 20 mL) and extraction with ethyl acetate (4 × 20 mL). The combined organic phases were dried over magnesium sulfate, and the solvent was evaporated under reduced pressure yielding colorless solid of DNBTO (40 mmol, 10.32 g, 80%). **^{1}H NMR** (270.17 MHz, DMSO-d_6, 25 °C, ppm) δ: 9.01 (s, 2H, OH); **^{13}C{^{1}H} NMR** (67.9 MHz, DMSO-d_6, 25 °C, ppm) δ: 154.9, 134.4; **EA** ($C_4H_2N_8O_6$, 258.11) calc.: C 18.61, H 0.78, N 43.41 %; found: C 18.74, H 0.95, N 42.18 %.

Dihydroxylammonium 3,3'-dinitro-5,5'-bis-1,2,4-triazole-1,1'-diolate (MAD-X1) [2a]

To the solution of DNBTO (10 mmol, 2.58 g) in ethanol (400 mL) water solution of hydroxylamine (50% wt., 20 mmol, 1.00 mL) was added. Precipitated orange product was collected by filtration and dried under reduced pressure at 60 °C for 6 hours (9.60 mmol, 3.11 g, 96%). **^{1}H NMR** (400.13 MHz, DMSO-d_6, 25 °C, ppm) δ: 10.24 (s, 6H, NH_3OH^+); **^{13}C{^{1}H} NMR** (100.6 MHz, DMSO-d_6, 25 °C, ppm) δ: 152.3, 133.3; **EA** ($C_4H_8N_{10}O_8$, 324.17) calc.: C 14.82, H 2.49, N 43.21 %; found: C 15.09, H 2.36, N 43.18 %.

PETNC[4]

Pentaerythritol Tetracarbamate

To suspended pentaerythritol (8 mmol, 1.09 g) in dry acetonitrile (40 mL) at 0 °C chlorosulfonyl isocyanate (40 mmol, 5.66 g) was slowly added followed by stirring for 2 hours at 0 °C and then at ambient temperature for 1 hour. Subsequently the reaction mixture was cooled to 5 °C and 20 mL of water was added with caution. The organic solvent was distilled under reduced pressure and the white precipitate of pentaerythritol tetracarbamate was filtered, washed with ice-cold water and dried under vacuum. Yield 99% (2.44 g). **^{1}H NMR** (400.18 MHz, DMSO-d_6, ppm) δ: 6.53 (s, 8H, NH_2), 3.92 (s, 8H, CH_2); **^{13}C{^{1}H} NMR** (100.6 MHz, DMSO-d_6, ppm) δ: 156.5, 62.1, 42.3; **EA** ($C_9H_{16}N_4O_8$, 308.25) calc.: C 35.07, H 5.23, N 18.18 %; found: C 34.98, H 5.34, N 18.11 %.

Pentaerythritol Tetranitrocarbamate (PETNC)

To the nitration mixture fuming nitric acid and concentrated sulfuric acid (8 mL, 1:1 *v/v*) at 0 °C pentaerythritol tetracarbamate (620 mg, 2.0 mmol) was slowly added followed by stirring for 15 minutes at 0 °C and then at ambient temperature for 1 hour. Afterward The reaction mixture was poured onto ice (400 g) and the precipitate was filtered, washed with water, diethyl ether and dried yielding 918 mg (94%) of PETNC. **^{1}H NMR** (400.18 MHz, DMSO-d_6, 25 °C, ppm) δ: 12.64 (s, 4H, NH), 4.15 (s, 8H, CH$_2$); **^{13}C{^{1}H} NMR** (100.5 MHz, DMSO-d_6, 25 °C, ppm) δ: 148.5, 63.8, 42.9; **EA** (C$_9$H$_{12}$N$_8$O$_{16}$, 488.24) calc.: C 22.14, H 2.48, N 22.95 %; found: C 22.06, H 2.69, N 21.60 %.

DAAF

Diaminoglyoxime (DAG)[10]

To ice cooled solution of sodium hydroxide (280 mmol, 11.20 g) in 32 mL of water, the hydroxylamine hydrochloride (256 mmol, 17.79 g) was slowly added. Subsequently glyoxal solution (40% wt., 64 mmol, 7.34 mL) was added in one portion. The reaction mixture was stirred for 15 minutes at 0 °C and then at 90 °C for 6 hours. During cooling of the reaction mixture to 0 °C yellow crystals of DAG was precipitated. Crude product was recrystallized from 32 mL of water, filtered and dried. Yield after recrystallization was 43% (3.25 g). **DTA** (5 °C·min^{-1}, onset): 202 °C (dec.); **^{1}H NMR** (270.17 MHz, DMSO-d_6, ppm) δ: 9.75 (s, 2H, OH), 5.16 (s, 4H, NH$_2$); **^{13}C{^{1}H} NMR** (67.9 MHz, DMSO-d_6, ppm) δ: 145.3; **IR** (ATR, 25 °C, cm^{-1}) $\tilde{v}$: 3466 (m), 3365 (m), 3092 (m), 2793 (w), 1680 (w), 1645 (m), 1602 (m), 1571 (s), 1505 (w), 1442 (m), 1419 (m), 1297 (m), 1112 (w), 976 (w), 936 (s), 739 (vs), 715 (vs); **Raman** (1064 nm, 300 mW, 25 °C, cm^{-1}) $\tilde{v}$: 1675 (100), 1588 (13), 1518 (57), 1467 (19), 1104 (32), 983 (12), 899 (17), 427 (16), 350 (30); **MS** (DEI+): m/z = 118.1 [M]$^+$; **EA** (C$_2$H$_6$N$_4$O$_2$, 118.09) calc.: C 10.34, H 5.12, N 47.44 %; found C 10.26, H 5.23, N 46.89 %.

Diaminofurazan (DAF)[10]

To solution of potassium hydroxide (80 mmol, 4.49 g) in 40 mL of water DAG (100 mmol, 11.81 g) was added. The suspension was placed in the stainless steel reactor and heated at 170 °C for 2 hours. White needle-like crystals of DAF were collected by filtration and dried under reduced pressure. Yield 50% (5.00 g). **DTA** (5 °C·min^{-1}, onset): 179 °C (melt.), 243 °C (dec.); **^{1}H NMR** (270.17 MHz, DMSO-d_6, ppm) δ: 5.78 (s, 4H, NH$_2$); **^{13}C{^{1}H} NMR** (67.9 MHz, DMSO-d_6, ppm) δ: 149.7; **IR** (ATR, 25 °C, cm^{-1}) $\tilde{v}$: 3420 (m), 3314 (w), 3258 (w), 3184 (w), 1623 (vs), 1585 (s), 1473 (m), 1417 (w), 1337 (s), 1300 (s), 970 (w),

888 (w), 859 (w), 774 (vs); **Raman** (1064 nm, 300 mW, 25 °C, cm^{-1}) $\tilde{\nu}$: 3425 (8), 3224 (8), 1644 (13), 1568 (29), 1473 (52), 1457 (41), 1159 (9), 961 (19), 886 (21), 877 (13), 780 (100), 653 (8); **MS** (DEI+): $m/z = 100.0$ [M]$^+$; **EA** (C$_2$H$_4$N$_4$O, 100.08) calc.: C 24.00, H 4.03, N 55.98 %; found C 23.24, H 3.53, N 54.73 %.

3,3'-Diamino-4,4'-azoxyfurazan (DAAF)[5, 11]

To aqueous solution of hydrogen peroxide (30% wt., 36.04 mL) of at 15 °C concentrated sulfuric acid (95% wt., 13.60 mL) was slowly added. After addition the solution was warmed to ambient temperature and kept for 15 minutes. Subsequently, finely powdered DAF (2 mmol, 2.00 g) under vigorous stirring was slowly added. After 24 h an orange solid was filtered, washed with ice cold water until the filtrate was neutral and dried. In order to remove the impurities, the crude product was dissolved in minimum amount of DMSO at 25 °C followed by slow addition of water as an antisolvent to give a pure DAAF (0.25 g, 59%).[9]

DTA (5 °C·min^{-1}, onset): 239 °C (dec.); **^{1}H NMR** (400.13 MHz, DMSO-d_6, ppm) δ: 6.94 (s, 2H, NH$_2$), 6.67 (s, 2H, NH$_2$); **^{13}C{^{1}H} NMR** (100.6 MHz, DMSO-d_6, ppm) δ: 153.5, 152.1, 150.7, 147.9; **IR** (ATR, 25 °C, cm^{-1}) $\tilde{\nu}$: 3424 (s), 3326 (s), 3257 (w), 3206 (w), 1634 (vs), 1589 (w), 1510 (m), 1461 (s), 1404 (vs), 1349 (m), 1296 (m), 1179 (w), 1124 (w), 1021 (vs), 946 (w), 917 (w), 875 (w), 847 (w), 773 (s), 732 (w), 683 (w), 663(w); **Raman** (1064 nm, 300 mW, 25 °C, cm^{-1}) $\tilde{\nu}$: 1511 (39), 1481 (80), 1424 (43), 1408 (25), 1352 (100), 1299 (13), 1035 (7), 922 (17), 731 (8); **MS** (DEI+): $m/z = 212.0$ [M]$^+$; **EA** (C$_4$H$_4$N$_8$O$_3$, 212.13) calc.: C 22.65, H 1.90, N 52.82 %; found: C 22.84, H 2.06, N 52.75 %; **IS**: 7 J; **FS**: > 360 N; **ESD**: 0.15 J.

4.6.4 References

[1]   a) R. K. Wharton, D. Chapman, *Propellants, Explos., Pyrotech.* **1997**, *22*, 71−73;
       b) J.-S. Lee, C.-K. Hsu, C.-L. Chang, *Thermochim. Acta* **2002**, *392−393*, 173−176.

[2]   a) A. A. Dippold, T. M. Klapötke, *J. Am. Chem. Soc.* **2013**, *135*, 9931−9938;
       b) C. S. Choi, E. Prince, *Acta Crystallogr., Sect. B: Struct. Crystallogr. Cryst. Chem.*
       1972, *28*, 2857−2862; c) R. Meyer, J. Köhler, A. Homburg, *Explosives*, 5th Edition,
       Wiley, Weinheim, Germany **2008**; d) J. P. Agrawal, *High Energy Materials:*
       Propellants, Explosives and Pyrotechnics, Wiley, Weinheim, Germany **2010**;
       e) P. Hakey, W. Ouellette, J. Zubieta, T. Korter, *Acta Cryst.* **2008**, *E64*, o1428;
       f) J. Deschamps, M. Frisch, D. Parrish, *J. Chem. Crystallogr.* **2011**, *41*, 966−970.

[3]   a) N. Fischer, D. Fischer, T. M. Klapötke, D. G. Piercey, J. Stierstorfer, *J. Mater. Chem.* **2012**, *22*, 20418−20422; b) X-ray density (for details see CCDC 872231, 872232; https://summary.ccdc.cam.ac.uk/structure-summary-form).

[4]   Q. J. Axthammer, B. Krumm, T. M. Klapötke, *Eur. J. Org. Chem.* **2015**, *2015*, 723−729.

[5]   E. G. Francois, D. E. Chavez, M. M. Sandstrom, *Propellants, Explos., Pyrotech.* **2010**, *35*, 529−534.

[6]   a) R. H. Cole, *Underwater Explosions*, Princeton Univ. Press, Princeton **1948**; b) S. Paterson, A. H. Begg, *Propellants, Explos., Pyrotech.* **1978**, *3*, 63−69; c) S. M. Kaye, H. L. Herman, J. Roth, *Encyclopedia of Explosives and Related Items*, US Army Armament Research and Development Command, Dover, New Jersey, **1983**; d) L. P. Orlenko, *Physics of Explosion*, Fizmatlit Publ., Moscow, **2002**.

[7]   G. Bjarnholt, R. Holmberg, *6th Symposium (International) on Detonation*, Coronado, California, USA, August 24−27, **1976**, p. 540−550.

[8]   I. V. Tselinskii, S. F. Mel'nikova, T. V. Romanova, *Russ. J. Org. Chem.* **2001**, *37*, 430−436.

[9]   A. A. Dippold, T. M. Klapötke, *Chem. Eur. J.* **2012**, *18*, 16742−16753.

[10]   A. K. Zelenin, M. L. Trudell, *J. Heterocycl. Chem.* **1997**, *34*, 1057−1060.

[11]   a) G. D. Solodyuk, M. D. Boldyrev, B. V. Gidaspov, V. D. Nikolaev, *Zh. Org. Khim.* **1981**, *17*, 861−865; b) M. Szala, A. Kruzel, L. Szymańczyk, *High-Energetic Materials* **2012**, *4*, 27−35.

5,5′-Bis(2,4,6-trinitrophenyl)-2,2′-bi(1,3,4-oxadiazole) (TKX-55): a Thermally Stable Explosive with Outstanding Properties

T_{dec} = 335 °C

FS > 360 N

IS = 5 J

ESD = 1.0 J

$\Delta_f H°$ = 197.6 kJ·mol^{-1}

ρ = 1.837 g·cm^{-3}

p_{C-J} = 27.3 GPa

V_{C-J} = 8030 m·s^{-1}
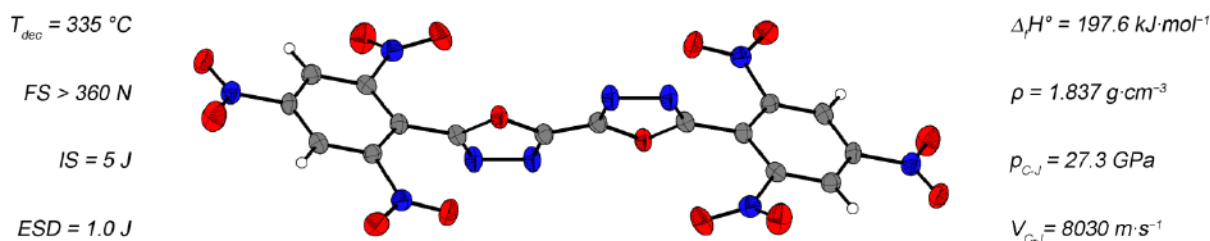
Abstract: The novel, thermally stable explosive 5,5′-bis(2,4,6-trinitrophenyl)-2,2′-bi(1,3,4-oxadiazole) (TKX-55) is reported. This compound can be prepared by means of a facile synthetic procedure and shows outstanding properties (detonation velocity, detonation pressure, sensitivity toward mechanical stimuli, and temperature of decomposition). TKX-55 was isolated and characterized by means of mass spectrometry, multinuclear (^{1}H, ^{13}C) NMR spectroscopy, and vibrational spectroscopy (IR and Raman). The structure in the crystalline state was determined by low-temperature single-crystal X-ray diffraction. From the calculated standard molar enthalpy of formation (CBS-4M) and the densities, the Chapman-Jouguet detonation properties were predicted by using the EXPLO5 V6.01 thermochemical computer code. The sensitivity of TKX-55 towards impact, friction, and electrostatic discharge was determined. The shock reactivity (explosiveness) of TKX-55 was measured by applying the small-scale shock reactivity test.

5.1 Introduction

Covalent compounds that contain a conjugated system with attached explosophore nitro groups are of particular interest in the development of new explosives which are stable at high temperatures. These explosives must also possess targeted performance properties (detonation velocity, specific energy), but, at the same time, show safety in handling and practicability for deep sea oil and gas exploitation as well as space exploration.[1] The known compound 2,2′,4,4′,6,6′-hexanitrobiphenyl (HNBP) consists of two directly connected trinitrophenyl moieties and shows a moderate decomposition temperature and good detonation parameters.[2] Inclusion of different moieties between the two picryl groups is one of the methodologies used in research in attempts to find heat-resistant explosives. The most prominent examples are 2,2′,4,4′,6,6′-hexanitrostilbene (HNS)[3] and 2,6-bis(picrylamino)-3,5-dinitropyridine (PYX).[1c, 4] The insertion of endothermic azole functionalities into the conjugated system improves the heat of formation of the final species. This also has a positive impact on the detonation parameters of the explosive. The connection of two picryl moieties through a 1,3,4-oxadiazole bridge was reported by Dacons and Sitzmann,[5] who reported the synthesis of 2,5-bis(2,4,6-trinitrophenyl)-1,3,4-oxadiazole (DPO), which had a decomposition temperature much higher than that of HNBP (Figure 1). Herein, the synthesis and investigation into the novel, thermally stable compound 5,5′-bis(2,4,6-trinitrophenyl)-2,2′-bi(1,3,4-oxadiazole) (TKX-55, **5**) is presented for the first time. In TKX-55, two 2,4,6-trinitrophenyl groups are connected by a di(1,3,4-oxadiazole) bridge (Figure 2).
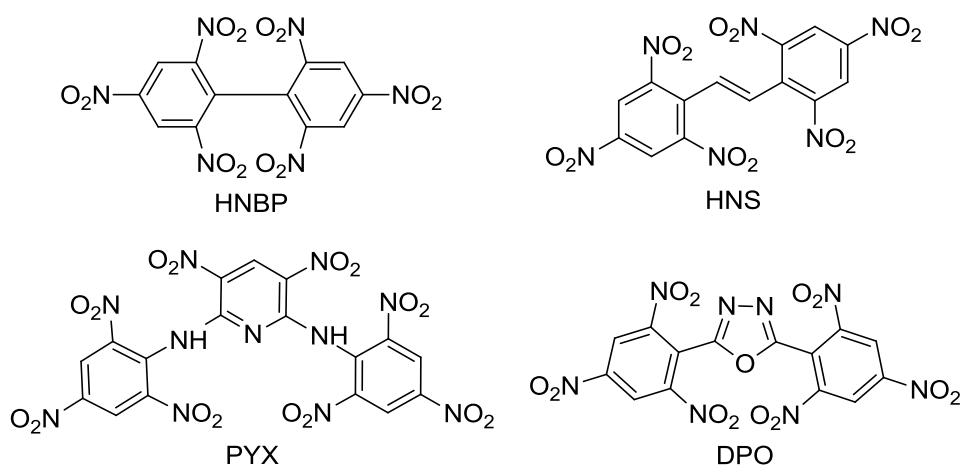
Figure 1. 2,2′,4,4′,6,6′-hexanitrobiphenyl (HNBP), 2,2′,4,4′,6,6′-hexanitrostilbene (HNS), 2,6-bis(picrylamino)-3,5-dinitropyridine (PYX), 2,5-bis(2,4,6-trinitrophenyl)-1,3,4-oxadiazole (DPO).
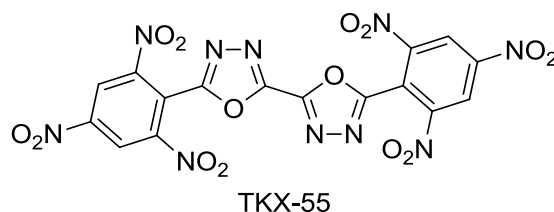
Figure 2. 5,5′-Bis(2,4,6-trinitrophenyl)-2,2′-bi(1,3,4-oxadiazole) (TKX-55).

5.2 Results and Discussion

The synthesis of TKX-55 is achieved in four steps from commercially available 2,4,6-trinitrotoluene (Scheme 1).
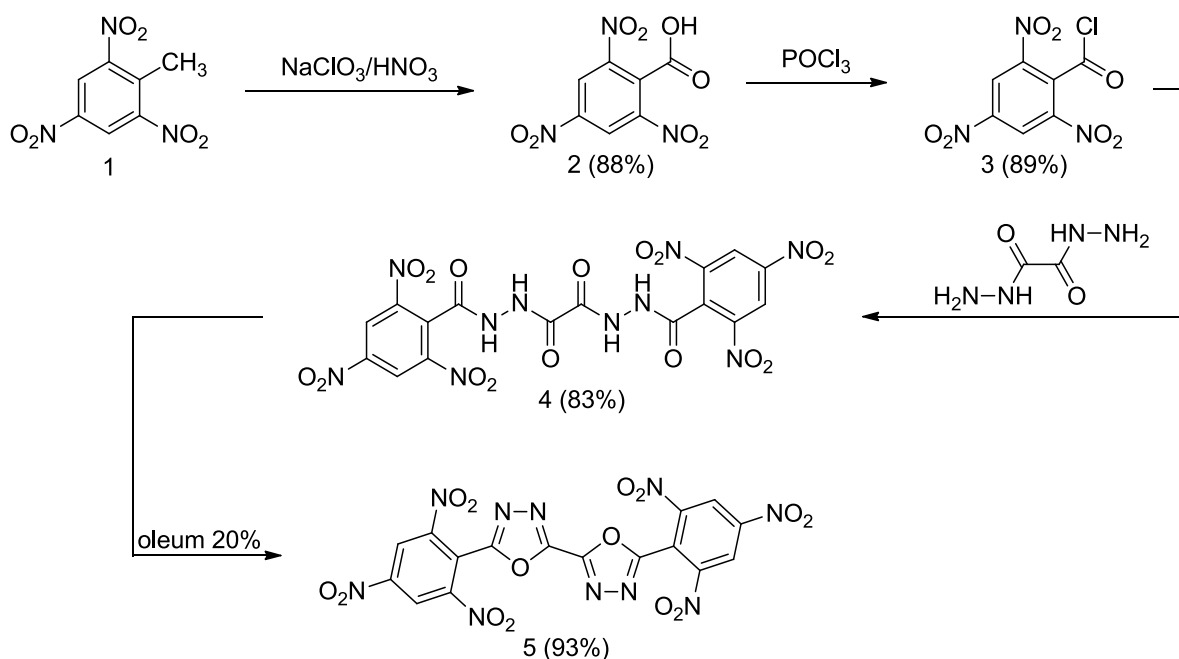
Scheme 1. Synthesis of TKX-55.

The synthetic route presented herein results in high yields of TKX-55 and selectivity of the desired compound. The intermediates and final product all precipitated from the reaction mixture without involving costly and time-consuming purification processes. It is worth noting that the process for synthesizing TKX-55 starts from 2,4,6-trinitrotoluene, which is also used as a starting material for the synthesis of HNS (the most commonly used heat-resistant explosive).

The first step in the synthesis of TKX-55 is oxidation of 2,4,6-trinitrotoluene to form 2,4,6-trinitrobenzoic acid (**1**) by using a mixture of $NaClO_3/HNO_3$ (yield 88%).[6] The second step involves chlorination of **1** with $POCl_3$ (yield 89%).[7] The next step involves the reaction of 2,4,6-trinitrobenzoyl chloride (**3**) with oxalyldihydrazide (which can be obtained in essentially quantitative yields through the reaction of diethyl oxalate with hydrazinium)

in tetrahydrofuran (yield 83%). In the final step, bis(2,4,6-trinitrobenzoyl)oxalohydrazide (**4**) is added to oleum (20%) and stirred at room temperature before the reaction mixture is poured onto crushed ice to yield TKX-55 (yield 93%). Compounds **4** and TKX-55 are pale, off-white solids that are practically insoluble in commonly used organic solvents.

The structure of TKX-55 in the crystalline state was determined by means of low-temperature single-crystal X-ray diffraction.[8] Selected crystallographic data, measurement parameters, and refinement details are given in the Supporting Information. TKX-55 crystallizes from hot 1,4-dioxane with three solvent molecules per TKX-55 molecule in the triclinic space group *P*-1, with a density of 1.625 g·cm^{-3} at 227 K and one molecule in the unit cell. The molecular structure of TKX-55 is shown in Figure 3.
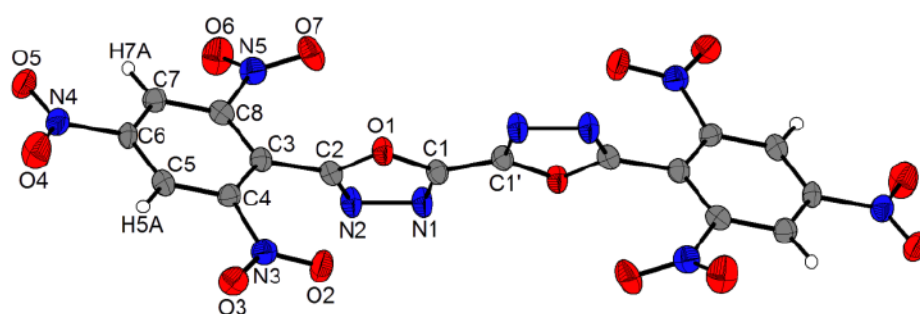
Figure 3. Molecular structure of TKX-55 in the crystal shown with thermal ellipsoids at the 50% probability level. Cocrystallized solvent molecules are removed for clarity.

The carbon–carbon bond connecting the 1,3,4-oxadiazole rings is involved in the conjugated π-electron system, and therefore, its length is shorter (1.449 Å) than that of a carbon–carbon single bond. 1,3,4-Oxadiazole rings are coplanar and twisted out of the plane of the 2,4,6-tri-nitrophenyl functionalities by 70.347(3)°. 2,4,6-Trinitrophenyl moieties are also parallel to each other. Two nitro groups are slightly twisted out of the benzene ring plane (∢C3-C4-N3-O3, 1.957(3)°; ∢C5-C6-N4-O4 5.667(3)°), whereas one *ortho*-nitro group is significantly bent (∢C3-C8-N5-O7, 36.061(3)°).

TKX-55 shows the desired properties required for a heat-resistant explosive: good detonation parameters, low sensitivity values, and a high decomposition temperature. The thermal stability of TKX-55 was measured by using differential scanning calorimetry (DSC), which showed that it decomposed above 335 °C. The measured density of the material is 1.837 g·cm^{-3} (obtained from a pycnometer measurement at 298 K), which is higher than the densities of both HNS and PYX.[3e] The calculated standard molar enthalpy of formation for TKX-55 is more than 2.5 times higher than that of HNS, and more than 4.5 times higher than that of PYX. The high density and high heat of formation result in very good detonation

parameters for TKX-55. The Chapman-Jouguet (C-J) characteristics: detonation velocity ($V_{C\text{-}J} = 8.030$ m·s^{-1}) and detonation pressure ($p_{C\text{-}J} = 27.3$ GPa) are both higher than the corresponding values for PYX and HNS.[2c–e] The nitrogen content of TKX-55 is enhanced owing to the inclusion of the oxadiazole moieties. The impact sensitivity of TKX-55 is 5 J, which is equal to the value reported for HNS, and the friction sensitivity of TKX-55 is higher than the measuring range of the friction tester apparatus (according to the STANAG regulations).[9] TKX-55 is also less sensitive toward electrostatic discharge (typical values for the human body are within the range 0.005–0.02 J) than PYX and HNS (Table 1).[1f] Moreover, TKX-55 is practically insoluble in water, which simplifies its isolation and purification. The combination of these properties makes TKX-55 unique among thermally stable explosives. Details on the measurements and computations are given in the Supporting Information.

Table 1. Physico-chemical properties of PYX, HNS and TKX-55.

	PYX	HNS	TKX-55
Formula	$C_{17}H_7N_{11}O_{16}$	$C_{14}H_6N_6O_{12}$	$C_{16}H_4N_{10}O_{14}$
IS[a] [J]	10	5[1f, 3e]	5
FS[b] [N]	360	240[1f, 3e]	> 360
ESD[c] [J]	0.5	0.8	1.0
N[d] [%]	24.80	18.67	25.00
Ω[e] [%]	−55.36	−67.6	−57.11
T_{dec}[f] [°C]	360[4a]	318[1f, 3e]	335
ρ[g] [g·cm^{-3}]	1.757[o]	1.74[3e]	1.837
$\Delta_f H^{\circ}$[h] [kJ·mol^{-1}]	43.7	78.2	197.6
EXPLO5 V6.01			
$-\Delta_E U^{\circ}$[i] [kJ·kg^{-1}]	4870	5142	4961
$T_{C\text{-}J}$[j] [K]	3609	3677	3681
$p_{C\text{-}J}$[k] [GPa]	25.1	24.3	27.3
$V_{C\text{-}J}$[l] [m·s^{-1}]	7757	7612	8030
Gas vol.[m] [dm^3·kg^{-1}]	633	602	604
f[n] [kJ·kg^{-1}]	1008	1008	1004

[a] Impact sensitivity (BAM drophammer, method 1 of 6); [b] Friction sensitivity (BAM drophammer, method 1 of 6); [c] Electrostatic discharge device (OZM research); [d] Nitrogen content; [e] Oxygen balance; [f] Temperature of decomposition; [g] Density at 298 K; [h] Standard molar enthalpy of formation; [i] Heat of detonation; [j] Detonation temperature; [k] Detonation pressure; [l] Detonation velocity; [m] Volume of detonation gases at standard temperature and pressure conditions; [n] Specific energy; [o] X-ray analysis.

To evaluate the explosive performance of TKX-55 on a small scale, a small-scale shock reactivity test (SSRT) was undertaken. The SSRT measures the shock reactivity (explosiveness) of potential energetic materials, often below the critical diameter, without requiring a transition to detonation.[10] TKX-55 was pressed into a perforated steel block. Initiation of the tested explosive was performed by using a commercially available detonator (Figures 4 and 5). The dent sizes were measured by filling them with finely powdered SiO$_2$

and measuring the resulting weight. For comparison, the corresponding values for PYX and HNS are also given (Table 2).
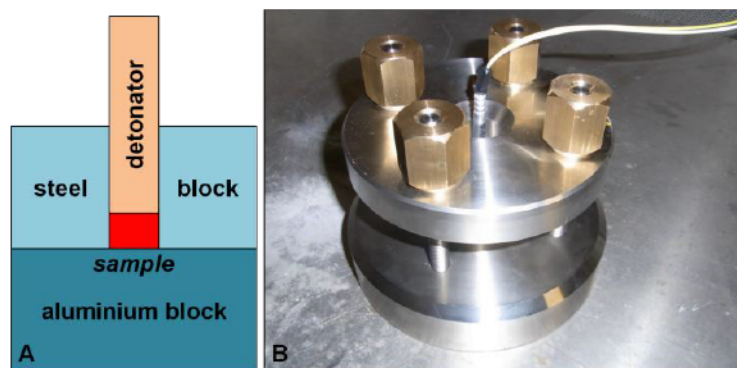
Figure 4. Details of the SSRT setup: schematic drawing (A); photograph of the test setup (B).
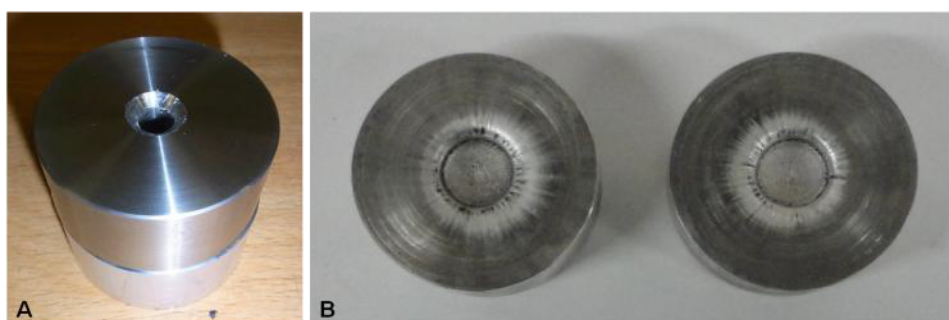
Figure 5. The SSRT results for TKX-55 : aluminum block and steel block filled with TKX-55 (A); dented aluminum blocks after initiation of the explosive with a commercial detonator (B).

Table 2. Results of the SSRT for PYX, HNS and TKX-55.

	PYX	**HNS**	**TKX-55**
m_E[a] [mg]	474	469	496
m_{SiO2}[b] [mg]	637	672	641

[a] Mass of the explosive: $m_E = V_s \cdot \rho \cdot 0.95$, ($V_s = 284 \text{ mm}^3$). [b] Mass of SiO_2.

From measuring the volumes of the dents (HNS > TKX-55 > PYX), it can be concluded that the performance of TKX-55 on a small scale is equivalent to the currently used heat-resistant explosives PYX and HNS.

It can be concluded that TKX-55 is one of the most thermally stable explosives. The density, enthalpy of formation, nitrogen content, detonation velocity, and detonation pressure values of TKX-55 are higher than those of the currently used heat-resistant explosives HNS and PYX. TKX-55 is insensitive to friction and its sensitivity to impact and electrostatic discharge are comparable with those of HNS. TKX-55 is practically insoluble in water (which avoids toxicity problems) and can be prepared by using a facile synthetic route. This combination of properties makes TKX-55 unique among thermally stable explosives.

5.3   Experimental Section

Bis(2,4,6-trinitrobenzoyl)oxalohydrazide (4): Oxalyldihydrazide (10 mmol, 0.59 g) was added in one portion to a solution of **3** (5 mmol, 2.76 g) in tetrahydrofuran (THF; 25 mL). The mixture was stirred for 72 h at ambient temperature. The precipitate was filtered off and washed with THF, acetone, and diethyl ether (2.48 g, 83%). **DSC** (5 °C·min^{-1}, onset): 307 °C (dec.); **^{1}H NMR** (400.18 MHz, DMSO-d_6, ppm) δ: 11.47 (s, 2H, NH), 11.42 (s, 2H, NH), 9.13 (s, 4H, CH)); **^{13}C{^{1}H} NMR** (100.0 MHz, DMSO-d_6, ppm) δ: 158.0, 157.5, 147.92, 147.91, 129.2, 124.1, ppm; **IR** (ATR, 25 °C, cm^{-1}) $\tilde{v}$: 3339 (m), 3295 (m), 3108 (w), 1714 (vs), 1671 (s), 1606 (m), 1552 (s), 1536 (vs), 1484 (m), 1452 (w), 1344 (vs), 1293 (m), 1230 (m), 11 81 (w), 1076 (w), 923 (s), 830 (w), 819 (w), 784 (w), 736 (s), 725 (s), 686 (m); **Raman** (1064 nm, 300 mW, 25 °C, cm^{-1}) $\tilde{v}$: 2589 (24), 2083 (7), 1734 (16), 1680 (10), 1626 (18), 1555 (26), 1546 (23), 1534 (17), 1490 (11), 1359 (100), 1295 (23), 1255 (10), 1198 (13), 1176 (11), 1098 (7), 1062 (8), 937 (16), 925 (17), 883 (19), 829 (29), 788 (7), 752 (8), 744 (7); **MS** (DEI+): $m/z = 596.1$ [M]$^+$; **EA** ($C_{16}H_8N_{10}O_{16}$, 596.29) calc.: C 32.23, H 1.35, N 23.49 %; found C 32.22, H 1.61, N 22.87 %.

5,5′-Bis(2,4,6-trinitrophenyl)-2,2′-bi(1,3,4-oxadiazole) (TKX-55, 5): Compound **4** (1 mmol, 0.60 g) was added to fuming sulfuric acid (20%, 10 mL). The mixture was stirred for 24 h at ambient temperature before being poured onto crushed ice. The precipitate formed was filtered off and washed with water until it was acid free, and was subsequently dried (0.52 g, 93%). **DTA** (5 °C·min^{-1}, onset): 335 °C (dec.); **^{1}H NMR** (399.78 MHz, DMSO-d_6, ppm) δ: 9.40 (s, 4H, CH); **^{13}C{^{1}H} NMR** (100.5 MHz, DMSO-d_6, ppm) δ: 158.1, 154.0, 150.3, 149.4, 125.3, 116.8; **IR** (ATR, 25 °C, cm^{-1}) $\tilde{v}$: 3089 (w), 1608 (m), 1541 (s), 1468 (w), 1403 (w), 1341 (s), 11 87 (w), 11 52 (m), 1064 (m), 993 (w), 966 (w), 955 (w), 923 (s), 925 (w), 780 (w), 759 (m), 740 (m), 722 (s), 694 (w), 673 (w), cm^{-1}; **Raman** (1064 nm, 200 mW, 25 °C, cm^{-1}) $\tilde{v}$: 1639 (100), 1565 (32), 1360 (66), 1026 (29), 977 (11), 967 (12), 924 (7), 825 (18), cm^{-1}; **MS** (DEI+): $m/z = 561. 1$ [M+1]$^+$; **EA** ($C_{16}H_4N_{10}O_{14}$, 560.26) calc.: C 34.30, H 0.72, N 25.00 %; found C 34.33, H 1.01, N 25.01 %; **IS**: 5 J (< 100 µm); **FS**: > 360 N (< 100 µm); **ESD**: 1.0 J (< 100 µm).

5.4   References

[1]   a) T. Urbański, *Chemistry and Technology of Explosives*, *Vol. 4*, Pergamon Press, Oxford, **1984**, p. 202–217; b) M. E. Sitzmann, *J. Energ. Mater.* **1988**, *6*, 129–144; c) J. P. Agrawal, Mehilal, U. S. Prasad, R. N. Surve, *New J. Chem.* **2000**, *24*, 583–585; d) H. S. Jadhav, M. B. Talawar, R. Sivabalan, D. D. Dhavale, S. N. Asthana,

V. N. Krishnamurthy, *Indian J. Heterocycl. Chem.* **2006**, *15*, 383–386; e) J. P. Agrawal, *Cent. Eur. J. Energ. Mater.* **2012**, *9*, 273–290; f) T. M. Klapötke, *Chemistry of High-Energy Materials*, Walter de Gruyter, Berlin, **2015**; g) J. P. Agrawal, *High Energy Materials: Propellants, Explosives and Pyrotechnics*, Wiley, Weinheim, **2015**.

[2]   a) F. Ullmann, J. Bielecki, *Ber. Dtsch. Chem. Ges.* **1901**, *34*, 2174–2185; b) P. E. Rouse, *J. Chem. Eng. Data* **1976**, *21*, 16–20; c) S. Zeman, *J. Therm. Anal.* **1980**, *19*, 207–214; d) M. Sućeska, *Propellants, Explos., Pyrotech.* **1991**, *16*, 197–202; e) M. Sućeska, in *32nd International Annual Conference of ICT*, Karlsruhe, Germany, **2001**, 110/111–110/113; f) M. Sućeska, *Mater. Sci. Forum* **2004**, *465–466*, 325–330.

[3]   a) K. G. Shipp, *J. Org. Chem.* **1964**, *29*, 2620–2623; b) F. Gerard, A. Hardy, *Acta Crystallogr., Sect. A: Found. Adv.* **1987**, *43*, C167; c) F. Gerard, A. Hardy, *Acta Crystallogr., Sect. C: Struct. Chem.* **1988**, *44*, 1283–1287; d) J.-S. Lee, C.-K. Hsu, C.-L. Chang, *Thermochim. Acta* **2002**, *392–393*, 173–176; e) R. Meyer, J. Köhler, A. Homburg, *Explosives*, 6th edn., Wiley, Weinheim, **2007**, p. 174.

[4]   a) M. D. Coburn, J. L. Singleton, *J. Heterocycl. Chem.* **1972**, *9*, 1039–1044; b) M. D. Coburn, *Pat. US 3678061A*, Atomic Energy Commission, Washington D.C., USA, **1972**; c) R. Kuboszek, W. Pawłowski, *Pat. PL 186580 B1*, Warsaw University of Technology, Poland, **1997**; d) H. S. Jadhav, M. B. Talawar, R. Sivabalan, D. D. Dhavale, S. N. Asthana, V. N Krishnamurthy, *Indian J. Heterocycl. Chem.* **2006**, *15*, 383-386.

[5]   J. C. Dacons, M. E. Sitzmann, *J. Heterocycl. Chem.* **1977**, *14*, 1151–1155.

[6]   Z.-L. Yao, R.-B. Wang, H.-L. Liu, *Applied Chemical Industry* **2009**, *38*, 1153–1155.

[7]   G. Zlotin, G. Kislitsin, V. Samet, A. Serebryakov, D. Konyushkin, V. V. Semenov, A. A. Gakh, *J. Org. Chem.* **2000**, *65*, 8430–8438.

[8]   CCDC 1450558 contains the supplementary crystallographic data for this paper. The data can be obtained free of charge from The Cambridge Crystallographic Data Centre via www.ccdc.cam.ac.uk/structures.

[9]   a) NATO Standardization Agreement 4489 (STANAG 4489), Explosives, Impact Sensitivity Tests, **1999**; b) NATO Standardization Agreement 4487 (STANAG 4487), Explosives, Friction Sensitivity Tests, **2002**.

[10] a) H. W. Sandusky, R. H. Granholm, and D.G. Bohl, *IHTR 2701*, Naval Surface Warfare Center, Indian Head Division, MD, USA, 12 August, **2005**; b) J. E. Felts, H. W. Sandusky, R. H. Granholm, *AIP Conf. Proc.* **2009**, *1195*, 233–236.

5.5   Supplementary information

The analytical methods, general procedures, Small-Scale Shock Reactivity Test and computational details are described in the appendix of this thesis.

5.5.1 X-ray Diffraction

TKX-55 crystallizes from hot 1,4-dioxane with three species of the solvent per one molecule of TKX-55 in the triclinic space group P-1 with a density of 1.625 g·cm^{-3} at 227 K and one molecule in the unit cell (Table 1). The molecule of TKX-55·3C$_4$H$_8$O$_2$ is shown in Figure 1.
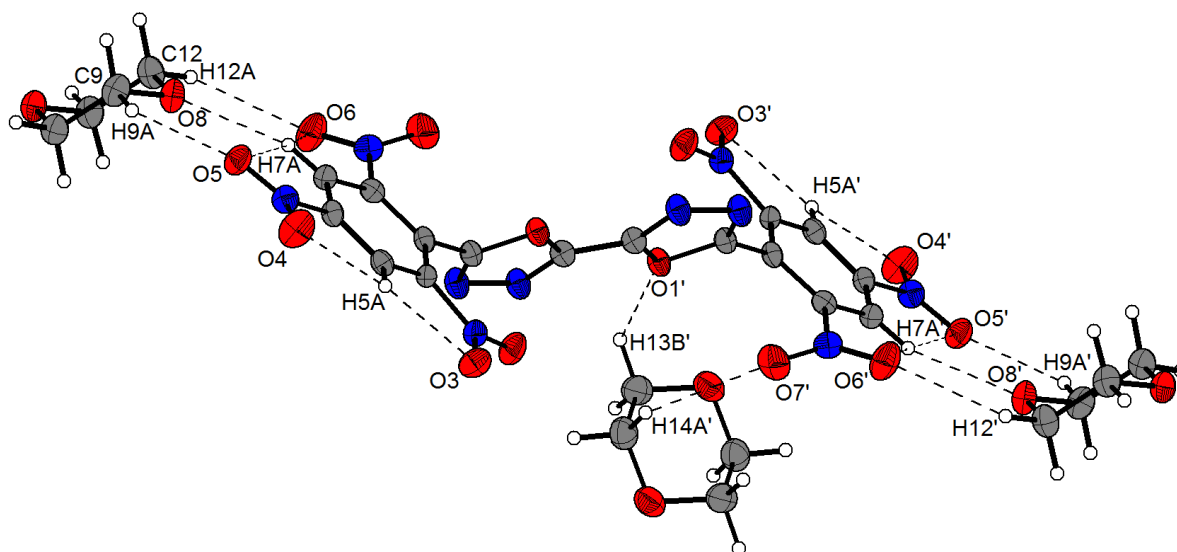
Figure 1.   Molecular   structure   of   5,5′-bis(2,4,6-trinitrophenyl)-2,2′-bi(1,3,4-oxadiazole) tris(1,4-dioxane) solvate (**5**·3C$_4$H$_8$O$_2$) in the crystal shown with 50% probability thermal ellipsoids.

CCDC 1450558 contains the supplementary crystallographic data for this paper. These data can be obtained free of charge from the Cambridge Crystallographic Data Centre *via* www.ccdc.cam.ac.uk/data_request/cif.

Table 1. Crystallographic data and refinement parameters of compound **5**·3C$_4$H$_8$O$_2$.

	5·3C$_4$H$_8$O$_2$
Chemical formula	C$_{16}$H$_4$N$_{10}$O$_{14}$·3(C$_4$H$_8$O$_2$)
Molecular weight [g·mol^{-1}]	824.58
Color, habit	colorless plate
Size [mm]	0.32x0.13x0.02
Crystal system	Triclinic
Space group	P-1 (No. 2)
a [Å]	6.6985(8)
b [Å]	7.7673(6)
c [Å]	16.6519(15)
α [°]	98.627(7)
β [°]	99.922(9)
γ [°]	91.635(8)
V [Å^3]	842.46(14)
Z	1
ρ_{calc} [g·cm^{-3}]	1.625
μ [mm^{-1}]	0.141
$\lambda_{MoK\alpha}$[Å]	0.71073
F(000)	426.0
ϑ min-max [°]	4.19–26.37
T [K]	227
Dataset h	$-6 \leq h \leq 8$
Dataset k	$-9 \leq k \leq 9$
Dataset l	$-19 \leq l \leq 20$
Reflections collected	5895
Independent reflections	3440
Observed reflections	2271
Number of parameters	304
R$_{int}$	0.0377
S	0.998
R$_1$, wR$_2$ (I>σI$_0$)	0.0468, 0.0757
R$_1$, wR$_2$ (all data)	0.0821, 0.0927
Weighting scheme (x, y)[a]	0.0211, 0.0
Remaining density [e·Å^{-3}]	−0.274, 0.287
Device type	Oxford XCalibur3 CCD
Solution	SIR-97
Refinement	SHELXL-97
Absorption correction	multi-scan
CCDC	1450558

[a] wR$_2$ = [Σ[w(F$_0^2$−F$_c^2$)^2]/Σ[w(F$_0$)^2]]$^{1/2}$ where w = 1/[σ$_c^2$(F$_0^2$)+(xP)^2+yP] and P = (F$_0^2$+2F$_c^2$)/3

Experimental Study on the Heat Resistant Explosive 5,5′-Bis(2,4,6-trinitrophenyl)-2,2′-bi(1,3,4-oxadiazole) (TKX-55): the Jet Penetration Capability and Underwater Explosion Performance
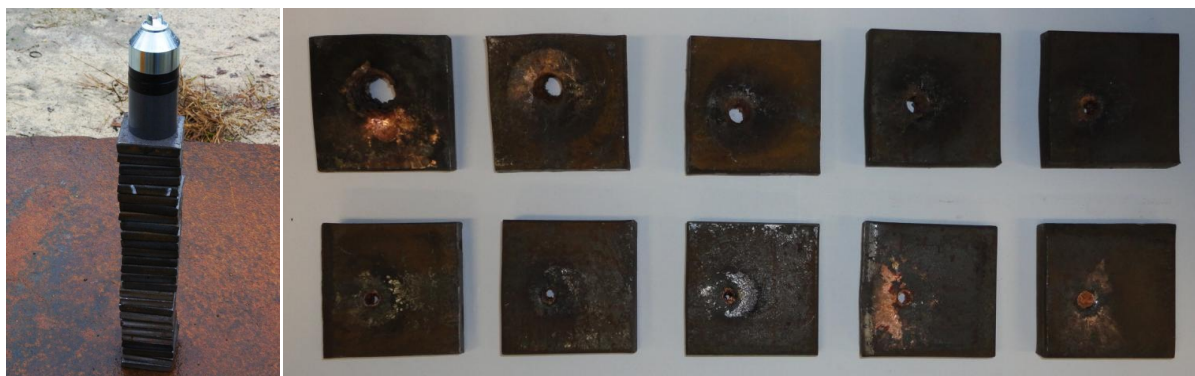
Abstract: Ongoing research to find new explosives which are stable at high temperatures focuses on compounds which comply with the strict requirements which must be fulfilled in order for a compound to be of use in deep oil-well and gas drilling applications. Great efforts have been focused on the development of new, thermally stable explosives which are stable at even higher temperatures than hexanitrostilbene, and which also show superior performance. In the group of recently synthesized thermally stable explosives, 5,5′-bis(2,4,6-trinitrophenyl)-2,2′-bi(1,3,4-oxadiazole) (TKX-55) is one of the most promising prospective candidates for use in practical applications, due to its physicochemical properties as well as its convenient synthesis. Therefore, further investigation into the performance of TKX-55 in shaped charge applications was undertaken. This study was focused on the investigation of the jet penetration capability of conical shaped charges filled with TKX-55, in comparison with recently used other explosives. The kinetic energy of the jet depends on the brisance of the explosive which is used. In order to experimentally investigate the shattering effect of TKX-55, the Underwater Explosion Test was applied. Based on the collected data, the total energy, as the sum of the primary shock wave energy (the brisance) and the bubble gas energy (the heaving effect), was calculated.

Keywords: thermally stable explosive · TKX-55 · shaped charge · underwater detonation

6.1   Introduction

Research on thermally stable explosives is conducted in many research groups worldwide.[1-8] However, there are strict demands which thermally stable explosives must meet: tailored performance, sensitivity, stability, vulnerability, environmental safety, low solubility in water, longevity and compatibility. Explosives which are stable at high temperatures and low pressures are used in perforating charges in the mining industry to obtain oil and gas from wells. Perforation with shaped charges is currently a common method of achieving a connection between the deposit and the geological borehole. It is also used for uncovering other deposits, such as mineral water, geothermal sources, shell gas, sulfur resources, as the most cost-effective method.[9] In this area of research, the following explosives have received particular interest: 1,3,5-triamino-2,4,6-trinitrobenzene (TATB),[10-17] 2,2′,4,4′,6,6′-hexanitrostilbene (HNS)[16-24] and 2,6-bis(picrylamino)-3,5-dinitropyridine (PYX).[4, 25-28] Other interesting heat resistant explosives such as 2,2′,2″,4,4′,4″,6,6′,6″-nona-nitroterphenyl (NONA) and 2,6-diamino-3,5-dinitropyrazine-1-oxide (LLM-105),[29-31] (Figure 1) are currently under investigation.
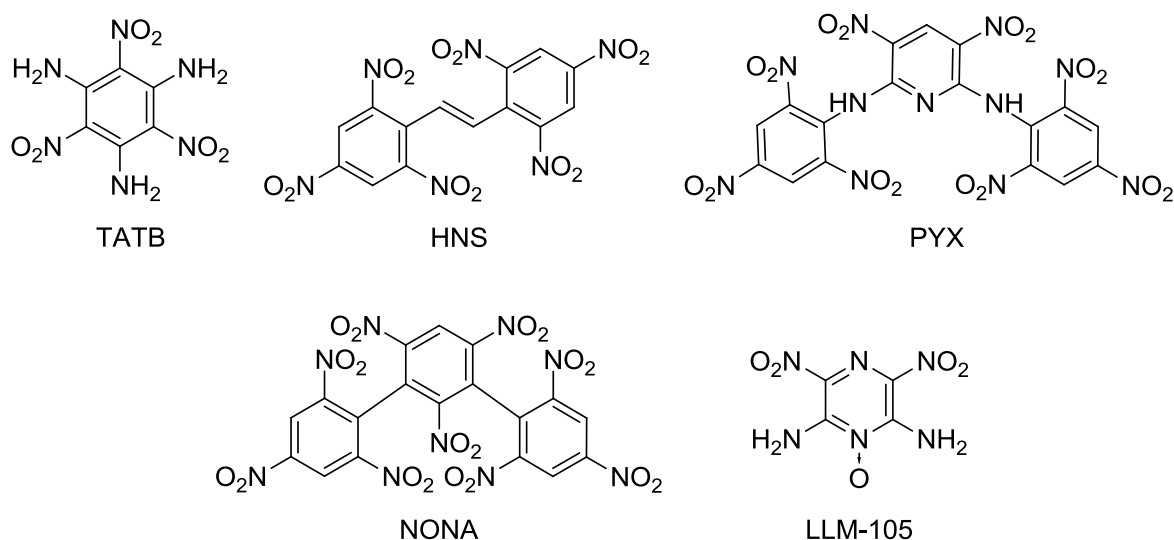
Figure 1.   1,3,5-Triamino-2,4,6-trinitrobenzene (TATB), 2,2′,4,4′,6,6′-hexanitrostilbene (HNS), 2,6-bis(picrylamino)-3,5-dinitropyridine (PYX), 2,2′,2″,4,4′,4″,6,6′,6″-nonanitroterphenyl (NONA) and 2,6-diamino-3,5-dinitropyrazine-1-oxide (LLM-105).

Many research groups are currently trying to find new heat resistant explosives which show lower sensitivity and better performance than HNS. Among the recently reported heat resistant explosives, 5,5′-bis(2,4,6-trinitrophenyl)-2,2′-bi(1,3,4-oxadiazole) (TKX-55) is one of the most promising candidates for application, because of its good physicochemical properties as well as its convenient synthesis (Scheme 1).[32]
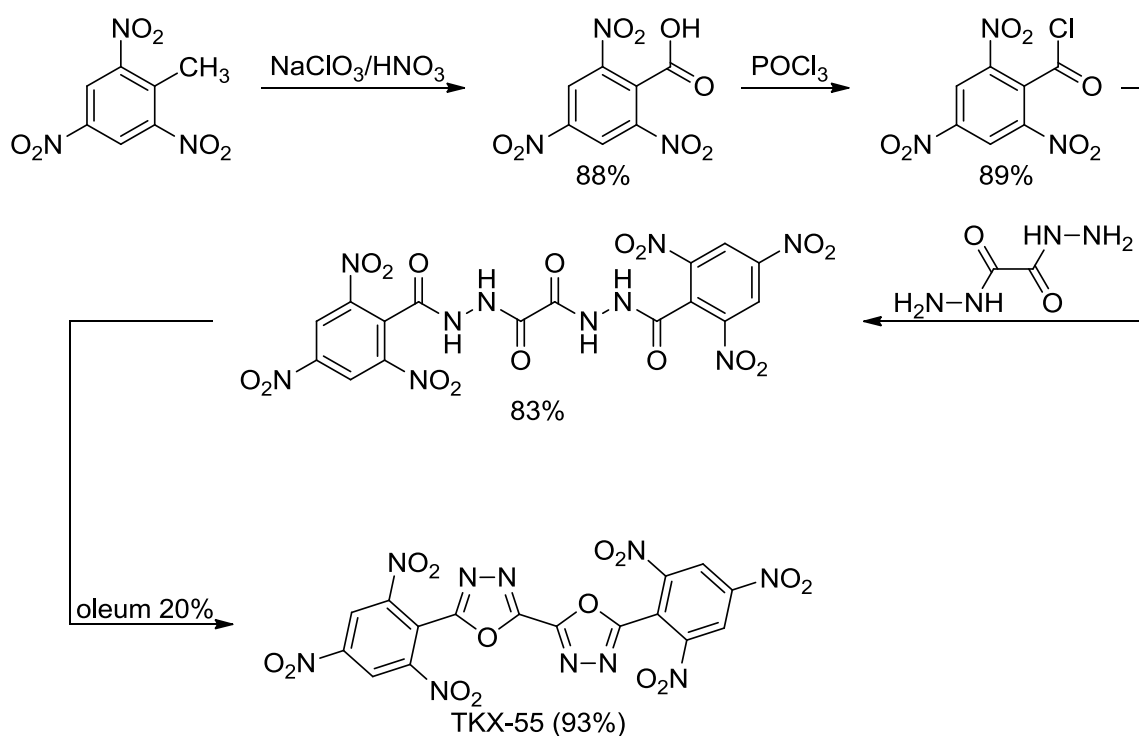
Scheme 1. Synthesis of 5,5′-bis(2,4,6-trinitrophenyl)-2,2′-bi(1,3,4-oxadiazole) (TKX-55).[32]

TKX-55 is a covalent species consisting of a conjugated system with six nitro explosophore functionalities attached to it. Moreover, the inclusion of the endothermic 1,3,4-oxadiazole heterocyclic moieties into the conjugated system increases the heat of formation of the final compound. The calculated standard molar enthalpy of formation for TKX-55 (197.6 kJ·mol^{-1}) is more than 2.5 times higher than that of HNS, and more than 4.5 times higher than that of PYX (78.2 and 43.7 kJ·mol^{-1}, respectively).[32] The measured density of TKX-55 is 1.837 g·cm^{-3} (pycnometer measurement at 298 K) which is higher than the reported densities of HNS and PYX.[32] The high density, as well as the high value for the heat of formation, are the reasons for the high detonation parameters of TKX-55 (computed using the EXPLO5 V6.01 thermochemical computer code):[33] detonation velocity ($V_{C-J} = 8030$ m·s^{-1}) and detonation pressure ($p_{C-J} = 27.3$ GPa).[32] The thermal stability of TKX-55 is high, with decomposition at 335 °C (onset value) determined using differential scanning calorimetry (DSC, $\beta = 5$ °C·min^{-1}).[32] The friction sensitivity of TKX-55 is lower (> 360 N) than the measuring range of the friction testing apparatus. The impact sensitivity of TKX-55 is 5 J, which is equal to the value reported for HNS. TKX-55 is also less sensitive toward electrostatic discharge than PYX and HNS.[8, 32] Since the properties of TKX-55 are remarkable in comparison with those of HNS and PYX, we decided to perform further investigations into TKX-55.

This study focused on an investigation of both the effective perforation of conical shaped charges filled with the new thermally stable explosive (TKX-55), and the initiating capability of detonators containing TKX-55 as a base charge (applying the Underwater Explosion Test).

6.2   The Jet Penetration Capability

In order to study the jet penetration capability of shaped charges containing TKX-55 as a base charge, the methodology described in the standard (PN-C- 86045:1997, Explosives – shaped charges) was applied.[34] The essential impact on the depth of the jet penetration have the symmetry and homogeneity of the liner. In order to meet all of the requirements which are desired for the geometry and structure of the liners, powder metallurgy technology was applied.[9, 35-37] Liners were manufactured by compression molding of electrolytic copper powder (ECu, the diameter of the spherical copper grains was approximately 10 μm), followed by low temperature sintering of the liners in an inert atmosphere. The symmetry and homogeneity of the powder liners were assessed on a spinning table workstation and by measuring the liners' wall thickness at predetermined measurement points.[9] The liners which were obtained had the following characteristics: outer diameter (34.70 ± 0.01 mm), apex angle (60.00 ± 0.01°), mass (18.00031 ± 0.00002 g), and density (8.40 ± 0.01 g·cm^{-3}) – Figure 2.

Figure 2. Liners made from copper (ECu) powder.

Further factors which have a significant impact on the jet penetration capability are the physicochemical properties of the explosive that is used as the main charge. In our experiments, TKX-55 was investigated and the results compared with those obtained using RDX and RDX phlegmatized with 1.5% polyfluoroethylene.[32, 38] The mass of the base charge which was used for each shaped charge was constant (16.00 ± 0.01 g). The explosive plus liner were press-molded into a steel case at ambient temperature under a pressure of 215 MPa. For each explosive, five shaped charges were prepared. The densities for TKX-55, RDX, and RDX + 1.5% PTFE charges which were obtained were equal to: 1.43, 1.46, and 1.51 g·cm^{-3}, respectively. An example of the shaped charge which was used for assessing the jet penetration capability and a schematic drawing are shown in Figure 3.
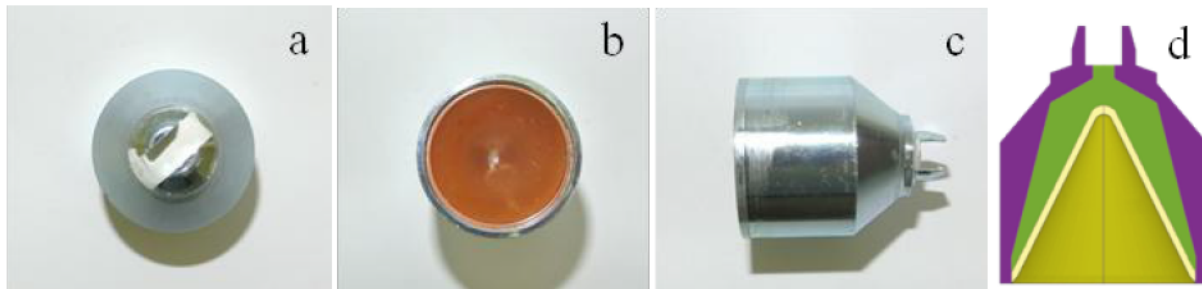
Figure 3. Views of a shape charge filled with 16.00 g of TKX-55 (a-c), and a schematic drawing of the shaped charges which were used in this work (d).

The shaped charges which were under investigation, were placed at a standoff distance equal to 1.5 caliber of the liner, above a stack of steel plates (steel grade St3, thickness 10.00 ± 0.01 mm). The shaped charges were connected using an RDX detonating cord in a lead case with a commercially available detonator (NITROERG – ERGODET 0.2 A). The test arrangement for the firing of the shaped charges is shown in Figure 4.

Figure 4. The test arrangement for firing the shaped charge: view of the shaped charge filled with TKX-55 placed at the standoff distance on the stack of witness plates (left) and the complete arrangement for the test (right).

After the shaped charges had been fired, the depth of penetration (h), inlet diameter (φ_i) and volume of the crater (V) were determined (Table 1). The results of the action of the shaped charge filled with TKX-55 as a base charge is shown in Figure 5.
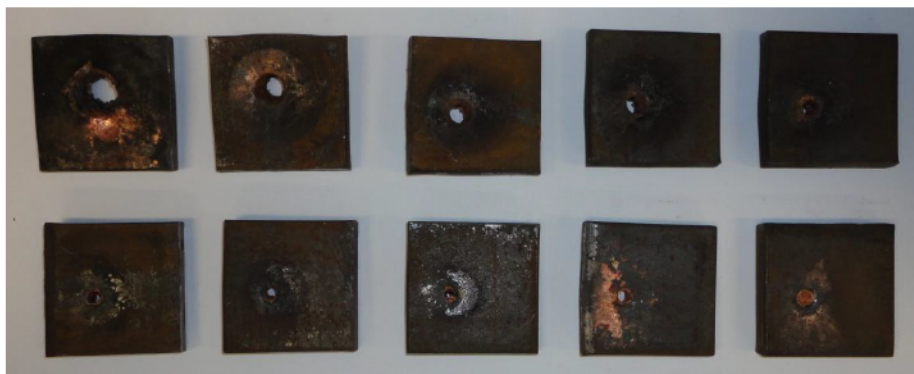
Figure 5. Steel witness plates after firing of the shaped charge filled with TKX-55.

Table 1. Values of h, φ_i, and V obtained for the investigated shaped charges.

Explosive	h [mm]	φ_i [mm]	V [mm^3]
RDX	127.3 (1.9)	14.1 (2.4)	5800 (2.9)
RDX + 1.5% PTFE	124.1 (2.2)	11.3 (2.6)	5500 (3.3)
TKX-55	91.2 (1.8)	13.4 (2.7)	3200 (3.0)

Coefficient of variation (C_V, %) is given in parentheses.

The largest values for the depth of penetration, inlet diameter and volume of the crater were obtained when RDX was used. The introduction of 1.5% PTFE resulted in a decrease in h, φ_i, and V in comparison to RDX (97.49, 80.14, and 94.83% of RDX values respectively). TKX-55 gave smaller h, φ_i, and V values than RDX (71.64, 95.04, and 55.17% of RDX values respectively).

6.3 The Initiating Capability of Detonators

In order to determine the initiating capability of detonators containing TKX-55 and PYX as a base charge, the underwater explosion test was used.[39-45] The investigated explosives (0.2, 0.5 and 0.7 g) were pressed into aluminum shells under a pressure of 4.40 MPa. Each of the tests using the explosive samples were carried out five times. For the 0.5 and 0.7 g base charge masses, two identical loading operations were undertaken (2×0.25 g and 2×0.35 g, respectively). The priming charge (lead azide, 300 mg) was compressed at 4.40 MPa into an inner cup, and placed onto the base charge by applying a pressure of 4.40 MPa. Afterwards, an electric fuse-head with a sealing plug and leading wires was fixed to the loaded detonator shell and an inner cup filled with lead azide. In order to carry out the underwater explosion tests, a water tank was constructed from energy-absorbing and non-reflecting material, with a positioning system for the sensor and detonator (Figure 6).

Figure 6. The arrangement for the underwater explosion tests (left) and the positioning system with the sensor and detonator (right).

A voltage mode tourmaline pressure sensor (PCB Piezotronics, Inc, model 138A05) and oscilloscope (Agilent, model 54622A) were used to collect the data. The testing conditions during measurements were constant and as follows: water temperature 11 °C, atmospheric pressure 982 hPa. The overpressures which were generated in the water were recorded by a piezoelectric transducer. Subsequently, the collected data ($I = f(t)$), by using the characteristics of the pressure sensor, was transferred into $P = f(t)$ relationship. The characteristics of the primary shock wave generated in water were used to determine the maximum of the overpressure (P_{max}), and the time at which the sensor output had decreased to $P_{\theta} = P_{max} \cdot e^{-1}$ (θ), and to calculate the primary shock-wave energy (E_{SW}) and the shock energy equivalent (E_S) (Figure 7, Tables 2 and 3).
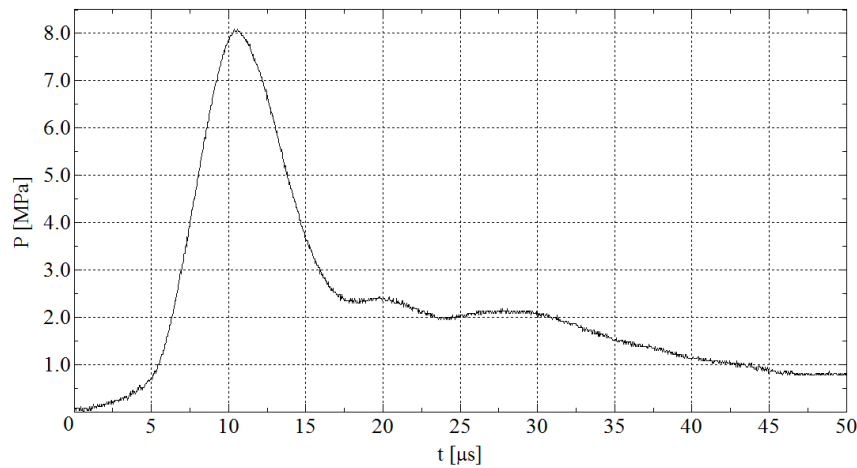
Figure 7. The primary shock wave generated in water by firing a detonator filled with 0.7 g TKX-55 as the base charge.

Using the data which was obtained, the time interval between the shock-wave pressure peak and the first collapse of the gas bubble (t_b) was determined, and the bubble gas energy (E_{BW}), and bubble energy equivalent (E_B) were calculated (Figure 8, Tables 2 and 3).
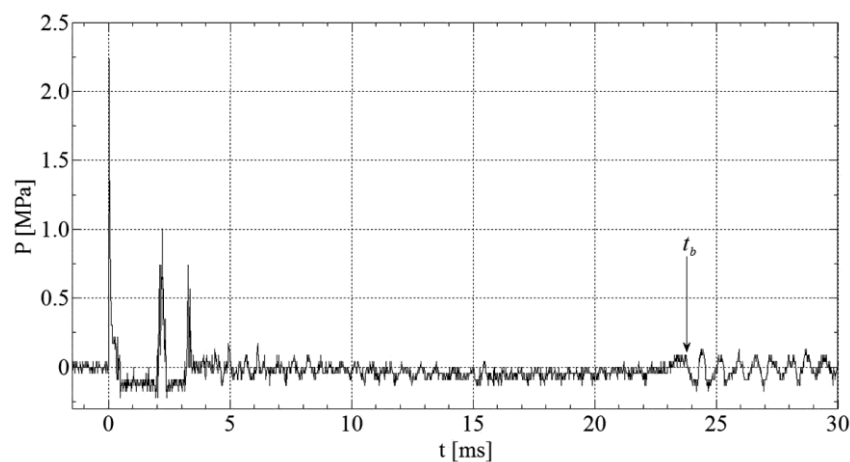
Figure 8. Overpressure generated in water by firing a detonator containing 0.7 g TKX-55 as the base charge.

Table 2. Values of the experimental shock wave parameters P_{max}, P_Θ, Θ and t_b for PYX and TKX-55.

Explosive	m [g]	ρ [g·cm^{-3}]	P_{max} [MPa]	P_Θ [MPa]	Θ [μs]	t_b [ms]
PYX	0.20 (0.28)	1.05 (0.34)	5.45 (3.54)	2.01	16.52 (2.70)	16.35 (0.83)
	0.50 (0.57)	1.40 (0.63)	7.41 (0.74)	2.73	16.46 (0.77)	22.07 (0.45)
	0.70 (0.18)	1.42 (0.57)	8.41 (1.37)	3.09	16.16 (3.31)	23.88 (0.49)
TKX-55	0.20 (0.36)	1.25 (0.40)	5.38 (0.73)	1.98	13.79 (1.76)	18.21 (0.28)
	0.50 (0.33)	1.18 (0.39)	7.09 (0.97)	2.61	15.14 (1.95)	22.10 (0.69)
	0.70 (0.17)	1.17 (0.39)	8.25 (0.76)	3.04	16.34 (1.37)	24.09 (0.48)

Coefficient of variation (C_V, %) is given in parentheses.

Table 3. Values of the calculated shock wave parameters E_S, E_{SW}, E_B, E_{BW}, and E for PYX and TKX-55.

Explosive	m [g]	$E_S \cdot 10^8$ [Pa^2·s]	E_{SW} [J]	$E_B \cdot 10^{-6}$ [s^3]	E_{BW} [J]	E [J]
PYX	*0.20*	1.46	198.27	4.37	339.85	538.12
	0.50	2.84	385.68	10.75	835.88	1221.56
	0.70	3.67	498.39	13.62	1058.87	1557.26
TKX-55	*0.20*	1.45	196.91	6.04	469.54	666.45
	0.50	2.60	353.08	10.79	839.30	1192.38
	0.70	3.46	469.87	13.98	1087.05	1556.92

The total energy (E) generated in water by PYX and TKX-55 (0.2, 0.5, 0.7 g) is summarized as a graph in Figure 9.
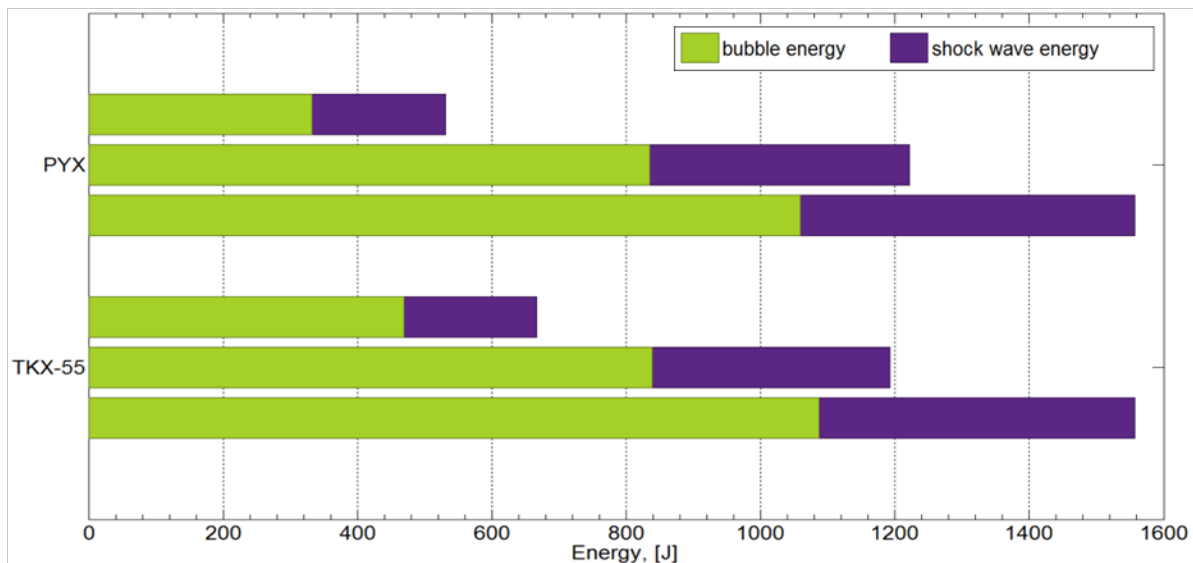
Figure 9. Total energies (E) generated in water by PYX and TKX-55 (0.2, 0.5, 0.7 g).

The densities obtained during the experiments were lower than the maximum determined densities. These differences in the densities are due to the methodology which was used, which is described in the European Standard,[41] *i.e.* the same pressing pressure (4.40 MPa) for the investigated explosives. The lowest density for PYX was obtained for base charges of 0.2 g. In the case of TKX-55 the opposite was observed. This has a direct impact on the experimental shock wave parameters (P_{max}, P_Θ, Θ, t_b), as well as the values for E_S, E_{SW}, E_B, E_{BW}, E, which were calculated using the experimental shock wave parameters. Nevertheless, the value of the pressing pressure was kept constant for comparative reasons. Additionally, the underwater test results were supported by the calculated detonation parameters at the recorded densities. The values of the peak overpressure of TKX-55 were slightly lower than those registered for PYX. The time required for the decrease in the overpressure to $P_{max} \cdot e^{-1}$ are comparable for TKX-55 and PYX. These two factors confirm that the primary shock waves (and thus brisance) generated by TKX-55 and PYX are similar. Moreover, the first bubble collapse registered for TKX-55 and PYX are also comparable. This indicates similar action (heaving power) for TKX-55 and PYX at larger distances from the point of initiation. Finally, the calculated total energies, as the sum of the primary shock wave energy and the bubble gas energy of TKX-55 (for 0.5 and 0.7 g base charges), are similar to those obtained for PYX, while for the 0.2 g base charges, TKX-55 generates a larger amount of bubble energy and therefore the total energy released by TKX-55 is higher than that of the total energy of PYX.

6.4   Detonation Parameters

The gas-phase absolute molar enthalpies at 298 K and 1 atm were calculated theoretically using the modified complete basis set method (CBS-4M; M referring to the use of minimal population localization) with the GAUSSIAN 09 software.[46-48] Gas-phase standard molar enthalpies of formation ($\Delta_f H_{(g)}°$) at 298 K were computed using the atomization energy method.[49-52] Standard molar enthalpies of formation ($\Delta_f H°$) were calculated using $\Delta_f H_{(g)}°$ and the standard molar enthalpies of sublimation by applying Trouton's rule.[53-54] The Chapman-Jouguet (C-J) characteristics, (*i.e.* detonation temperature, T_{C-J}; detonation pressure, p_{C-J}; detonation velocity V_{C-J}) based on the calculated standard molar enthalpy of formation values (PYX: 43.7, HNS: 78.2, TKX-55: 197.6 kJ·mol^{-1}) and the densities were performed with the CHEETAH (version 2.0) thermochemical code.[32, 55] The calculations for the explosives assume ideal behaviour. The Becker-Kistiakowsky-Wilson equation of state (BKW EOS) for gaseous detonation products with the BKWC product library and the BKWC

set of parameters ($\alpha = 0.49912$, $\beta = 0.40266$, $\kappa = 10.864$, $\Theta = 5441.8$) were used in the calculations. The total detonation energy (E_0) as the sum of the mechanical and thermal energies was calculated assuming frozen expansion of the detonation products at 2145 K (Table 4).

Table 4. Calculated values of T_{C-J}, p_{C-J}, V_{C-J} and E_0 for PYX, HNS and TKX-55.

	ρ [g·cm^{-3}]	$\rho \cdot \rho_{TMD}^{-1}$ ·100[%]	T_{C-J}[a] [K]	p_{C-J}[b] [GPa]	V_{C-J}[c] [m·s^{-1}]	$-E_0$[d] [kJ·cm^{-3}]
PYX	1.757	100.00	3974	24.44	7462	8.215
	1.42	80.82	3970	15.04	6463	6.075
	1.40	79.68	3965	14.59	6404	5.956
	1.05	59.76	3829	8.13	5385	4.032
HNS	1.74	100.00	4048	23.24	7227	8.406
TKX-55	1.837	100.00	4059	27.02	7630	8.684
	1.25	68.05	4004	11.45	5948	5.049
	1.18	64.24	3972	10.17	5747	4.673
	1.17	63.69	3967	10.00	5718	4.620

[a] Detonation temperature; [b] detonation pressure; [c] detonation velocity; [d] detonation energy.

The calculated detonation parameters (for the maximum density of the explosive charges) using the CHEETAH (version 2.0) code, differed from those obtained using EXPLO5 (version 6.01). The largest differences were found for the detonation temperature, with the CHEETAH values being much higher than those obtained using EXPLO5. Nevertheless, the calculated values have the same tendency.[32] TKX-55 was calculated as showing a higher detonation temperature, detonation pressure, detonation velocity, and detonation energy than PYX or HNS.

6.5 Synthesis

TKX-55 and PYX were synthesized according to the methods given in the literature.[27, 28, 32] Industrially produced explosives were supplied by Chemical Works "NITRO-CHEM" S.A.

TKX-55

Bis(2,4,6-trinitrobenzoyl)oxalohydrazide:[32] Oxalyldihydrazide (5 mmol, 0.59 g) was added in one portion to a solution of 2,4,6-trinitrobenzoyl chloride (10 mmol, 2.76 g) in tetrahydrofuran (THF, 25 mL). The mixture was stirred for 72 h at ambient temperature. The precipitate was filtered off and washed with THF, acetone, and diethyl ether (yield 2.48 g, 83%). **^{1}H NMR** (400.18 MHz, DMSO-d_6, ppm) δ: 11.47 (s, 2H, NH), 11.42 (s, 2H, NH); 9.13 (s, 4H, CH); **^{13}C{^{1}H} NMR** (100.0 MHz, DMSO-d_6, ppm) δ: 158.0, 157.5, 147.92, 147.91, 129.2, 124.1; **EA** ($C_{16}H_8N_{10}O_{16}$, 596.29) calc.: C 32.23, H 1.35, N 23.49 %; found: C 32.22, H 1.61, N 22.87 %.

5,5'-Bis(2,4,6-trinitrophenyl)-2,2'-bi(1,3,4-oxadiazole), TKX-55:[32] Bis(2,4,6-trinitrobenzo-yl)oxalohydrazide (1 mmol, 0.60 g) was added to fuming sulfuric acid (20%, 10 mL). The mixture was stirred for 24 hours at ambient temperature before being poured onto crushed ice. The precipitate which formed was filtered off and washed with water until it was acid free, and was subsequently dried (yield 0.52 g, 93%). **^{1}H NMR** (400.18 MHz, DMSO-d_6, ppm) δ: 9.40 (s, 4H, CH); **^{13}C{^{1}H} NMR** (100.0 MHz, DMSO-d_6, 25 °C, ppm) δ: 158.1, 154.0, 150.3, 149.4, 125.3, 116.8; **EA** ($C_{16}H_4N_{10}O_{14}$, 560.26) calc.: C 34.30, H 0.72, N 25.00 %; found: C 34.33, H 1.01, N 25.01 %.

PYX

2,6-Bis(picrylamino)pyridine (Pre-PYX):[28] Magnesium hydroxide (1.05 g, 18 mmol) and 2,6-diaminopyridine (0.98 g, 9 mmol) were added to a solution of picryl chloride (4.95 g, 20 mmol) in *p*-xylene (40 mL). The reaction mixture was heated at 140 °C for 3 h and then allowed to cool to room temperature. Toluene (30 mL) was then added and the product was collected by filtration, washed with methanol, 10% HCl and with water until it was acid free. Yield: 62%, 2.97 g. **^{1}H NMR** (400.18 MHz, DMSO-d_6, ppm) δ: 10.37 (s, 2H, NH), 8.77 (s, 4H, CH), 7.75 (t, 1H, J = 8.02 Hz, CH), 7.75 (d, 2H, J = 8.02 Hz, CH); **^{13}C{^{1}H} NMR** (100.0 MHz, DMSO-d_6, ppm) δ: 154.7, 143.1, 139.4, 139.1, 136.7, 125.7, 99.2; **EA** ($C_{17}H_9N_9O_{12}$, 531.31) calc.: C 38.43, H 1.71, N 23.73 (%); found: C 38.29, H 1.88, N 23.57 (%).

2,6-Bis(picrylamino)-3,5-dinitropyridine (PYX):[27] 2,6-Bis(picrylamino)pyridine (1.06 g, 2 mmol) was carefully added to fuming nitric stirred acid (11 mL) at −20 °C. The resulting solution was allowed to warm to room temperature, stirred for 2 h, then heated under reflux for 5 h before being cooled and diluted with 65% nitric acid (21 mL) at 0 °C. The precipitated product was filtered off, washed with 70% nitric acid (3 mL), water until HNO_3 free, and finally with methanol (21 mL). The product which was obtained was dried at 150 °C. Yield: 67%, 0.83 g. **^{1}H NMR** (400.18 MHz, DMSO-d_6, ppm) δ: 11.25 (s, 2H, NH), 9.19 (s, 1H, CH), 8.90 (s, 4H, CH); **^{13}C{^{1}H} NMR** (100.0 MHz, DMSO-d_6, ppm) δ: 161.2, 144.4, 142.3, 137.7, 131.2, 125.1, 124.0; **EA** ($C_{17}H_7N_{11}O_{16}$, 621.30): calc.: C 32.86, H 1.14, N 24.80 %; found: C 32.68, H 1.38, N 24.29 %.

6.6 Conclusions

TKX-55 shows excellent properties (V_{C-J}, p_{C-J}, E_0, *FS*, *IS*, *ESD* and temperature of decomposition) and an easy and straightforward method of synthesis, which makes

TKX-55 remarkable in comparison to HNS and PYX. The jet penetration capability of TKX-55 is much lower than that of RDX, however, RDX would be inadequate as an explosive which must be stable at very high temperatures since it decomposes at temperatures as low as 210 °C. For a better comparison of the jet penetration capability, shaped charges containing PYX and HNS as the base charge should be performed. The primary shock waves (and thus brisance) generated by TKX-55 and PYX are similar. The first bubble collapse obtained for TKX-55 and PYX are also comparable. This indicates a similar action (heaving power) of TKX-55 and PYX at larger distances from the point of initiation.

6.7   References

[1]   T. Urbański, *Chemistry and Technology of Explosives*, Volume 4, Pergamon Press, **1984**; ISBN 0-08-026206-6.

[2]   M. E. Sitzmann, *J. Energ. Mater.* **1988**, *6*, 129−144.

[3]   J. P. Agrawal, Mehilal, U. S. Prasad, R. N. Surve, *New J. Chem.* **2000**, *24*, 583−585.

[4]   H. S. Jadhav, M. B.Talawar, R. Sivabalan, D. D. Dhavale, S. N. Asthana, V. N. Krishnamurthy, *Indian J. Heterocycl. Chem.* **2006**, *15*, 383−386.

[5]   H. Gao, J. M. Shreeve, *Chem. Rev.* **2011**, *111*, 7377−7436.

[6]   J. P. Agrawal, *Cent. Eur. J. Energ. Mater.* **2012**, *9*, 273−290.

[7]   J. P. Agrawal, *High Energy Materials: Propellants, Explosives and Pyrotechnics*, Wiley, Weinheim, **2015**, ISBN 978-3-527-80268-5.

[8]   T. M. Klapötke, *Chemistry of High-energy Materials*, 3rd edn., De Gruyter, Berlin, **2015**, ISBN 978-3-11-043932-8.

[9]   B. Zygmunt, Z. Wilk, *Propellants, Explos., Pyrotech.* **2008**, *33*, 482−487.

[10] N. L. Coleburn, B. E. Drimmer, *The Explosive Properties of the Amino-substituted, Symmetrical Trinitrobenezenes*, Defense Technical Information Center, United States Naval Ordnance Laboratory, White Oak, Silver Spring, Maryland, USA, **1963**.

[11] H. H. Cady, A. C. Larson, *Acta Crystallogr.* **1965**, *18*, 485−496.

[12] S. M. Kaye, H. L. Herman, *Encyclopedia of Explosives and Related Items*, U.S. Army Armament Research and Development Command, Large Caliber Weapon Systems Laboratory, **1978**.

[13] C. L. Jackson, J. F. Wing, *Am. Chem. J.* **1888**, *10*, 283−294.

[14] I. Akst, Heat of Detonation, the Cylinder Test, and Performance in Munitions, *9th Symposium (Int.) on Detonation*, Portland, Oregon, USA, August 28 – September 1, **1989**.

[15] B. M. Dobratz, *The Insensitive High Explosive Triaminotrinitrobenzene (TATB): Development and Characterization – 1888-1994*, Report LA-13014-H, UC-741, **1995**.

[16] D. Skinner, D. Olson, A. Block-Bolten, *Propellants, Explos., Pyrotech.* **1998**, *23*, 34−42.

[17] R. Meyer, J. Köhler, A. Homburg, *Explosives*, 6th edn., Wiley, Weinheim, **2007**, ISBN 978-3-527-31656-4.

[18] K. G. Shipp, *J. Org. Chem.* **1964**, *29*, 2620−2623.

[19] J. A. Crutchmer, *HNS Critical Diameter Feasibility Study*, MHSMP-78-53, **1978**.

[20] F. Gerard, A. Hardy, *Acta Crystallogr., Sect. A: Found. Adv.* **1987**, *43*, C167.

[21] F. Gerard, A. Hardy, *Acta Crystallogr., Sect. C: Struct. Chem.* **1988**, *44*, 1283−1287.

[22] M. A. Hiskey, D. E. Chavez, D. L. Naud, *Insensitive High-nitrogen Compounds*, LA-UR-01-1493, **2001**.

[23] J.-S. Lee, C.-K. Hsu, C.-L. Chang, *Thermochim. Acta* **2002**, *392−393*, 173−176.

[24] B. Singh, R. K. Malhotra, *Def. Sci. J.* **2014**, *33*, 165−176.

[25] M. D. Coburn, J. L. Singleton, *J. Heterocycl. Chem.* **1972**, *9*, 1039−1044.

[26] M. D. Coburn, *2,6-Bis(picrylamino)-3,5-dinitropyridine and a Method for Its Preparation*, Pat. US 3678061, **1972**.

[27] R. Kuboszek, W. Pawłowski, *A method for preparation of 2,6-bis(picrylamino)-3,5-dinitropyridine*, Pat. PL 186580, **1997**.

[28] W. Pawłowski, R. Kuboszek, *Chemical Industry* **2002**, *81*, 237−240.

[29] R. S. Riggs, *1,3,5-Trinitro-2,4,6-tripicrylbenzene*, Pat. US 4861924, **1989**.

[30] M. E. Sitzmann, *Method for Making Nonanitroterphenyl*, Pat. US 6476280, **2002**.

[31] P. F. Pagoria, M. X. Zhang, Synthesis of Pyrazines Including 2,6-Diaminopyrazine-1-oxide (DAPO) and 2,6-Diamino-3,5-dinitropyrazine-1-oxide (LLM-105), *Pat. WO 2010123806*, **2010**.

[32] T. M. Klapötke, T. G. Witkowski, *ChemPlusChem* **2016**, *81*, 357–360.

[33] M. Sućeska, *EXPLO5, Version 6.01*, Zagreb, Croatia, **2013**.

[34] PN-C-86045:1997, *Explosives - Charges Directional for Jet Perforating*, **1997**.

[35] Z. Wilk, B. Zygmunt, W. Skóra, Z. Kupidura, M. Kroczek, T. Kuśnierz, *Liner for the Conical Shaped Charges*, Pat. PL 182314, **1996**.

[36] K. Jach, R. Świerczyński, Z. Wilk, *J. Tech. Phys. (Warsaw, Pol.)* **2004**, *45*, 31–54.

[37] B. Zygmunt, Z. Wilk, *Arch. Min. Sci.* **2007**, *52*, 121–133.

[38] Z. Wilk, B. Zygmunt, Research of High Energy Explosives with Fluoropolymer Binders, *4ᵗʰ New Trends in Research of Energetic Materials*, Pardubice, Czech Republic, **2001**.

[39] G. Bjarnholt, R. Holmberg, Explosive Expansion Works in Underwater Detonations, *6ᵗʰ Symposium (Int.) on Detonation*, Coronado, California, USA, August 24 - 27, **1976**.

[40] M. H. Lefebvre, Determination of the Power Output of Detonators, *6ᵗʰ New Trends in Research of Energetic Materials*, Pardubice, Czech Republic, **2003**.

[41] EN 13763-15: 2004 *Explosives for Civil Uses - Detonators and Relays - Part 15: Determination of Equivalent Initiating Capability*.

[42] J. Paszula, A. Maranda, T. Szydłowska, *Cent. Eur. J. Energ. Mater.* **2006**, *3*, 73–82.

[43] P. Koślik, J. Staś, Z. Wilk, A. Zakrzewski, *Cent. Eur. J. Energ. Mater.* **2007**, *4*, 3–13.

[44] S. Cudziło, W. A. Trzciński, J. Paszula, M. Nita, *Cent. Eur. J. Energ. Mater.* **2014**, *11*, 539–552.

[45] T. M. Klapötke, T. G. Witkowski, Z. Wilk, J. Hadzik, *Propellants, Explos., Pyrotech.* **2016**, *41*, 92–97.

[46] J. W. Ochterski, G. A. Petersson, J. A. Montgomery, *J. Chem. Phys.* **1996**, *104*, 2598–2619.

[47] J. A. Montgomery, M. J. Frisch, J. W. Ochterski, G. A. Petersson, *J. Chem. Phys.* **2000**, *112*, 6532–6542.

[48] *Gaussian 09, Revision C.01*, M. J. Frisch, G. W. Trucks, H. B. Schlegel, G. E. Scuseria, M. A. Robb, J. R. Cheeseman, G. Scalmani, V. Barone, B. Mennucci, G. A. Petersson, H. Nakatsuji, M. Caricato, X. Li, H. P. Hratchian, A. F. Izmaylov, J. Bloino, G. Zheng, J. L. Sonnenberg, M. Hada, M. Ehara, K. Toyota, R. Fukuda, J. Hasegawa, M. Ishida, T. Nakajima, Y. Honda, O. Kitao, H. Nakai, T. Vreven, J. A. Montgomery, Jr., J. E. Peralta, F. Ogliaro, M. Bearpark, J. J. Heyd, E. Brothers, K. N. Kudin, V. N. Staroverov, R. Kobayashi, J. Normand, K. Raghavachari, A. Rendell, J. C. Burant, S. S. Iyengar, J. Tomasi, M. Cossi, N. Rega, J. M. Millam, M. Klene, J. E. Knox, J. B. Cross, V. Bakken, C. Adamo, J. Jaramillo, R. Gomperts, R. E. Stratmann, O. Yazyev, A. J. Austin, R. Cammi, C. Pomelli, J. W. Ochterski, R. L. Martin, K. Morokuma, V. G. Zakrzewski, G. A. Voth, P. Salvador, J. J. Dannenberg, S. Dapprich, A. D. Daniels, Ö. Farkas, J. B. Foresman, J. V. Ortiz, J. Cioslowski, and D. J. Fox, Gaussian, Inc., Wallingford CT, **2009**.

[49] L. A. Curtiss, K. Raghavachari, P. C. Redfern, J. A. Pople, *J. Chem. Phys.* **1997**, *106*, 1063–1079.

[50] B. M. Rice, S. V. Pai, J. Hare, *Combust. Flame* **1999**, *118*, 445–458.

[51] E. F. C. Byrd, B. M. Rice, *J. Phys. Chem. A* **2006**, *110*, 1005–1013.

[52] P. J. Linstrom, W. G. Mallard, *NIST Standard Reference Database Number 69*, National Institute of Standards and Technology, Gaithersburg MD, 20899.

[53] F. Trouton, *Philos. Mag. (1876-1900)* **1884**, *18*, 54–57.

[54] M. S. Westwell, M. S. Searle, D. J. Wales, D. H. Williams, *J. Am. Chem. Soc.* **1995**, *117*, 5013–5015.

[55] *CHEETAH 2.0*, Energetic Materials Center, Lawrence Livermore National Laboratory, USA, **1998**.

Synthesis and Investigation of Advanced Energetic Materials

Based on Bispyrazolylmethanes
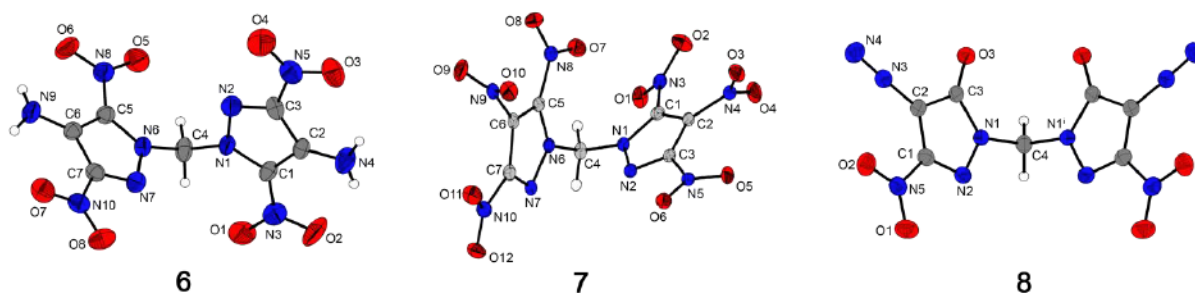
Abstract: Herein we present the preparation and characterization of three new bispyrazolyl-based energetic compounds with great potential as explosive materials. The reaction of sodium 4-amino-3,5-dinitropyrazolate (**5**) with dimethyl iodide yielded bis(4-amino-3,5-dinitropyrazolyl)methane (**6**), which is a secondary explosive with high heat resistance ($T_{dec} = 310\ °C$). The oxidation of this compound afforded bis(3,4,5-trinitro-pyrazolyl)methane (**7**), which is a combined nitrogen- and oxygen-rich secondary explosive with very high theoretical and experimental detonation performance ($V_{C\text{-}J} = 9304\ \mathrm{m \cdot s^{-1}}$ *versus* $V_{LASEM} = 9910 \pm 310\ \mathrm{m \cdot s^{-1}}$) in the range of that of CL-20. Also, the thermal stability ($T_{dec} = 205\ °C$) and sensitivities of **7** are auspicious. The reaction of **6** with *in situ* generated nitrous acid yielded the primary explosive bis(4-diazo-5-nitro-3-oxopyrazolyl)methane (**8**), which showed superior properties to those of currently used diazodinitrophenol (DDNP).

7.1 Introduction

"Safer, greener, stronger …" are the main keywords in the development of new explosives for civil but also military purposes. The new materials must meet many different requirements, for example, high performance, insensitivity toward accidental stimuli, stability, vulnerability, low solubility in water, hydrolytic stability, longevity, compatibility, and environmental safety.[1] On the basis of their sensitivities or the time of their deflagration-to-detonation transition, explosives can be classified as secondary and primary explosives. Both groups are divided into subgroups depending on their application. For example, the mining and fracking industry uses heat-resistant explosives, such as hexanitrostilbene (Scheme 1), for deeper drill holes. In contrast, the military is undertaking research toward the development of more powerful and effective explosives (such as CL-20, Scheme 1) for use in future unmanned-vehicle missions. DDNP (Scheme 1) is an example of a more sensitive energetic material and is used in lead-free priming compositions. It is used as an initiating explosive that is more powerful than mercury fulminate and slightly less explosive than lead azide.[2] Nevertheless, DDNP is characterized by a relatively low decomposition temperature.[2]
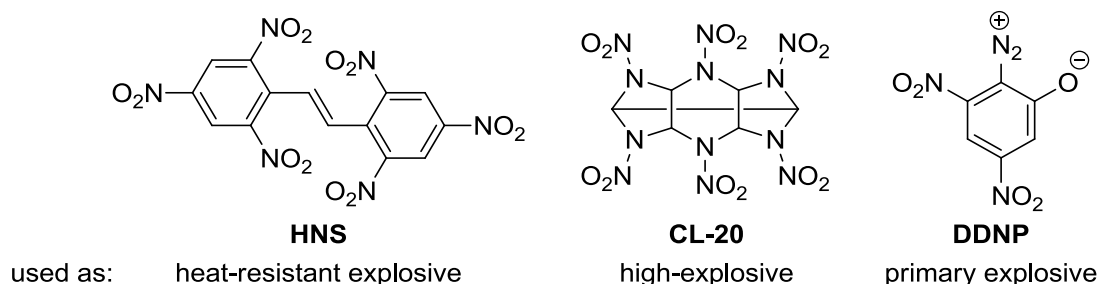
Figure 1. Examples of prominent explosives belonging to different classes: heat-resistant explosives (hexanitrostilbene, HNS), high explosives (hexanitrohexaazaisowurtzitane, CL-20), and primary explosives (DDNP, diazadinitrophenole).

In the current study, three different explosives, **6–8**, belonging to the above-mentioned classes were found to show very promising performance and sensitivity characteristics. They are all based on methylene-bridged pyrazoles. Nitropyrazoles have been described as powerful energetic materials.[3] Furthermore, ethylene-bridged pyrazoles, the synthesis of which is more trivial, have been described; however, they have been shown to have weaker performance values.[3b]

7.2 Results and Discussion

The present synthetic protocol has been optimized partly on the basis of previous studies. Pyrazole (**1**) was chlorinated to give 4-chloropyrazole (**2**) with chlorine generated *in situ*

(NaClO/HCl; Scheme 2).[4] The nitration of **2** was carried out by the use of a H_2SO_4/HNO_3(100%) mixture.[5] The third step involved the reaction of 4-chloro-3,5-di-nitropyrazole (**3**) with ammonia to give 4-amino-3,5-dinitropyrazole (**4**),[5] followed by reaction with sodium hydroxide to yield sodium 4-amino-3,5-dinitropyrazolide (**5**) as a monohydrate salt.[6] The sodium salt **5** was treated with diiodomethane to give bis(4-amino-3,5-dinitropyrazolyl)methane (**6**),[6] which could be oxidized to bis(3,4,5-trinitropyrazolyl)methane (**7**) by stirring in a H_2O_2(50%)/H_2SO_4 mixture. The final step to provide bis(4-diazo-5-nitro-3-oxopyrazolyl)methane (**8**) was carried out by diazotation and the generation of HNO_2 ($NaNO_2 + H_2SO_4$) at 0 °C.
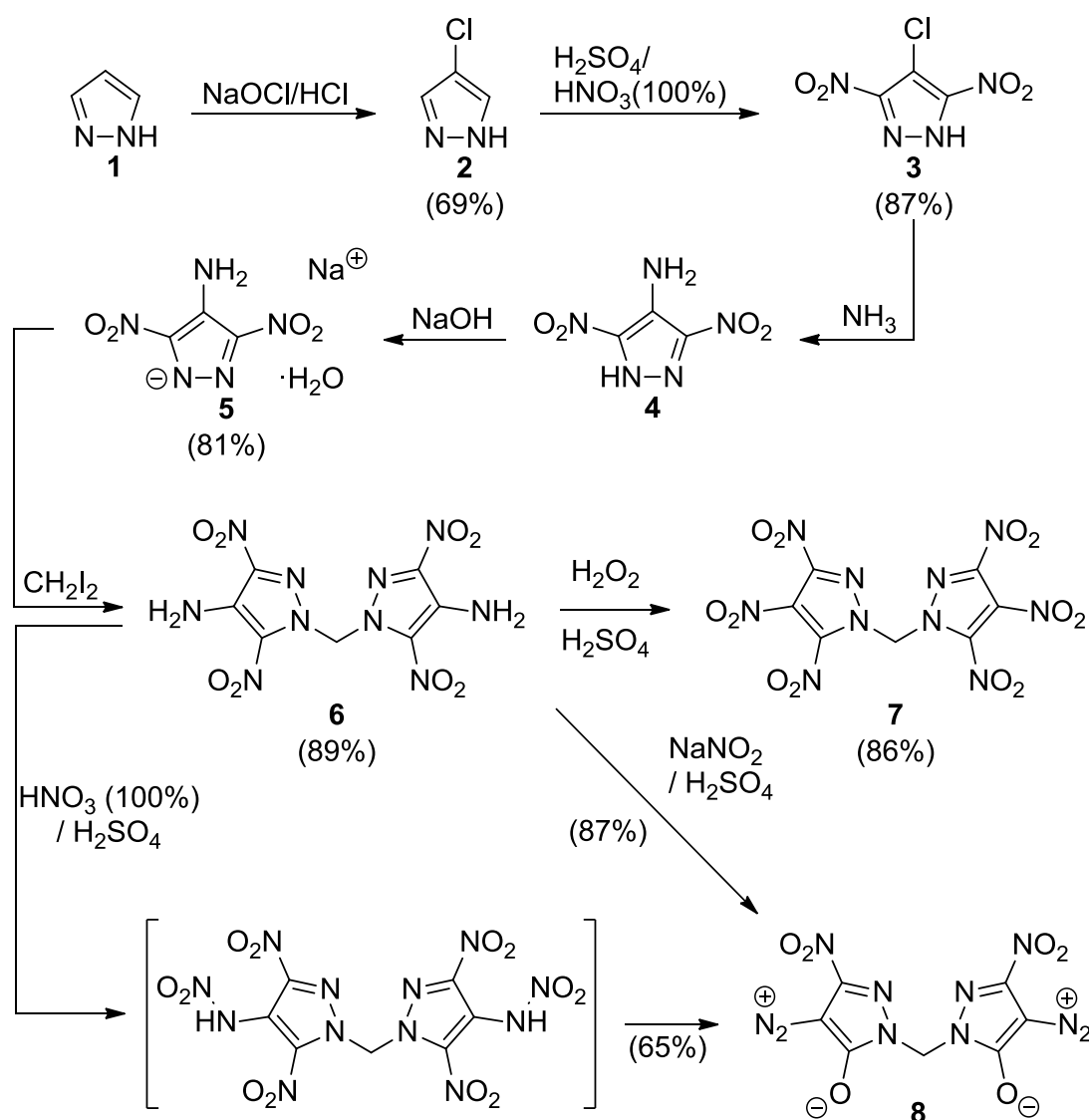
Scheme 1. Synthesis of bis(4-amino-3,5-dinitropyrazolyl)methane (**6**), bis(3,4,5-trinitropyrazolyl)methane (**7**), and bis(4-diazo-5-nitro-3-oxopyrazolyl)methane (**8**).

The solid-state structures of compounds **3** and **5**–**8** were determined by XRD. All compounds crystallize in common space groups (**3**: $P2_1/c$; **5**: P-1; **6**: *Pbca*, **7**: $P2_1/n$; **8**: *Pnma*). Especially

for **6** (1.836 g·cm^{-3} at 173 K) and **7** (1.970 g·cm^{-3} at 173 K), high densities were observed, as desired for secondary explosives. The molecular moieties are shown in Figure 2. Further details can be found in the Supporting Information. In the case of **5** and **6**, the 3,5-di-nitro-4-aminopyrazole moiety was observed to be nearly planar owing to the intramolecular hydrogen bonds, which are also found in TATB (1,3,5-triamino-2,4,6-trinitrobenzene) and FOX-7 (1,1-diamino-2,2-dinitroethylene).[1b] The diazonium N4−N3 bond length of 1.112(2) Å is nearly equal to those found in various diazonium inner salts[7] and cations,[8] thus proving the same a triple character of the N4−N3 bond ($d_{N\equiv N} = 1.10$ Å).[9] The bond between the C2 and N3 atoms has a length of 1.320(2) Å, which is between the expected lengths of first- and second-order bonds between carbon and nitrogen atoms ($d_{C-N} = 1.47$ Å; $d_{C=N} = 1.28$ Å).[10] The C3−O3 bond length of 1.215(2) Å is virtually equal to the expected value for doubly bonded (keto) oxygen atoms ($d_{C=O} = 1.20$ Å[9]) and is in agreement with previously reported data for this functionality.[7b, 7d]
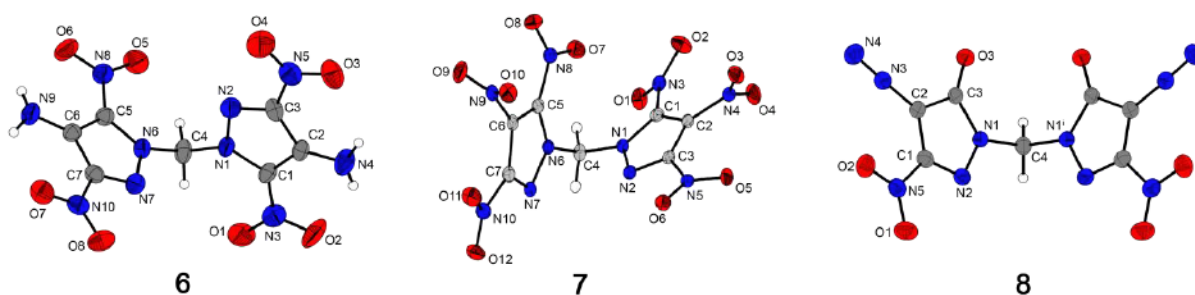
Figure 2. Molecular structures of **6–8** in the crystals with atom labels. Thermal ellipsoids represent the 50% probability level.

Compounds **6–8** are valuable energetic materials with moderate sensitivities toward impact, friction, and electrostatic discharge. The measured sensitivity values (according to the German Bundesanstalt für Materialforschung und -prüfung (BAM)) are gathered in Table 1. The impact sensitivities (**6**: 11, **7**: 4 J) are in the range of those of HNS and pentaerythritol tetranitrate (PETN). Compound **8** is more sensitive (1.5 J) and should therefore be classified as a primary explosive. Positive enthalpies of formation were calculated for **6–8** (**6**: 205, **7**: 379, **8**: 497 kJ·mol^{-1}; see the Supporting Information for details of the computations). With these values, several detonation parameters (Table 1) were calculated by using the EXPLO5 computer code.

The thermal stability of **6–8** at a heating rate of 5 °C·min^{-1} was investigated, and excellent decomposition values were found (**6**: 310, **7**: 205, **8**: 226 (T_m: 194 °C)). The decomposition temperature of **8** is lower than the value determined for 1,2-ethylenebis(4-diazo-nium-3-nitro-1*H*-pyrazol-5-olate)[3b] but still higher than that of DDNP (Table 1).

Table 1. Energetic properties and detonation parameters of **6**–**8** and comparison with state-of-the-art compounds.

	6	HNS	7	RDX	CL-20	8	DDNP
Formula	$C_7H_6N_{10}O_8$	$C_{14}H_6N_6O_{12}$	$C_7H_2N_{10}O_{12}$	$C_3H_6N_6O_6$	$C_6H_6N_{12}O_{12}$	$C_7H_2N_{10}O_6$	$C_6H_2N_4O_5$
IS[a] [J]	11	5[b]	4	7.5	3	1.5	1
FS[c] [N]	>360	> 360[b]	144	120	96	40	5
ESD[d] [J]	>1.5	1.0[b]	0.1	0.2	0.1	0.10	0.012
Ω[e] [%]	−40.20	−67.6	−11.48	−21.6	−11.0	−44.70	−60.92
T_{dec}[f] [°C]	310	320[12]	205	210	195	226 (dec.)	157
ρ[g] [g·cm^{-3}]	1.802	1.745[13]	1.934	1.806[14]	2.035[15]	1.732	1.719[16]
$\Delta_f H°$[h] [kJ·mol^{-1}]	205	78	379	86	365	497	139
EXPLO5 6.01							
$-\Delta_E U°$[i] [kJ·kg^{-1}]	4942	5146	6147	5853	6130	4862	4987
$p_{C\text{-}J}$[j] [GPa]	29.6	24.5	39.1	33.8	44.9	26.0	23.8
$V_{C\text{-}J}$[k] [km·s^{-1}]	8332	7629	9304	8803	9673	8016	7651
Gas vol.[l] [dm^3·kg^{-1}]	719	601	720	891	724	700	633

[a] Impact sensitivity (BAM drop hammer, method 1 of 6); [b] Determined at LMU; [c] Friction sensitivity (BAM friction tester, method 1 of 6); [d] OZM electrostatic discharge device; [e] Oxygen balance ($\Omega = xO − 2C − 1/2H)·1600·M^{-1}$); [f] Decomposition temperature from DSC/DTA (β = 5 °C·min^{-1}); [g] Determined by X-ray diffraction and converted into room-temperature values; [h] Calculated (CBS-4M) heat of formation; [i] Energy of explosion; [j] Detonation pressure; [k] Detonation velocity; [l] Volume of detonation gases assuming only gaseous products.

The very promising detonation velocity of **7** (*e.g.* V_{C-J} = 9304 m·s^{-1}) was corroborated by the estimated detonation velocity determined in a LASEM experimental setup (V_{LASEM} = 9910 ± 310 m·s^{-1}). In LASEM, the laser-induced air shock velocity is measured by schlieren imaging and correlated to the laser-induced shock velocities of conventional energetic materials to estimate the detonation velocity of the tested energetic material (see the Supporting Information for a closer description of this method[11]). The average measured characteristic laser-induced shock velocity for **7** is shown in Table 2 (along with 95% confidence intervals). The LASEM results suggest that **7** has a higher detonation velocity (at the theoretical maximum density; TMD) than CL-20, and the value is almost 600 m·s^{-1} higher than that predicted by EXPLO5 V6.01. However, LASEM is applied as a screening method, and the obtained data are not definitive, but only serve as an indicator of promising performance. Therefore, further testing will be performed to confirm the LASEM results.

Table 2. Measured laser-induced air shock velocity and detonation velocity estimated by LASEM (V_{LASEM}), along with the theoretically predicted detonation velocity (V_{C-J}).

Sample	Laser-induced Shock Velocity [m·s^{-1}]	Estimated V_{LASEM} [km·s^{-1}]	EXPLO5 V6.01 V_{C-J} [km·s^{-1}]	Measured VOD at TMD
7	849.54 ± 12.50	9.91 ± 0.31	9.304	*nd*
RDX	806.83 ± 7.74	8.85 ± 0.19	8.834	8.833[11b]
CL-20	835.41 ± 9.52	9.56 ± 0.24	9.673	9.57[11b]

In summary, we have introduced three new methylene-bridged nitropyrazole derivatives with potential use as explosives for different applications. Bis(4-amino-3,5-dinitropyrazolyl)methane (**6**) is a secondary explosive with a high heat resistance (T_{dec} = 310 °C), enhanced detonation parameters in comparison to those of HNS, and lower sensitivity to external stimuli. The NH2→NO2 oxidation product bis(3,4,5-trinitropyrazolyl)methane (**7**) shows excellent detonation velocity (approximately equal to that of CL-20, the current high-explosive benchmark) according to the theoretical value and the value estimated by the LASEM method, and is described in a recently submitted patent application. The reaction of **6** with nitrous acid generated *in situ* yielded the primary explosive bis(4-diazo-5-nitro-3-oxopyrazolyl)methane (**8**), the higher performance and better thermal stability of which relative to DDNP make this compound a competitive candidate as a green primary explosive. The synthetic approach presented herein resulted in three new compounds which not only fall into different classes of explosives but also show improved or comparable properties to those of corresponding representatives of each group (HNS, CL-20, DDNP). Moreover, all compounds can be synthesized economically.

7.3   Experimental Part

General methods, the preparation of **2–5**, and more experimental data on **6–8** can be found in the Supporting Information.

Bis(4-amino-3,5-dinitropyrazolyl)methane (6): Sodium 3,5-dinitro-4-aminopyrazolate monohydrate (4.29 g, 22 mmol) was suspended in *N,N*-dimethylformamide (15 mL), and diiodomethane (2.68 g, 805 µL, 10 mmol) was added. The mixture was stirred at 90 °C for 16 h and then poured into water (100 mL). A small quantity of sodium thiosulfate solution is added to reduce the precipitated iodine until the suspension was a clean yellow color. The precipitated product was filtered, washed with a little water, and dried in air to give **6** (3.18 g, 89%) as yellow solid. **DSC** (5 °C·min^{-1}, onset): 310 °C (dec.); **^{1}H NMR** (400.18 MHz, DMSO-d_6, ppm) δ: 7.29, 7.16; **^{13}C\{^{1}H\} NMR** (100.0 MHz, DMSO-d_6, ppm) δ: 142.1, 131.7, 130.9, 67.2; **^{15}N NMR** (40.6 MHz, DMSO-d_6, ppm) δ: −23.8 (s, NO_2), −29.3 (s, NO_2), −73.7 (t, J_{NH} = 2.7 Hz, N_{pyr}–CH$_2$), −192.8 (t, J_{NH} = 1.1 Hz, N_{pyr}), −314.1 (t, J_{NH} = 93.7 Hz, NH_2); **EA** ($C_7H_6N_{10}O_8$, 258.19) calc.: C 23.47, H 1.69, N 39.10 %; found: C 23.73, H 1.81, N 38.90 %; **IS**: 11 J (< 100 µm); **FS**: > 360 N (< 100 µm); **ESD** > 1 J (< 100 µm).

Bis(3,4,5-trinitropyrazolyl)methane (7): A solution of **6** (1.00 g, 2.80 mmol) in concentrated H_2SO_4 (5 mL) was added dropwise to a mixture of 50% H_2O_2 (7.5 mL) and H_2SO_4 (25 mL) at 0 °C. The reaction mixture was stirred at 0 °C for 3 h and then overnight at room temperature. Subsequently, the reaction mixture was poured onto ice (100 g). Finally, the resulting precipitate was isolated by filtration, washed with water, and dried in air to give **7** (1.00 g, 86%). **DSC** (5 °C·min^{-1}, onset): 205 °C (dec.); **^{1}H NMR** (400.18 MHz, acetone-d_6, ppm) δ: 7.84; **^{13}C\{^{1}H\} NMR** (100.0 MHz, acetone-d_6, ppm) δ: 144.2, 138.8, 123.8, 67.3; **^{14}N NMR** (28.9 MHz, acetone-d_6, ppm) δ: −29.1 (NO_2), −31.0 (NO_2), −33.5 (NO_2); **EA** ($C_7H_2N_{10}O_{12}$, 418.15) calc.: C 20.11, H 0.48, N 33.50 %; found: C 19.91, H 0.82, N 32.55 %; **IS**: 4 J (< 100 µm); **FS**: 112 N (< 100 µm); **ESD**: 0.6 J (< 100 µm).

Bis(4-diazo-5-nitro-3-oxopyrazolyl)methane (8), method A: **6** (3 mmol, 1.075 g) was dissolved in sulfuric acid (15 mL) and cooled to 0 °C. A solution of sodium nitrite (**9** mmol, 0.621 g) in water (2 mL) was then added dropwise. The reaction mixture was stirred at 0 °C for 2 h and then for 4 h at ambient temperature, and was then poured onto ice. The yellow precipitate was filtered and washed with a small amount of cold water. The water phase was extracted with ethyl acetate (3 × 25 mL), dried over magnesium sulfate, and evaporated under reduced pressure to give **8** (0.84 g, 87%; for method B, please see the Supporting

Information). **DSC** (5 °C·min^{-1}, onset): 194 °C (melt.), 226 °C (dec.); **^{1}H NMR** (400.18 MHz, DMSO-d_6, ppm) δ: 5.88 (s, 2H, CH_2); **^{13}C{^{1}H} NMR** (101.0 MHz, DMSO-d_6, ppm) δ: 161.3 (*C*O$^-$), 145.1 (*C*NO$_2$), 65.6 (*C*N$_2^+$), 53.8 (*C*H$_2$); **^{14}N NMR** (28.9 MHz, DMSO-d_6, ppm) δ: −24.9 (*N*O$_2$), −139.9 (*N*$^+$≡N); **^{15}N NMR** (40.6 MHz, DMSO-d_6, ppm) δ: −16.0 (N$^+$≡*N*), −28.7 (*N*O$_2$), −84.1 (t, J_{NH} = 2.8 Hz, N_{pyr}–CH$_2$), −139.6 (*N*$^+$≡N), −193.0 (N_{pyr}); **EA** (C$_7$H$_2$N$_{10}$O$_6$, 322.15, %) calc.: C 26.10, H 0.63, N 43.48; found: C 26.03, H 0.83, N 43.33; **IS**: 1.5 J (< 100 μm); **FS**: 40 N (< 100 μm); **ESD**: 0.10 J (< 100 μm).

7.4 References

[1] a) H. Gao, J. M. Shreeve, *Chem. Rev.* **2011**, *111*, 7377–7436; b) T. M. Klapötke, *Chemistry of High-energy Materials*, 3rd edn., De Gruyter, Berlin, **2015**.

[2] R. Matyáš, J. Pachmáň, *Primary Explosives*, Springer, Heidelberg, **2013**, 157–166.

[3] a) G. Hervé, C. Roussel, H. Graindorge, *Angew. Chem. Int. Ed.* **2010**, *49*, 3177–3181; b) P. Yin, J. Zhang, D. A. Parrish, J. M. Shreeve, *Chem. Europ. J.* **2014**, *20*, 16529–16536.

[4] a) U. Baus, W. Reuther, *Patent DE 38 40 342 A1* **1990**; b) S. Ek, N. V. Latypov, *J. Heteroc. Chem.* **2014**, *51*, 1621–1627.

[5] a) I. L. Dalinger, I. A. Vatsadze, T. K. Shkineva, G. P. Popova, S. A. Shevelev, *Mendeleev Comm.* **2012**, *22*, 43–44; b) I. L. Dalinger, I. A. Vatsadze, T. K. Shkineva, G. P. Popova, S. A. Shevelev, *Synthesis* **2012**, *44*, 2058–2064.

[6] D. Fischer, PhD Dissertation, *High Performing and Nitrogen-rich High Energy Density Materials,* Ludwig-Maximilian University of Munich, Germany **2015**.

[7] a) A. A. Dippold, T. M. Klapötke, F. A. Martin, S. Wiedbrauk, *Europ. J. Inorg. Chem.* **2012**, *2012*, 2429–2443; b) C. He, J. Zhang, D. A. Parrish, J. M. Shreeve, *J. Mater.Chem.* **2013**, *A1*, 2863–2868; c) T. M. Klapötke, B. Krumm, C. Pflüger, *J. Org. Chem.* **2016**, *81*, 6123–6127; d) D. Izsák, T. M. Klapötke, A. Preimesser, J. Stierstorfer, *Z. Anorg. Allg. Chem.* **2016**, *642*, 48–55.

[8] a) M. Cygler, M. Przybylska, R. M. Elofson, *Canad. J. Chem.* **1982**, *60*, 2852–2855; b) R. P. Brint, D. J. Coveney, F. L. Lalor, G. Ferguson, M. Parvez, P. Y. Siew, *J. Chem. Soc., Perkin Trans. 2* **1985**, *1985*,139–145.

[9] J. Huheey, E. Keiter, R. Keiter, *Anorganische Chemie, Prinzipien von Struktur und Reaktivität*, De Gruyter, Berlin, **2014**.

[10] A. F. Holleman, E. Wiberg, N. Wiberg, *Lehrbuch der Anorganischen Chemie*, De Gruyter, Berlin, **2007**.

[11] a) J. L. Gottfried, *Phys. Chem. Chem. Phys.* **2014**, *16*, 21452–21466; b) J. L. Gottfried, *Propellants, Explos., Pyrotech.* **2015**, *40*, 674–681.

[12] R. Meyer, J. Köhler, A. Homburg, *Explosives*, 5th ed., Wiley, Weinheim, **2008**

[13] F. Gerard, A. Hardy, *Acta Crystallogr.* **1988**, C*44*, 1283–1287.

[14] C. S. Choi, E. Prince, *Acta Crystallogr.* **1972**, *B28*, 2857–2862.

[15] N. B. Bolotin, M. J. Hardie, R. L. Speer Jr, A. A. Pinkerton, *J. Appl. Crystallogr.* **2004**, *37*, 808–814.

[16] C. K. Lowe-Ma, R. A. Nissar, W. S. Wilson*, Diazophenols – Their Structure and Explosive Properties,* AD-A197439, **1987**.

7.5 Supplementary information

The analytical methods, general procedures, Small-Scale Shock Reactivity Test and computational details are described in the appendix of this thesis.

7.5.1 X-ray Diffraction
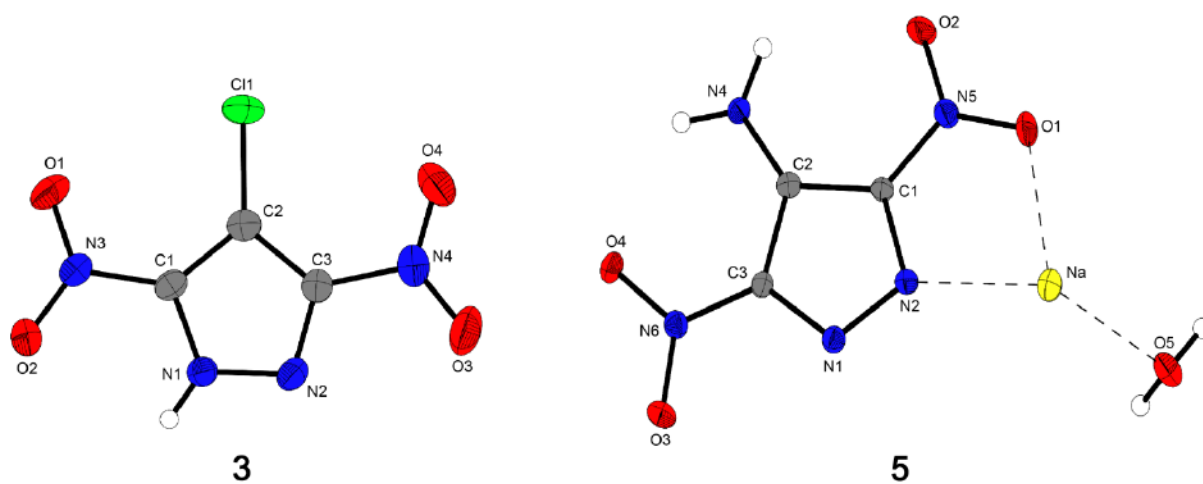
Figure 1. Molecular structures of of **3** and **5** in the crystals with atom labels. Thermal ellipsoids represent the 50% probability level.

Table 1. Crystallographic data and refinement parameters of compound **3** and **5**.

	3	5
Chemical formula	$C_3HClN_4O_4$	$C_3H_4N_5NaO_5$
Molecular weight [g·mol^{-1}]	192.53	213.10
Color, habit	Colorless plate	Colorless block
Size [mm]	0.08 x 0.21 x 0.34	0.10 x 0.15 x 0.21
Crystal system	Monoclinic	Triclinic
Space group	$P2_1/c$ (No. 14)	P-1 (No. 2)
a [Å]	11.7640(4)	6.2999(6)
b [Å]	11.0150(5)	6.4504(6)
c [Å]	10.1644(5)	9.7685(10)
α [°]	90	102.597(8)
β [°]	90.952(4)	95.339(8)
γ [°]	90	106.809(8)
V [Å^3]	1316.93(10)	365.64(7)
Z	8	2
ρ_{calc} [g·cm^{-3}]	1.942	1.936
μ [mm^{-1}]	0.560	0.226
$\lambda_{MoK\alpha}$[Å]	0.71073	0.71073
F(000)	768	216
ϑ min-max [°]	4.1–26.0	4.3–26.0
T [K]	173	173
Dataset h	$-14 \leq h \leq 14$	$-7 \leq h \leq 7$
Dataset k	$-13 \leq k \leq 13$	$-7 \leq k \leq 7$
Dataset l	$-11 \leq l \leq 12$	$-11 \leq l \leq 12$
Reflections collected	9763	2513
Independent reflections	2576	1422
Observed reflections	2064	1214
Number of parameters	225	143
R_{int}	0.028	0.024
S	1.02	1.04
R_1 (obs)	0.0308	0.0327
wR_2 (all data)	0.0826	0.0794
Remaining density [e·Å^{-3}]	−0.26, 0.24	−0.25, 0.24
Device type	Oxford XCalibur3 CCD	Oxford XCalibur3 CCD
Solution	SIR-92	SIR-92
Refinement	SHELXL-97	SHELXL-97
Absorption correction	multi-scan	multi-scan
CCDC	1500793	1500794

Table 2. Crystallographic data and refinement parameters of compounds **6–8**.

	6	7	8
Chemical formula	$C_7H_6N_{10}O_8$	$C_7H_2N_{10}O_{12}$	$C_7H_2N_{10}O_6$
Molecular weight [$g \cdot mol^{-1}$]	358.22	418.19	322.19
Color, habit	Colorless plate	Yellow block	Yellow block
Size [mm]	0.08 x 0.20 x 0.20	0.07 x 0.09 x 0.10	0.10 x 0.15 x 0.20
Crystal system	Orthorhombic	Monoclinic	Orthorhombic
Space group	$Pbca$ (No. 61)	$P2_1/n$ (No. 14)	$Pnma$ (No. 62)
a [Å]	12.2107(8)	8.6118(3)	10.3877(5)
b [Å]	9.6010(7)	16.5734(5)	21.8875(10)
c [Å]	22.1100(12)	29.794(1)	5.2966(3)
α [°]	90	90	90
β [°]	90	95.938(1)	90
γ [°]	90	90	90
V [Å^3]	2592.1(3)	4229.6(2)	1204.24(11)
Z	8	12	4
ρ_{calc} [$g \cdot cm^{-3}$]	1.836	1.970	1.777
μ [mm^{-1}]	0.167	0.189	0.157
$\lambda_{MoK\alpha}$[Å]	0.71073	0.71073	0.71073
$F(000)$	1456	2520	648
ϑ min-max [°]	4.1–26.0	2.6–26.0	4.3–26.4
T [K]	173	173	123
Dataset h	$-15 \leq h \leq 14$	$-10 \leq h \leq 10$	$-12 \leq h \leq 12$
Dataset k	$-9 \leq k \leq 11$;	$-20 \leq k \leq 20$	$-26 \leq k \leq 27$
Dataset l	$-27 \leq l \leq 26$	$-36 \leq l \leq 36$	$-6 \leq l \leq 6$
Reflections collected	12394	73555	7968
Independent reflections	2524	8289	1256
Observed reflections	1437	7169	1051
Number of parameters	250	784	108
R_{int}	0.096	0.035	0.035
S	1.03	1.05	1.05
R_1 (obs)	0.0577	0.0355	0.0424
wR_2 (all data)	0.1405	0.0911	0.1196
Remaining density [$e \cdot Å^{-3}$]	−0.25, 0.40	−0.29, 0.42	−0.19, 1.45
Device type	Oxford XCalibur3 CCD	Oxford XCalibur3 CCD	Oxford XCalibur3 CCD
Solution	SHELXS-97	SIR-92	SIR-92
Refinement	SHELXL-97	SHELXL-97	SHELXL-97
Absorption correction	multi-scan	multi-scan	multi-scan
CCDC	1500792	1500795	1494362

7.5.2 Small-Scale Shock Reactivity Test (SSRT)

Table 3. Results of the SSRT for **6**, **7** and **8**.

	6	**7**	**8**
$m_E^{[a]}$ [mg]	486	522	467
$m_{SiO2}^{[b]}$ [mg]	726	895	639

[a] Mass of the explosive: $m_E = V_s \cdot \rho \cdot 0.95$, ($V_s = 284$ mm^3); [b] Mass of SiO$_2$.

7.5.3 ^{15}N NMR spectroscopy
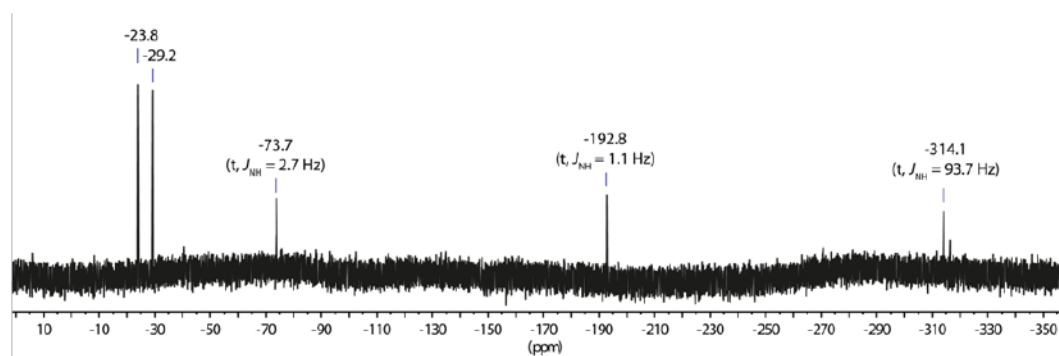
Figure 2. ^{15}N NMR spectrum of **6**.
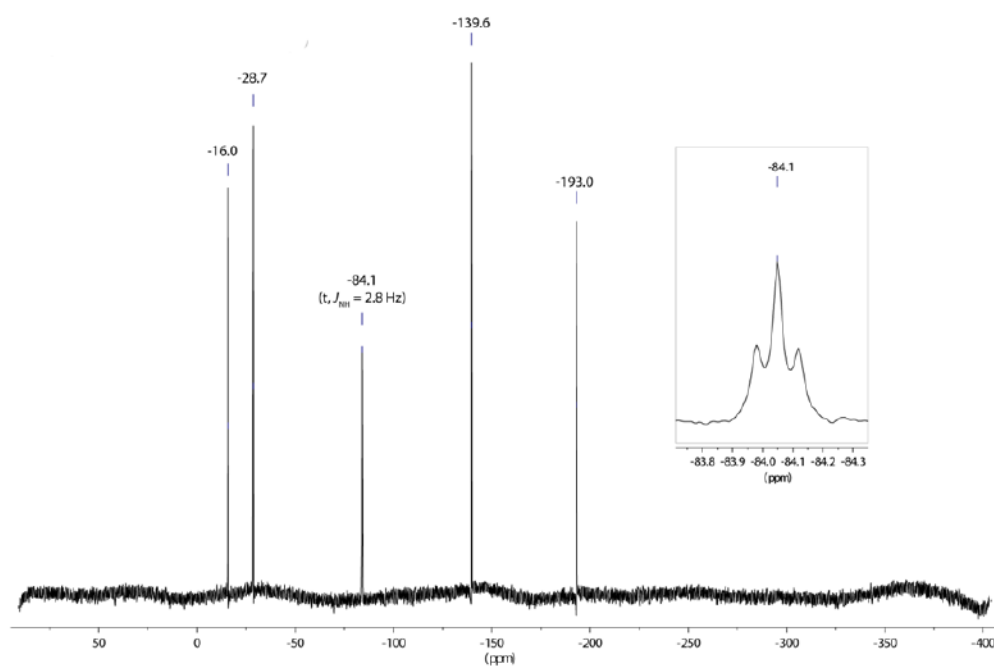
Figure 3. ^{15}N NMR spectrum of **8**.

7.5.4 Thermal Stability

The following plot compares the thermal stability of compound **6** with a commercially available sample of hexanitrostilbene (HNS). The temperatures of decomposition at a DSC heating rate of $5\ °\cdot min^{-1}$ are very similar.
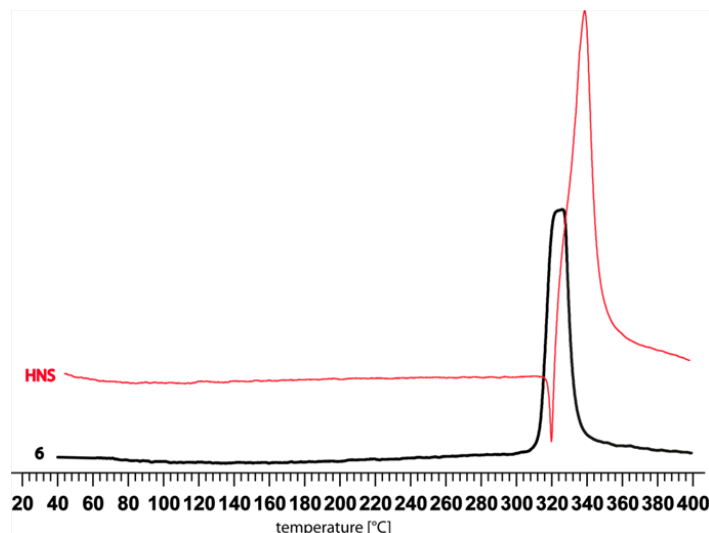
Figure 4. DSC measurements of **6** and HNS (heating rate $5\ °\cdot min^{-1}$).
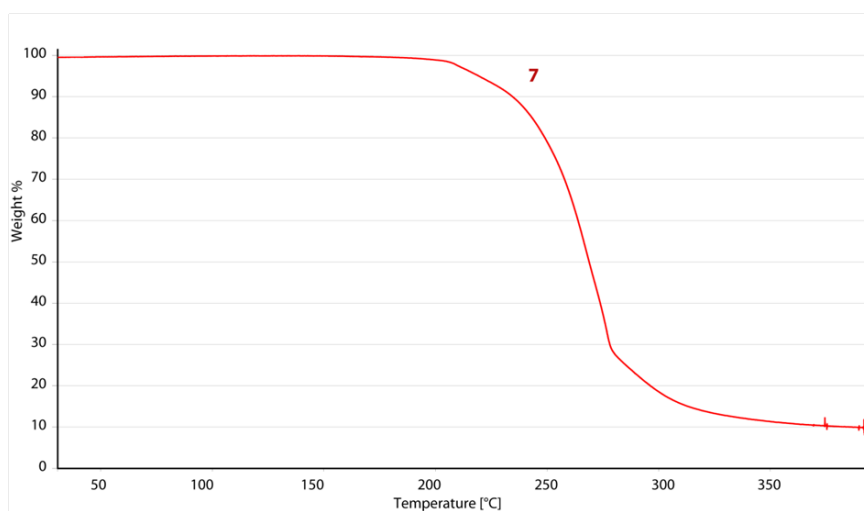
Figure 5. Thermal gravimetric measurement of **7** (heating rate $2\ °\cdot min^{-1}$).

7.5.5 Experimental Part

4-Chloropyrazole (2):[1] Pyrazole (0.50 mol, 34.00 g) was dissolved in water (100 mL). To the stirred solution a sodium hypochlorite solution (12.50 mol, 350.00 mL, 13% active chlorine) in water (100 mL) was added dropwise in that manner that the temperature of the reaction mixture did not rise above 35 °C. Subsequently, the reaction solution was stirred for 1 h at room temperature. Afterwards, concentrated hydrochloric acid was added to the mixture until pH = 1. The formed precipitate was filtered and washed with ice water. The mother liquor was extracted with ethyl acetate (1 × 100 mL, 2 × 50 mL). The solvent

was removed and the solid was recrystallized from hot water (100 mL). The product crystallizes as a colorless solid. Yield: 35.40 g (69.1%). **^{1}H NMR** (400.18 MHz, DMSO-d_6, ppm) δ: 13.11 (s, 1H, NH), 7.75 (s, 2H, CH); **^{13}C{^{1}H} NMR** (100.0 MHz, DMSO-d_6, ppm) δ: 131.5 (2C, C-3, C-5), 108.5 (1C, C-4).

4-Chloro-3,5-dinitropyrazole (3):[2] 4-Chloropyrazole (**2**) (0.12 mol, 15.60 g) was dissolved in concentrated sulfuric acid (190 mL). To the resulting reaction solution fuming nitric acid (20 mL) was added dropwise under cooling (temperature below 40 °C). The mixture was carefully heated to 100 °C, followed by stirring for 5 h at 100 °C. Afterwards, the reaction mixture was cooled to room temperature and added to ice water (2 L). The solution was extracted with ethyl acetate (3 x 300 mL) and the organic phase was washed with water (50 mL). The organic phase was dried over magnesium sulfate and evaporated under nitrogen. 4-Chloro-3,5-dinitropyrazole crystallizes in pale yellow-green blocks. Yield: 19.98 g (86.7%). **^{1}H NMR** (400.18 MHz, DMSO-d_6, ppm) δ: 11.83 (s, 1H, NH); **^{13}C{^{1}H} NMR** (100.0 MHz, DMSO-d_6, ppm) δ: 149.0 (2C, C-3, C-5), 103.8 (1C, C-4); **^{14}N NMR** (28.9 MHz, DMSO-d_6, ppm) δ: −26.3 (NO_2).

Sodium 4-amino-3,5-dinitropyrazolate monohydrate (5):[2] 4-Chloro-3,5-dinitropyrazole (**3**) (0.14 mol, 27.00 g) was dissolved in concentrated ammonia solution (250 mL). The resulting suspension was transferred to a steel autoclave and placed in an oven for 10 h at 170 °C. Subsequently, the autoclave was cooled to room temperature and the reaction mixture was acidified using concentrated hydrochloric acid to pH = 1. The cooled solution was extracted with ethyl acetate (3 x 100 mL). The organic phase was dried over magnesium sulfate and concentrated to dryness on a rotary evaporator. The resulting yellowish solid was dissolved in hot water (150 mL) and brought to pH = 9 using sodium hydroxide solution. The reaction mixture was cooled to a temperature of 5 °C and under vigorous stirring ethanol (500 mL) was added slowly. The precipitated solid was filtered and washed with ethanol and diethyl ether. The product precipitates as an orange microcrystalline powder. Yield: 24.20 g (81.1%). **^{1}H NMR** (400.18 MHz, DMSO-d_6, ppm) δ: 6.66 (s, 2H, NH$_2$), **^{13}C{^{1}H} NMR** (100.0 MHz, DMSO-d_6, ppm) δ: 144.1 (2C, C-3, C-5), 132.4 (1C, C-4).

Bis(4-amino-3,5-dinitropyrazolyl)methane (6): Sodium 3,5-dinitro-4-aminopyrazolate mono-hydrate (**5**) (22 mmol, 4.29 g) was suspended in 15 mL DMF and diiodomethane (10 mmol, 2.68 g, 805 µl) was added. The mixture was stirred at 90 °C for 16 h and poured on 100 mL water. A little sodium thiosulfate solution is added to reduce the precipitated iodine until

the suspension gives a nice and clean yellow colour. The precipitated product was filtered and washed with little water and dried in air to give 3.18 g **6** (89%) as yellow solid. **DSC** (5 °C·min^{-1}, onset): 310 °C (dec.); ^{1}**H NMR** (400.18 MHz, DMSO-d_6, ppm) δ: 7.29, 7.16; ^{13}**C{^{1}H} NMR** (100.6 MHz, DMSO-d_6, ppm) δ: 142.1, 131.7, 130.9, 67.2; ^{15}**N NMR** (40.6 MHz, DMSO-d_6, ppm) δ: −23.8 (s, NO_2), −29.3 (s, NO_2), −73.7 (t, J_{NH} = 2.7 Hz, N_{pyr}−CH$_2$), −192.8 (t, J_{NH} = 1.1 Hz, N_{pyr}), −314.1 (t, J_{NH} = 93.7 Hz, NH_2); **IR** (ATR, 25 °C, cm^{-1}) $\tilde{v}$: 3484 (w), 3462 (w), 3368 (w), 3349 (w), 1642 (s), 1579 (w), 1508 (m), 1477 (s), 1445 (m), 1386 (m), 1352 (w), 1300 (s), 1274 (vs), 1234 (m), 1218 (m), 1150 (w), 1103 (w), 1063 (w), 1004 (m), 886 (w), 827 (m), 803 (w), 785 (m), 759 (m), 743 (w), 736 (w); **Raman** (1064 nm, 300 mW, 25 °C, cm^{-1}) $\tilde{v}$: 3352 (3), 3032 (2), 1639 (22), 1568 (8), 1471 (8), 1446 (5), 1407 (7), 1391 (27), 1375 (100), 1352 (39), 1316 (4), 1294 (4), 1274 (6), 1238 (10), 1209 (2), 1151 (2), 1007 (6), 834 (46), 802 (6), 792 (12), 740 (11), 676 (2), 638 (5), 358 (9), 226 (2); **MS** (DEI+): m/z = 358.2 [M]$^+$; **EA** (C$_7$H$_6$N$_{10}$O$_8$, 258.19) calc.: C 23.47, H 1.69, N 39.10 %; found: C 23.73, H 1.81, N 38.90 %; **IS**: 11 J (< 100 μm); **FS**: > 360 N (< 100 μm); **ESD:** > 1 J (< 100 μm).

Bis(3,4,5-trinitropyrazolyl)methane, BTNPM (7): The solution of **6** (2.80 mmol, 1.00 g) in 5 mL of conc. H$_2$SO$_4$ was added dropwise to a mixture of 7.5 mL of 50% H$_2$O$_2$ and 25 mL of H$_2$SO$_4$ at 0 °C. The reaction mixture was stirred at 0 °C for 3 h and then overnight at room temperature. Subsequently, the reaction mixture was poured on 100 g of ice. Finally, **7** was isolated by filtration and washed with water and dried in air (86%, 1.00 g). **DSC** (5 °C·min^{-1}, onset): 205 °C (dec.); ^{1}**H NMR** (400.18 MHz, acetone-d_6, ppm) δ: 7.84; ^{13}**C{^{1}H} NMR** (100.0 MHz, acetone-d_6, ppm) δ: 144.2, 138.8, 123.8, 67.3; ^{14}**N NMR** (28.9 MHz, acetone-d_6, ppm) δ: −29.1 (NO_2), −31.0 (NO_2), −33.5 (NO_2); **IR** (ATR, 25 °C, cm^{-1}) $\tilde{v}$: 1586 (w), 1566 (w), 1541 (vs), 1471 (w), 1363 (w), 1332 (s), 1300 (m), 1263 (w), 1204 (w), 1084 (w), 1072 (w), 1000 (w), 906 (s), 844 (s), 806 (s), 775 (m), 742 (w), 673 (w), 598 (w); **Raman** (1064 nm, 300 mW, 25 °C, cm^{-1}) $\tilde{v}$: 3007 (11), 1573 (14), 1474 (6), 1453 (12), 1427 (100), 1411 (13), 1368 (35), 1334 (61), 1266 (10), 846 (60), 808 (6), 744 (13), 536 (5), 494 (5), 325 (17), 234 (6); **MS** (DEI+): m/z = 372.1 [M–NO$_2$]$^+$; **EA** (C$_7$H$_2$N$_{10}$O$_{12}$, 418.15) calc.: C 20.11, H 0.48, N 33.50 %; found: C 19.91, H 0.82, N 32.55 %; **IS**: 4 J (< 100 μm); **FS**: 112 N (< 100 μm); **ESD**: 0.6 J (< 100 μm).

Bis(4-diazo-5-nitro-3-oxopyrazolyl)methane (8): Method a: **6** (3 mmol, 1.075 g) was dissolved in 15 mL of sulfuric acid and cooled to 0 °C. Afterwards a solution of sodium nitrite

(9 mmol, 0.621 g) in 2 mL of water was added dropwise. The reaction mixture was stirred at 0 °C for 2 hours and then for 4 hours at ambient temperature followed by pouring it onto ice. The yellow precipitate was filtered and washed with small amount of cold water. The water phase was extracted using ethyl acetate (3 x 25 mL), dried over magnesium sulfate, and evaporated under reduced pressure. Yield: 87%, 0.84 g. Method b: A cooled to 0 °C solution of **6** (3 mmol, 1.075 g) in 10 mL of sulfuric acid was added dropwise to 10 mL of fuming nitric acid at 0 °C. The reaction mixture was stirred at 0 °C for 4 hours and then poured onto crushed ice and after ice melted water faze was extracted using ethyl acetate (3 x 50 mL). The collected organic phase was dried over magnesium sulfate. Throughout the solution nitrogen was bubbled until crude product was obtained which was recrystallized from ethyl acetate. Yield: 65%, 0.63 g. **DSC** (5 °C·min^{-1}, onset): 194 °C (melt.), 226 °C (dec.); **^{1}H NMR** (400 MHz, DMSO-d_6, ppm) δ: 5.88 (s, 2H, CH2); **^{13}C{^{1}H} NMR** (101 MHz, DMSO-d_6, ppm) δ: 161.3 (CO^-), 145.1 (CNO_2), 65.6 (CN_2^+), 53.8 (CH_2); **^{14}N NMR** (28.9 MHz, DMSO-d_6, ppm) δ: −24.9 (NO_2), −139.9 ($N^+\equiv$N); **^{15}N NMR** (40.6 MHz, DMSO-d_6, ppm) δ: −16.0 (N$^+\equiv N$), −28.7 (NO_2), −84.1 (t, J_{NH} = 2.8 Hz, N_{pyr}−CH$_2$), −139.6 ($N^+\equiv$N), −193.0 (N_{pyr}); **IR** (ATR, 25 °C, cm^{-1}) $\tilde{v}$: 3021 (w), 2152 (vs), 1730 (vs), 1684 (m), 1557 (w), 1502 (vs), 1446 (m), 1447 (s), 1430 (m), 1370 (m), 1362 (m),1291 (vs), 1265 (m), 1251 (m), 1204 (s), 1078 (m), 1062 (m), 958 (w), 935 (w), 915 (w), 799 (s), 764 (s), 750 (s),742 (m), 722 (w), 704 (m); **Raman** (1064 nm, 300 mW, cm^{-1}) $\tilde{v}$: 3022 (1), 2976 (13), 2159 (29), 1705 (10), 1558 (14), 1524 (37), 1514 (38), 1469 (39), 1451 (43), 1430 (12), 1362 (55), 1334 (48), 1297 (19), 1253 (21), 1205 (100), 1081 (59), 1068 (30), 959 (21), 936 (11), 796 (19), 765 (13), 753 (8), 743 (6), 723 (10), 708 (7), 624 (9), 569 (10), 419 (12), 401 (9), 366 (9), 243 (14), 167 (24), 134 (42), 98 (66); **MS** (DEI+): m/z = 322.1 [M]$^+$; **EA** (C$_7$H$_2$N$_{10}$O$_6$, 322.15) calc.: C 26.10, H 0.63, N 43.48 %; found: C 26.03, H 0.83, N 43.33 %; **IS**: 1.5 J (< 100 μm); **FS**: 40 N (< 100 μm); **ESD**: 0.10 J (< 100 μm).

7.5.6 LASEM Procedure

The laser-induced air shock from energetic materials (LASEM) experimental setup to measure the laser-induced air shock velocity using schlieren imaging and estimate the detonation velocity of an energetic material has been described previously.[3] Briefly, single-shot pulses from a Nd:YAG laser (1064 nm, 900 mJ, 6 ns) were focused just below the sample surface in order to ablate the residue material, exciting and ionizing the sample to form a high temperature microplasma lasting tens of microseconds. The temperature

and pressure mismatch between the laser-induced plasma and the surrounding air resulted in the formation of a laser-induced shock wave, which was further accelerated by the exothermic chemical reactions of the reacting energetic material in the plasma. The expansion of the laser-induced shock wave into the air above the sample was recorded with high-speed color camera (Photron SA5 at 84,000 frames-per-second, 1.0 μs shutter, 64×648 pixels image size) incorporated into a Z-type schlieren imaging system (10.8 cm diameter mirrors, 114 cm focal length) illuminated with a 200 W mercury-xenon arc lamp. The camera was focused 33 cm in front of the focus of the ablation laser with a zoom lens (Nikon Nikkor 24–85 mm f/2.8–4D IF) in order to provide the greatest contrast for visualization of the shock wave.

The characteristic laser-induced shock velocity in air for each sample was determined by finding the y-intercept of a polynomial fit to the velocity versus time curve. Since the calibration fit for estimating detonation velocity from the characteristic laser-induced shock velocity of a sample was previously developed for conventional military explosives by correcting the measured values from large-scale detonation testing to the theoretical maximum density (TMD), the LASEM technique estimates the maximum detonation velocity for a sample (assuming the material detonates and the charge was prepared at the TMD). Residue samples of **7** (approximately 60 mg·mm^{-2}) were prepared by spreading the material on double-sided tape affixed to a glass slide; the material was pressed into the tape to confine the material and enhance the laser-material interaction. Excess material was gently removed from the slide by tapping the edge. The samples were allowed to air dry for approximately 30 minutes after being spread on the tape to remove residual water, until the measured mass was stable (as measured by a balance accurate to 1.0 μg). A total of 15 laser shots were acquired from 4 different sample slides. An exhaust outlet was located next to laser ablation region to remove scattered particulates and product gases.

7.5.7 References

[1]   a) U. Baus, W. Reuther, *Patent DE 38 40 342 A1* **1990**; b) S. Ek, N. V. Latypov, *J. Heteroc. Chem.* **2014**, *51*, 1621−1627.

[2]   a) I. L. Dalinger, I. A. Vatsadze, T. K. Shkineva, G. P. Popova, S. A. Shevelev, *Mendeleev Comm.* **2012**, *22*, 43-44; b) I. L. Dalinger, I. A. Vatsadze, T. K. Shkineva, G. P. Popova, S. A. Shevelev, *Synthesis* **2012**, *44*, 2058−2064.

[3]   a) J. L. Gottfried, *Phys. Chem. Chem. Phys.* **2014**, *16*, 21452−21466; b) J. L. Gottfried, *Propellants, Explos., Pyrotech.* **2015**, *40*, 674−681.

Estimated Detonation Velocities for TKX-50, MAD-X1, BDNAPM, BTNPM, TKX-55 and DAAF using the Laser-induced Air Shock from Energetic Materials Technique
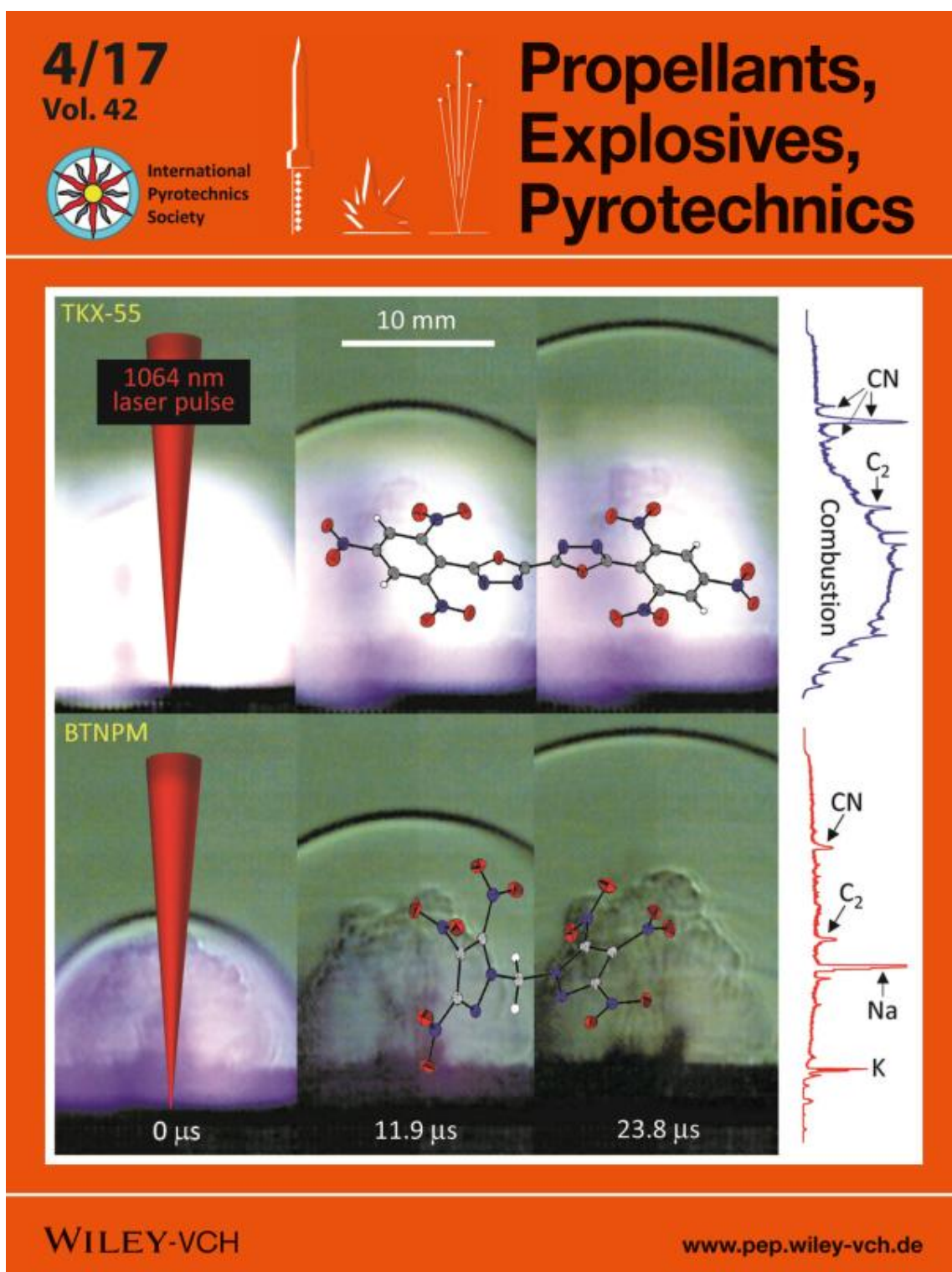
Abstract: Since new energetic materials are initially produced in very small quantities for both safety and cost reasons, laboratory-scale methods for characterizing their performance are essential for determining the most promising candidates for scale-up. Laser-induced air shock from energetic materials (LASEM) is a promising new method for estimating the detonation velocity of novel explosives using milligram amounts of material while simultaneously investigating their high temperature chemical reactions. LASEM has been applied to 6 new explosives for the first time: TKX-50, MAD-X1, BDNAPM, BTNPM, TKX-55, and DAAF. Emission spectroscopy of the laser excited materials revealed the formation of the high pressure bands of C_2 during the ensuing exothermic reactions. The low thermal sensitivity of the materials also led to unusual laser-material interactions, visualized with high-speed video. The estimated detonation velocities for the 6 explosives were compared to predicted values from EXPLO5 and CHEETAH. The LASEM results suggest that TKX-55, BDNAPM, and BTNPM have higher detonation velocities than predicted by the thermochemical codes, while the estimated detonation velocities for MAD-X1 and TKX-50 are slightly lower than those predicted.

8.1   Introduction

Laser-induced air shock from energetic materials (LASEM) is a laboratory-scale technique for estimating the detonation velocity of energetic materials.[1, 2] A focused nanosecond laser pulse is used to ablate and excite an energetic material residue, forming a laser-induced plasma. Exothermic chemical reactions in the plasma accelerate the laser-induced shock wave generated by the plasma formation – thus, energetic materials produce faster shock waves than inert materials (as measured on the microsecond timescale by a high-speed camera). The measured laser-induced air shock velocity can be correlated to measured detonation velocities from large-scale testing and used to estimate the detonation velocity of the material. Although the energetic material is not detonated by the laser, and therefore LASEM only provides an estimate of the maximum attainable detonation velocity for a material, it has the distinct advantage of requiring only milligram quantities of energetic material. New candidate energetic materials are often initially synthesized in small quantities for safety reasons, and scale-up to multiple gram quantities can be costly. While the shot-to-shot variation in the measured laser-induced shock velocities can be significant due to the stochastic nature of the laser-material interaction, many laser shots can be acquired to obtain a reproducible average at minimal expense (especially compared to large-scale detonation testing, where significant safety hazards increase the cost of testing). The method was originally demonstrated by comparison of the laser-induced air shock velocities of inert and energetic materials,[1] then calibrated by correlating the measured laser-induced air shock velocities from conventional military explosives to measured detonation velocities from large-scale detonation testing.[2] The calibration fit was validated using conventional energetic materials (both monomolecular and composite) not used to develop the correlation. Estimated detonation velocities for materials without measured detonation velocities were also determined for nanoscale cyclotrimethylene trinitramine (*nano*-RDX) and three high-nitrogen explosives. This method has also recently been extended to mixtures of military explosives with metal additives (aluminum or boron).[3]

Here, the estimated detonation velocities of 6 new explosives, dihydroxylammonium 5,5′-bistetrazole-1,1′-diolate (TKX-50), dihydroxylammonium 5,5′-bis(3-nitro-1,2,4-triazo-late-1*N*-oxide) (MAD-X1), bis(4-amino-3,5-dinitropyrazol-1-yl)methane (BDNAPM), bis(3,4,5-trinitropyrazol-1-yl)methane (BTNPM), 5,5′-bis(2,4,6-trinitrophe-nyl)-2,2′-bi(1,3,4-oxadiazole) (TKX-55), and 3,3′-diamino-4,4′-azoxyfurazan (DAAF), have been determined and compared to theoretical predictions of the detonation velocities using two different thermochemical codes (EXPLO5 V6.01 and CHEETAH V8.0). TKX-50,[4]

MAD-X1,[5] BDNAPM,[6] BTNPM,[6] TKX-55,[7] and DAAF[8, 9] are within the group of recently synthesized explosives which are the most promising prospective candidates for use in practical applications (Figure 1).
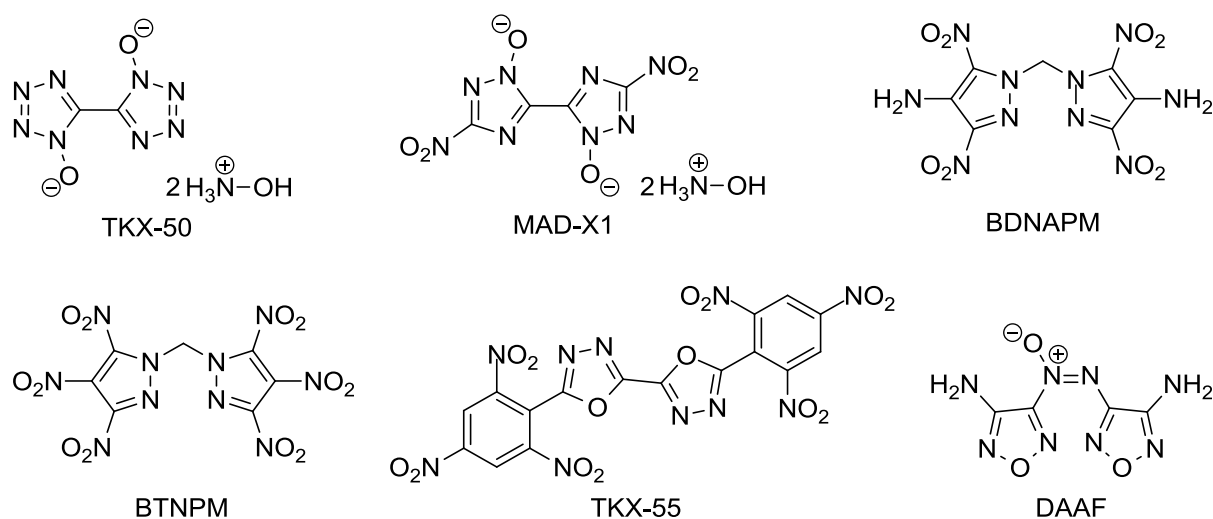
Figure 1. Chemical structures of TKX-50, MAD-X1, BDNAPM, BTNPM, TKX-55 and DAAF.

These explosives are characterized by high decomposition temperatures ($200 \leq T_{dec} \leq 335\ °C$) and high densities ($1.802 \leq \rho \leq 1.934\ \mathrm{g \cdot cm^{-3}}$). All of them are endothermic compounds with standard molar enthalpy of formation between $198\ \mathrm{kJ \cdot mol^{-1}}$ and $447\ \mathrm{kJ \cdot mol^{-1}}$. Theoretically calculated Chapman-Jouguet (C-J) characteristics of these explosives from EXPLO5 V6.01 (detonation pressure, 27.3−40.0 GPa; detonation velocities, 8030−9767 $\mathrm{m \cdot s^{-1}}$) also make these molecules interesting for possible applications. Therefore, we decided to perform the LASEM investigations of those molecules.

8.2 Experimental Section

8.2.1 Synthesis

The explosives TKX-50, MAD-X1, BDNAPM, BTNPM, TKX-55 and DAAF were synthesized according to the methods given in the literature (see Supporting Information).[4-10] A comprehensive list of the physico-chemical properties of the explosives are also given in the supporting information, along with a comparison of the detailed results from the thermodynamic codes EXPLO5 and CHEETAH (Table 1, SI). For comparison, the physico-chemical properties and thermodynamic results for several conventional military explosives are listed in Table 2.

8.2.2   Sample Preparation for LASEM

Residue samples of energetic materials were prepared by spreading the material on double-sided tape affixed to a glass slide; the material was pressed into the tape with a stainless steel spatula to confine the material. Excess material was gently removed from the slide by tapping the edge. Confinement of the material in the tape enhances the laser-material interaction and helps distribute the residue layer (approximately 60 µg·mm^2) evenly across the substrate. The samples were allowed to air dry for approximately 30 minutes after being spread on the tape to remove residual water, until the measured mass was stable (as measured by a balance accurate to 1 µg). At least two slides were prepared for each sample in order to get 15 laser shots per material. Some materials, such as TKX-55 and BTNPM, did not stick to the tape as well and a large amount of material surrounding the laser spot was scattered into the air following the shock wave, resulting in fewer shots per slide. Other materials, such as the MAD-X1 and DAAF were tacky and adhered to the tape extremely well.

8.2.3   LASEM

The experimental setup for LASEM analysis has been described previously.[1, 2]   Briefly, a 6-ns pulsed Nd:YAG laser (1064 nm, 900 mJ) was focused just below the sample surface with a 10 cm lens. The focused laser pulse ablated the sample residue into the air above the sample surface, generating a laser-induced plasma and subsequent shock wave. A Z-type schlieren imaging system (10.8 cm diameter mirrors, 114 cm focal length) with a high-speed color camera (Photron SA5) was used to record the expansion of the laser-induced shock wave into the surrounding air above the sample, which was illuminated by a 200 W Hg-Xe arc lamp. A zoom lens (Nikon Nikkor 24–85 mm f/2.8–4D IF) on the camera was focused 33 cm in front of the focus of the ablation laser. This focal position was optimized to provide the greatest contrast for visualization of the shock wave. The following camera settings were used for imaging the shock waves: 84,000 frames-per-second, 1.0 µs exposure time, 64 × 648 pixels image size. Shock data from 15 laser shots were acquired for each sample.

The characteristic laser-induced shock velocity in air for each sample was determined by finding the y-intercept of a polynomial fit to the velocity versus time curve. The calibration fit for estimating detonation velocity from the characteristic laser-induced shock velocity of a sample was previously developed for conventional military explosives by correcting the measured values from large-scale detonation testing to the theoretical maximum density (TMD) and determining the linear correlation between the characteristic laser-induced shock

velocities of the tested materials and their corrected detonation velocities, therefore the LASEM technique estimates the maximum detonation velocity for a sample (assuming the material detonates and the charge was prepared at the TMD). In addition to imaging the shock wave, a CCD spectrometer (Ocean Optics USB4000, 200-890 nm, 100-ms integration time) was added to investigate the chemical reactions and elemental composition of the ablated material following the initial plasma formation, and an infrared-sensitive photoreceiver (New Focus Model 2053, 900-1700 nm) was added to measure the peak intensity and duration of the subsequent combustion reactions. An exhaust outlet was located next to laser ablation region to remove scattered particulates and product gases.

8.3   Results and Discussion

8.3.1   Emission spectra

The emission spectra for the explosives investigated in this study are shown in Figure 2, along with the blank tape substrate for comparison.
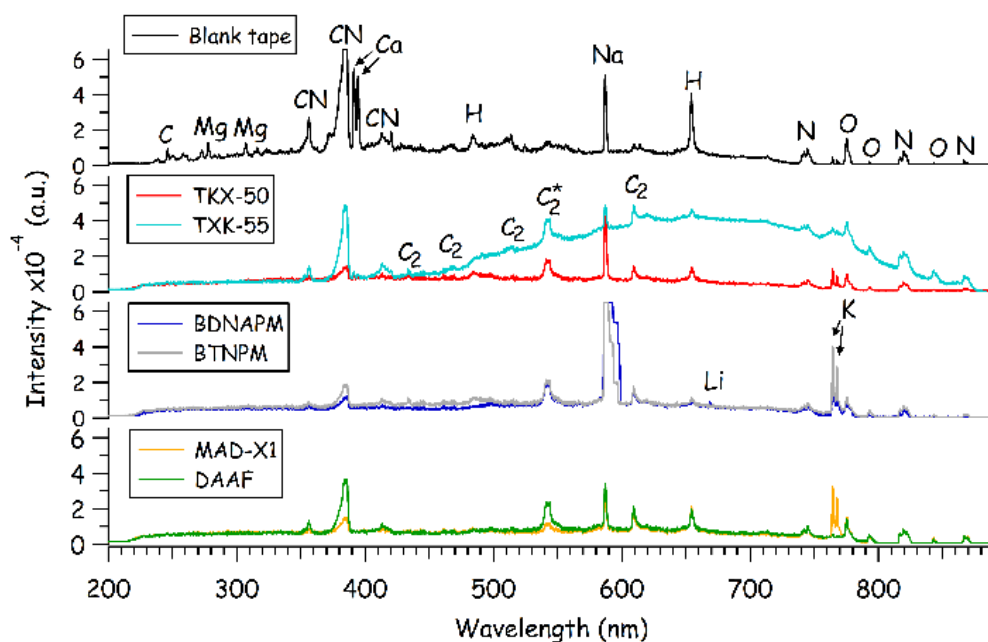
Figure 2. Emission spectra from the laser excitation of the 6 explosive materials and the blank tape substrate; C_2^* denotes the high pressure band of C_2.

The emission spectra can be used to identify metal impurities in the energetic materials, as well as to provide insight into the chemical reactions that occur in the laser-induced plasma[11] and/or the laser-induced deflagration[12], depending on the gate width of the spectrometer. For this work, a spectrometer with a long gate (100 ms) was used to capture all emission from the laser excitation of the energetic materials. Discrete atomic and ionic emission features (C, H, N, O, Ca, Na, K, Li, Mg)[13] are due to emission from the laser-induced plasma, while molecular emission features (CN, C_2)[14, 15] result primarily

from recombination reactions in the plasma (microsecond timescale) and in the deflagrating material (millisecond timescale). Table 1 lists the species observed in the emission spectra of the energetic materials (not including the Mg, which was only observed in the blank tape) and their accepted wavelengths. Most of the O and N emission is due to entrainment of air in the laser-induced plasma, while Ca, Na, and K are relatively common contaminants introduced by sample handling. Li was only observed in the spectra of BDNAPM.

Table 1. Observed species from the emission spectra of laser-excited explosive residues

Observed Species	Wavelength [nm] (wavelengths from references[13-15])
C	247.856
CN	358.39-.59.04, 385.09-388.34, 415.24-421.6
Ca	393.366, 396.847
C_2	467.86-473.71, 512.93, 516.52, 612.21, 619.12
C_2^*	434-437, 465-473, 538-546
Na	588.995/589.592, 819.482
H	486.133, 656.285
Li	670.776
N	742.364, 744.229, 746.831, 818.487/818.802, 868.028
K	766.490, 769.896
O	777.194/777.417, 794.755/795.080, 844.636

All of the energetic materials have a strong emission feature near 543 nm due to the high pressure band of C_2 (C_2^*);[15] selective excitation of the $A^3\Pi_g[v=6]$ state results from collisional excitation of C_2 in lower vibrational states, suppressing the prominent Swan bands $A^3\Pi_g$-$X'^3\Pi_u$. Background-corrected peak emission intensities for the blank tape and 6 explosives are shown in Figure 3. A comparison of the relative intensities of the emission features shows that the blank tape has stronger C, H, C_2, and CN emission compared to the explosives. However, the C_2^* emission is significantly stronger in the explosives – likely indicating higher temperature plasmas with more collisional excitation. Calculation of temperatures from the recorded emission spectra was not possible because of the long integration time and lack of suitable emission features from the same species with widely varying excited state levels. Notably, significant broadband emission was observed from the burning of condensed phase particles of TKX-55 scattered into the air by the laser-induced shock wave; when the ejected particles entered the region of air heated by the plasma and subsequent chemical reactions they began deflagrating.[1] The emission from laser-induced deflagration indicates extended energy release on the millisecond timescale, as discussed in the next section.[12]
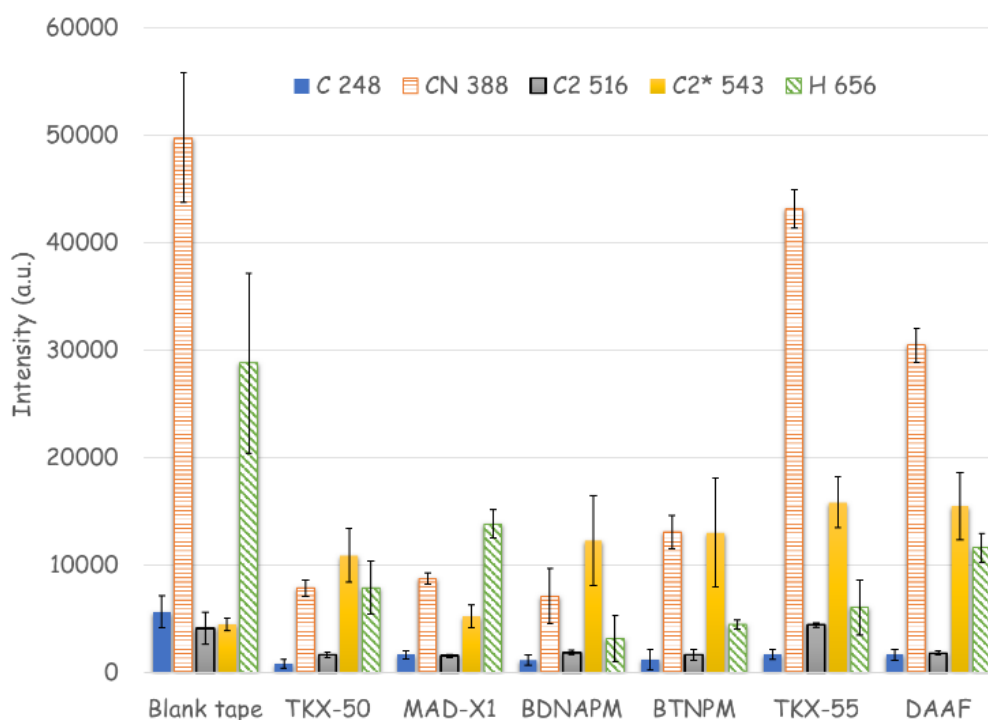
Figure 3. Background-corrected peak emission intensities for the blank tape substrate, TKX-50, MAD-X1, BDNAPM, BTNPM, TKX-55, and DAAF.

8.3.2 Time-resolved emission

The time-resolved emission from the laser excitation of materials gives an indication of the extent of combustion of the energetic material in the air on the millisecond-timescale. For example, carbon-rich explosives like trinitrotoluene (TNT) or hexanitrostilbene (HNS) undergo extended combustion reactions following laser excitation, resulting in significant emission on the millisecond timescale (*i.e.,* laser-induced deflagration[3, 12]). The more powerful military explosives, with high detonation velocities (and correspondingly higher laser-induced air shock velocities), did not undergo extensive combustion reactions on the millisecond timescale since most of the exothermic chemical reactions took place in the laser-induced plasma. Thus, the time-resolved emission can be used as a measure of the slow energy release of a material (compared to the fast, microsecond-timescale energy release during the laser-induced plasma and shock wave formation).

Figure 4 shows the average time-resolved emission from the 6 explosives from all laser shots. While shot-to-shot variation in the deflagration intensities were significant as a result of the stochastic nature of the ejection of energetic material particles from the sample surface, the average relative intensities of the combustion emission were reproducible between sample slides (see Figures 1 and 2 in the supporting information). TKX-55 has the lowest oxygen balance ($\Omega = -57.11\%$), and undergoes the most significant combustion on the millisecond

timescale. Although DAAF has the second lowest Ω (−52.79%), the laser-induced deflagration was extremely weak – likely because the tacky nature of the material prevents significant ejection of particles surrounding the laser impact region following the laser-induced shock wave. Of the conventional military explosives, the similarly tacky composite explosive C-4 did not deflagrate either (unpublished results). The BDNAPM produced the second largest deflagration ($\Omega = -40.20\%$), followed by the TKX-50 ($\Omega = -27.10\%$) and BTNPM ($\Omega = -11.48\%$). Like DAAF, the MAD-X1 ($\Omega = -19.74\%$) is very tacky and the particles did not scatter into the air above the sample following the laser-induced shock wave.
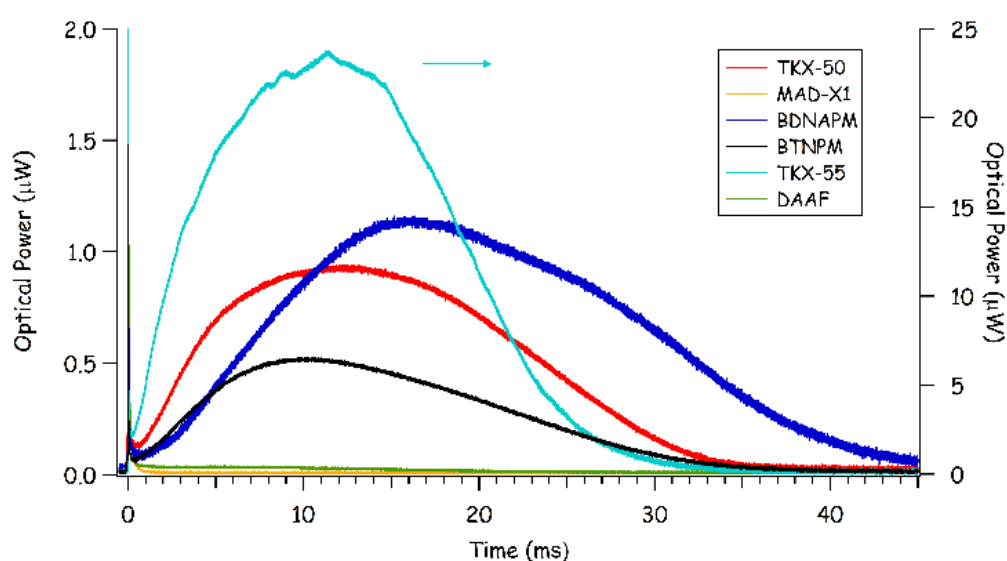
Figure 4. Infrared emission from the laser-induced plasma (sharp initial spike) and laser-induced deflagration (millisecond-timescale emission) of the explosive materials.

8.3.3 High-speed video

Figure 5 shows snapshots from the high-speed video of the laser excitation of the 6 explosives; the selected videos represent the typical laser shot for each material. The brightness was increased (+ 40%) for all images in the figure for enhanced visualization. Adjustment of the brightness and/or contrast for the first few frames was necessary during measurement of the shock wave position to improve visualization of the shock wave in the presence of the defocused plasma emission; the few individual shots where the plasma emission completely obscured the shock wave position in the first frame were discarded (however, a total of 15 videos with measurable shock waves in the first frame were obtained for all samples). Since the camera was focused in front of the laser-induced plasma to enhance visualization of the shock wave, the plasma emission is slightly defocused. The purple light

in the snapshots is a result of the strong CN emission (Figure 2), while the white light is residual continuum emission from the laser-induced plasma. The TKX-55 (Figure 5a) and DAAF (Figure 5d) produce the most intense plasma emission, followed by TKX-50 (Figure 5b), BDNAPM (Figure 5e) and MAD-X1 (Figure 5f). BTNPM (Figure 5c) produced very little visible plasma emission following laser excitation. In general, it was previously observed that the most powerful energetic materials produce the least amount of visible plasma emission.[1]

In Figure 5d-f, a thin, dark string of excited material coincident with laser beam (center of images) is particularly visible in the later frames; it also appears to a lesser extent in Figure 5b (TKX-50) and in later frames of TKX-55 once the plasma emission has decreased (not shown). The structure of the plasma plume region is also distinct for these energetic materials (DAAF, BDNAPM, MAD-X1). The only conventional military explosive observed to show similar features was TATB,[1] which could indicate that these effects are related to the low thermal sensitivity of these energetic materials. BTNPM, which is the only explosive in this set that does not show similar interaction with the laser beam, has the lowest decomposition temperature and has higher impact and friction sensitivity compared to most of the other materials (Table 1, SI).
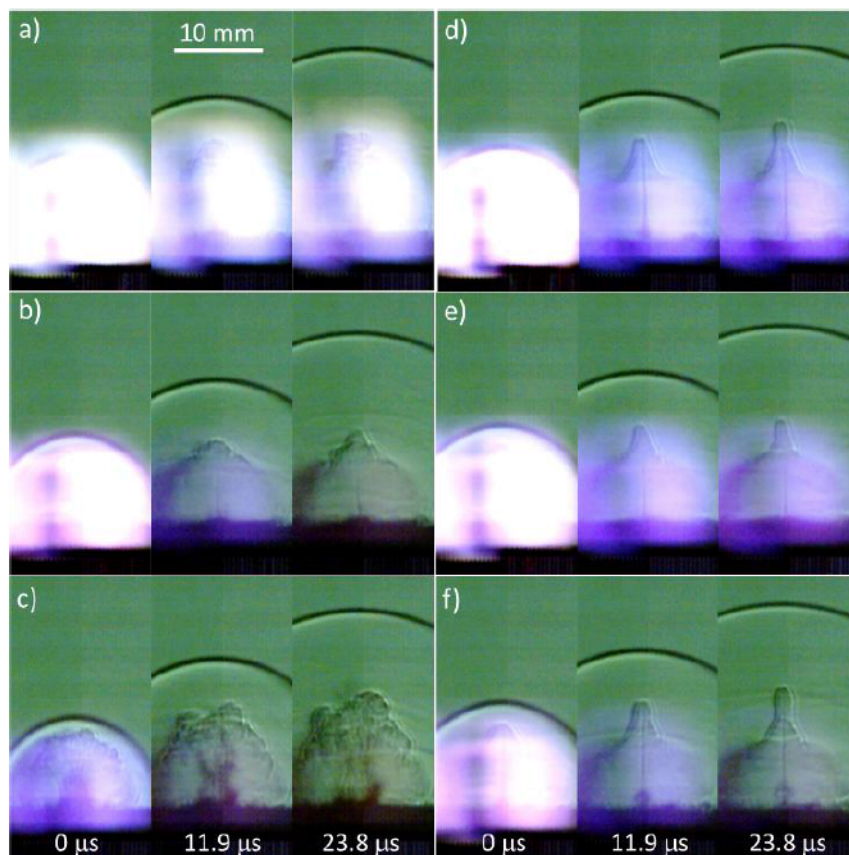
Figure 5. Selected snapshots from the high-speed video of the laser excitation of a) TKX-55, b) TKX-50, c) BTNPM, d) DAAF, e) BDNAPM), and f) MAD-X1.

Occasionally, unusual features appeared in the high-speed video for random laser shots of a few of the energetic materials. For example, in Figure 6, distortion of the leading edge of the laser-induced shock wave in air is shown for a) TKX-50, b) BTNPM, and c) MAD-X1, in order of increasing degree of severity. For these, a second, much smaller plume of reacting material appeared to form near the top of main laser-induced plasma (coincident with the laser beam). This distortion is so severe in the MAD-X1 shot that a bubble was formed in the main shock wave which persisted for tens of microseconds. The cause of this behavior is currently unknown, but it was never observed in the high-speed videos of the conventional military explosives.
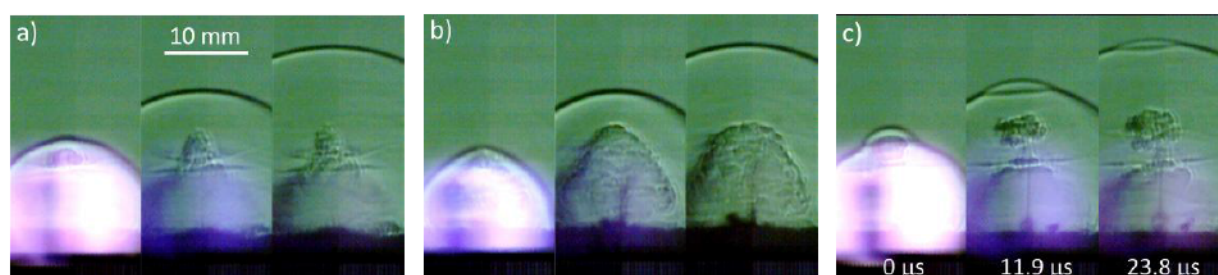
Figure 6. Selected snapshots from the high-speed video of the laser excitation of a) TKX-50, b) BTNPM, and c) MAD-X1.

8.3.4 Laser-induced shock velocities

The measured characteristic laser-induced air shock velocities (with 95% confidence intervals), along with the estimated and theoretically predicted detonation velocities using two thermochemical codes (EXPLO5 V6.01[16-20] and CHEETAH V8.0[21]) are shown in Table 2 (full results from the calculations provided in Tables 1 and 2 in the supporting information). The velocity *vs.* time curves used to determine the characteristic laser-induced shock velocity for each sample, along with shock velocities from individual laser shots and the 95% confidence intervals for the polynomial fits are shown in Figures 3-9 in the supporting information. For comparison, the average measured detonation velocities from large-scale detonation testing of some conventional military explosives[2] are also listed in Table 2. The percentage difference between the predicted or measured detonation velocities and the estimated detonation velocities from LASEM are given in parentheses. The average difference between the estimated detonation velocities and EXPLO5 predictions is 3.1% (3.6% for the 6 explosives studied here and 2.5% for the conventional military explosives). For CHEETAH predictions, the average difference is 3.9% (4.8% for the 6 explosives and 2.8% for the conventional military explosives). Note that the TMD and heats of formation given in Tables 1 and 2 in the supporting information were used for the CHEETAH

calculations. Using the values in the CHEETAH database, the average difference between the estimated and predicted values for CHEETAH was 2.4% (1.0% for TXK-50 and DAAF; 3.0% for the conventional military explosives).

Table 2. LASEM results with comparison to theoretical predictions and large-scale detonation test results (% difference from estimated detonation velocity indicated in parentheses).

Sample	Laser-induced shock velocity [m·s^{-1}]	Estimated V_{LASEM} [km·s^{-1}]	EXPLO5 v6.01 V_{C-J} [km·s^{-1}]	CHEETAH v8.0 V_{C-J} [km·s^{-1}]	Measured $V_{det.}$ at TMD [km·s^{-1}]
TKX-50	835.41 ± 11.20	9.56 ± 0.28	9.767 (2.1%)	9.735 (1.8%)	9.432 (−1.4%)
MAD-X1	807.19 ± 8.96	8.86 ± 0.22	9.195 (3.6%)	9.267 (4.4%)	*nd*
BDNAPM	797.65 ± 8.56	8.63 ± 0.21	8.332 (−3.6%)	8.171 (−5.6%)	*nd*
BTNPM	849.54 ± 12.50	9.91 ± 0.31	9.304 (−6.5%)	9.276 (−6.8%)	*nd*
TKX-55	781.72 ± 10.72	8.23 ± 0.26	8.030 (−2.5%)	7.548 (−9.0%)	*nd*
DAAF	774.16 ± 10.63	8.05 ± 0.26	8.316 (3.2%)	8.124 (0.9%)	8.11 ± 0.03 (1.0%)
TNT	731.26 ± 9.28	6.99 ± 0.23	7.286 (4.1%)	7.192 (2.8%)	7.026 ± 0.119 (0.5%)
HNS	739.96 ± 8.43	7.20 ± 0.21	7.629 (5.6%)	7.499 (4.0%)	7.200 ± 0.071 (0.0%)
NTO	784.34 ± 10.29	8.30 ± 0.25	8.420 (1.4%)	8.656 (4.1%)	8.335 ± 0.120 (0.4%)
RDX	806.83 ± 7.74	8.85 ± 0.19	8.834 (−0.2%)	8.803 (−0.5%)	8.833 ± 0.064 (-0.2%)
CL-20	835.41 ± 9.52	9.56 ± 0.24	9.673 (1.2%)	9.833 (2.8%)	9.57 (0.1%)

In contrast to the predicted detonation velocities, the difference between estimated detonation velocities and measured large-scale detonation velocities for the conventional military explosives is only 0.2%. The accuracy of LASEM for estimating detonation velocities of the high-nitrogen energetic materials is not known since few large-scale results have been reported in the published literature, other than for DAAF[9, 22] and TKX-50.[23] The estimated detonation values agree with the reported detonation velocities for DAAF and TKX-50 within less than 1.5%. The LASEM results suggest that TKX-55, BDNAPM, and BTNPM have higher detonation velocities than predicted by the thermochemical codes, while the estimated detonation velocities for MAD-X1 and TKX-50 are slightly lower than those predicted by EXPLO5 or CHEETAH. A comparison of the two thermochemical codes show that while the magnitude of the difference between the estimated detonation velocities and predicted

detonation velocities may differ (especially for TKX-55), the predicted detonation velocities are typically either both higher or both lower than the estimated (or measured) detonation velocities.

8.4   Conclusions

The emission spectra obtained from the laser excitation of the investigated explosives show that TKX-55, similar to other explosives containing the *sym*-tinitrobenzene moiety in the chemical structure (TNT, HNS), and therefore low $\Omega = -52.79\%$, undergoes extended combustion reactions following laser excitation, resulting in considerable emission on the millisecond timescale. BDNAPM produced the second largest deflagration, followed by TKX-50 and BTNPM. The tacky nature of DAAF resulted in extremely weak laser-induced deflagration, despite the low oxygen balance (-52.79%), similar to the C-4 explosive composition. The emission spectra also showed the presence of the high-pressure bands of C_2, which might provide some insight into the mechanisms for the combustion reactions of the excited explosive materials.

High-speed video investigation confirms that the most powerful explosive among those investigated in this study is BTNPM (it produced the least intense plasma emission); the weakest are TKX-55 and DAAF. Moreover, the structure of the plasma plume region of DAAF, BDNAPM, MAD-X1, and TKX-55 appears to reflect the low thermal sensitivity of these energetic materials and the high thermal sensitivity of BTNPM.

The estimated detonation velocities of the investigated explosives, based on the measured characteristic laser-induced air shock velocities, are in very good agreement with calculated detonation velocities using EXPLO5 V6.01 and CHEETAH V8.0 thermochemical codes. The average difference between the estimated detonation velocities and calculated using EXPLO5 is 3.6% while using CHEETAH is 4.8%. The LASEM results show that TKX-55, BDNAPM, and BTNPM have higher detonation velocities than those calculated using EXPLO5 or CHEETAH, while the estimated detonation velocities for MAD-X1 and TKX-50 are somewhat inferior to those calculated using the thermochemical codes. The calculated detonation velocities using EXPLO5 and CHEETAH slightly differ from each other (especially for TKX-55), nevertheless they show the same tendency (in general, the values are either both higher or both lower than the estimated – or measured – detonation velocities). In comparison to the predicted detonation velocities (EXPLO5: 2.5%; CHEETAH: 2.8%), the difference between estimated detonation velocities and measured large-scale detonation velocities for the conventional military explosives is only 0.2%. Moreover, for DAAF

and TKX-50 the estimated detonation values are in agreement with the reported detonation velocities to within less than 1.5%.

We have demonstrated that the LASEM technique can be successfully used not only as a laboratory-scale technique for estimating the detonation velocity of explosives, but it also gives insight into the high temperature chemical reactions which occur during and after decomposition of the explosives in the laser-induced plasma. While not a replacement for larger scale detonation testing, LASEM serves as a valuable pre-screening tool for investigating the performance of new energetic materials prior to scale-up into multi-gram quantities.

8.5   References

[1]   J. L. Gottfried, *Phys. Chem. Chem. Phys.* **2014**, *16*, 21452−21466.

[2]   J. L. Gottfried, *Propellants Explos. Pyrotech.* **2015**, *40*, 674–681.

[3]   J. L. Gottfried, E. J. Bukowski, *Appl. Opt.* **2016**, *56*, B47–B57.

[4]   N. Fischer, D. Fischer, T. M. Klapötke, D. G. Piercey, J. Stierstorfer, *J. Mater. Chem.* **2012**, *22*, 20418–20422.

[5]   A. A. Dippold, T. M. Klapötke, *J. Am. Chem. Soc.* **2013**, *135*, 9931–9938.

[6]   a) D. Fischer, *High Performing and Nitrogen-Rich High Energy Density Materials*, PhD Thesis, **2015**, Department of Chemistry, Ludwig-Maximilian University of Munich, Germany; b) D. Fischer, J. L. Gottfried, T. M. Klapötke, K. Karaghiosoff, J. Stierstorfer, T. G. Witkowski, *Angew. Chem. Int. Ed. Engl.*, **2016** , *55*, 16132–16135.

[7]   T. M. Klapötke, T. G. Witkowski, *ChemPlusChem* **2016**, *81*, 357–360.

[8]   G. D. Solodyuk, M. D. Boldyrev, B. V. Gidaspov, V. D. Nikolaev, *Zh. Org. Khim.*, **1981**, *17*, 861–865.

[9]   M. Szala, A. Kruzel, L. Szymańczyk, *High-Energ. Mater.* **2012**, *4*, 27–35.

[10]   T. M. Klapötke, T. G. Witkowski, Z. Wilk, J. Hadzik, *Propellants Explos. Pyrotech.*, **2016**, *41*, 92–97.

[11]   J. L. Gottfried, *Appl. Opt.*, **2012**, *51*, B13–B21.

[12]   E. S. Collins, J. L. Gottfried, *Laser-Induced Deflagration of Energetic Materials*, Insensitive Munitions and Energetic Materials Technology Symposium, Rome, Italy, **2015**.

[13]   A. E. Kramida, Y. Ralchenko, J. Reader, N. A. Team, *NIST Atomic Spectra Database (version 5.1)*, National Institute of Standards and Technology, Gaithersburg, MD, **2013**.

[14] R. W. B. Pearse, A. G. Gaydon, The Identification of Molecular Spectra, 4th edition, Wiley, New York, **1976**.

[15] H. Meinel, G. Messerle, *Astrophys. J.* **1968**, *154*, 381–384.

[16] M. Sućeska, *Propellants Explos. Pyrotech.* **1991**, *16*, 197–202.

[17] M. Sućeska, *Propellants. Explos. Pyrotech.* **1999**, *24*, 280–285.

[18] M. Sućeska, *Computer Program for Calculation of Detonation Parameters*, Proceedings of the 32nd Int. Annual Conference of ICT, Karlsruhe, Germany, **2001**, 110(1–13).

[19] M. Sućeska, *Mater. Sci. Forum* **2004**, *465–466*, 325–330.

[20] M. Sućeska, *EXPLO5*, Version 6.01, Zagreb, Croatia, **2013**.

[21] S. Bastea, L. E. Fried, K. R. Glaesemann, W. M. Howard, I.-F. W. Kuo, P. C. Souers, P. A. Vitello, *CHEETAH 8.0*, Energetic Materials Center, Lawrence Livermore National Laboratory, Livermore, CA.

[22] E. G. Francois, D. E. Chavez, M. M. Sandstrom, *Propellants Explos. Pyrotech.* **2010**, *35*, 529–534.

[23] W. P. Zhang, F. Q. Bi, Y. S. Wang, T. F. Huang, W. X. Li, C. L. Wang and S. X. Zhao, *Chin. J. Explos. Propellants* **2015**, *38*, 67–71.

8.6 Supplementary information

The analytical methods, general procedures, and computational details are described in the appendix of this thesis.

8.6.1 Physico-chemical properties of the investigated explosives

Table 1. Physico-chemical properties of TKX-50, MAD-X1, BDNAPM, BTNPM, TKX-55, and DAAF

	TKX-50[1]	MAD-X1[2]	BDNAPM[3]	BTNPM[3]	TKX-55[4]	DAAF
Formula	$C_2H_8N_{10}O_4$	$C_4H_8N_{10}O_8$	$C_7H_6N_{10}O_8$	$C_7H_2N_{10}O_{12}$	$C_{16}H_4N_{10}O_{14}$	$C_4H_4N_8O_3$
MW [g·mol^{-1}]	236.15	324.2	358.19	418.15	560.26	212.13
IS[a] [J]	20	>40	11	4	5	7[5]
FS[b] [N]	120	>360	>360	144	> 360	>360[5]
ESD[c] [J]	0.10	0.50	>1	0.6	1.0	0.0625[5]
N[d] [%]	59.31	43.21	39.10	33.50	25.00	52.82
Ω[e] [%]	−27.10	−19.74	−40.20	−11.48	−57.11	−52.79
T_m[f] [°C]	−	−	−	−	−	−
T_{dec}[g] [°C]	221	217	310	200	335	229[5]
ρ[h] [g·cm^{-3}]	1.877	1.90	1.802	1.934	1.837	1.745[6]
$\Delta_f H^o$[i] [kJ·mol^{-1}]	447	213	205	379	198	443$^{i)}$[5]
EXPLO5 V6.01						
$-\Delta_E U^o$[j] [kJ·kg^{-1}]	5892	5631	4942	6147	4962	5081
T_{C-J}[k] [K]	3623	3722	3554	4526	3683	3589
p_{C-J}[l] [GPa]	40.0	39.3	29.6	39.1	27.3	27.5
V_{C-J}[m] [m·s^{-1}]	9767	9195	8332	9304	8030	8316
Gas vol.[n] [dm^3·kg^{-1}]	913	786	719	720	604	758
CHEETAH v8.0						
$-\Delta_E U^o$[j] [kJ·kg^{-1}]	5862	5792	4854	6132	4560	4853
T_{C-J}[k] [K]	2845	3248	3205	4375	3498	3061
p_{C-J}[l] [GPa]	42.4	38.3	28.0	38.8	24.9	26.3
V_{C-J}[m] [m·s^{-1}]	9735	9267	8171	9276	7548	8124
Gas vol.[n] [dm^3·kg^{-1}]	925	865	766	757	660	777

[a] Impact sensitivity; [b] Friction sensitivity; [c] Electrostatic discharge device (OZM research); [d] Nitrogen content; [e] Oxygen balance; [f] Melting temperature; [g] Temperature of decomposition; [h] Density at 298 K; [i] Standard molar enthalpy of formation ($^{i)}$ measured); [j] Heat of detonation; [k] Detonation temperature; [l] Detonation pressure; [m] Detonation velocity; [n] Volume of detonation gases at standard temperature and pressure conditions.

Table 2. Physico-chemical properties of TNT, HNS, NTO, RDX, and ε-CL-20.

	TNT	HNS	NTO	RDX	ε-CL-20
Formula	$C_7H_5N_3O_6$	$C_{14}H_6N_6O_{12}$	$C_2H_2N_4O_3$	$C_3H_6N_6O_6$	$C_6H_6N_{12}O_{12}$
MW [g·mol^{-1}]	227.13	450.23	130.06	222.12	438.19
$IS^{[a]}$ [J]	15[7]	5[7, 8]	>120[7]	7.5[7]	4[7]
$FS^{[b]}$ [N]	> 353[7]	240[7, 8]	>353[7]	120[7]	48[7]
$ESD^{[c]}$ [J]	*nd*	0.8	>4.5[9]	0.20[1, 10]	0.13[1, 10]
$N^{[d]}$ [%]	18.50	18.67	43.08	37.84	38.3
$\Omega^{[e]}$ [%]	−73.96	−67.52	−24.60	−21.61	−10.95
$T_m^{[f]}$ [°C]	81[11]	318[7]	271[12]	205[13]	–
$T_{dec}^{[g]}$ [°C]	290[14]	318[7]	271[12]	210[2]	219[15]
$\rho^{[h]}$ [g·cm^{-3}]	1.648[16]	1.745[17]	1.916[18]	1.806[19]	2.035[20]
$\Delta_f H°^{[i]}$ [kJ·mol^{-1}]	−56	78	−129[i)][21]	86	365
EXPLO5 V6.01					
$-\Delta_E U°^{[j]}$ [kJ·kg^{-1}]	4925	5146	3673	5798	6130
$T_{C-J}^{[k]}$ [K]	3422	3675	2868	3831	4102
$p_{C-J}^{[l]}$ [GPa]	21.1	24.5	30.6	35.4	44.9
$V_{C-J}^{[m]}$ [m·s^{-1}]	7286	7629	8420	8834	9673
Gas vol.$^{[n]}$ [dm^3·kg^{-1}]	646	601	734	792	724
CHEETAH v8.0					
$-\Delta_E U°^{[j]}$ [kJ·kg^{-1}]	4476	4597	3685	5853	6139
$T_{C-J}^{[k]}$ [K]	3240	3518	2346	3482	3771
$p_{C-J}^{[l]}$ [GPa]	20.0	22.9	34.5	33.8	43.8
$V_{C-J}^{[m]}$ [m·s^{-1}]	7192	7499	8656	8803	9833
Gas vol.$^{[n]}$ [dm^3·kg^{-1}]	716	695	751	891	816

8.6.2 References

[1] N. Fischer, D. Fischer, T. M. Klapötke, D. G. Piercey, J. Stierstorfer, *J. Mater. Chem.* **2012**, *22*, 20418–20422.

[2] A. A. Dippold, T. M. Klapötke, *J. Am. Chem. Soc.* **2013**, *135*, 9931–9938.

[3] a) D. Fischer, *High Performing and Nitrogen-Rich High Energy Density Materials*, PhD Thesis, **2015**, Department of Chemistry, Ludwig-Maximilian Univeristy of Munich, Germany; b) D. Fischer, J. L. Gottfried, T. M. Klapötke, K. Karaghiosoff, J. Stierstorfer, T. G. Witkowski; *Angew. Chem. Int. Ed. Engl.*, **2016** , *55*, 16132–16135.

[4] T. M. Klapötke, T. G. Witkowski, *ChemPlusChem* **2016**, *81*, 357–360.

[5] E. G. Francois, D. E. Chavez, M. M. Sandstrom, *Propellants, Explos., Pyrotech.* **2010**, *35*, 529–534.

[6] R. Gilardi, X-ray density (for details see CCDC 134715; https://summary.ccdc.cam.ac.uk/structure-summary-form).

[7] R. Meyer, J. Köhler, A. Homburg, *Explosives*, 7th Edition, Wiley, Weinheim, **2016**.

[8] T. M. Klapötke, *Chemistry of High-energy Materials*, 3th Edition, De Gruyter, Berlin, **2015**.

[9] R. J. Spear, C. N. Louey, M. G. Wolfson, *A Preliminary Assessment of 3-Nitro-1,2,4-Triazol-5-One (NTO) as an Insensitive High Explosive*, ADA215063. Materials Research Laboratory, Australia, **1989**.

[10] J. L. Gottfried, *Phys. Chem. Chem. Phys.* **2014**, *16*, 21452–21466.

[11] R. M. Vrcelj, J. N. Sherwood, A. R. Kennedy, H. G. Gallagher, T. Gelbrich, *Cryst. Growth Des.* **2003**, *3*, 1027–1032.

[12] M. Szala, S. Cudziło, R. Lewczuk, *Bull. Mil. Univ. Technol.* **2011**, *60*, 407–419.

[13] J. P. Agrawal, *High Energy Materials: Propellants, Explosives and Pyrotechnics*, Wiley, **2010**.

[14] J. Zhu, S. Jin, L. Wan, C. Zhang, L. Li, S. Chen, Q. Shu, *Dalton Trans.* **2016**, *45*, 3590–3598.

[15] R. Turcotte, M. Vachon, Q. S. M. Kwok, R. Wang, D. E. G. Jones, *Thermochim. Acta* **2005**, *433*, 105–115.

[16] N. I. Golovina, A. N. Titkov, A. V. Raevskii, L. O. Atovmyan, *J. Solid State Chem.* **1994**, *113*, 229–238.

[17] F. Gerard, A. Hardy, *Acta Crystallogr., Sect. C: Struct. Chem.* **1988**, *44*, 1283–1287.

[18] N. Bolotina, K. Kirschbaum, A. A. Pinkerton, *Acta Crystallogr., Sect. B: Struct. Sci., Cryst. Eng. Mater.* **2005**, *61*, 577–584.

[19] C. S. Choi, E. Prince, *Acta Crystallogr., Sect. B: Struct. Sci., Cryst. Eng. Mater.* **1972**, *28*, 2857–2862.

[20] N. B. Bolotin, M. J. Hardie, R. L. Speer Jr, A. A. Pinkerton, *J. Appl. Crystallogr.* **2004**, *37*, 808–814.

[21] A. Finch, P. J. Gardner, A. J. Head, H. S. Majdi, *J. Chem. Thermodyn.* **1991**, *23*, 1169–1173.

Synthesis and Characterization of

5-methyl-2,4,6-trinitrobenzene-1,3-diol and its Energetic Cesium Salt
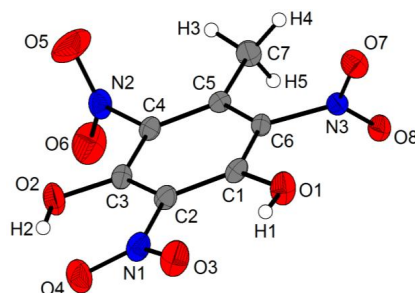
Abstract: The synthesis and characterization of the primary explosive cesium 5-methyl-2,4,6-trinitrobenzene-1,3-diolate (**3**) as well as its precursor compounds is described. The compounds were isolated as pure substances and characterized using multinuclear (^{1}H, ^{13}C) NMR spectroscopy, vibrational (IR and Raman) spectroscopy, mass spectrometry and elemental analysis. The thermal behavior of the compounds was established using differential scanning calorimetry. The solid state structure of 5-methyl-2,4,6-tri-nitrobenzene-1,3-diol (**2**) was determined using low temperature single crystal X-ray diffraction. The friction and impact sensitivity tests were carried out using the BAM friction tester and BAM drophammer respectively. The sensitivities of the compounds towards electrostatic discharge (ESD) were determined using a small-scale ESD device (OZM). The gas phase absolute molar enthalpy at 298.15 K and 1 atm for **2** was computed applying the CBS-4M method using the GAUSSIAN 09 program package. Gas phase standard molar enthalpy of formation ($\Delta_f H_{(g)}°$) for **2** at 298 K was computed using the atomization energy method. Standard molar enthalpy of formation ($\Delta_f H°$) for **2** was calculated using $\Delta_f H_{(g)}°$ and the standard molar enthalpy of sublimation by applying Trouton's rule. The detonation parameters for the covalent compounds which were investigated were calculated using EXPLO5 V6.03 thermochemical computer code, using the calculated $\Delta_f H°$ values and the densities which were either obtained from X-ray diffraction at 298.15 K or were recalculated from values obtained at 173 K.

Keywords: primary explosives · structure elucidation · 2,4,6-trinitroorcinol · energetic materials

9.1 Introduction

Primary explosives are highly sensitive to different sources of stimuli (*e.g.* impact, friction, electrostatic discharge, light, flame, and heat). Furthermore, primary explosives show a much faster transition from deflagration to detonation (DDT) than secondary explosives and generate a detonation wave which is able to trigger high performing but less sensitive secondary explosives or propellants.[1] The first primary explosive that found widespread application was mercury fulminate (MF), which was used by Alfred Nobel in metal blasting cap detonators to initiate dynamite.[1-9] During the last century, MF was replaced by lead azide (LA) and lead styphnate (LS) which show lower toxicity, improved performance and better thermal stability.[10-14] LA has many advantageous properties which makes it still the most commonly used primary explosive: LA is resistant to heat and moisture, not very hygroscopic, more effective than MF even in smaller quantities, higher triggering rate than MF. Moreover, in contrast to MF, LA cannot be dead pressed.[11, 13, 15]

Unfortunately, LA is highly sensitive to friction and needs to be phlegmatized.[1, 13] Moreover, it slowly decomposes in presence of moist air containing carbon dioxide to form extremely toxic hydrazoic acid (HN_3) and basic lead carbonate.[13, 16] Hydrazoic acid can further react with copper metal in the encapsulating casing to give the highly sensitive to impact and friction copper(II) azide.[13, 16] LA decomposes in the presence of acids.[13, 17] Finally, the environmental concerns associated with the toxicity of lead are also one of the most important drawbacks of LA.[13, 16]

Therefore, research concerned with finding suitable replacements for lead containing primary explosives is an essential aspect of present investigations in the energetic materials field. For a compound to be considered as a possible LA replacement, it has to meet the following minimum requirements: (*a*) insensitivity to light; (*b*) sensitivity to detonation but not too sensitive to handle and transport; (*c*) thermal stability of at least 200 °C, (*d*) chemically stable for long periods time; (*e*) free of toxic metals; and (*f*) free of toxic perchlorate.[18]

Among recently synthesized metal-containing ionic primary explosives, the following are the promising candidates for possible application as primary explosives: iron and copper complexes of the type $[cat]^+_2[M(NT)_4(H_2O)_2]$ ($[cat]^+ = NH_4^+$, Na^+; $M = Fe^{2+}$, Cu^{2+}; NT = 5-nitrotetrazolate),[18] copper(II) bis(1-methyl-5-nitriminotetrazolate),[19] copper(I) 5-nitrotetrazolate (DBX-1),[20] calcium 5-nitriminotetrazolate,[21] potassium 5,7-dinitro-[2,1,3]-benzoxadiazol-4-olate-3-oxide (KDNP)[22] and potassium 1,1'-dinitramino-5,5'-bis(tetrazolate) (K₂DNABT).[23]

Until now, the most mostly investigated energetic materials containing both, a 2,4,6-trinitrobenzene moiety and hydroxy functionalities were based on picric acid (PA) and styphnic acid (SA) (Figure 1).

Building on our current extensive research in the field of energetic materials, we decided to focus on decreasing the sensitivity to external stimuli of 2,4,6-trinitrobenzene-1,3-diol (SA) based salts by inserting a methyl group in the five-position of the benzene ring (5-methyl-2,4,6-trinitrobenzene-1,3-diol, TNO – Figure 1)
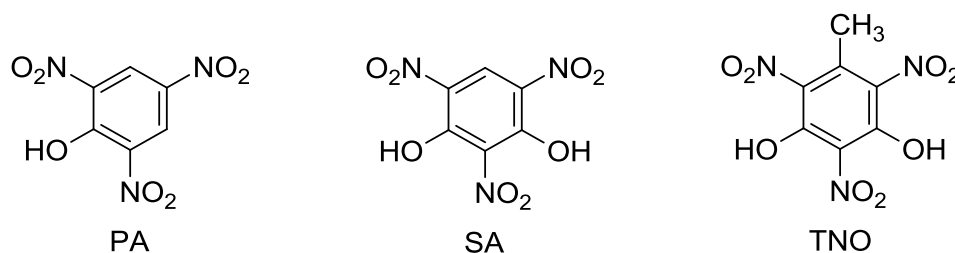
Figure 1. Chemical structures of PA, SA and TNO.

The synthesis of PA from phenol using nitric acid was reported in 1841 by Laurent.[24] In 1871 Sprengel reported that PA can be detonated.[25] The explosive power of picric acid is slightly superior to that of 2,4,6-trinitrotoluene (TNT).[15] The main drawback of PA is its tendency to form impact sensitive metal salts (picrates) when it is in direct contact with metal shell walls.[15] Among investigated picric acid salts, the best known is lead picrate which was used in various initiating compositions and in mixtures for electric fuseheads.[14] Handling of anhydrous lead picrate has the same risk level as handling LS.[14] Unfortunately, the environmental concerns associated with the toxicity of lead excluded further practical application of lead picrate. SA is a relatively weak explosive which can be obtained *via* nitration of either resorcinol or 2-nitroresorcinol using sulfuric acid and potassium nitrate.[15, 26] The most important salt of SA is, as described above, LS. Barium styphnate is not very sensitive to impact and its brisance is lower than for LS.[14] It is used in delay compositions, as an ingredient of primary compositions.[14] Silver styphnate is characterized by sensitivity to impact similar to LS and high sensitivity to flames. It has been proposed as a primary explosive.[14]

Herein, we present the synthesis and investigation of 5-methyl-2,4,6-trinitrobenzene-1,3-diol and its energetic cesium salt. The nitration of 3,5-dihydroxytoluene monohydrate using mixture of concentrated nitric acid and concentrated sulfuric acid was performed accordingly to the methodology presented by Marchand and Reddy[27] while synthesis and characterization of the cesium salt is presented for the first time.

9.2 Results and Discussion

9.2.1 Synthesis

The first step in the synthesis of cesium 5-methyl-2,4,6-trinitrobenzene-1,3-diolate (**3**) is the nitration of 3,5-dihydroxytoluene monohydrate (**1**) using concentrated nitric and sulfuric acids to form 5-methyl-2,4,6-trinitrobenzene-1,3-diol (**2**) following a modified method of Marchand and Reddy.[27] The next step is the reaction of **2** with cesium hydroxide monohydrate to give the final product **3** (Scheme 1).
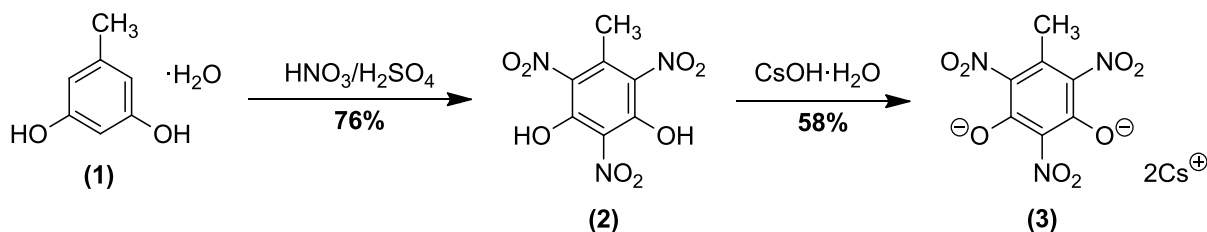
Scheme 1. Synthesis of cesium 5-methyl-2,4,6-trinitrobenzene-1,3-diolate (**3**).

9.2.2 Single-crystal X-ray analysis

The single crystal X-ray diffraction dataset of **2** was collected using an Oxford Xcalibur3 diffractometer with a Spellman generator (voltage 50 kV, current 40 mA), enhanced molybdenum $K\alpha$ radiation source ($\lambda = 0.71073$ Å), Oxford Cryostream cooling unit, four circle kappa platform and a Sapphire CCD detector. By using the CRYSALISPRO software, the data collection and reduction were performed.[28] The structure was solved with SIR-97,[29] refined by full-matrix least-squares on F^2 with SHELXL-97,[30, 31] and checked with PLATON,[32-34] which are all integrated within the WINGX software suite.[35] The non-hydrogen atoms were refined anisotropically and the hydrogen atoms were located and freely refined. The finalized CIF file was checked with CHECKCIF.[36] Illustrations of molecular structures were drawn with DIAMOND 4.[37] CCDC 1476881 contains the supplementary crystallographic data for this paper. These data can be obtained free of charge from the Cambridge Crystallographic Data Centre *via* www.ccdc.cam.ac.uk/data_request/cif.

5-Methyl-2,4,6-trinitrobenzene-1,3-diol (**2**) crystallizes from ethyl acetate in the orthorhombic space group $P2_12_12_1$ with a calculated density of 1.759 g·cm^{-3} at 123 K and four molecules in the unit cell (Table 1). The molecular structure of **2** is shown in Figure 2.

Table 1. Crystallographic data and refinement parameters of **2**.

	2
Chemical formula	$C_7H_5N_3O_8$
Molecular weight [$g \cdot mol^{-1}$]	259.14
Color, habit	pale yellow rod
Size [mm]	0.40x0.10x0.03
Crystal system	Orthorhombic
Space group	$P2_12_12_1$ (No. 19)
a [Å]	5.5309(2)
b [Å]	8.0469(3)
c [Å]	21.9802(8)
α [°]	90
β [°]	90
γ [°]	90
V [$Å^3$]	978.26(6)
Z	4
ρ_{calc} [$g \cdot cm^{-3}$]	1.759
μ [mm^{-1}]	0.165
$\lambda_{MoK\alpha}$ [Å]	0.71073
$F(000)$	528
θ min-max [°]	4.125-30.499
T [K]	123(2)
Dataset h	$-7 \leq h \leq 7$
Dataset k	$-11 \leq k \leq 11$
Dataset l	$-31 \leq l \leq 31$
Reflections collected	10066
Independent reflections	2973
Observed reflections	2627
Number of parameters	173
R_{int}	0.0303
GoF on F^2	1.062
R_1, wR_2 ($I>\sigma I_0$)	0.0366, 0.0866
R_1, wR_2 (all data)	0.0446, 0.0925
Weighting scheme (x, y)[a]	0.0419, 0.1917
Remaining density [$e \cdot Å^{-3}$]	-0.191, 0.267
Device type	Oxford XCalibur3 CCD
Solution	SIR-97
Refinement	SHELXL-97
Absorption correction	multi-scan
CCDC	1476881

[a] $wR_2 = \{\Sigma[w(F_o^2 - F_c^2)^2] / \Sigma[w(F_o^2)^2]\}^{1/2}$ where $w = 1 / [\sigma_c^2(F_o^2) + (xP)^2 + yP]$ and $P = (F_o^2 + 2F_c^2) / 3$
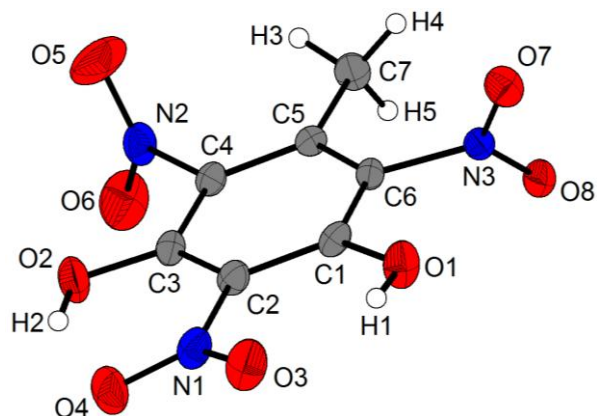
Figure 2. Molecular structure of 5-methyl-2,4,6-trinitrobenzene-1,3-diol (**2**) in the crystal. Thermal ellipsoids are drawn at the 50% probability level, and H atoms are shown as spheres of arbitrary radii. Selected bond lengths [Å]: C1−C2 1.414(3), C1−C6 1.389(2), C1−O1 1.332(2), C2−C3 1.403(3), C2−N1 1.443(3), C3−C4 1.390(3), C3−O2 1.335(3), C4−C5 1.390(3), C4−N2 1.464(2), C5−C6 1.387(2), C5−C7 1.501(3), C6−N3 1.468(2), N1−O3 1.232(2), N1−O4 1.236(3), N2−O5 1.214(3), N2−O6 1.210(3), N3−O7 1.227(2), N3−O8 1.220(2). Selected bond angles [°]: C1−C6−N3 115.4(2), C2−C1−O1 124.9(2), C2−N1−O3 119.0(2), C2−N1−O4 118.7(2), C3−C2−N1 120.1(2), C4−C3−O2 116.0(2), C4−N2−O5 117.1(2), C4−N2−O6 118.5(2), C5−C4−N2 119.7(2), C6−C5−C7 122.8(2), C6−N3−O7 117.5(2), C6−N3−O8 118.1(2).

In the solid state structure of **2**, the *ortho*-nitro groups are significantly twisted out of the benzene ring plane (∡C5–C4–N2–O6, 101.8(2)°; ∡C5–C6–N3–O7 114.1(2)°), while the *para*-nitro group is only slightly twisted out of the ring plane (∡C1–C2–N1–O3, 7.9(3)°). Two strong intramolecular O–H⋯O hydrogen bonding interactions are observed in the solid state structure of **2** (Table 2), which are similar to those reported for the related compound 5-methoxy-2,4,6-trinitro-1,3-benzenediol by Deschamps and Straessler.[38]

Table 2. Intramolecular hydrogen bonds within the crystal structure of **2**.

D–H⋯A	**d(D–H) [Å]**	**d(H⋯A) [Å]**	**d(D⋯A) [Å]**	**∡DHA [°]**
O1–H1⋯O3	0.78(4)	1.93(4)	2.570(2)	139(4)
O2–H2⋯O4	0.83(3)	1.88(3)	2.591(2)	143(3)

9.2.3 Thermal Stabilities and Sensitivities

The thermal stabilities of **2**, and **3** were measured using differential scanning calorimetry (DSC, $\beta = 5\,°C\cdot min^{-1}$). Thermal decomposition of **2** occurs at 223 °C (onset value) while compound **3** exhibits superior thermal stability with an onset value for exothermic decomposition at 255 °C.

For initial safety testing, the impact, friction, and electrostatic discharge sensitivities were determined. The impact sensitivity of **2** was measured to be 17.5 J and the friction sensitivity is lower (*FS* > 360 N) than the measuring range of the friction tester apparatus. In terms of *IS* and *FS*, **2** is less sensitive than picric acid (PA) and styphnic acid (SA). Moreover, **2** shows low sensitivity to electrostatic discharge (*ESD* = 0.75 J; typical values for the human body are

within the range $5 - 20$ mJ).[1] The lower sensitivities of **2** to external stimuli make it a suitable starting material for the synthesis of primary explosives.

The cesium salt (**3**) is much more sensitive to impact ($1 < IS < 2$ J; $IS_{LA} = 2.4$ J[1]), friction ($FS = 24$ N; $FS_{LA} = 0.1$ N[1]), and electrostatic discharge ($ESD = 5$ mJ; $ESD_{LA} = 4.7$ mJ[1]) than its precursor **2**. Based on this data, **3** can be placed in the most sensitive classes in terms of its both friction and impact sensitivity according to the UN Recommendations on the Transport of Dangerous Goods (*impact: insensitive >40 J, less sensitive ≥35 J, sensitive ≥4 J, very sensitive ≤3 J; friction: insensitive > 360 N, less sensitive = 360 N, sensitive <360 N and >80 N, very sensitive ≤80 N, extremely sensitive ≤10 N*).[39]

A preliminary flame test using a small amount of **3** (approximately 5 mg) - in which the compound was heated on a spatula using a lighter but without direct flame contact - showed that compound **3** detonated upon reaching its ignition temperature.

9.2.4   Energetic Properties

The gas-phase absolute molar enthalpy at 298 K and 1 atm for **2** was calculated theoretically using the modified complete basis set method (CBS-4M) with the GAUSSIAN 09 software.[40-42] The atomization-energy method was applied in order to calculate the gas phase standard molar enthalpy of formation ($\Delta_f H_{(g)}°$) at 298.15 K.[42-45] In order to obtain the standard molar enthalpy of formation ($\Delta_f H°$) the value of the standard molar enthalpy of sublimation (estimated using Trouton's rule) was subtracted from $\Delta_f H_{(g)}°$.[46, 47] The values of $\Delta_f H°$ for PA and SA were taken from the literature (Table 3).[48, 49]

The Chapman-Jouguet (C-J) characteristics (detonation temperature, detonation pressure, detonation velocity) for the precursor (**2**) of the primary explosive (**3**), were calculated using EXPLO5 V6.03 thermochemical computer code.[50] Additionally, for comparison reasons, calculations were also performed for PA and SA (Table 4).

The detonation parameters were calculated based on the $\Delta_f H°$ values and the densities using the EXPLO5 V6.03 thermochemical computer code.[50] In the cases of PA and SA, the theoretical maximum densities obtained from X-ray diffraction measurements at 298 K were used,[51, 52] while for **2**, the density was re-calculated from the single crystal density determined at 123 K using the Equation 1[53] and the coefficient of volume expansion (α_v) of 2,4,6-trinitrotoluene (the orthorhombic form, $\alpha_v = 19.8 \times 10^{-5}$ K^{-1}).[54]

$$\rho_{298} = \frac{\rho_T}{1 + \alpha_v(298 - T)} \tag{1}$$

The calculations for explosives assume ideal behavior and estimation of the detonation parameters is based on the chemical equilibrium steady-state model of detonation.[50]

The thermodynamic functions of the detonation products in the standard state are calculated from the enthalpy (which is expressed in a fourth degree polynomial form as a function of temperature).[50] The Becker-Kistiakowsky-Wilson equation of state (BKW EOS) with the BKWN set of constants: $\alpha = 0.5$, $\beta = 0.38$, $\kappa = 9.4$, and $\Theta = 4120$ for gaseous detonation products, and the Murnaghan equation of state for condensed products (compressible solids and liquids) were applied.[50] The calculation of the equilibrium composition of the detonation products uses a modified version of White, Johnson and Dantzig's free energy minimization technique.[50]

Table 3. Physico-chemical properties of PA, SA and **2**.

	PA	**SA**	**2**
Formula	$C_6H_3N_3O_7$	$C_6H_3N_3O_8$	$C_7H_5N_3O_8$
$IS^{[a]}$ [J]	7.4[15]	7.4[15]	17.5
$FS^{[b]}$ [N]	> 353[15]	353[15]	> 360
$ESD^{[c]}$ [J]	*nd*	*nd*	0.75
$N^{[d]}$ [%]	18.34	17.15	16.22
$\Omega^{[e]}$ [%]	−45.39	−35.9	−52.48
$T_m^{[f]}$ [°C]	122 (I polymorph)[55] 105 (II polymorph)[55] 75 (III polymorph)[55]	181.6[56]	172
$T_{dec}^{[g]}$ [°C]	*nd*	*nd*	223
$\rho^{[h]}$ [g·cm^{-3}]	1.769[51]	1.829[52]	1.700
$\Delta_f H°^{[i]}$ [kJ·mol^{-1}]	−218[48]	−468[49]	−410
EXPLO5 V6.03			
$-\Delta_E U°^{[j]}$ [kJ·kg^{-1}]	4537	4146	4079
$T_{C-J}^{[k]}$ [K]	3440	3203	3091
$p_{C-J}^{[l]}$ [GPa]	23.4	24.0	20.1
$V_{C-J}^{[m]}$ [m·s^{-1}]	7436	7522	6986
Gas vol.$^{[n]}$ [dm^3·kg^{-1}]	631	623	641

[a] Impact sensitivity (BAM drophammer, method 1 of 6); [b] friction sensitivity (BAM drophammer, method 1 of 6); [c] electrostatic discharge device (OZM research); [d] nitrogen content; [e] oxygen balance; [f] Melting point; [g] temperature of decomposition; [h] density at 298 K; [i] standard molar enthalpy of formation; [j] heat of detonation; [k] detonation temperature; [l] detonation pressure; [m] detonation velocity; [n] volume of detonation gases at standard temperature and pressure conditions.

9.3   Conclusions

The introduction of the second hydroxy group to the PA molecule has practically no influence on the *IS* and *FS*. However, SA has a higher melting point, density and oxygen balance than PA. Incorporation of the methyl group in the five-position of the SA molecule results in a decrease in the sensitivities to external stimuli (*IS*, *FS*). This is of great importance in terms of safety. The presence of the methyl group in **2** results in a reduction in the nitrogen content, oxygen balance, and density compared to PA and SA. The lower density and the relatively low enthalpy of formation of **2** are reflected in the lower values

of the detonation parameters of **2**. Nevertheless, these important factors are still relatively high, and therefore **2** could be used as a starting material in the synthesis of energetic salts.

The cesium salt (**3**) is characterized by high decomposition temperature (255 °C, onset). Sensitivity investigations shows that **3** is more sensitive to impact than LA, electrostatic sensitivity is in the range of LA while its sensitivity to friction is much lower than this determined for LA. The preliminary flame test and sensitivity to external stimuli measurements show that **3** have properties of primary explosive. Further research in order to determine the ability to initiate of detonation in secondary explosives has to be performed.

9.4   Experimental Section

The analytical methods, general procedures, and computational details are described in the appendix of this thesis.

Caution! All materials prepared are energetic compounds with sensitivities to various stimuli and only small quantities should be prepared and handled. Although we encountered no issues in the handling of these materials, proper protective measures (e.g., face shield, ear protection, body armor, Kevlar gloves, and earthed equipment) should be used, especially if working with primary explosive 3.

5-Methyl-2,4,6-trinitrobenzene-1,3-diol (2):[27] A mixture of concentrated sulfuric (14.0 mL) and concentrated nitric (2.8 mL) acids was cooled to 0 °C. Subsequently, 3,5-dihydroxytoluene monohydrate (4.0 mmol, 568 mg) was dissolved in concentrated sulfuric acid (10 mL) and added slowly in a dropwise manner to the cooled acids. After addition was complete, the reaction mixture was stirred for 1 h at 0 °C. Afterwards, the mixture was poured onto crushed ice (50 mL). The product was extracted from the aqueous phase with ethyl acetate (4 x 50 mL). The extract was evaporated under low pressure. Finally, after drying at high vacuum, the desired product was obtained as fine yellow rods (yield 790 mg, 76%). **DSC** (5 °C·min^{-1}, onset): 172 °C (melt.), 223 °C (dec.); **^{1}H NMR** (400.13 MHz, DMSO-d_6, 26 °C, ppm) δ: 10.66 (s, 2H, OH), 2.25 (s, 3H, CH$_3$), ppm; **^{13}C NMR{^{1}H}** (100.6 MHz, DMSO-d_6, ppm) δ: 152.5, 131.9, 131.4, 129.3, 15.9; **IR** (ATR, cm^{-1}) $\tilde{v}$: 3228 (w), 1608 (m), 1590 (s), 1535 (vs), 1461 (w), 1419 (m), 1362 (vs), 1306 (s), 1258 (m), 1160 (vs), 1144 (vs), 1067 (m), 1045 (m), 914 (w), 897 (s), 829 (w), 802 (m), 784 (s), 751 (m), 739 (m), 717 (w), 694 (s); **Raman** (1064 nm, 300 mW, cm^{-1}) $\tilde{v}$: 2938 (4), 1633 (18), 1540 (10), 1364 (27), 1305 (100), 1273 (11), 1184 (12), 829 (44);**MS** (DEI+): *m/z* = 259.0 [M]$^+$; **EA** (C$_7$H$_5$N$_3$O$_8$, 259.13) calc.: C 32.45, H 1.94,

N 16.22 %; found: C 32.44, H 1.97, N 16.19 %; **IS**: 17.5 J ($< 100\,\mu m$); **FS**: $> 360\,N$ ($<100\,\mu m$); **ESD**: 0.75 J ($<100\,\mu m$).

Cesium 5-methyl-2,4,6-trinitrobenzene-1,3-diolate (3): 5-Methyl-2,4,6-trinitrobenze-ne-1,3-diol (0.48 mmol, 124 mg) was dissolved in 20 mL of ethanol and a solution of cesium hydroxide monohydrate (0.96 mmol, 161 mg) in 5 mL of ethanol was added dropwise. During addition of the cesium hydroxide solution, a red solid immediately precipitated. After addition of the hydroxide was complete, the reaction mixture was heated for 2 hours under reflux. The precipitate was then filtered off and dried under high vacuum yielding red platelets (yield 145 mg, 58%). **DSC** ($5\,°C·min^{-1}$, °C): 255 °C (dec., onset); **^{1}H NMR** (400.13 MHz, DMSO-d_6, 26 °C, ppm) δ: 1.97 (s, 3H, CH_3), ppm; **^{13}C NMR{^{1}H}** (100.6 MHz, DMSO-d_6, 26 °C, ppm) δ: 161.3, 135.6, 131.2, 128.5, 16.1; **IR** (ATR, cm^{-1}) $\tilde{v}$: 2996 (vw), 1567 (vs), 1513 (w), 1494 (m), 1467 (m), 1412 (m), 1384 (w), 1376 (w), 1287 (s), 1232 (vs), 1180 (vs), 1047 (s), 1026 (m), 922 (m), 811 (w), 786 (s), 756 (m), 738 (w), 724 (s), 692 (s), 675 (s); **Raman** (1064 nm, 10 mW, cm^{-1}) $\tilde{v}$: 3006 (2), 2948 (3), 1423 (7), 1379 (7), 1295 (100), 1053 (10), 815 (91), 697 (7); **MS** (FAB^+): $m/z = 133.1$ $[Cs]^+$; (FAB^-): $m/z = 258.2$ $[C_7H_4N_3O_8]^-$; **EA** ($C_7H_3N_3O_8Cs_2$, 522.92) calc.: C 16.08, H 0.58, N 8.04 %; found: C 16.03, H 0.58, N 7.98 %; **IS**: $1 < IS < 2$ J ($<100\,\mu m$); friction tester: 24 N ($< 100\,\mu m$); **ESD**: 5 mJ ($< 100\,\mu m$).

9.5 References

[1] T. M. Klapötke, *Chemistry of High-Energy Materials*, 3rd edition, Walter de Gruyter, Berlin, **2015**.

[2] H. Wieland, *Ber. Dtsch. Chem. Ges.* **1910**, *43*, 3362−3364.

[3] L. Wölhler, *Ber. Dtsch. Chem. Ges.* **1910**, *43*, 754−756.

[4] F. Kurzer, *J. Chem. Educ.* **2000**, *77*, 851−857.

[5] W. Beck, J. Evers, M. Göbel, G. Oehlinger, T. M. Klapötke, *Z. Anorg. Allg. Chem.* **2007**, *633*, 1417−1422.

[6] H. Kast, A. Haid, *Angew. Chem.* **1925**, *38*, 43−52.

[7] R. Matyáš, J. Pachmáň, *Primary Explosives. Fulminates*, Springer, Berlin, **2013**, 37−70.

[8] A. Nobel, *J. R. Soc. Arts* **1875**, *23*, 611−630.

[9] B. T. Fedoroff, O. E. Sheffield, *Encyclopedia of Explosives and Related Items*, Vol. 5, Picatinny Arsenal, Dover, NJ, USA, **1972**, D1588.

[10] B. T. Fedoroff, O. E. Sheffield, *Encyclopedia of Explosives and Related Items*, Vol. 6, Picatinny Arsenal, Dover, NJ, USA, **1974**, F217-F223.

[11] B. T. Fedoroff, O. E. Sheffield, *Encyclopedia of Explosives and Related Items*, Vol. 1, Picatinny Arsenal, Dover, NJ, USA, **1960**, A545-A555.

[12] B. T. Fedoroff, O. E. Sheffield, *Encyclopedia of Explosives and Related Items*, Vol. 5, Picatinny Arsenal, Dover, NJ, USA, **1972**, D1278-D1280.

[13] R. Matyáš, J. Pachmáň, *Primary Explosives. Azides. ,* Springer, Berlin, **2013**, 71−129.

[14] R. Matyáš, J. Pachmáň, *Primary Explosives. Salts of Polynitrophenols*, Springer, Berlin, **2013**, 131−155.

[15] R. Meyer, J. Köhler, A. Homburg, *Explosives*, 7th edition, Wiley, Weinheim, **2016**.

[16] J. J. Sabatini, K. D. Oyler, *Crystals* **2015**, *6*, 5(1−22).

[17] T. Curtius, J. Rissom, *J. Prakt. Chem.* **1898**, *58*, 261−309.

[18] M. H. Huynh, M. A. Hiskey, T. J. Meyer, M. Wetzler, *PNAS* **2006**, *103*, 5409−5412.

[19] G. Geisberger, T. M. Klapötke, J. Stierstorfer, *Eur. J. Inorg. Chem.* **2007**, *2007*, 4743−4750.

[20] J. W. Fronabarger, M. D. Williams, W. B. Sanborn, J. G. Bragg, D. A. Parrish, M. Bichay, *Propellants, Explos., Pyrotech.* **2011**, *36*, 541−550.

[21] N. Fischer, T. M. Klapötke, J. Stierstorfer, *J. Energ. Mater.* **2011**, *29*, 61−74.

[22] J. W. Fronabarger, M. D. Williams, W. B. Sanborn, D. A. Parrish, M. Bichay, *Propellants, Explos., Pyrotech.* **2011**, *36*, 459−470.

[23] D. Fischer, T. M. Klapötke, J. Stierstorfer, *Angew. Chem., Int. Ed.* **2014**, *53*, 8172−8175.

[24] A. Laurent, *Ann. Chim. Phys.* **1841**, *3*, 195−228.

[25] H. Sprengel, *J. Chem. Soc.* **1873**, *26*, 796−808.

[26] D. Srinivas, V. D. Ghule, K. Muralidharan, *New J. Chem.* **2014**, *38*, 3699−3707.

[27] A. P. Marchand, G. M. Reddy, *Synthesis* **1992**, *1992*, 261−262.

[28] *CrysAlisPro* 1.171.37.33, Agilent Technologies, **2014**.

[29] A. Altomare, M. C. Burla, M. Camalli, G. L. Cascarano, C. Giacovazzo, A. Guagliardi, A. G. G. Moliterni, G. Polidori, R. Spagna, *J. Appl. Crystallogr.* **1999**, *32*, 115−119.

[30] G. M. Sheldrick, *SHELXL-97*, Program for the Refinement of Crystal Structures. University of Göttingen, Germany, **1997**.

[31] G. M. Sheldrick, *Acta Crystallogr., Sect. A: Found. Adv.* **2008**, *64*, 112−122.

[32] A. L. Spek, *PLATON*, A Multipurpose Crystallographic Tool, Utrecht University, The Netherlands, **1999**.

[33] A. Spek, *J. Appl. Crystallogr.* **2003**, *36*, 7−13.

[34] A. Spek, *Acta Crystallogr., Sect. D: Biol. Crystallogr.* **2009**, *65*, 148−155.

[35] L. Farrugia, *J. Appl. Crystallogr.* **1999**, *32*, 837−838.

[36] http://checkcif.iucr.org/.

[37] H. Putz, K. Brandenburg, *Diamond, Version 4.1.2.*, Crystal Impact, Bonn, Germany, **2016**.

[38] J. R. Deschamps, N. A. Straessler, *J. Chem. Crystallogr.* **2011**, *41*, 971−975.

[39] UN Manual of Test and Criteria, *Recommendations on the Transport of Dangerous Goods*, 5th revised edition, United Nations Publication (ST/SG/AC.10/11/Rev.5), **2009**, Geneva.

[40] J. W. Ochterski, G. A. Petersson, J. A. Montgomery, *J. Chem. Phys.* **1996**, *104*, 2598−2619.

[41] J. A. Montgomery, M. J. Frisch, J. W. Ochterski, G. A. Petersson, *J. Chem. Phys.* **2000**, *112*, 6532−6542.

[42] *Gaussian 09, Revision C.01*, M. J. Frisch, G. W. Trucks, H. B. Schlegel, G. E. Scuseria, M. A. Robb, J. R. Cheeseman, G. Scalmani, V. Barone, B. Mennucci, G. A. Petersson, H. Nakatsuji, M. Caricato, X. Li, H. P. Hratchian, A. F. Izmaylov, J. Bloino, G. Zheng, J. L. Sonnenberg, M. Hada, M. Ehara, K. Toyota, R. Fukuda, J. Hasegawa, M. Ishida, T. Nakajima, Y. Honda, O. Kitao, H. Nakai, T. Vreven, J. A. Montgomery, Jr., J. E. Peralta, F. Ogliaro, M. Bearpark, J. J. Heyd, E. Brothers, K. N. Kudin, V. N. Staroverov, R. Kobayashi, J. Normand, K. Raghavachari, A. Rendell, J. C. Burant, S. S. Iyengar, J. Tomasi, M. Cossi, N. Rega, J. M. Millam, M. Klene, J. E. Knox, J. B. Cross, V. Bakken, C. Adamo, J. Jaramillo, R. Gomperts, R. E. Stratmann, O. Yazyev, A. J. Austin, R. Cammi, C. Pomelli, J. W. Ochterski, R. L. Martin, K. Morokuma, V. G. Zakrzewski, G. A. Voth, P. Salvador, J. J. Dannenberg, S. Dapprich, A. D. Daniels, Ö. Farkas, J. B. Foresman, J. V. Ortiz, J. Cioslowski, and D. J. Fox, Gaussian, Inc., Wallingford CT, **2009**.

[43] L. A. Curtiss, K. Raghavachari, P. C. Redfern, J. A. Pople, J. Chem. Phys. **1997**, *106*, 1063−1079.

[44] E. F. C. Byrd, B. M. Rice, J. Phys. Chem. A **2006**, *110*, 1005−1013.

[45] P. J. Linstrom, W. G. Mallard, *National Institute of Standards and Technology*, Gaithersburg MD, 20899.

[46] F. Trouton, *Philos. Mag. (1876-1900)* **1884**, *18*, 54−57.

[47] M. S. Westwell, M. S. Searle, D. J. Wales, D. H. Williams, *J. Am. Chem. Soc.* **1995**, *117*, 5013−5015.

[48] A. Finch, A. E. Smith, *Thermochim. Acta* **1982**, *52*, 317−319.

[49] A. Finch, J. Payne, *Thermochim. Acta* **1990**, *170*, 209−212.

[50] M. Sućeska, *EXPLO5 Version 6.03 User's Guide*, January **2015**.

[51] Y-X. Sun, Z-L. Ren, W-S. Meng, *Asian J. Chem.* **2013**, *25*, 6186−6188.

[52] G. Jerusalem, *J. Chem. Soc., Trans.* **1909**, *95*, 1275−1291.

[53] C. Xue, J. Sun, B. Kang, Y. Liu, X. Liu, G. Song, Q. Xue, *Propellants, Explos., Pyrotech.* **2010**, *35*, 333−338.

[54] R. M. Vrcelj, J. N. Sherwood, A. R. Kennedy, H. G. Gallagher, T. Gelbrich, *Cryst. Growth Des.* **2003**, *3*, 1027−1032.

[55] A. Kofler, M. Brandstätter, *Monatsh. Chem.* **1948**, *78*, 65−70.

[56] P. G. Farrell, F. Shahidi, F. Casellato, C. Vecchi, A. Girelli, *Thermochim. Acta* **1979**, *33*, 275−280.

Nitrogen-Rich Energetic 1,2,5-Oxadiazole-Tetrazole – Based Energetic Materials

H_2BTF　　　　$H_2BOTFAZ$　　　　$H_2BOTFOX$
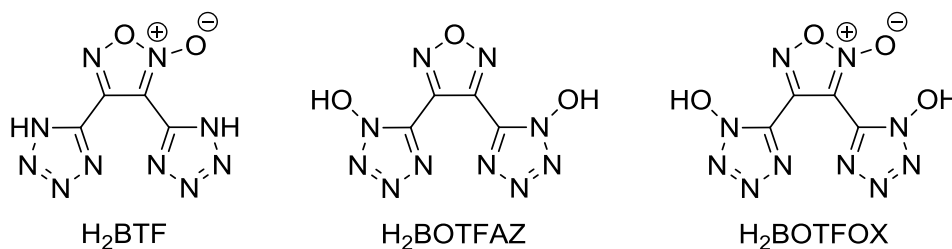
Abstract: Research for new energetic materials with tailored properties is of particular interest in many research groups. In order to meet challenging requirements heterocyclic systems have been investigated. One of the most promising area of research is synthesis of high nitrogen content compounds. Connection of highly endothermic moieties within one molecule attracted attention in recent time. The combination of nitrogen rich tetrazole and tetrazole oxides with oxygen containing furazan and furoxan is a new trend in synthesis of energetic materials with appropriate oxygen balance, high density, and good thermal stability. Various salts have been obtained in order to improve properties in comparison to covalent energetic materials. In this paper results in a recent research for nitrogen rich compounds containing 1,2,5-oxadiazole–tetrazoles species are presented.

Keywords: Furazan · Furoxan · Tetrazole · 1-Hydroxytetrazole · Energetic salts

10.1   Introduction

The energetic materials (EMs) may be characterized as materials whose chemical transformation is accompanied by energy release. Based on amount of the energy content in EMs and on the speed of its release, these materials can be divided into the primers, secondary explosives, "tertiary" explosives, propellants, pyrotechnics, and not least into materials that are dangerous in terms of possible (auto)-ignition (the materials, dangerous by explosion). An explosive on initiation undergoes a self-contained and self-sustained chemical reaction, during which a large amount of heat and gases within a short time are produced. Explosives are classified into different types in different ways depending on their susceptibility to initiation, usage etc. Based on the sensitivity to initiation explosives may be classified as primary and secondary explosives. The former are highly sensitive to different stimuli (*e.g.* heat, impact, friction, light, and electrostatic discharge), which are used to trigger less sensitive but high-performing secondary explosives (or propellants). Primary explosives undergo more rapidly than secondary explosives transition from combustion (or deflagration) to detonation (DDT). High (secondary) explosives are less sensitive than primary explosives and usually possess higher performance (the most important are: heat of explosion, detonation velocity, detonation pressure) than primaries. Propellants are substances or mixtures of substances that burn or deflagrate (in combustion chamber) and they do not undergo DDT. During decomposition a large amount of hot gas is produced as a result of which propulsion is provided. One of the most important performance parameters is the specific impulse (I_{sp}, the change in the impulse per mass unit of the propellant). Pyrotechnics are mostly mixtures of different substances which undergo self-liberating detonative (*e.g.* nona-thermites) or non-detonative exothermic reactions (with reaction rate higher than in the case of propellants), during which different audiovisual effects *e.g.* heat, flame, gas emission, smoke, sound, or a combination of these are generated.

Many EMs have been developed recently in order to meet key requirements including: tailored performance, insensitivity, stability, vulnerability, and environmental safety, low solubility in water and hydrolytic stability (for ecological, and toxicity reasons), longevity and compatibility.

It is of great importance to obtain explosives which contain the oxidizer and fuel in one molecule. In explosives such as TNT, PETN, RDX, HMX (Figure 1, Table 1) the oxidizer and fuel are combined within one molecule. During its detonation heat is released *via* oxidation of the carbon backbone.
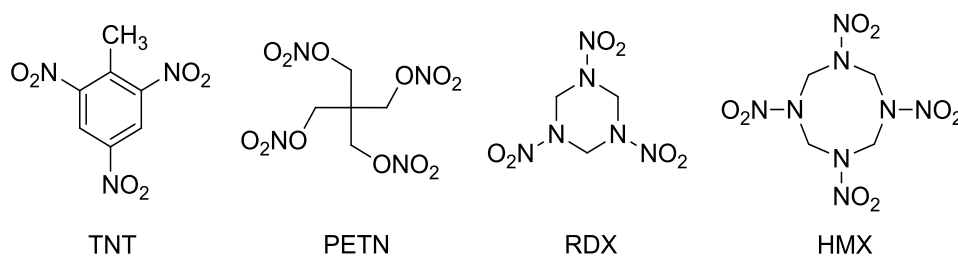
Figure 1. Commonly used explosives.

Table 1. Properties of selected explosives.

	TNT	PETN	RDX	β-HMX
$\rho^{[a]}$ [g·cm^{-3}]	1.713[b][1]/1.648[2]	1.845[3]/1.780[4]	1.858[c][5]/1.806[6]	1.944[d]/1.904[e][7]
$T_m^{[f]}$ [°C]	80[8]	143[9]	204[9]	281[9]
$T_{dec}^{[g]}$ [°C]	290	208[9]	237[9]	285[9]
$\Delta_f H°^{[h]}$ [kJ·mol^{-1}]	−55.5	−479.7	86.3	116.1
$p_{C\text{-}J}^{[i]}$ [GPa]	23.5	31.4	35.4	41.5
$V_{C\text{-}J}^{[j]}$ [m·s^{-1}]	7459	8447	8834	9221
$IS^{[k]}$ [J]	15.0[10]	3.0[10]	7.5[10]	7.4[10]
$FS^{[l]}$ [N]	353[10]	60[10]	120[10]	120[10]

[a] Density from X-ray diffraction, 173 K/298 K, [b] 90 K, [c] 100 K, [d] 123 K, [e] 293 K; [f] Melting temperature; [g] Decomposition temperature; [h] Enthalpy of formation calculated using the GAUSSIAN G09 program package; [i, j] Detonation pressure and detonation velocity calculated using EXPLO5 version 5.05; [k] Impact sensitivity; [l] Friction sensitivity.

EMs, which contain a strained ring or cage structure (TEX, CL-20, ONC, TNAZ, Figure 2), increase the energy of the molecule (comparing with unstrained system) and therein more energy is released during decomposition than in an unstrained system.
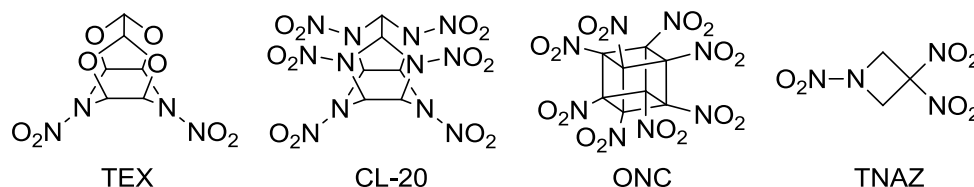
Figure 2. Strained ring or cage structure explosives.

A separate group of EMs are species with high nitrogen content which can be only endothermic. It is due to high nitrogen content. High difference in the bond energies for single, double, and triply bonded nitrogen atoms as well as their strength makes nitrogen a unique element. Therefore, synthesis of high nitrogen content EMs is most promising area for development of new EMs. Many theoretical investigations were conducted to answer the following question: is it possible to obtain poly-nitrogen species which during their decomposition will release only dinitrogen and high amount of energy? Synthesis of N_x species could give excellent EMs with high positive standard enthalpy of formation as well as high detonation parameters (heat of detonation, detonation pressure, detonation temperature), high propulsive or explosive power, high specific impulse and would solve the problem of compatibility (low erosion of gun barrels – no formation of iron carbide),

and toxicity (only N_2 formed as decomposition product). Until now, two homoleptic-nitrogen species are identified, which can be made on a large scale: dinitrogen – isolated in pure form independently by Rutherford, Scheele, Priestley, and Cavendish[11] and the azide anion firstly reported by Curtius.[12] In recent years, many different N_x species were investigated *e.g.*: N_3,[13] N_3^+,[14] N_4,[15] N_4^+,[11, 12, 13e, 14b, c, e, f, 16] N_5^-,[17] N_6,[13c, d, 14d, 18] N_6^{4-},[18a, 19] N_7^-,[20] N_8,[13d, 18a] N_{10},[20–21], N_{13}^+.[20] The thermodynamically most stable N_x systems are based on pentazole units.[22] Among the polynitrogen compounds the isomers of N_6 and N_8 are those which have been mostly investigated theoretically. Most of the theoretical efforts were focused on searching for possible minimum structures of the isomers and on the prediction of their stability. Nevertheless, until know there are no known EMs, which contain only nitrogen atoms. Recently synthesized high nitrogen content EMs contain different nitrogen rich species *e.g.*: hydrazoic acid,[23] tetraazidomethane (TAM),[24] hydrazinium azide,[25] ammonium azide,[26] 5-azido-1*H*-tetrazole (AzT),[27] 3,6-diazido-1,2,4,5-tetrazine (DiAT),[28] 1,1′-azobis(tetrazole) (ABTe),[29] 1,5-diamino-tetrazole (DAT),[30] 5,5′-bis(1*H*-tetrazol-yl)hydrazine (HBT),[31] tri(azido)-1,3,5-triazine (TAT),[32] bis(1*H*-tetrazolyl)amine (H$_2$BTA),[33] 4,4′,6,6′-tetra(azido)azo-1,3,5-triazine (TAAT),[34] 4,4′,6,6′-tetra(azido)hydra-zo-1,3,5-triazine (TAHT),[34] 3,6-dihydrazino-1,2,4,5-tetrazine (DHT),[28a, c, 35] 3,3′-azo-bis(6-amino-1,2,4,5-tetrazine) (DAAT),[35, 36] 2,4,6-triazido-5-(azidomethyl)-pyrimidine (TAAMP),[37] 2,5,8-triazido-*s*-heptazine (TAH),[28a, 38] (Figure 3 and Figure 4).
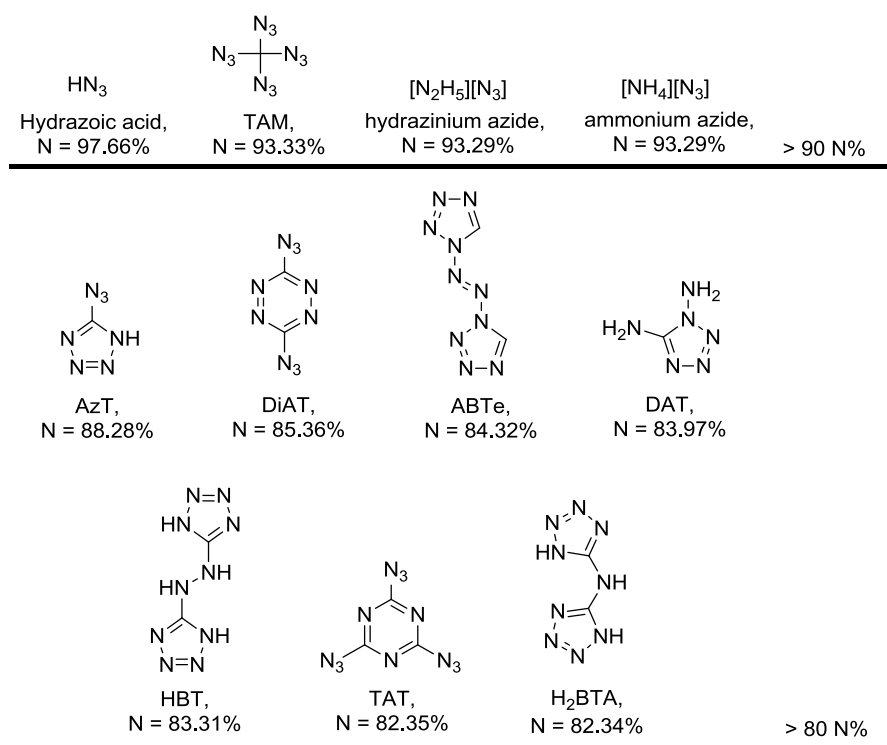
Figure 3. Selected nitrogen-rich chemical compounds (>80 N%).
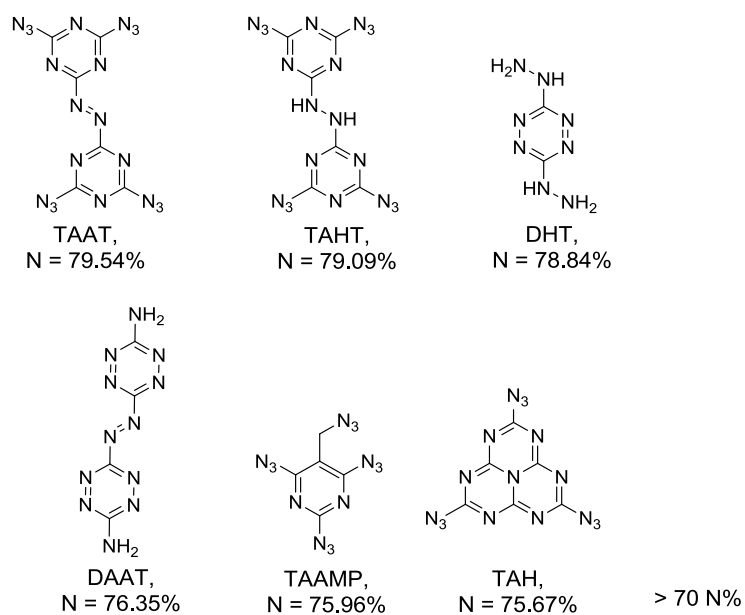
Figure 4. Selected nitrogen-rich chemical compounds (>70 N%).

A review in the field of EMs containing azoles moieties (tetrazole, triazole, imidazole, and pyrazole) is published by Shreeve and Gao.[39]

The combination of highly endothermic heterocycles containing nitrogen as well as oxygen is a new trend in the development of EMs. Numerous EMs containing tetrazole moieties connected with 1,2,5-oxadiazole were investigated. Recent achievements in this area are presented in this paper in order to highlight their properties and thermochemical values.

10.2   Tetrazole-1,2,5-oxadiazole connected Moieties as Energetic Materials

In 2009 Godovikova et al.[40] proposed two methods for synthesis of tetrazolyl-furazans (Scheme 1):

- reaction of 1,2,5-oxadiazole-3,4-dicarbonitrile with sodium azide;
- transformation of 1,2,5-oxadiazole-3,4-dicarbonitrile into corresponding amidrazone followed by its nitrosation with HNO_2.

Because of the higher yield of the final product and single-step synthesis of 3,4-bis(1*H*-tetrazol-5-yl)-1,2,5-oxadiazole from 1,2,5-oxadiazole-3,4-dicarbonitrile the first method is more attractive than synthesis *via* amidrazone (82%, 68%, respectively). Zhou et al. obtained 3,4-bis(1*H*-tetrazol-5-yl)furoxan and its monoanionic[41] and dianionic[42] salts. 3,4-Bis(1-hydroxytetrazolyl)furazan and 3,4-bis(1-hydroxytetrazolyl)furoxan were synthesized in similar manner by Klapötke et al.[43]
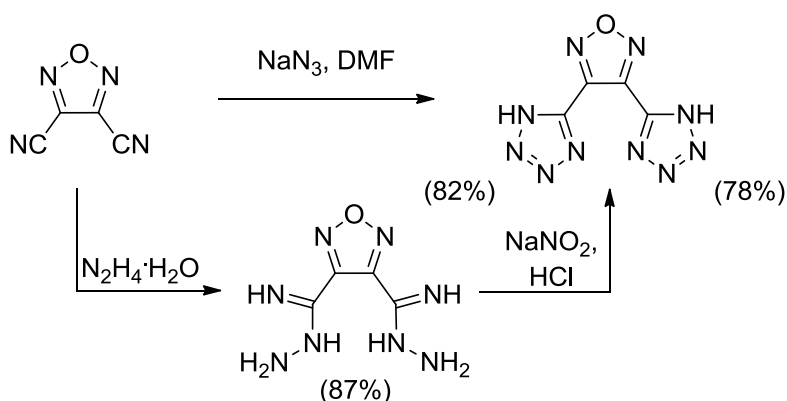
Scheme 1. Synthesis of 3,4-bis(1*H*-tetrazol-5-yl)-1,2,5-oxadiazole.

10.2.1 3,4-Bis(1*H*-tetrazol-5-yl)furoxan and its Energetic Salts

Monoanionic Salts of 3,4-Bis(1H-tetrazol-5-yl)furoxan

3,4-Bis(1*H*-tetrazol-5-yl)furoxan (H$_2$BTF) and its nitrogen-rich energetic monoanionic salts are synthesized by Zhou et. al[41] from 1,2,5-oxadiazole-3,4-dicarbonitrile, sodium azide, and ammonium chloride in DMF with 60% yield (Scheme 2).
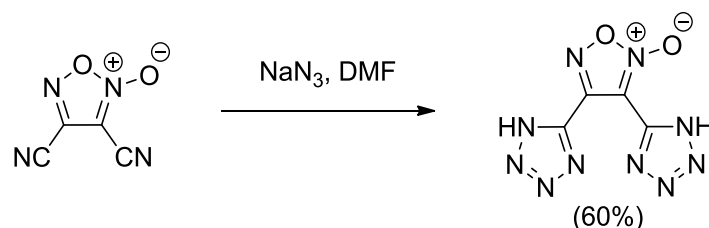
Scheme 2. Synthesis of 3,4-bis(1*H*-5-tetrazolyl)furoxan (H$_2$BTF).

H$_2$BTF was used for the preparation of energetic monoanionic salts, which contain following counter anions: hydrazinium (Hy), 1*H*-1,2,4-triazolium (H1,2,4Tr), 4-amino-1,2,4-triazolium (H1,2,4ATr), 3,4,5-triamino-1,2,4-triazolium (H1,2,4TATr), 1*H*-1,2,3-triazolium (H1,2,3Tr), 1-amino-1,2,3-triazolium (H1,2,3ATr), 5-aminotetrazolium (HAT), and 1,5-diamino-tetrazolium (HDAT) (Scheme 3).

H$_2$BTF decomposes without melting at 220 °C,[41] possess lower that common used explosives (TNT, RDX, HMX) detonation parameters (p_{C-J} = 23.9 GPa, V_{C-J} = 7778 m·s^{-1}), and is highly sensitive toward impact (*IS* < 2 J). Two monoaionic salts from presented by Zhou et al. decomposed without melting: 3,4,5-triamino-1,2,4-triazolium and 5-amino-tetrazolium salts of H$_2$BTF (T_{dec} = 251 °C and 218 °C, respectively). 3,4,5-Triami-no-1,2,4-triazolium salt has the highest thermal stability, high density (1.79 g·cm^{-3}), and high detonation parameters (p_{C-J} = 28.1 GPa, V_{C-J} = 8326 m·s^{-1}). Hydrazinium monoainioc salts of H$_2$BTF has a density of 1.82 g·cm^{-3} (which is equal to RDX) and the highest values

of detonation parameters (p_{C-J}, V_{C-J}) among presented salts, which are lower than those for RDX (Table 1, Table 2 and Table 3).
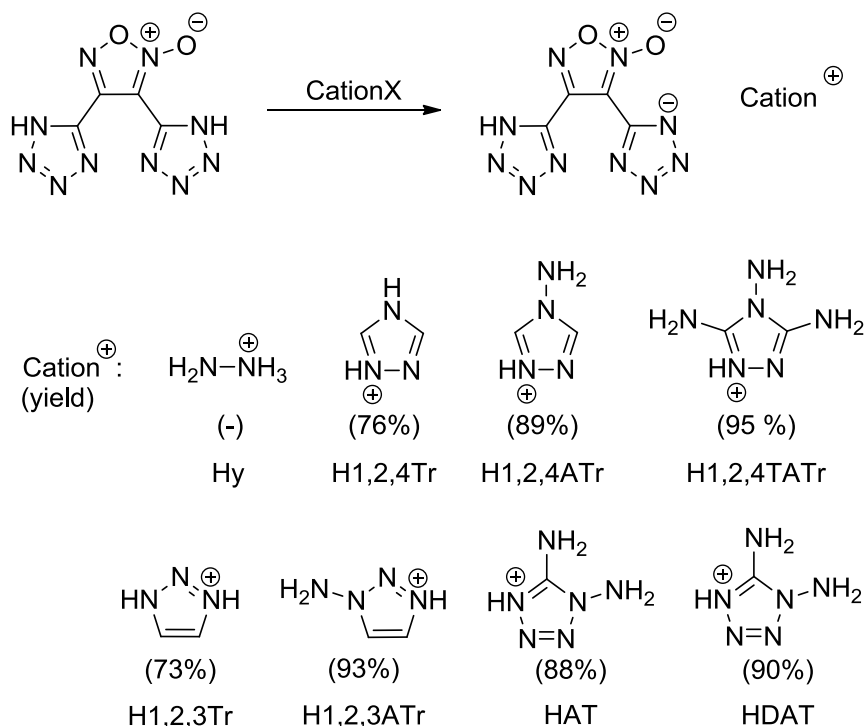
Scheme 3. Synthesis of 3,4-bis(1H-5-tetrazolyl)furoxan (H$_2$BTF)-based energetic salts.

Table 2. Physical properties and thermochemical values of H$_2$BTF and its monoanionic salts.[41, 42]

	H$_2$BTF	Hy-HBTF	H1,2,4Tr-HBTF	H1,2,4ATr-HBTF	H1,2,4TATr-HBTF
$\rho^{[a]}$ [g·cm^{-3}]	1.62	1.82[b]	1.78	1.76	1.79
T_m [°C]	dec	–[c]	205	197	dec
T_{dec} [°C]	220, 229	–[c]	225	225	251
$\Delta_f H°$ [kJ·mol^{-1}]	727.8	775.2	859.8	968.4	883.1
p_{C-J} [GPa]	23.9	32.5	27.3	27.9	28.1
V_{C-J} [m·s^{-1}]	7778	8790	8188	8278	8326
IS [J]	<2	–[c]	8	8	9

[a] Measured density at 298 K (gas pycnometer); [b] From X-ray diffraction; [c] Information not presented.

Table 3. Physical properties and thermochemical values of HBTF monoanionic salts.[41, 42]

	H1,2,3Tr-HBTF	H1,2,3ATr-HBTF	HAT-HBTF	HDAT-HBTF
$\rho^{[a]}$ [g·cm^{-3}]	1.63	1.78	1.67	1.68
T_m [°C]	192	173	dec	172
T_{dec} [°C]	223	177	218	204
$\Delta_f H°$ [kJ·mol^{-1}]	946.9	1063.5	1014.3	1062.0
p_{C-J} [GPa]	23.1	29.6	25.6	26.4
V_{C-J} [m·s^{-1}]	7740	8469	8049	8153
IS [J]	25	4	14	9

[a] Measured density at 298 K (gas pycnometer).

Dianionic Salts of 3,4-Bis(1H-tetrazol-5-yl)furoxan

Nitrogen-rich energetic dianionic salts of 3,4-bis(1H-5-tetrazolyl)furoxan were synthesized and characterized by Zhou et al.[42, 44] The synthesis of dianionic salts of H_2BTF is based on metathesis reactions of either barium salt of H_2BTF with one amount of the corresponding sulfate salts prepared before or generated by treatment of iodide or chloride salts with Ag_2SO_4. Following nitrogen-containing counter anions were chosen for preparation of energetic salts: ammonium (A), hydrazinium (Hy), guanidinium (G), aminoguanidinium (AG), diaminoguanidinium (DAG), triaminoguanidinium (TAG), N-carbamoylguanidinium (CG), 1-methyl-3,4,5-triamino-1,2,4-triazolium (H1,2,4TAMTr), and 1-amino-3-methyl-1,2,3-triazolium (H1,2,3AMTr) (Scheme 4).
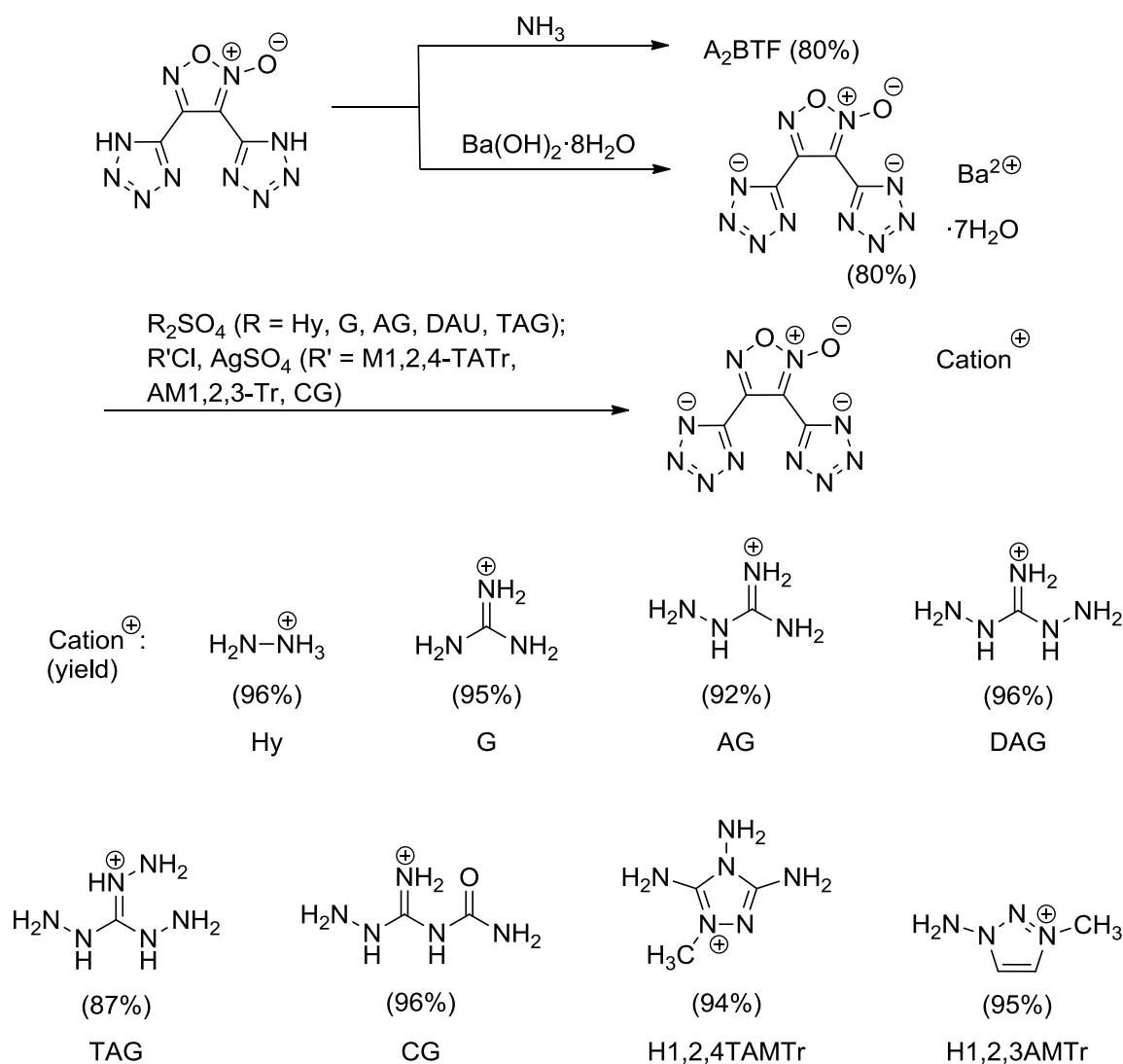
Scheme 4. Synthesis of 3,4-bis(1H-5-tetrazolyl)furoxan-based dianionic energetic salts.

Most dianionic salts of H_2BTF show higher decomposition temperatures than the neutral molecule. TAG_2BTF has the lowest decomposition temperature ($T_{dec} = 220\,°C$), the highest thermal stability is shown by the barium ($T_{dec} = 297\,°C$) and diaminoguanidinium ($T_{dec} = 290\,°C$) salts. The densities of presented dianionic salts of H_2BTF with energetic counterions are between 1.56 and 1.85 $g·cm^{-3}$. Moreover all of them are endothermic compounds (enthalpy of formation ranged from 471.6 to 1762.0 $kJ·mol^{-1}$). Those values of densities and enthalpies of formation are the cause of high values of detonation parameters (Table 4, Table 5). Hy_2BTF shows the highest detonation properties ($p_{C-J} = 32.0\,GPa$, $V_{C-J} = 8915\,m·s^{-1}$) similar to those for RDX and similar detonation pressure but higher detonation velocity than monoaionic hydrazinium analog. The reaction of H_2BTF with one or two equivalent amounts of hydrazine yields in a mixture of the monoanionic salt HyHBTF and the dianionic salt Hy_2BTF.

Table 4. Physical properties and thermochemical values of dianionic salts of H_2BTF (part 1).[42]

	BaBTF	**A_2BTF**	**Hy_2BTF**	**G_2BTF**	**AG_2-BTF**
$\rho^{[a]}$ [$g·cm^{-3}$]	2.07	1.71	1.68	1.71	1.64
T_m [°C]	dec	dec	200	dec	dec
T_{dec} [°C]	297	262	233	264	241
$\Delta_f H°$ [$kJ·mol^{-1}$]	—[b]	810.2	1163.6	851.6	1093.8
p_{C-J} [GPa]	—[b]	31.2	32.0	26.9	26.3
V_{C-J} [$m·s^{-1}$]	—[b]	8765	8915	8288	8278
IS [J]	>30	4	14	14	28

[a] Measured density at 298 K (gas pycnometer); [b] Information not presented.

Table 5. Physical properties and thermochemical values of dianionic salts of H_2BTF (part 2).[42]

	DAG_2BTF	**TAG_2BTF**	**CG_2BTF**	**(H1,2,4T-AMTr)$_2$BTF**	**(H1,2,3A-MTr)$_2$BTF**
$\rho^{[a]}$ [$g·cm^{-3}$]	1.68	1.62	1.85	1.56	1.59
T_m [°C]	dec	dec	dec	220	133
T_{dec} [°C]	290	220	253	252	239
$\Delta_f H°$ [$kJ·mol^{-1}$]	1321.5	1574.5	471.6	1719.8	1762.0
p_{C-J} [GPa]	29.3	28.4	29.5	23.4	24.8
V_{C-J} [$m·s^{-1}$]	8641	8597	8495	7939	8062
IS [J]	12	7	29	5	6

[a] Measured density at 298 K (gas pycnometer).

10.2.2 3,4-Bis(1-hydroxytetrazolyl)furazan, -furoxan and their Energetic Salts

High energetic materials containing furazan or furoxan moieties connected with tetrazole-1-oxides within one molecule were prepared by Klapötke et al.[43] 3,4-Bis(1-hydroxytetrazolyl)furazan ($H_2BOTFAZ$) and 3,4-bis(1-hydroxytetrazolyl)furoxan ($H_2BOTFOX$) were made from the corresponding nitriles by reaction with hydroxylamine

in order to obtain corresponding aminohydroximoyl species. The following steps are: diazotization in HCl, substitution of chlorine atom by azide moiety yielding hydroximoylazides [3,4-bis(azidohydroximoyl)-furazan, 3,4-bis(azidohydroximoyl)-furoxan] followed by tetrazole ring closure yielding H$_2$BOTFAZ and H$_2$BOTFOX (Scheme 5).[43]
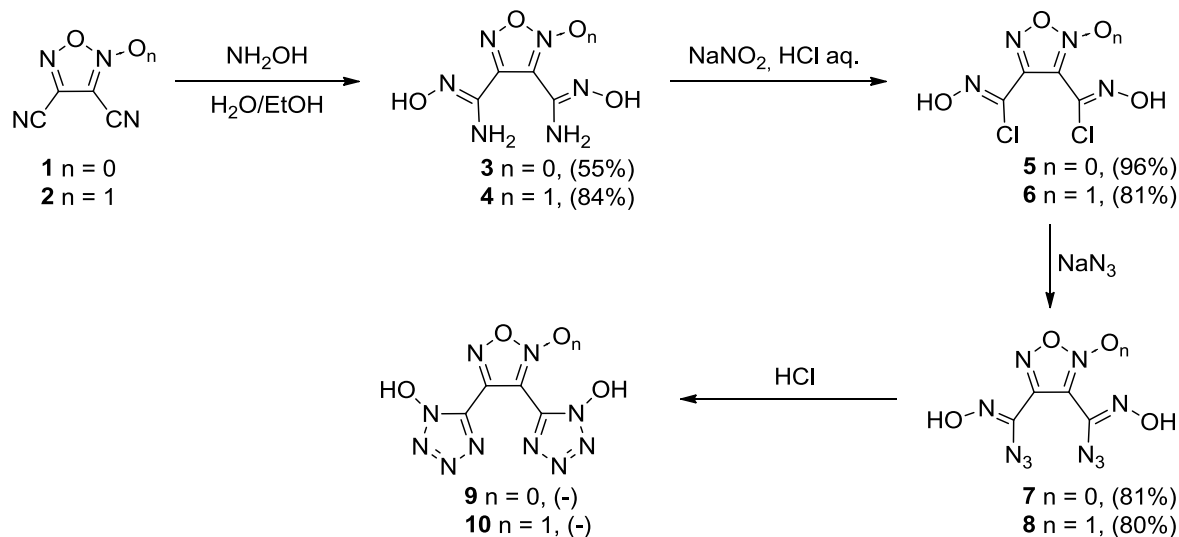
Scheme 5. Synthesis of 3,4-bis(1-hydroxytetrazolyl)furazan (H$_2$BOTFAZ) and its furoxan analog (H$_2$BOTFOX).

Subsequently, those compounds were used as precursors for energetic salts. Addition of a base or the corresponding carbonates (or bicarbonates) to aqueous solutions of H$_2$BOTFAZ and H$_2$BOTFOX yields energetic salts. The silver salt of H$_2$BOTFOX precipitated upon the addition of aqueous solution of silver nitrate. Counterions for H$_2$BOTFAZ are: potassium, ammonium (A), hydrazinium (Hy), hydroxylammonium (HA), and guanidinium (G) (Scheme 6); for H$_2$BOTFOX: silver, potassium, ammonium (A), hydrazinium (Hy), hydroxylammonium (HA), guanidinium (G), aminoguanidinium (AG), and diaminouronium (HDAU) (Scheme 7, Table 6).
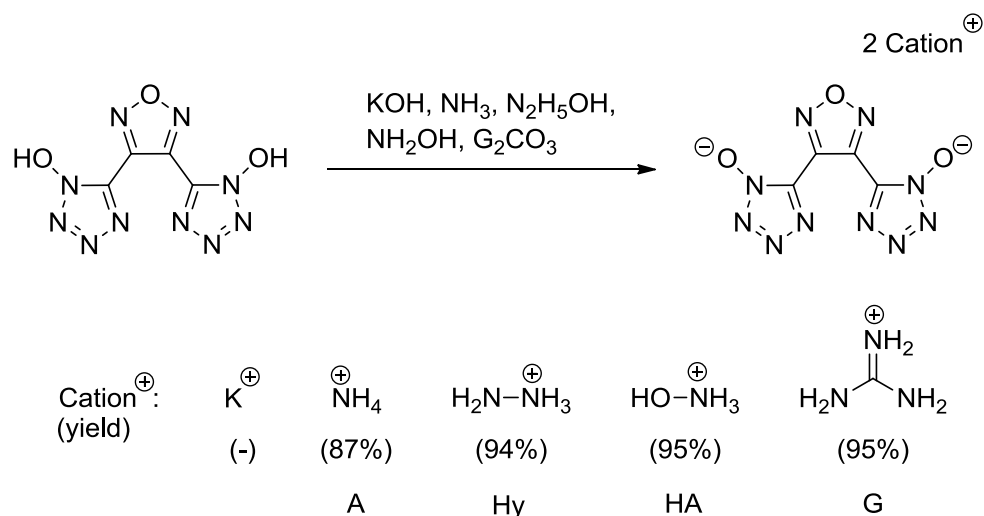
Scheme 6. Synthesis of 3,4-bis(hydroxytetrazolyl)furazan (H$_2$BOTFAZ) energetic salts.
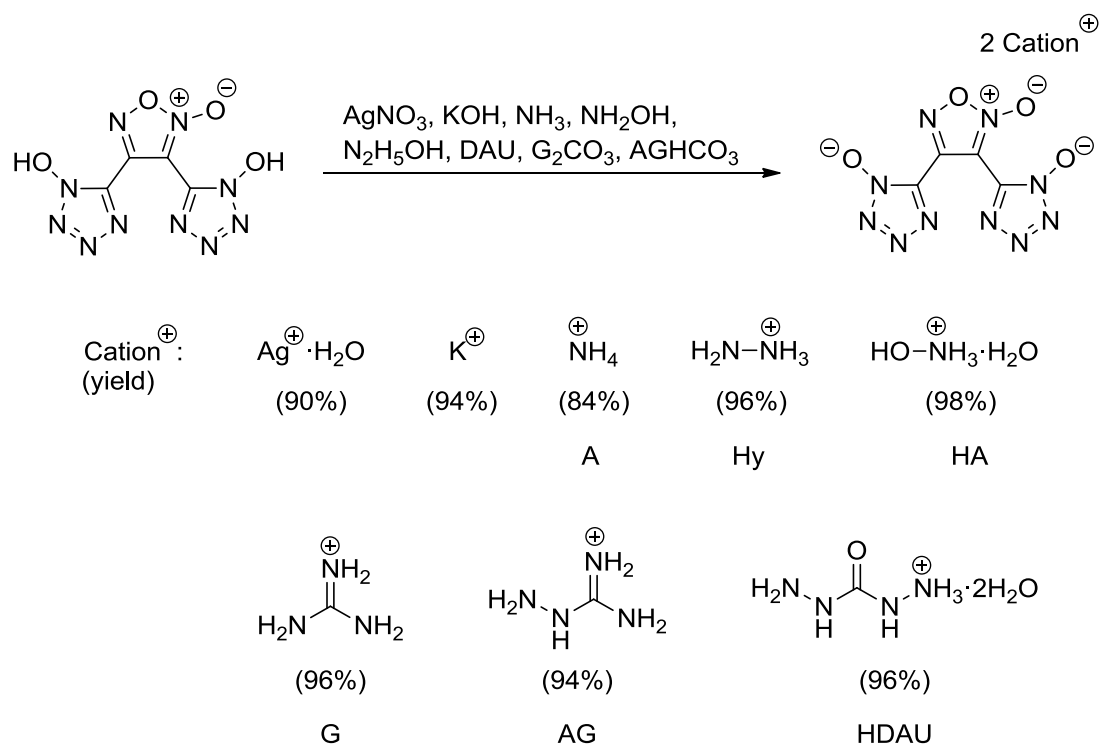
Scheme 7. Synthesis of 3,4-bis(hydroxytetrazolyl)furoxan (H$_2$BOTFOX) energetic salts.

Table 6. Properties of H$_2$BOTFAZ and H$_2$BOTFOX salts.[43]

	A$_2$BOT-FAZ	A$_2$BOT-FOX	Hy$_2$BOT-FAZ	G$_2$BOT-FOX	AG$_2$BOT-FOX
ρ[a] [g·cm^{-3}]	1.686[d]	1.748[d]	1.727[c]/1.71	1.739[b]/1.69	1.692[b]/1.64
T_{dec} [°C]	259	234	211	197	165
$\Delta_f H°$ [kJ·mol^{-1}]	625.6	621.7	947.5	638.3	885.4
$p_{C\text{-}J}$ [GPa]	27.9	31.3	31.8	26.1	26.1
$V_{C\text{-}J}$ [m·s^{-1}]	8364	8671	8843	8161	8224
IS [J]	9	10	7	30	8
FS [N]	>360	240	>360	>360	>360

[a] From X-ray diffraction, 173 K/298 K (values for 298 K were calculated with $\rho_{298\,K} = \rho_T/(1+\alpha_v(298-T)$, $\alpha_v = 1.5\times10^{-4}$ K^{-1} [45]), [b] 100 K, [c] 236 K, [d] 293 K.

The presented furoxans show generally lower thermal stabilities than the corresponding furazans. The most thermal stable are the potassium salts of 3,4-bis(1-hydroxytetrazolyl)furazan and 3,4-bis(1-hydroxytetrazolyl)furoxan which decompose at 277 °C and 265 °C, respectively. Investigated EMs possess lower sensitivities in comparison to RDX ($IS = 7.5$ J, $FS = 120$ N). Dihydrazinium 3,4-bis(1-oxidotetrazolyl)furazan has the highest heat of formation ($\Delta_f H° = 947.5$ kJ·mol^{-1}) and the highest detonation velocity (8843 m·s^{-1}), which is better than RDX (8763 m·s^{-1}).

10.3 Summary

1,2,5-Oxadiazole–tetrazole connected energetic materials are the new and promising research area for finding replacement for currently used energetic materials (including common used explosives). Most of the presented compounds have high density ranging from 1.59 for bis(1-amino-3-methyl-1,2,3-triazolium) 3,4-bis(1H-5-tetrazolyl)furoxan to 1.82 g·cm^{-3} for hydrazinium hydrogen 3,4-bis(1H-5-tetrazolyl)furoxan. Heat of formation is in the range of 471.6 for bis(N-carbamoylguanidinium) 3,4-bis(1H-tetrazol-5-yl)furoxan to 1762.0 kJ·mol^{-1} for bis(1-amino-3-methyl-1,2,3-triazolium) 3,4-bis(1H-5-tetrazolyl)furoxan. The values of densities and heat of formation reflect in high detonation properties of those compounds. The most insensitive toward friction and impact within presented EMs are 3,4-bis(1-hydroxytetrazolyl)furazan and -furoxan based compounds. Presented EMs possess mostly good oxygen balance, great density, and high thermal stability. Therefore, 1,2,5-oxadiazole–tetrazoles functionality provides considerable skeletons for synthesis novel EMs.

10.4 References

[1] R. M. Vrcelj, J. N. Sherwood, A. R. Kennedy, H. G. Gallagher, T. Gelbrich, Polymorphism in 2,4,6 Trinitrotoluene, *Cryst. Growth Des.* **2003**, *3*, 1027–1032.

[2] N. I. Golovina, A. N. Titkov, A. V. Raevskii, L. O. Atovmyan, *J. Solid State Chem.* **1994**, *113*, 229–238.

[3] E. A. Zhurova, A. I. Stash, V. G. Tsirelson, V. V. Zhurov, E. V. Bartashevich, V. A. Potemkin, A. A. Pinkerton, *J. Am. Chem. Soc.* **2006**, *128*, 14728–14734.

[4] J. Trotter, *Acta Crystallogr.* **1963**, *16*, 698–699.

[5] P. Hakey, W. Ouellette, J. Zubieta, T. Korter, *Acta Crystallogr., Sect. E* **2008**, *64*, o1428.

[6] C. S. Choi, E. Prince, *Acta Crystallogr., Sect. B* **1972**, *28*, 2857–2862.

[7] J. Deschamps, M. Frisch, D. Parrish, *J. Chem. Crystallogr.* **2011**, *41*, 966–970.

[8] A. Ksia czak, T. Ksia czak, *Thermochim. Acta* **1996**, *275*, 27–36.

[9] J.-S. Lee, C.-K. Hsu, C.-L. Chang, *Thermochim. Acta* **2002**, *392–393*, 173–176.

[10] R. Meyer, J. Köhler, A. Homburg, Explosives, 5th Edition, Wiley-VCH, Weinheim **2002**, p. 68 (RDX), 239 (HMX), 253 (PETN), 340 (TNT).

[11] P. Enghag, Encyclopedia of the Elements: Technical Data – History – Processing – Applications, Wiley, New York, **2008**, p. 971.

[12] T. Curtius, *Ber. Dtsch. Chem. Ges.* **1890**, *23*, 3023–3033.

[13] a) N. Hansen, A. M. Wodtke, *J. Phys. Chem. A* **2003**, *107*, 10608–10614; b) A. M. Wodtke, N. Hansen, J. C. Robinson, N. E. Sveum, S. J. Goncher, D. M. Neumark, *Chem. Phys. Lett.* **2004**, *391*, 334–337; c) P. C. Samartzis, J. J.-M. Lin, T.-T. Ching, C. Chaudhuri, S.-H. Lee, A. M. Wodtke, *J. Chem. Phys.* **2007**, *126*, 041101–1–5; d) P. C. Samartzis, A. M. Wodtke, *Phys. Chem. Chem. Phys.* **2007**, *9*, 3054–3066; e) K. Yuan, Y. Cheng, F. Wang, X. Yang, *J. Phys. Chem. A* **2008**, *112*, 5332–5337.

[14] a) D. Babikov, V. A. Mozhayskiy, A. I. Krylov, *J. Chem. Phys.* **2006**, *125*, 084306-1-14; b) C. Larson, Y. Ji, P. C. Samartzis, A. Quinto-Hernandez, J. J.-M. Lin, T.-T. Ching, C. Chaudhuri, S.-H. Lee, A. M. Wodtke, *J. Phys. Chem. A* **2008**, *112*, 1105–1111; c) A. Quinto-Hernandez, J. Doehla, W.-T. Huang, C.-Y. Lien, W.-Y. Lin, J.-M. Lin, A. M. Wodtke, *J. Phys. Chem. A* **2012**, *116*, 4695–4704; d) J. S. Wright, *J. Am. Chem. Soc.* **1974**, *96*, 4753–4760; e) D. Babikov, *J. Chem. Phys.* **2011**, *134*, 114305-1-7; f) D. Babikov, B. K. Kendrick, *J. Chem. Phys.* **2010**, *133*, 174310-1-9; g) I. S. K. Kerkines, Z. Wang, P. Zhang, K. Morokuma, *J. Chem. Phys.* **2008**, *129*, 171101-1-5.

[15] a) T. J. Lee, J. E. Rice, *J. Chem. Phys.* **1991**, *94*, 1215–1221; b) K. M. Dunn, K. Morokuma, *J. Chem. Phys.* **1995**, *102*, 4904–4908; c) E. M. Shustorovich, *J. Struct. Chem.* **1969**, *10*, 154–156; d) W. J. Lauderdale, J. F. Stanton, R. J. Bartlett, *J. Phys. Chem.* **1992**, *96*, 1173–1178; e) M. M. Francl, J. P. Chesick, *J. Phys. Chem.* **1990**, *94*, 526–528.

[16] a) W. Lindinger, I. Dotan, D. L. Albritton, F. C. Fehsenfeld, *J. Chem. Phys.* **1978**, *68*, 2607–2611; b) G. Kemister, J. B. Peel, *Org. Mass Spectrom.* **1993**, *28*, 311–315; c) C. Léonard, P. Rosmus, S. Carter, N. C. Handy, *J. Phys. Chem. A* **1999**, *103*, 1846–1852; d) H. Bohringer, F. Arnold, D. Smith, N. Adams, *Int. J. Mass Spectrom. Ion Processes* **1983**, *52*, 25–41; e) T. Ruchti, T. Speck, J. P. Connelly, E. J. Bieske, H. Linnartz, J. P. Maier, *J. Chem. Phys.* **1996**, *105*, 2591–2594; f) S. C. de Castro, H. F. Schaefer, R. M. Pitzer, *J. Chem. Phys.* **1981**, *74*, 550–558; g) J. H. Langenberg, I. B. Bucur, P. Archirel, *J. Chem. Phys.* **1997**, *221*, 225–236; h) K. Sohlberg, *J. Mol. Struct.* **1995**, *339*, 195–199; i) G. P. Smith, L. C. Lee, *J. Chem. Phys.* **1978**, *69*, 5393–5399; j) L. B. Knight, K. D. Johannessen, D. C. Cobranchi, E. A. Earl, D. Feller, E. R. Davidson, *J. Chem. Phys.* **1987**, *87*, 885–897; k) K. Hiraoka, G. Nakajima, *J. Chem. Phys.* **1988**, *88*, 7709–7714; l) W. E. Thompson, M. E. Jacox, *J. Chem. Phys.* **1990**, *93*, 3856–3862.

[17] M. N. Glukhovtsev, P. von Rague Schleyer, C. Maerker, *J. Phys. Chem.* **1993**, *97*, 8200–8206.

[18] a) A. Vij, J. G. Pavlovich, W. W. Wilson, V. Vij, K. O. Christe, *Angew. Chem. Int. Ed.* **2002**, *41*, 3051–3054; b) M. G. Papadopoulos, J. Waite, *J. Chem. Phys.* **1985**, *82*, 1435–1436.

[19] J. Li, C.-W. Liu, J.-X. Lu, *J. Mol. Struct.* **1993**, *280*, 223–231.

[20] H. H. Michels, J. A. Montgomery Jr., K. O. Christe, D. A. Dixon, *J. Phys. Chem.* **1995**, *99*, 187–194.

[21] K. F. Ferris, R. J. Bartlett, *J. Am. Chem. Soc.* **1992**, *114*, 8302–8303.

[22] M. N. Glukhovtsev, H. Jiao, P. von Rague Schleyer, *Inorg. Chem.* **1996**, *35*, 7124–7133.

[23] P. Gray, *Q. Rev. Chem. Soc.* **1963**, *17*, 441–473.

[24] K. Banert, Y.-H. Joo, T. Rüffer, B. Walfort, H. Lang, *Angew. Chem. Int. Ed.* **2007**, *46*, 1168–1171.

[25] a) T. Curtius, *Ber. Dtsch. Chem. Ges.* **1891**, *24*, 3341–3349; b) A. Hammerl, T. M. Klapötke, H. Piotrowski, G. Holl, M. Kaiser, *Propellants Explos. Pyrotech.* **2001**, *26*, 161–164.

[26] a) W. S. Frost, J. C. Cothran, A. W. Browne, *J. Am. Chem. Soc.* **1933**, *55*, 3516–3518; b) C. O. Obenland, D. J. Mangold, M. P. Marino, T. R. Musgrave, R. N. Keller, *Inorg. Synth.* **2007**, *8*, 53–56.

[27] a) J. Stierstorfer, T. M. Klapötke, A. Hammerl, R. D. Chapman, *Z. Anorg. Allg. Chem.* **2008**, *634*, 1051–1057; b) T. M. Klapötke, J. Stierstorfer, *J. Am. Chem. Soc.* **2008**, *131*, 1122–1134.

[28] a) M. H. V. Huynh, M. A. Hiskey, D. E. Chavez, D. L. Naud, R. D. Gilardi, *J. Am. Chem. Soc.* **2005**, *127*, 12537–12543; b) H. J. Marcus, A. Remanick, *J. Org. Chem.* **1963**, *28*, 2372–2375; c) M. H. V. Huynh, M. A. Hiskey, J. G. Archuleta, E. L. Roemer, R. Gilardi, *Angew. Chem. Int. Ed.* **2004**, *43*, 5658–5661.

[29] T. M. Klapötke, D. G. Piercey, *Inorg. Chem.* **2011**, *50*, 2732–2734.

[30] a) R. Raap, *Can. J. Chem.* **1969**, *47*, 3677–3681; b) J. C. Gálvez-Ruiz, G. Holl, K. Karaghiosoff, T. M. Klapötke, K. Löhnwitz, P. Mayer, H. Nöth, K. Polborn, C. J. Rohbogner, M. Suter, J. J. Weigand, *Inorg. Chem.* **2005**, *44*, 4237–4253; c) Y.-H. Joo, B. Twamley, S. Garg, J. M. Shreeve, *Angew. Chem. Int. Ed.* **2008**, *47*, 6236–6239.

[31] T. M. Klapötke, C. M. Sabaté, *Chem. Mater.* **2008**, *20*, 3629–3637.

[32] a) E. Ott, E. Ohse, *Ber. Dtsch. Chem. Ges.* **1921**, *54*, 179–186; b) E. Keßenich, T. M. Klapötke, J. Knizek, H. Nöth, A. Schulz, *Eur. J. Inorg. Chem.* **1998**, *1998*, 2013–2016.

[33] T. M. Klapötke, P. Mayer, J. Stierstorfer, J. J. Weigand, *J. Mater. Chem.* **2008**, *18*, 5248–5258.

[34] a) M.-H. V. Huynh, M. A. Hiskey, E. L. Hartline, D. P. Montoya, R. Gilardi, *Angew. Chem. Int. Ed.* **2004**, *43*, 4924–4928; b) M. H. V. Huynh, M. A. Hiskey, C. J. Pollard, D. P. Montoya, E. L. Hartline, R. Gilardi, *J. Energ. Mater.* **2004**, *22*, 217–229.

[35] M. B. Talawar, R. Sivabalan, N. Senthilkumar, G. Prabhu, S. N. Asthana, *J. Hazard. Mater.* **2004**, *113*, 11–25.

[36] a) J. Kerth, S. Löbbecke, *Propellants, Explos., Pyrotech.* **2002,** *27*, 111–118; b) D. E. Chavez, M. A. Hiskey, R. D. Gilardi, *Angew. Chem. Int. Ed.* **2000**, *39*, 1791–1793.

[37] C. Ye, H. Gao, J. A. Boatz, G. W. Drake, B. Twamley; J. M. Shreeve, *Angew. Chem. Int. Ed.* **2006**, *45*, 7262–7265.

[38] D. R. Miller, D. C. Swenson, E. G. Gillan, *J. Am. Chem. Soc.* **2004**, *126*, 5372–5373.

[39] H. Gao, J. M. Shreeve, *Chem. Rev.* **2011**, *111*, 7377–7436.

[40] T. I. Godovikova, S. K. Vorontsova, L. D. Konyushkin, S. I. Firgang, O. A. Rakitin, *Russ. Chem. Bull.* **2009**, *58*, 406–409.

[41] H. Huang, Z. Zhou, L. Liang, J. Song, K. Wang, D. Cao, W. Sun, C. Bian, M. Xue, *Chem. Asian J.* **2012**, *7*, 707–714.

[42] H. Huang, Z. Zhou, L. Liang, J. Song, K. Wang, D. Cao, C. Bian, W. Sun, M. Xue, *Z. Anorg. Allg. Chem.* **2012**, *638*, 392–400.

[43] D. Fischer, T. M. Klapötke, M. Reymann, J. Stierstorfer, M. B. R. Völkl, *New J. Chem.* **2015**, *39*, 1619–1627.

[44] Z. Zhou; H. Huang; L. Liang, J. Song, K. Wang, D. Cao, C. Bian, *3,4-Bis(1-hydro-5-tetrazolyl)furoxan Ionic Salt Containing Energy and Preparation Method Thereof*, Patent CN 102952124, Beijing Institute of Technology, Beijing, P. R. China, **2013**.

[45] C. Xue, J. Sun, B. Kang, Y. Liu, X. Liu, G. Song, Q. Xue *Propellants, Explos., Pyrotech.* **2010**, *35*, 333–338.

Covalent and Ionic Insensitive High-Explosives
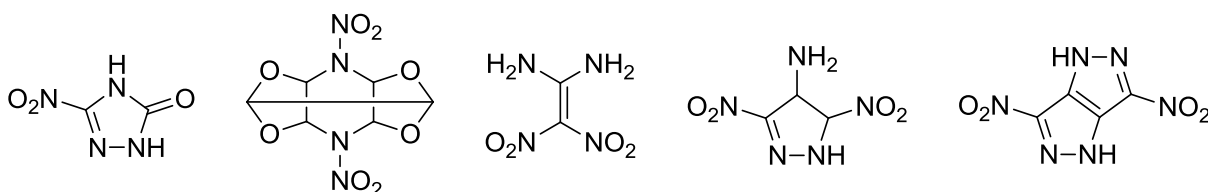
Abstract: Ongoing research into new insensitive energetic materials with low sensitivity toward accidental stimuli, high thermal stability and high performance characteristics is undertaken in many research groups worldwide. In order to obtain promising compounds, which fulfill the sensitivity, stability, and performance requirements, researchers use many different strategies. One of the most promising approaches is the synthesis of novel explosives with tailored physico-chemical properties. In this review the synthesis and properties of some both covalent (NTO, TEX, FOX-7, ADNP, DNPPs) and ionic (salts of ANDP and DNPP) insensitive explosives are presented, which are of high interest to this field of research.

Keywords: Insensitive explosives · NTO · TEX · FOX-7 · ADNP · DNPP

11.1 Introduction

Explosives which show both high performance (heat of explosion, detonation velocity, detonation pressure, explosion temperature, and volume of gas released) but low sensitivity to external stimuli (friction, impact, electrostatic discharge, and heat) have long fascinated scientists due to their potential applications for military as well as for civilian purposes. Throughout the past decades, there have been considerable efforts by many research groups worldwide to synthesis compounds which will meet such a challenging combination of requirements. Modern weaponry still high relies on explosives, which can be used in insensitive munitions (IM). IMs are both safe to handle and difficult to initiate when subjected to accidental stimuli (*e.g.* heat, shock, bullet or fragment impact, electromagnetic pulse), but at the same time their performance characteristics and reliability fulfill all of the requirements, which are necessary in order to complete a specific mission.[1] The IMs can be tested and classified into six categories: no reaction (NR), burning (V), deflagration (IV), explosion (III), partial detonation (II), detonation (I). In order to evaluate the characteristics of munition, the following tests are applied: bullet impact (BI ≥ V), fragment impact (FI ≥ V), fast cook-off test (FCO ≥ V), slow cook-off test (FCO ≥ V) and sympathetic reaction (SR ≥ III).[1b, c] The safety and sensitivity of IMs are directly connected with the properties of the energetic materials applied therein.[2]

The essential role in the ignition of explosives is the phenomena of the conversion of accidentally applied energy. Ignition (initiation) of the explosive involves interaction between heat releasing and heat dissipating processes.[3] If the release of chemical energy is larger than that dissipated, the reaction grows. In general it is assumed that initiation of an explosive is thermal in origin and other energies (*e.g.* mechanical, electrical) are converted into heat in localized regions, which results in the formation of so-called hot-spots.[4] The ignition (initiation) of secondary explosives can occur by the shock excitation of internal vibrations *via* multiphonon up-pumping. The leading mechanism for up-pumping is the anharmonic coupling of excited phonon modes with low frequency molecular vibrations (*doorway mode*). The explosive is heated to a certain temperature, which – if is high enough – results in bond breaking taking place (ignition, the critical hot-spots) and deflagration, and/or an extremely fast (pico to nanoseconds time scale) multistep, exothermic chemical reaction occurs (detonation).[4, 5] Some of the hot-spots necessary for the initiation of explosives, which have crystal structures that show piezoelectricity might be produced by electrical breakdown of the crystal due to a generated piezoelectric field.[6] Maycock and Grabenstein proposed an explanation for accidental explosions of primary

explosives (lead azide), which is based on the exceedingly strained crystals, in which generation of a piezoelectric voltage with subsequent explosion take part.[6a] The hot-spots, depending on their position in the explosive particles (granules, crystals), can be classified into external (placed on the surface of particles) and internal (situated inside of the explosive particles).[7] Therefore strategies for the development of novel insensitive explosives can be either to: eliminate the critical hot-spots and/or increase the ratio of dissipated energy (mostly by increasing the thermal effusivity) in currently used explosives, or synthesize novel explosives, which can be ignited only by a relatively large amount of energy. Therefore, the development of insensitive energetic materials can be conducted in many different ways; most of them can be classified into the following groups:

a) Preparation of formulations containing currently used explosives and different additives (binders, surfactants) *e.g.* polymer bonded explosive (PBX), which is a composite consisting of an energetic material (filler) embedded in a polymeric matrix (*e.g.*: 1,3,5-trinitro-1,3,5-triazacyclohexane (RDX),[8] 2-oxo-1,3,5-trinitro-1,3,5-triaza-cyclohexane (K-6, keto-RDX),[9] 1,3,5,7-tetranitro-1,3,5,7-tetraazacyclo-octane (HMX),[8a, b, d, e, 10] 2,4,6-trinitrotoluene (TNT),[8b, d] pentaerythritol tetranitrate (PETN),[8e, 11] 2,4,6-triamino-1,3,5-trinitrobenzene (TATB),[8e, 12] 2,4,6,8,10,12-hexa-nitro-2,4,6,8,10,12-hexaazaisowurtzitane (HNIW, CL-20),[8e, 10c, 13] 1,3,3-trinitro-azetidine (TNAZ),[8e, 14] 3-nitro-1,2,4-triazol-5-one (NTO),[8b, d, 15] 1,1-diamino-2,2-di-nitroethylene (FOX-7, DADNE),[8e] *N*-guanylurea-dinitramide (FOX-12, GUDN)[8e]. The polymer matrix (elastomer), which is added, tends to absorb shocks, thereby decreasing the sensitivity to external stimuli. Therefore PBX charges mostly show considerably reduced vulnerability towards different stimuli;[1a]

b) Decreasing the particle size (minimization of the intercrystalline heterogeneities such as defects, undesirable inclusions, voids etc.) of the explosive (*e.g.*: submicro-RDX,[8c, 16] nano-RDX,[8c, f, 16–17] nano-keto-RDX,[18] micro-HMX,[10d] nano-HMX,[10d, 17e, 19] nano-PETN,[17b] micro-TATB,[20] nano-TATB,[20] nano-CL-20,[13b, 17e, 21] nano-FOX-7,[22]);

c) Synthesis of novel explosives with tailored physicochemical properties.

The design and synthesis of novel secondary explosives with tailored properties seems to be the most convenient method in the development of novel insensitive species, since it has many advantages compared to the preparation of formulations. In 1888 Jackson and Wing prepared the most prominent 2,4,6-triamino-1,3,5-trinitrobenzene (TATB) by reaction of 1,3,5-tribromo-2,4,6-trinitrobenzene (TBTNB) with ammonia as a pale yellow solid.[23]

TATB is considered to be the first and most prominent example of a thermally stable explosive species, TATB has a "graphite-like", layered crystalline structure with strong inter- and intramolecular hydrogen bonds, which have a strong impact on its high crystal density (1.94 g·cm^{-3})[24] and high thermal stability (exotherm starts at 310 °C[25]). Moreover, TATB has a high measured detonation velocity and pressure (V_{C-J} = 7.66 km·s^{-1}, p_{C-J} = 28.7 GPa at density 1.854 g·cm^{-3}; cylinder test).[26] It is characterized by low impact sensitivity, low friction sensitivity, and low electrostatic discharge ignition (> 50 J, > 353 N, > 2.56 J, respectively).[27] The initiation sensitivity of TATB is relatively low (300 mg of lead azide).[28] The extensive hydrogen bonding network results in the low solubility of TATB in commonly used organic solvents. Therefore, it is necessary to develop a solvent system in which TATB will show much better solubility. High solubility is needed for the production of high-quality crystals with improved processability. In order to break the hydrogen bonds, different ionic liquids have been investigated.[29] The authors reported that 3-ethyl-1-methyl-imidazolium acetate (EMImOAc) is the best ionic liquid for dissolving TATB among those that were investigated, and dissolves 10 ± 1.0 wt-% of TATB. Crystallization of TATB *via* the non-agitated cooling method in EMImOAc yields TATB crystals with improved morphology in comparison with the starting materials. Cooling by natural convection yields 10–50 μm sized crystals, whereas cooling the solution at a rate of 1 K·min^{-1} produces 200–500 μm sized crystals.[29]

Amongst different classes of chemical species, the molecules, which meet a variety of key standards for insensitive explosives may contain the following structure features: acyclic (1,1-diamino-2,2-dinitroethylene), heterocyclic (3-nitro-1,2,4-triazol-5-one, 4-amino-3,5-di-nitropyrazole), caged (4,10-dinitro-2,6,8,12-tetraoxa-4,10-diazaisowurtzitane), fused (3,6-dinitropyrazolo[4,3-*c*]pyrazoles), and ionic (salts of 4-amino-3,5-dinitropyrazole and 3,6-dinitropyrazolo[4,3-*c*]pyrazole). In the next part of this review, the synthesis and properties of the above-mentioned species as well as their applications as insensitive munitions are given.

11.2   3-Nitro-1,2,4-triazol-5-one (NTO, ONTA)

In 1905, Manchot and Noll prepared 3-nitro-1,2,4-triazol-5-one (oxynitrotriazole, NTO, ONTA, pK_a = 3.63)[30] by nitration of 1,2,4-triazol-3-one (TO) using fuming nitric acid.[31] However, due to lack of precise techniques for the structural determination, the authors incorrectly assigned the structure to be the hydroxy tautomer (5-hydroxy-3-nitro-1,2,4-tri-azole). In 1966, Chipen et al. correctly identified the chemical structure of NTO,[32] and its

detonation properties were investigated by Coburn et al.[33] Most of the methods reported for the synthesis of NTO are based on a two-step process. In the first step TO is synthesized and in the second step it is nitrated to give NTO (Scheme 1). TO can be obtained by:

a) Reaction of semicarbazide with formic acid (the originally reported method for the synthesis of TO);[34]

b) Reaction of semicarbazide hydrochloride with formic acid (b₁),[33, 35] or trimethyl orthoformate (b₂),[36] or triethyl orthoformate (b₃)[37];

c) Reaction of acetone semicarbazone with formic acid;[32]

d) Deamination of 4-amino-1,2,4-triazol-5-one with nitrous acid (generated *in situ*);[38]

e) Thermal decarboxylation of 5-oxo-4,5-dihydro-1,2,4-triazole-3-carboxylic acid.[32, 39]

All of the reported syntheses of NTO were achieved using one of the following nitrating agents: fuming nitric acid[31, 35f] nitric acid of different concentrations[32, 33, 35d, f] or nitrating mixtures.[35f, 40]

The nitration of TO using concentrated nitric acid (85–100%) shows little dependence on the ratio of the reagents, the temperature, and the dilution of the reactant acid.[35b, 41] Zbarsky and Yudin analyzed the kinetics and mechanism of the nitration of TO in 72–100% HNO₃[42] and found that the nitration can be described by pseudo-first-order reaction kinetics. At HNO₃ concentrations exceeding 77%, 1-nitro-1,2,4-triazol-5-one (*N*-NTO) is formed within the first minutes of the reaction. When H_0 is lower than −1, a denitration reaction forming TO occurs. However, when $H_0 > 1$ total destruction of the ring is observed.[42]
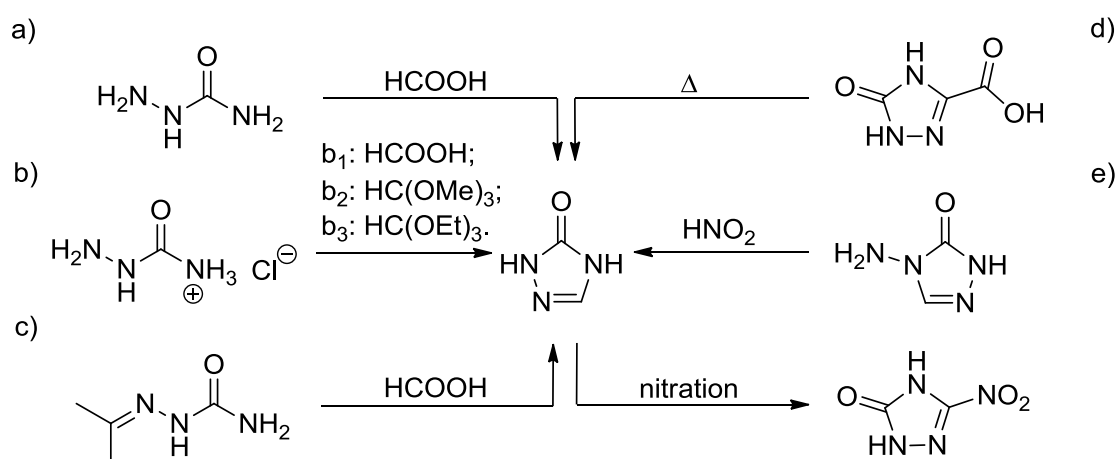
Scheme 1. Synthetic routes for TO and NTO.

For concentrations of HNO₃ in the 96–100 % range, there is a sharp decrease in the NTO yield.[42] This is because the activation energy of the *N*-NTO decomposition process in 100% HNO₃ is higher than the activation energy for the nitration of TO, which causes the NTO

yield to decrease with increasing reaction temperature.[42] The kinetic study reported by Zbarskii et al. showed that NTO is formed from *N*-NTO *via* hydrolysis to form TO, followed by subsequent nitration of the latter – rather than *via* a rearrangement.[43] *N*-NTO can be synthesized by the reaction of TO with nitric acid in acetic anhydride, and can also act as nitrating agent.[43] *N*-NTO is an extremely unstable substance and undergoes hydrolysis very readily in aqueous solutions with pH $\geq$ 7.[42, 43]. *N*-NTO has a measured ignition point of 84 °C,[42] and burn velocities at 0.1 MPa and 10 MPa of 10.8 mm·s^{-1} and 100 mm·s^{-1}, respectively.[42] On the basis of kinetic studies, Zbarsky and Yudin proposed a mechanism for the nitration of TO (Scheme 2).[42]
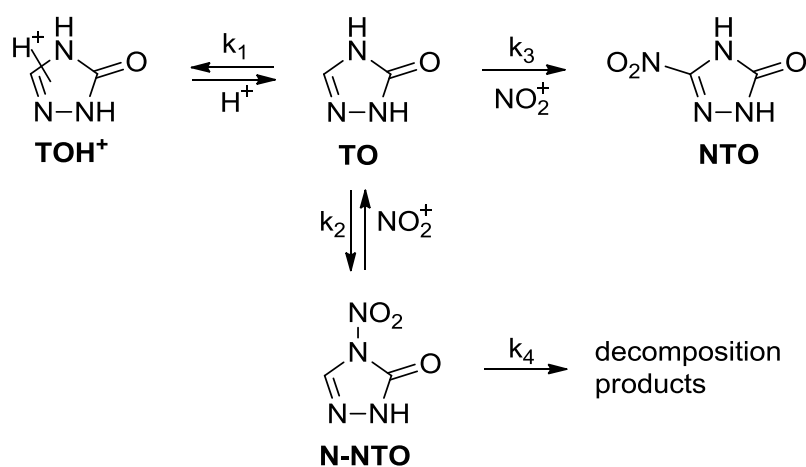
Scheme 2. The suggested mechanism for the TO nitration process.[42]

Further research into the nitration of TO was undertaken by Trzciński et al.[44] The authors investigated the heat of reaction of TO nitration using a differential reaction calorimeter. The average heat of reaction value for the nitration of TO using various nitration mixtures was determined (60% HNO$_3$, 20% H$_2$SO$_4$, 20% H$_2$O, 1320 $\pm$ 40 J·g^{-1}; 70% HNO$_3$, 30% H$_2$O, 1195 $\pm$ 2 J·g^{-1}; 85% HNO$_3$, 15% H$_2$O, 1360 $\pm$ 30 J·g^{-1}). Additionally, the heat of dissolution of TO in concentrated sulfuric acid was determined (80% H$_2$SO$_4$, 20% H$_2$O, 260 $\pm$ 20 J·g^{-1}; 95% H$_2$SO$_4$, 5% H$_2$O, 580 $\pm$ 20 J·g^{-1}). The authors investigated the synthesis of NTO in an aqueous solution of sulfuric acid and nitric acid, and also in only nitric acid (if the nitric acid concentration is below 85 %, *N*-NTO is not formed). Arrhenius equation parameters were determined for the nitrating mixtures: 60 % HNO$_3$, 20 % H$_2$SO$_4$, 20 % H$_2$O (E_a = 88.2 kJ·mol^{-1}), 85 % HNO$_3$, 15% H$_2$O (E_a = 79.6 kJ·mol^{-1}), and 70% HNO$_3$, 30% H$_2$O (E_a = 92.0 kJ·mol^{-1}).

NTO has been investigated as filler in many different low-sensitivity formulations, among which the most known are: IMX-101, IMX-104 (OSX-7), and PAX-48

(OSX-8).[1c, 8b, 15b, 35b, 45] The insensitive munitions explosive 101 (IMX-101) consists of a melt-castable mixture (T_m = 95 °C; T_{dec} = 212 °C, onset) of 43.5% 2,4-dinitroanisole (DNAN, binder), 36.8% nitroguanidine (NQ, filler), and 19.7% NTO (filler).[45d] IMX-101 has passed standardized performance, stability, and aging tests and was qualified by the U.S. Army for use as an insensitive TNT replacement explosive for artillery ammunitions. During fast cook-off, slow cook-off, bullet impact, fragment impact, and sympathetic detonation tests, IMX-101 does not detonate, but undergoes a rapid deflagration – in contrast to TNT-based formulations.[1c, 15b, 35b, 45c–e] Two other important formulations for insensitive munitions applications – IMX-104 and PAX-48 – are DNAN/NTO based melt-castable mixtures with different nitramine components: IMX-104 contains RDX, whereas PAX-48 utilizes HMX.[45b] IMX-104 consists of NTO (filler), DNAN (binder), and RDX (filler), and is characterized by a higher melting point (T_m = 89 °C) than Composition B (60% RDX, 39% TNT, 1% wax; T_m = 80 °C, T_{dec} = 215 °C), slightly lower decomposition temperature (T_{dec} = 213 °C, DSC-onset) and comparable detonation velocity ($V_{C\text{-}J}$ = 98% of Composition B).[1c, 45b] PAX-48 is characterized by a higher melting and decomposition temperature than IMX-104 (T_m = 93 °C, T_{dec} = 231 °C, onset), while its $V_{C\text{-}J}$ corresponds to 96 % of that of Composition B.[45b] The evaluation of the thermal stabilities, sensitivities, and efflux viscosity has shown that both IMX-104 and PAX-48 are show comparable or superior results in comparison to traditional mortar fillings.[45b, h] Moreover, both IMX-104 and PAX-48 achieve high order detonation, in a similar manner to Composition B.[45b] IMX-104 is a moderately low cost replacement for Composition B, since its production utilizes existing manufacturing equipment in both mixing and high volume loading operations, meaning that significant investment in new technology or in equipment is not required.[1c, 45b] IMX-104 satisfied all of the requirements outlined by the US Army and was selected as the lead explosive for an insensitive Composition B replacement for mortar applications.[45b, e]

11.3   4,10-Dinitro-2,6,8,12-tetraoxa-4,10-diazaisowurtzitane (TEX)

In 1990, Boyer et al. reported the synthesis of the insensitive explosive 4,10-di-nitro-2,6,8,12-tetraoxa-4,10-diazaisowurtzitane (TEX), which is synthesized by the base catalyzed formation of 1,4-diformyl-2,3,5,6-tetrahydroxypiperazine (DFTHP) followed by condensation of trimeric glyoxal with DFTHP in acidic solution and subsequent nitration (Scheme 3).[46]
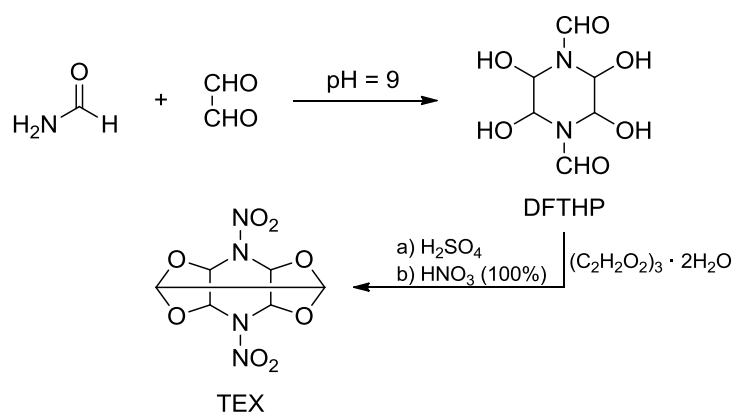
Scheme 3. Synthesis of 4,10-dinitro-2,6,8,12-tetraoxa-4,10-diazaisowurtzitane (TEX).

A single-crystal X-ray diffraction study of TEX was performed and the structure in the solid state was determined by Klapötke et al.[47] The seven-membered rings introduce strain to the cage and consequently raise the energy content of the molecule in comparison to unstrained system. The molecule is compact and − excluding the nitro groups − can be described as being nearly spherical, which may explain the extremely high density of TEX ($\rho = 2.008$ g·cm^{-3} at 200 K, $\rho = 1.987$ g·cm^{-3} at 298.15 K).[47, 48] TEX decomposes without melting at 304 °C.[48] The calculated enthalpy of formation ($\Delta_f H°$, isodesmic reaction, density functional theory B3LYP method with 6-31+G** basis set) of TEX is equal to −448.37 kJ·mol^{-1},[50] which is close to the experimentally determined value (−445.60 kJ·mol^{-1}).[51] The values for the density and enthalpy of formation are reflected in its high detonation parameters ($p_{C-J} = 34.3$ GPa, $V_{C-J} = 8615$ m·s^{-1}).[52] Moreover, TEX possesses lower sensitivities toward friction and impact (> 360 N, 22.5 J, respectively) than TNT, PETN, RDX, and HMX,[53] while its sensitivity toward electrostatic discharge is in the range of those explosives.

The critical diameters of an explosive (upper and lower limiting diameters) are one of the most important factors of an explosive and have a large influence on their potential for practical application. The lower critical diameter of the phlegmatized TEX (3.5% Svit 3RV wax, $\rho = 1.836$ g·cm^{-3}, $V_{C-J} = 6028$ m·s^{-1}) oscillates around 21 mm. The detonation velocity remains almost constant (upper limiting diameter) for charge diameters greater than 60 mm ($\rho = 1.815$ g·cm^{-3}, $V_{C-J} = 7446$ m·s^{-1}).[53b] Due to the lower inner pressability of the explosive, the density of phlegmatised-TEX charges decreased with increasing diameter of the pellets. Therefore, the authors concluded that the area of the ideal detonation of TEX may be larger than a diameter of 95 mm.[53b] Review in the field of TEX and TEX-based formulations have been written by Koch.[54]

144

11.4 1,1-Diamino-2,2-dinitroethylene (DADNE, FOX-7)

In 1998, Latypov et al. reported the synthesis of 1,1-diamino-2,2-dinitroethylene,[55] an acyclic explosive with a density of 1.894 $g \cdot cm^{-3}$[56] and a heat of formation of -133 $kJ \cdot mol^{-1}$.[27b, 57] The authors synthesized FOX-7 by treating 2-(dinitromethylene)-4,5-imidazolidinedione with an aqueous ammonia solution (pH = 8–9).[55] The synthesis of FOX-7 can be divided into two main steps: nitration of a heterocyclic species followed by hydrolysis to produce FOX-7 (Scheme 4).[58]
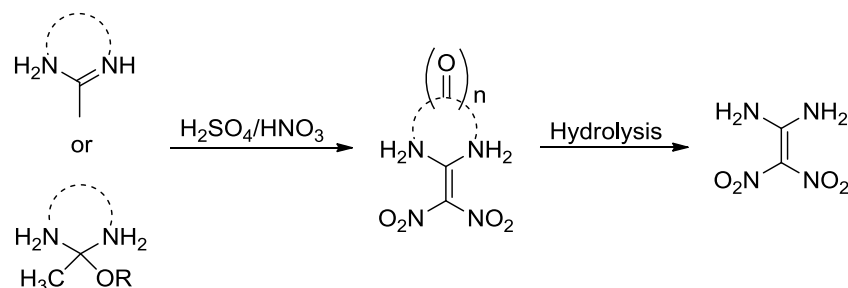
Scheme 4. Synthesis of 1,1-diamino-2,2-dinitroethylene (FOX-7).

In 1998, Bemm and Östmark first determined the crystal structure of α-FOX-7 (monoclinic crystal system, $P2_1/n$ space group, $\rho = 1.907$ $g \cdot cm^{-3}$, $T = 173$ K).[59] In 2005 Kempa and Herrmann conducted research into the phase behavior of FOX-7 using temperature dependent X-ray diffraction.[60] They observed a complete phase transition on heating at about 386 K ($\alpha \rightarrow \beta$). On cooling, the β phase fully transformed back to α phase. On further heating at 446 K, a second complete phase transition ($\beta \rightarrow \gamma$) occurs. On cooling, the authors observed only one transition ($\gamma \rightarrow \alpha$, below 348 K, incomplete).[60] Subsequently, polymorphs of FOX-7 in the range from 200 to 423 K using single-crystal X-ray and powder diffraction were investigated by Evers et al.[56] At 389 K, α-FOX-7 is transformed into orthorhombic β-FOX-7.[56] The $\alpha \rightarrow \beta$ phase transformation in FOX-7 is displacive and first order. Additionally, using single-crystal X-ray diffraction, the crystal structures of α-FOX-7 ($\rho = 1.924$ $g \cdot cm^{-3}$, $T = 200$ K; $\rho = 1.894$ $g \cdot cm^{-3}$, $T = 298$ K; $\rho = 1.880$ $g \cdot cm^{-3}$, $T = 333$ K) and β-FOX-7 at 393 K (orthorhombic crystal system, $P2_12_12_1$ space group, $\rho = 1.907$ $g \cdot cm^{-3}$, $T = 173$ K) were solved.[56] This research showed that α- and β-FOX-7 are structurally related. In order to determine the crystal structure of γ-FOX-7, Klapötke et al. slowly heated a single crystal of the β polymorph of FOX-7 to 440 K.[61] The crystal structures of the β polymorph at different temperatures ($\rho = 1.811$ $g \cdot cm^{-3}$, $T = 403$ K; $\rho = 1.807$ $g \cdot cm^{-3}$, $T = 413$ K; $\rho = 1.802$ $g \cdot cm^{-3}$, $T = 423$ K) and of the γ polymorph at 200 K (monoclinic crystal system, $P2_1/n$ space group, $\rho = 1.901$ $g \cdot cm^{-3}$) were determined. The authors were able to show that the $\beta \rightarrow \gamma$ phase transition in FOX-7 at 446 K is reconstructive and of first order.

Therefore, a single crystal of γ-FOX obtained at 450 K could be quenched to 200 K.[61] FOX-7 can be described as a push-pull ethylene containing electron donating amino groups ("*head*") and electron withdrawing nitro groups ("*tail*") within the same species. The crystal structure of FOX-7 consists of molecules with strong π conjugation. In all three phases of dipolar FOX-7, the molecules are packed "*head-to-tail*" in layers with widespread intra- and intermolecular hydrogen bonding within the layers and weak van der Waals interactions between the layers.[59, 69] The total number of hydrogen bonds formed per molecule increases from 14 in the α phase to 18 in both the β and γ phases of FOX-7.[56] Moreover, the single-crystal investigations as a function of time show that the oxygen atoms belong to the very active part of the FOX-7 molecule and therefore the four oxygen atoms, in the C-NO$_2$ groups of FOX-7, could also play a main part in triggering of the detonation.[56] (Figure 1).[61]
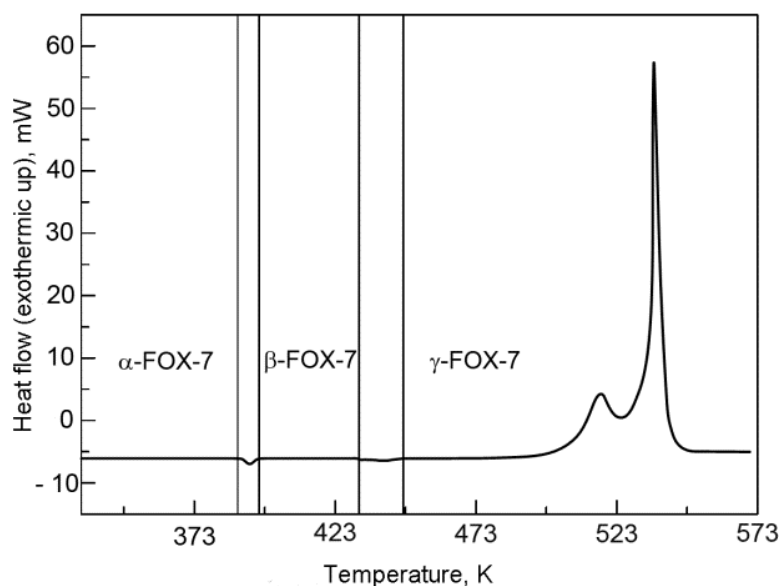
Figure 1. Differential scanning calorimetry curve of FOX-7.[1c]

Using a cylinder test, Trzciński et al. determined the detonation velocity ($\rho = 1.780$ g·cm^{-3}), Gurney energy, and Gurney velocity (8295 m·s^{-1}, 3620 kJ·kg^{-1}, and 2691 m·s^{-1}, respectively) for FOX-7.[62] In addition, the detonation energy was estimated ($E_0 = 5060$ kJ·kg^{-1}) using data obtained from cylindrical tests.[62] Moreover, Trzciński et al. determined the sensitivity of FOX-7 toward shockwaves ($\rho = 1.610$ g·cm^{-3}, diameter of charge: 25 mm) using the gap test (separating medium – ertalon): 52 mm (without detonation), 54 mm (detonation).[70] Furthermore, using the semi-empirical water test method the estimated detonation pressure ($\rho = 1780$ g·cm^{-3}, charge of FOX-7: diameter 25 mm, length 250 mm) has been reported. The obtained exponent of isentrope of the detonation products ($\gamma = 3.39$)

146

and $V_{C\text{-}J}$ (8375 m·s^{-1}) were used to calculate $p_{C\text{-}J}$ (28.4 GPa).[70] Moreover, the determined coefficients of the equations of state of the detonation products (Jones-Wilkins-Lee) are also given (Table 1).[70]

Table 1. Detonation pressure and the JWL isentrope.

$p_{C\text{-}J}$ [GPa]	E_0 [GPa]	A [GPa]	B [GPa]	C [GPa]	R_1	R_2	ω
28.4	9.0	14.1434	21.6637	1.2341	5.54	1.51	0.32

These data show that FOX-7 can be classified as an explosive, which shows low sensitivity toward mechanical stimuli (Table 2). Therefore, FOX-7 could be considered as a replacement of RDX.

Table 2. Physico-chemical properties of NTO, FOX-7, TEX in comparison to TATB, RDX, and HMX.

	NTO	FOX-7	TEX	TATB	RDX	HMX
Formula	$C_2H_2N_4O_3$	$C_2H_4N_4O_4$	$C_6H_6N_4O_8$	$C_6H_6N_6O_6$	$C_3H_6N_6O_6$	$C_4H_8N_8O_8$
MW [g·mol^{-1}]	130.06	148.08	262.13	258.15	222.12	296.16
IS [J]	>120[53a]	25[1c]	22.5[53b]	>50[27]	7.5[27b]	7.4[27b]
FS [N]	>353[53a]	>353[62]	>360[53b]	>353[27]	120[27b]	120[27b]
ESD [J]	>4.5[63]	ca. 4.5[1c]	0.25[53b]	2.5–4.24[1c, 27]	0.20[1c]	0.20[1c]
N [wt-%]	43.08	37.84	21.37	32.55	37.84	37.84
Ω [wt-%]	−24.60	−21.6	−42.72	−55.78	−21.61	−21.61
T_m [°C]	271[35f]	–	–	–	204[64]	281[64]
T_{dec} [°C]	271[35f]	220[58]	304[49]	360[1c]	237[64]	285[64]
ρ [g·cm^{-3}]	1.916[65]	1.894[56]	1.987	1.937[24]	1.806[66]	1.904[67]
$\Delta_f H°$ [kJ·mol^{-1}]	−129.4[a][68]	−133.9[a][27b, 57]	445.60[a][51]	−105.73	86.3	116.1
EXPLO5 V6.02[52]						
$-\Delta_E U°$ [kJ·kg^{-1}]	3748	4860[a][62]/4740	4488	4489	5910	5921
$T_{C\text{-}J}$ [K]	2866	3205	3044	3026	3844	3753
$p_{C\text{-}J}$ [GPa]	30.5	35.0	34.3	32.4	34.8	39.44
$V_{C\text{-}J}$ [m·s^{-1}]	8543	8910	8615	8693	8878	9263
Gas vol. [dm^3·kg^{-1}]	730	778	639	677	784	765

[a] Measured.

FOX-7 is shows detonation parameters similar to those of RDX, while its sensitivity toward external stimuli is comparable to that of TNT. FOX-7 formulations have been investigated by Trzciński et al. amongst others.[71] The measured detonation velocity and brisance of its formulations are higher than those measured for TNT and phlegmatized RDX. The sensitivity of phlegmatized FOX-7 toward to mechanical stimuli (impact and friction, and shock) is comparable or even less than the sensitivity of TNT. The composition based on phlegmatized FOX-7 and HMX is less sensitive than phlegmatized RDX.[71]

11.5 4-Amino-3,5-dinitropyrazole (LLM-116, ADNP)

Another explosive, which has low sensitivity towards external stimuli due to alternating electron donating and withdrawing groups and which may be used in low vulnerability ammunition is 4-amino-3,5-dinitropyrazole (LLM-116, ADNP), which can be obtained by (Scheme 5):

(a) Amination of 3,5-dinitropyrazole by vicarious nucleophilic substitution of hydrogen (VNS[72]) using 1,1,1-trimethylhydrazinium iodide (TMHI)[73] or 4-amino-1,2,4-triazole (4-AT);[74]

(b) Nucleophilic substitution of the 4-positioned group in 3,4,5-trinitropyrazole[75] or 4-chloro-3,5-dinitro-pyrazole (ClDNP);[76]

(c) Nitration of protected 4-aminopyrazole-3,5-dicarboxylic acid or 4-ethylcarbethoxy-amino-1-ethylcarbethoxypyrazole.[74]

R_1= NO$_2$ (b$_1$), Cl (b$_2$); c$_1$: R$_2$= COOH, R$_3$= H; c$_2$: R$_2$= H, R$_3$= COOEt.
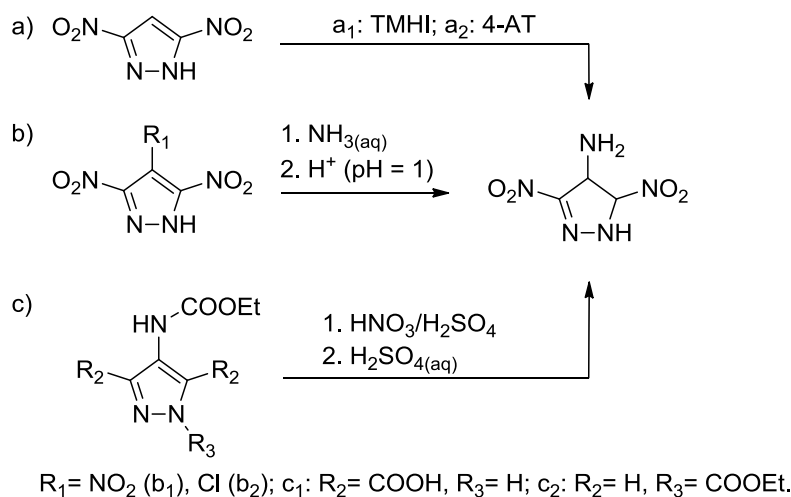
Scheme 5. Synthesis of 4-amino-3,5-dinitropyrazole, LLM-116.

Depending on the choice of the starting materials for the synthesis of LLM-116, different conclusions can be drawn. The shortest synthetic route with the highest overall yield (61%) is the synthesis of LLM-116 from 4-chloropyrazole (nitration followed by substitution of the chlorine atom in 3,4,5-trinitropyrazole).[74] Moreover, this procedure is characterized by only a small amount of waste and no unfavorable solvents. Therefore, this process was scaled up to a small pilot plant scale.[74] In 2001 Schmidt et al. determined the structure of LLM-116 in the solid state at 294 K (orthorhombic crystal system, $P2_12_12_1$ space group, $\rho = 1.900 \ \text{g·cm}^{-3}$).[73]

The calculated enthalpy of formation ($\Delta_f H°$, isodesmic reaction, density functional theory B3LYP method with 6-311++G(d, p) basis set) of LLM-116 corresponds to 96.3 kJ·mol^{-1}.[79] Energetic salts based on ADNP (pK_a = 3.42[75b]) were prepared by Shreeve et al.[77] Salts of ADNP with the following counter anions were prepared: ammonium (A),

hydrazinium (Hy), guanidinium (G), aminoguanidinium (AG), diaminoguanidinium (DAG), triaminoguanidinium (TAG), biguanidinium (BG), diaminouronium (HDAU), N-carbamoylguanidinium (CG), 1,2,4-triazolium (HT), 3-amino-1,2,4-triazolium (H3AT), 4-amino-1,2,4-triazolium (H4AT), 3,5-diamino-1,2,4-triazolium (HDAT), 1,4-dimethyl-5-aminotetrazolium (HDMAT) and 1,5-diamino-4-methyltetrazolium (HDAMT) (Scheme 6; Table 3, Table 4).
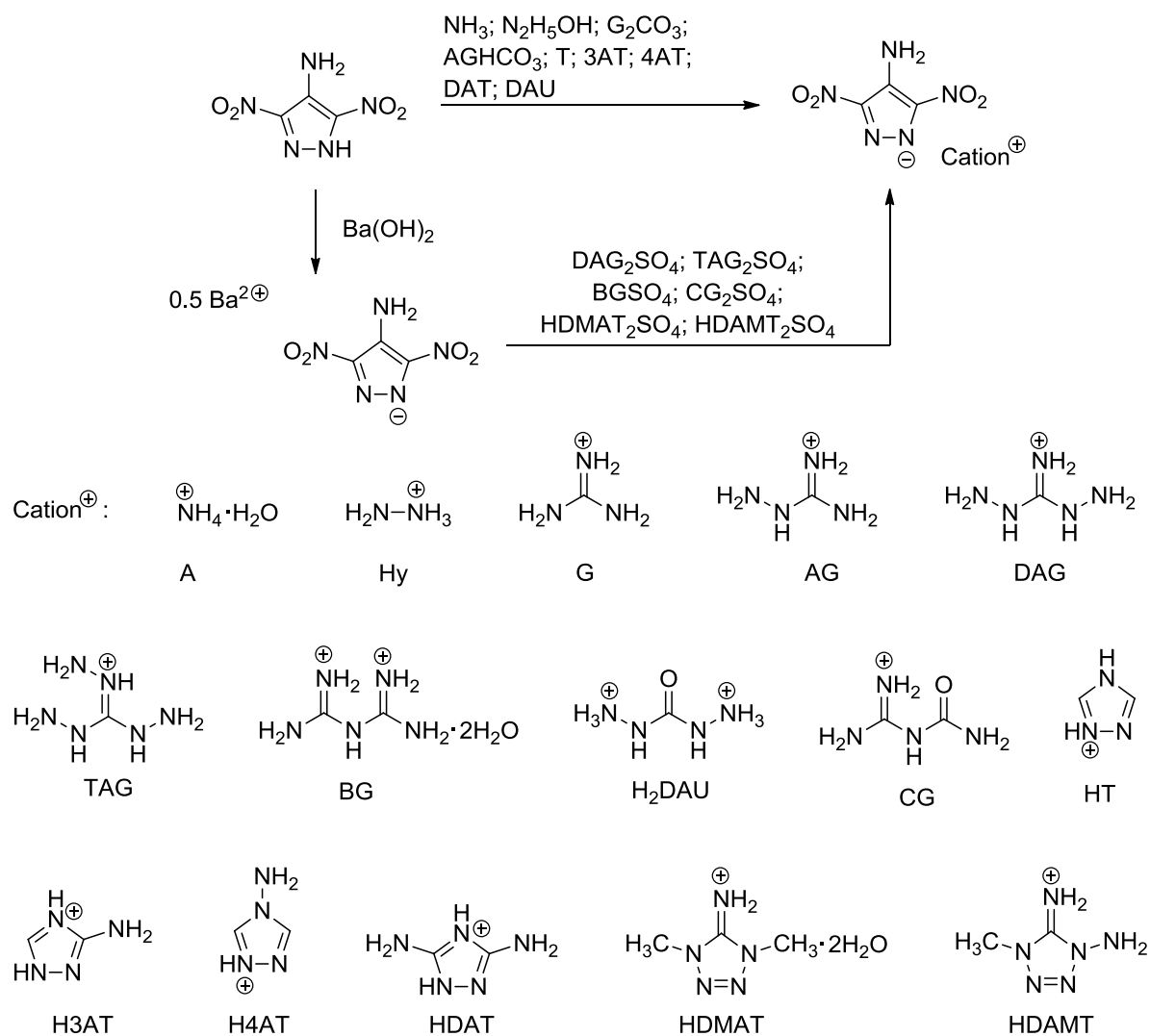
Scheme 6. Synthesis of ADNP-based energetic salts.

Table 3. Physical properties and thermochemical values of ADNP and its salts.[77]

	ADNP	A-ADNP	Hy-ADNP	G-ADNP	AG-ADNP	DAG-ADNP	TAG-ADNP	BG-ADNP$_2$	H$_2$DAU-ADNP$_2$	CG-ADNP	HT-ADNP
Formula	$C_3H_3N_5O_4$	$C_3H_6N_6O_4$	$C_3H_7N_7O_4$	$C_4H_8N_8O_4$	$C_4H_9N_9O_4$	$C_4H_{10}N_{10}O_4$	$C_4H_{11}N_{11}O_4$	$C_8H_{13}N_{15}O_8$	$C_7H_{12}N_{14}O_9$	$C_5H_9N_9O_5$	$C_5H6N_8O_4$
MW [g·mol^{-1}]	173.09	190.12	205.13	232.16	247.17	262.19	277.20	447.28	436.26	275.18	242.15
IS [J]	12[78], >40[79]	>60	>60	>60	>60	>60	>60	>60	>60	>60	>60
FS [N]	>360[78]	nd	nd	nd	nd	nd	nd	nd	nd	nd	nd
N [wt-%]	40.00	44.20	47.80	48.27	51.00	53.42	55.58	46.97	44.95	45.81	46.27
Ω [wt-%]	−32.35	−42.08	−42.90	−55.13	−55.02	−54.92	−54.83	−51.86	−40.34	−55.23	−59.46
T_m [°C]	166–168[75b] 164[79]	–	–	–	223	201	–	–	193	243	–
T_{dec} [°C]	178[79, 80]	275	221	303	223	201	229	169	193	243	179
ρ[a] [g·cm^{-3}]	1.900[b][73]	1.63	1.64	1.63	1.69	1.67	1.71	1.72	1.84	1.73	1.62
$\Delta_f H°$ [kJ·mol^{-1}]	96.3[79]	64.8	222.6	36.1	140.1	250.5	356.9	100.4	211.9	−166.3	310.4
$-\Delta_E U°$ [kJ·kg^{-1}]	5206	5015	5558	4308	4572	4793	4985	4341	5006	3717	4929
EXPLO5 V6.02[52]											
$T_{C\text{-}J}$ [K]	3584	3395	3600	2968	3010	3086	3102	3014	3308	2654	3433
$p_{C\text{-}J}$ [GPa]	35.0	24.3	26.6	22.1	25.6	26.5	29.6	24.6	32.5	23.2	22.3
$V_{C\text{-}J}$ [m·s^{-1}]	8894	8036	8383	7863	8414	8563	8995	8139	8886	7990	7749
Gas vol. [dm^3·kg^{-1}]	712	838	865	846	866	885	898	804	791	820	767

[a] Gas pycnometer (25 °C); [b] X-ray measurement; *nd* (not determined).

Table 4. Physico-chemical properties of ADNP salts.[77]

	H3AT-ADNP	H4AT-ADNP	HDAT-ADNP	HDMAT-ADNP	HDAMT-ADNP
Formula	$C_5H_7N_9O_4$	$C_5H_7N_9O_4$	$C_5H_8N_{10}O_4$	$C_6H_{10}N_{10}O_4$	$C_5H_9N_{11}O_4$
MW [g·mol^{-1}]	257.17	257.17	272.18	286.21	287.2
IS [J]	> 60	> 60	> 60	> 60	> 60
N [wt-%]	49.02	49.02	51.46	48.94	53.65
Ω [wt-%]	−59.10	−59.10	−58.78	−72.67	−58.49
T_m [°C]	257	188	270	184	173
T_{dec} [°C]	257	223	270	206	173
ρ [g·cm^{-3}]	1.67	1.73	1.79	1.54	1.60
$\Delta_f H°$ [kJ·mol^{-1}]	283.6	411.1	241.6	389.3	471.8
EXPLO5 V6.02[52]					
$-\Delta_E U°$ [kJ·kg^{-1}]	4710	5200	4460	4821	5031
T_{C-J} [K]	3241	3437	3000	3182	3356
p_{C-J} [GPa]	23.7	27.3	27.9	20.2	23.2
V_{C-J} [m·s^{-1}]	8001	8441	8616	7652	8055
Gas vol. [dm^3·kg^{-1}]	787	783	807	820	836

The salts shown in Scheme 6 have densities between 1.54 and 1.84 g·cm^{-3}, and all show an impact sensitivity higher than 60 J. The most thermally stable is the guanidinium salt which decomposes at 303 °C. The salts which were investigated possess lower sensitivities than that of RDX.

The diaminouronium (p_{C-J} = 32.5 GPa, V_{C-J} = 8886 m·s^{-1}) and triaminoguanidinium (p_{C-J} = 29.6 GPa, V_{C-J} = 8995 m·s^{-1}) are comparable with TATB (Table 2) and can be classed as extremely insensitive energetic salts with high detonation parameters.

11.6 3,6-Dinitropyrazolo[4,3-*c*]pyrazoles (DNPPs)

Molecular modeling and explosive performance calculations resulted in the development of the novel explosive 3,6-dinitropyrazolo[4,3-*c*]pyrazole (DNPP), which was successfully synthesized in 1993 by Shevelev et al.[81] An alternative method for the synthesis of DNPP, which shows a higher overall yield was developed in the Lawrence Livermore National Laboratory by Pagoria et al.[82] Further improvements to the LLNL synthetic method for DNPP increased the overall yield of DNPP starting from acetylacetone to 33%. In this process, 4-amino-3,5-dimethylpyrazole is prepared by a one-pot reaction starting from acetylacetone followed by diazotization, cyclization, oxidation, and nitrative decarboxylation to give DNPP (Scheme 7).[80, 83]
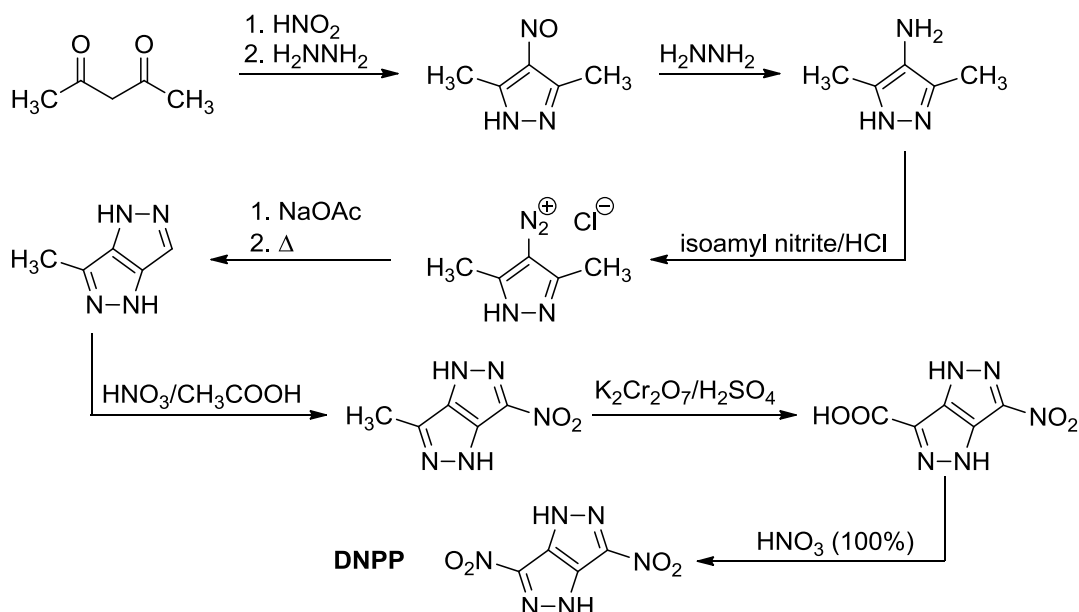
Scheme 7. Synthesis of DNPP.

DNPP shows high thermal stability (exothermic peak on the DSC at 330 °C)[80] and low sensitivity towards mechanical stimuli: $Dh_{50} = 68$ cm (HMX = 32 cm;[80] $IS = 15$ J, $FS = 160$ N[84]). The calculated $\Delta_f H°$ (isodesmic reaction, density functional theory B3LYP method with 6-31+G** basis set) of DNPP is equal to +322.6 kJ·mol^{-1}[84] and differs from the measured value of +271.96 kJ·mol^{-1}.[80] DNPP has a slightly lower density than FOX-7,[80] which is also reflected in its high detonation parameters ($p_{C-J} = 32.0$ GPa, $V_{C-J} = 8687$ m·s^{-1}). Moreover, DNPP has two acidic hydrogen atoms ($pK_{a1} = 5.39$, $pK_{a2} = 8.54$)[81] and can therefore be used as a starting material for the synthesis of energetic ionic compounds. Salts containing the mono or dianion of DNPP were investigated by Stern et al.[85] and later by Shreeve et al.[84] and the following nitrogen-containing counter cations were chosen for the synthesis of energetic salts – either in a straightforward manner or by metathesis reactions (Scheme 8): ammonium (A), hydroxylammonium (HA), hydrazinium (Hy), guanidinium (G), aminoguanidinium (AG), diaminoguanidinium (DAG), triaminoguanidinium (TAG), 3,5-diamino-triazolium (HDAT), 3,4,5-triamino-triazolium (HTAT) and 2-iminium-5-nitriminooctahydroimidazo[4,5-d]imidazole (INI).[84] In addition, metal salts of DNPP were obtained in the simple reaction of DNPP with sodium hydroxide, potassium hydroxide, or silver nitrate (Scheme 8).[84]

Scheme 8. Synthesis of DNPP-based energetic salts.

Most of the salts, shown in Scheme 8, have lower impact and friction sensitivities than DNPP and most DNPP salts show high decomposition temperatures. DAG$_2$DNPP has the lowest decomposition temperature (T_{dec} = 209 °C), whereas the highest thermal stabilities are shown by the disodium (T_{dec} = 395 °C) and dipotassium (T_{dec} = 365 °C) salts. The densities of the DNPP salts are between 1.68 (G$_2$DNPP) and 1.85 g·cm^{-3} (Ag$_2$DNPP). All of the DNPP salts with energetic counterions shown in Scheme 8 are endothermic compounds ($\Delta fH°$ ranges from 158.5 to 963.8 kJ·mol^{-1}). The highest values for the detonation parameters (p_{C-J}, V_{C-J}) are shown by the dihydroxylammonium, dihydrazinium, diaminoguanidinium, and monotriaminoguanidinium salts of DNPP (Table 5). Finally, DNPP is also used as a precursor for many other covalent energetic materials.[83a] One of the most promising candidates for application as an insensitive munition is 1,4-diami-no-3,6-dinitropyrazolo[4,3-c]pyrazole (LLM-119, DADNP). DADNP can be obtained by N-amination of DNPP using hydroxylamine-O-sulfonic acid[86] or O-(mesitylenesulfo-nyl)hydroxylamine.[87] The second method results in a higher yield and purity of DADNP (Scheme 9).

Table 5. Physical properties and thermochemical values of DNPP and its salts.[84]

	DNPP	A₂-DNPP	HA₂-DNPP	Hy₂-DNPP	HDAT-DNPP	HTAT₂-DNPP	G₂-DNPP	AG₂-DNPP	DAG₂-DNPP	TAG-DNPP	INI-DNPP·H₂O
Formula	$C_4H_2N_6O_4$	$C_4H_8N_8O_4$	$C_4H_8N_8O_6$	$C_4H_{10}N_{10}O_4$	$C_6H_7N_{11}O_4$	$C_8H_{14}N_{18}O_4$	$C_6H_{12}N_{12}O_4$	$C_6H_{14}N_{14}O_4$	$C_6H_{16}N_{16}O_4$	$C_5H_{10}N_{12}O_4$	$C_8H_{11}N_{13}O_7$
MW [g·mol⁻¹]	198.10	232.16	264.16	262.19	297.19	426.31	316.24	346.27	376.30	302.21	401.26
IS [J]	15	>40	29	16	>40	>40	>40	>40	>40	12	23
FS [N]	160	360	360	160	360	360	360	360	360	80	160
N [wt-%]	42.42	48.27	42.42	53.42	51.84	59.14	53.15	56.63	59.56	55.62	45.38
Ω [wt-%]	−40.38	−55.12	−36.34	−54.92	−91.91	−71.30	−70.83	−69.30	−68.02	−58.23	−60.53
T_m [°C]	–	160	174	–	–	–	318	213	–	208	–
T_{dec} [°C]	330[80]/336	328	327	247	287	289	324	222	209	215	238
ρ[a] [g·cm⁻³]	1.865[b][80]/1.85	1.69	1.82	1.72	1.71	1.67	1.68	1.69	1.71	1.76	1.79[c]
$\Delta_fH°$ [kJ·mol⁻¹]	322.6/271.96[80]	158.5	274.2	501.0	481.9	963.8	173.3	477.0	679.6	605.5	505.6
EXPLO5 V6.02[52]											
$-\Delta_EU°$ [kJ·kg⁻¹]	5297	4830	5942	5732	4748	4780	3853	4486	4754	5335	4840
T_{C-J} [K]	3801	3173	3723	3462	3287	3078	2599	2825	2879	3333	3279
p_{C-J} [GPa]	32.0	25.6	34.9	31.3	24.9	26.3	23.9	27.7	30.6	31.0	27.8
V_{C-J} [m·s⁻¹]	8687	8335	9084	9128	8154	8605	8287	8836	9260	9092	8463
Gas vol. [dm³·kg⁻¹]	680	843	804	884	763	825	842	869	888	846	745

154
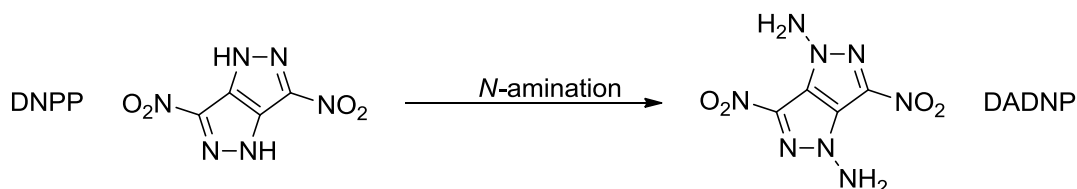
Scheme 9. Synthesis of DADNP.

DADNP decomposes without melting at 253 °C and is more sensitive towards impact than HMX (Dh_{50} value of 24 cm; HMX = 32 cm). Tests have shown that it is not friction or spark sensitive.[80] DADNP has a density of 1.845 g·cm^{-3} which is lower than that of DNPP. The decrease in the density and thermal stability of DADNP in comparison with DNPP is due to the fact that the amino groups are orthogonal to the plane of the molecule in DADNP.[80] The measured $\Delta_f H°$ value of +476.98 kJ·mol^{-1}[80] and moderately high density are the reason for the high detonation parameters: $-\Delta_E U° = -5697$ kJ·kg^{-1}, $T_{C-J} = 3846$ K, $p_{C-J} = 34.13$ GPa; $V_{C-J} = 8973$ m·s^{-1}, Gas vol. = 736 dm^3·kg^{-1}.[52] The introduction of the two amino groups increases the heat of detonation, detonation temperature, detonation pressure, and detonation velocity.

11.7 Conclusions

It is clear that there is an ever-increasing interest in the development of insensitive explosives within the energetic materials community. This is not only because of increasing demands with respect to tailoring the properties of explosives, but also in finding convenient production methods for such compounds. For this purpose researchers have investigated numerous new explosives. Some of the compounds recently investigated as insensitive explosives have been described and can be separated into two categories: covalent (NTO, TEX, FOX-7, ADNP, DNPPs) and ionic species (ANDP and DNPP). Some of them are currently used in combination with other ingredients in order to improve their properties (generally NTO and FOX-7). Recently, pyrazole-based ionic species were synthesized, which are promising as insensitive explosives. Such energetic materials are characterized by low sensitivity toward external stimuli and generally show high detonation parameters. Most of the compounds, which have been discussed possess high densities and are endothermic. The high densities and heats of formation are reflected in the high detonation parameters, which are reported for these compounds.

11.8 References

[1]   a) R. E. Bowen, *Insensitive Munitions Technical Requirements*, OMB No. 0704-0188, Naval Sea Systems Command, Insensitive Munitions Office, Washington D.C., USA, **1990**; b) J. Isler, The Transition to Insensitive Munitions (IM), *Propellants Explos. Pyrotech.* **1998**, *23*, 283–291; c) T. M. Klapötke, *Chemistry of High-Energy Materials*, 3ʳᵈ edition, Walter de Gruyter, Berlin, **2015**.

[2]   J. P. Agrawal, Some New High Energy Materials and their Formulations for Specialized Applications, *Propellants Explos. Pyrotech.* **2005**, *30*, 316–328.

[3]   a) N. N. Semenov, *Z. Phys.* **1928**, *48*, 571–582; b) O. M. Todes, *Zh. Fiz. Khim.* **1933**, *4*, 78–81.

[4]   J. E. Field, *Acc. Chem. Res.* **1992**, *25*, 489–496.

[5]   a) F. J. Zerilli, E. T. Toton, *Phys. Rev. B* **1984**, *29*, 5891–5902; b) M. D. Fayer, A. Tokmakoff, D. D. Dlott, *Mat. Res. Soc. Symp. Proc.* **1992**, *296*, 379–384; c) A. Tokmakoff, M. D. Fayer, D. D. Dlott, *J. Phys. Chem.* **1993**, *97*, 1901–1913; d) C. M. Tarver, S. K. Chidester, A. L. Nichols, Critical Conditions for Impact- and Shock-Induced Hot Spots in Solid Explosives, *J. Phys. Chem.* **1996**, *100*, 5794–5799; e) T. Shan, A. P. Thompson, *J. Phys. Conf. Ser.* **2014**, *500*, 172009; f) M. A. Wood, M. J. Cherukara, E. M. Kober, A. Strachan, *J. Phys. Chem. C* **2015**, *119*, 22008–22015.

[6]   a) J. N. Maycock, D. E. Grabenstein, *Science* **1966**, *152*, 508–509; b) K. Raha, J. S. Chhabra, *Def. Sci. J.* **1991**, *41*, 295–304.

[7]   B. Zygmunt, The Detonation Properties of Explosive-Water Mixtures, *Propellants Explos. Pyrotech.* **1982**, *7*, 107–109.

[8]   a) A. van der Steen, R. Verbeek, *Propellants Explos. Pyrotech.* **1990**, *15*, 19–21; b) W. A. Trzciński, L. Szymańczyk, *J. Energ. Mater.* **2005**, *23*, 151–168; c) A. E. van der Heijden, Y. L. Creyghton, E. Marino, R. H. Bouma, G. J. Scholtes, W. Duvalois, M. C. Roelands, *Propellants Explos. Pyrotech.* **2008**, *33*, 25–32; d) P. P. Vadhe, R. B. Pawar, R. K. Sinha, S. N. Asthana, A. Subhananda Rao, *Combust. Explos. Shock Waves (Engl. Transl.)* **2008**, *44*, 461–477; e) Q.-L. Yan, S. Zeman, A. Elbeih, *Thermochim. Acta* **2012**, *537*, 1–12; f) B. He, V. Stepanov, H. Qiu, L. N. Krasnoperov, *Propellants Explos. Pyrotech.* **2015**, *40*, 659–664.

[9]   S P. Felix, G. Singh, A. K. Sikder, J. P. Agrawal, *Thermochim. Acta* **2005**, *426*, 53–60.

[10] J.-S. Lee, C.-K. Hsu, *Thermochim. Acta* **2002**, *392–393*, 153–156; b) G. Singh, S. F. Prem, P. Soni, *Thermochim. Acta* **2003**, *399*, 153–165; c) S. S. Samudre, U. R. Nair, G. M. Gore, R. K. Sinha, A. K. Sikder, S. N. Asthana, *Propellants Explos. Pyrotech.* **2009**, *34*, 145–150; d) B. Risse, F. Schnell, D. Spitzer, *Propellants Explos. Pyrotech.* **2014**, *39*, 397–401.

[11] K. S. Jaw, J. S. Lee, *J. Therm. Anal. Calorim.* **2008**, *93*, 953–957.

[12] a) M. B. Talawar, A. P. Agarwal, M. Anniyappan, G. M. Gore, S. N. Asthana, S. Venugopalan, *J. Hazard. Mater.* **2006**, *137*, 1848–1852; b) C. M. Tarver, *J. Phys. Chem. A* **2010**, *114*, 2727–2736.

[13] a) R. L. Simpson, P. A. Urtiew, D. L. Ornellas, G. L. Moody, K. J. Scribner, D. M. Hoffman, *Propellants Explos. Pyrotech.* **1997**, *22*, 249–255; b) J. Li, T. B. Brill, *Propellants Explos. Pyrotech.* **2006**, *31*, 61–69.

[14] J. Z. Li, F. Q. Zhao, R. Z. Hao, *J. Therm. Anal. Calorim.* **2006**, *85*, 779–784.

[15] a) W. A. Trzciński, L. Szymańczyk, *Bull. Mil. Univ. Technol.* **2003**, *52*, 63–72; b) J. C. Oxley, J. L. Smith, M. A. Donnelly, K. Colizza, S. Rayome, *Propellants Explos. Pyrotech.* **2015**, *41*, 98–113.

[16] N. Radacsi, A. I. Stankiewicz, Y. L. Creyghton, A. E. van der Heijden, J. H. ter Horst, *Chem. Eng. Technol.* 2011, **34**, 624–630.

[17] a) V. Stepanov, L. N. Krasnoperov, I. B. Elkina, X. Zhang, *Propellants Explos. Pyrotech.* **2005**, *30*, 178–183; b) D. Spitzer, C. Baras, M. R. Schäfer, F. Ciszek, B. Siegert, *Propellants Explos. Pyrotech.* **2011**, *36*, 65–74; c) J. T. Essel, A. C. Cortopassi, K. K. Kuo, C. G. Leh, J. H. Adair, *Propellants Explos. Pyrotech.* **2012**, *37*, 699–706; d) R. Kumar, P. F. Siril, P. Soni, *Propellants Explos. Pyrotech.* **2014**, *39*, 383–389; e) J. Liu, W. Jiang, Q. Yang, J. Song, G. Hao, F. Li, *Def. Technol.* **2014**, *10*, 184–189.

[18] L. Blas, M. Klaumünzer, F. Pessina, S. Braun, D. Spitzer, *Propellants Explos. Pyrotech.* **2015**, *40*, 938–944.

[19] a) Y. X. Zhang, D. B. Liu, C. X. Lv, *Propellants Explos. Pyrotech.* **2005**, *30*, 438–441; b) B. Risse, D. Spitzer, D. Hassler, F. Schnell, M. Comet, V. Pichot, H. Muhr, *Chem. Eng. J.* **2012**, *203*, 158–165; c) Y. Bayat, S. M. Pourmortazavi, H. Iravani, H. Ahadi, *J. Supercrit. Fluids* **2012**, *72*, 248–254.

[20] G. Yang, F. Nie, H. Huang, L. Zhao, W. Pang, *Propellants Explos. Pyrotech.* **2006**, *31*, 390–394.

[21] Y. Bayat, V. Zeynali, *J. Energ. Mater.* **2011**, *29*, 281–291.

[22] B. Gao, P. Wu, B. Huang, J. Wang, Z. Qiao, G. Yang, F. Nie, *New J. Chem.* **2014**, *38*, 2334–2341.

[23] C. L. Jackson, J. F. Wing, *Am. Chem. J.* **1888**, *10*, 283–294.

[24] H. H. Cady, A. C. Larson, *Acta Crystallogr.* **1965**, *18*, 485–496.

[25] B. M. Dobratz, *The Insensitive High Explosive Triamino-trinitrobenzene (TATB): Development and Characterization – 1888–1994*, Report LA-13014-H, UC-741, Los Alamos National Laboratory, Los Alamos, NM, USA, **1995**.

[26] I. Akst, Heat of Detonation, the Cylinder Test, and Performance Munitions, *9th International Symposium on Detonation*, Portland, OR, USA, August 28 - September 1, **1989**, p. 478.

[27] a) D. Skinner, D. Olson, *Propellants Explos. Pyrotech.* **1998**, *23*, 34–42; b) R. Meyer, J. Köhler, A. Homburg, Explosives, 6th edition, Wiley-VCH, Weinheim, **2007**.

[28] S. M. Kaye, H. L. Herman, Encyclopedia of Explosives and Related Items, Vol. 9, U.S. Army Armament Research and Development Command, Large Caliber Weapon Systems Laboratory, Washington D.C., USA, **1978**.

[29] T. Y.-J. Han, P. F. Pagoria, A. E. Gash, A. Maiti, C. A. Orme, A. R. Mitchell, L. E. Fried, *New J. Chem.* **2009**, *33*, 50–56.

[30] J. Schmidt, H. Gehlen, *Z. Chem.* **1965**, *5*, 304–304.

[31] W. Manchot, R. Noll, *Justus Liebigs Ann. Chem.* **1905**, *343*, 1–27.

[32] G. I. Chipen, R. P. Bokalder, V. Y. Grinshtein, *Chem. Heterocycl. Compd.* **1966**, *2*, 79–83.

[33] a) K.-Y. Lee, L. B. Chapman, M. D. Coburn, *J. Energ. Mater.* **1987**, *5*, 27–33; b) K. Lee, M. D. Coburn, *Pat. US 4733610*, The United States Department of Energy, Washington D.C., USA, **1988**.

[34] O. Widman, A. Cleve, *Ber. Dtsch. Chem. Ges.* **1898**, *31*, 378–381.

[35] a) E. Bojarska-Olejnic, L. Stefaniak, M. Witanowski, G. A. Webb, *Bull. Pol. Acad. Sci. Chem.* **1986**, *34*, 295–303; b) A. Becuwe, A. Delclos, *Propellants Explos. Pyrotech.* 1993, **18**, 1–10; c) D. C. Sorescu, T. R. L. Sutton, D. L. Thompson, D. Beardall, C. A. Wight, *J. Mol. Struct.* **1996**, *384*, 87–99; d) L. Fan, C. Dass, T. J. Burkey, *J. Labelled Compd. Radiopharm.* **1996**, *38*, 87–94; e) J. Zhang, T. Zhang, G. Ma, K. Yu, *J. Heterocycl. Chem.* **2006**, *43*, 503–508; f) M. Szala, S. Cudziło, R. Lewczuk, *Bull. Mil. Univ. Technol.* **2011**, *60*, 407–419; g) M. Szala, S. Cudziło, R. Lewczuk, *Bull. Mil. Univ. Technol.* **2012**, *61*, 299–308.

[36] C. J. Cowden, *Pat. US 2003187274*, Merck Co. Inc., Rahway, NJ, USA, **2003**.

[37] a) C.-F. Kröger, P. Selditz, M. Mutscher, *Chem. Ber.* **1965**, *98*, 3034–3039; b) D. R. Haines, N. J. Leonard, D. F. Wiemer, *J. Org. Chem.* **1982**, *47*, 474–482.

[38] C.-F. Kröger, L. Hummel, M. Mutscher, H. Beyer, *Chem. Ber.* **1965**, *98*, 3025–3033.

[39] Y. A. Rozin, N. A. Belyaev, V. A. Bakulev, I. Leban, Y. A. Azev, *Chem. Heterocycl. Compd.* **2011**, *46*, 1534–1535.

[40] H. S. Kim, E. M. Goh, B. S. Park, *Pat. US 6583293*, The Agency for Defense Development (KR), Seoul, South Korea, **2003**.

[41] S. Cudziło, W. A. Trzciński, *J. Energ. Mater.* **2001**, *19*, 1–21.

[42] V. L. Zbarsky, N. V. Yudin, *Propellants Explos. Pyrotech.* **2005**, *30*, 298–302.

[43] V. L. Zbarskii, V. V. Kužmin, N. V. Yudin, *Russ. J. Org. Chem.* **2004**, *40*, 1069–1070.

[44] W. A. Trzciński, M. Szala, W. Rejmer, *Propellants Explos. Pyrotech.* **2015**, *40*, 498–505.

[45] a) A. Bąk, A. Maranda, J. Nowaczewski, M. Szerszeń, *Cent. Eur. J. Energ. Mater.* **2006**, *3*, 53–64; b) V. Fung, C. Patel, M. Ervin, B. Alexander, P. Samuels, Development and Manufacture of an Insensitive Composition B Replacement Explosive IMX-104 for Mortar Applications, *Insensitive Munitions and Energetic Materials Technology Symposium – International Progress in Insensitive Munitions and Energetic Materials*, Munich, Germany, 11–13 October, **2010**; c) W. B. Hummers, The Insensitive TNT Replacement Explosive IMX-101 and IMX-104 Qualifiation, *Insensitive Munitions and Energetic Materials Technology Symposium – International Progress in Insensitive Munitions and Energetic Materials*, Munich, Germany, 11–13 October, **2010**; d) K. E. Lee, W. A. Balas-Hummers, A. R. Di Stasio, C. H. Patel, J. Samuels, Qualification Testing of the Insensitive TNT Replacement Explosive IMX-101, *Insensitive Munitions and Energetic Materials Technology Symposium – International Progress in Insensitive Munitions and Energetic Materials*, Munich, Germany, 11–13 October, **2010**; e) J. J. Sabatini, K. D. Oyler, *Crystals* **2016**, *6*, 1–22; f) C. Spyckerelle, C. Songy, G. Eck, IM Melt Cast Compositions Based on NTO, *Insensitive Munitions and Energetic Materials Technology Symposium – International Progress in Insensitive Munitions and Energetic Materials*, Munich, Germany, 11–13 October, **2010**; g) W. A. Trzciński, S. Cudziło, S. Dyjak, M. Nita, *Cent. Eur. J. Energ. Mater.* **2014**, *11*, 443–455; h) D. Zaloga, K. Patel, B. Travers, P. Samuels, A. Di Stasio, S. Singh, Initiation Trials of IMX-104 in 81 mm Mortars, *Insensitive Munitions and Energetic Materials Technology Symposium –*

International Progress in Insensitive Munitions and Energetic Materials, Munich, Germany, 11–13 October, **2010**.

[46] V. T. Ramakrishnan, M. Vedachalam, J. H. Boyer, *Heterocycles* **1990**, *31*, 479–480.

[47] K. Karaghiosoff, T. M. Klapötke, A. Michailovski, G. Holl, *Acta Crystallogr., Sect. C* **2002**, *58*, o580–o581.

[48] Y. V. Gatilov, T. V. Rybalova, O. A. Efimov, A. A. Lobanova, G. V. Sakovich, S. V. Sysolyatin, *J. Struct. Chem.* **2005**, *46,* 566–571.

[49] S. A. Headrick, H. G. Johnston, Development Toward the Large-Scale Synthesis of TEX, *Insensitive Munitions and Energetic Materials Technology Symposium – Lower Cost Solutions for 21ˢᵗ Century IM/EM Requirements*, Tucson, AZ, USA, 11–14 May, **2009**.

[50] X. L. Zeng, X. H. Ju, H. X. Gao, *Adv. Mater. Res.* **2012**, *554–556*, 1618–1623.

[51] G. K. Lund, T. K. Highsmith, P. C. Braithwaite, R. B. Wardle, *Pat. US 5529649*, Assignee: Thiokol Corporation, Ogden, UT, USA, **1996**.

[52] M. Sućeska, *Explo5, Version 6.02*, Zagreb, Croatia, **2014**.

[53] a) R. Meyer, J. Köhler, A. Homburg, Explosives, 5ᵗʰ edition, Wiley-VCH, Weinheim, **2002**; b) J. Vágenknecht, P. Mareček, W. A. Trzciński, *J. Energ. Mater.* **2002**, *20*, 245–253.

[54] E.-C. Koch, *Propellants Explos. Pyrotech.* **2015**, *40*, 374–387.

[55] N. V. Latypov, J. Bergman, A. Langlet, U. Wellmar, U. Bemm, *Tetrahedron* **1998**, *54*, 11525–11536.

[56] J. Evers, T. M. Klapötke, P. Mayer, G. Oehlinger, J. Welch, *Inorg. Chem.* **2006**, *45*, 4996–5007.

[57] H. Östmark, A. Langlet, H. Bergman, N. Wingborg, U. Wellmar, U. Bemm, FOX-7 – A New Explosive with Low Sensitivity and High Performance, in *11ᵗʰ International Detonation Symposium*, Snowmass Village, CO, USA, 31 August – 4 September, **1998**, p. 807.

[58] N. Latypov, A. Langlet, U. Wellmar, *Pat. US 6312538*, Totalforsvarets Forskningsinstitut, Stockholm, Sweden, **2001**.

[59] U. Bemm, H. Östmark, *Acta Crystallogr., Sect. C* **1998**, *54*, 1997–1999.

[60] P. B. Kempa, M. Herrmann, *Part. Part. Syst. Charact.* **2005**, *22*, 418–422.

[61] M.-J. Crawford, J. Evers, M. Göbel, T. M. Klapötke, P. Mayer, G. Oehlinger, J. M. Welch, *Propellants Explos. Pyrotech.* **2007**, *32*, 478–495.

[62] W. A. Trzciński, S. Cudziło, Z. Chyłek, L. Szymańczyk, *Bull. Mil. Univ. Technol.* **2006**, *55*, 145–157.

[63] R. J. Spear, C. N. Louey, M. G. Wolfson, *A Preliminary Assessment of 3-Nitro-1,2,4-triazol-5-one (NTO) as an Insensitive High Explosive*, *ADA215063*, Materials Research Laboratory, Canberra, Australia, **1989**.

[64] J.-S. Lee, C.-K. Hsu, C.-L. Chang, *Thermochim. Acta* **2002**, *392–393*, 173–176.

[65] N. Bolotina, K. Kirschbaum, A. A. Pinkerton, *Acta Crystallogr., Sect. B* **2005**, *61*, 577–584.

[66] C. S. Choi, E. Prince, *Acta Crystallogr., Sect. B* 1972, **28**, 2857–2862.

[67] J. R. Deschamps, M. Frisch, D. Parrish, *J. Chem. Crystallogr.* **2011**, *41*, 966–970.

[68] A. Finch, P. J. Gardner, A. J. Head, H. S. Majdi, *J. Chem. Thermodyn.* **1991**, *23*, 1169–1173.

[69] a) U. Bemm, H. Östmark, *Acta Crystallogr., Sect. C* **1998**, *54*, 1997–1999; b) CCDC-127539 contains the supplementary crystallographic data for this paper. The data can be obtained free of charge from The Cambridge Crystallographic Data Centre via www.ccdc.cam.ac.uk/structures.

[70] W. A. Trzciński, S. Cudziło, Z. Chyłek, L. Szymańczyk, *Bull. Mil. Univ. Technol.* **2007**, *56*, 283–296.

[71] W. A. Trzciński, S. Cudziło, Z. Chyłek, L. Szymańczyk, *J. Energ. Mater.* **2013**, *31*, 72–85.

[72] M. Makosza, J. Winiarski, *Acc. Chem. Res.* **1987**, *20*, 282–289.

[73] R. D. Schmidt, G. S. Lee, P. F. Pagoria, A. R. Mitchell, R. Gilardi, Synthesis of 4-Amino-3,5-dinitro-1*H*-pyrazole Using Vicarious Nucleophilic Substitution of Hydrogen, *J. Heterocycl. Chem.* **2001**, *38*, 1227–1230.

[74] S. Ek, N. V. Latypov, *J. Heterocycl. Chem.* **2014**, *51*, 1621–1627.

[75] a) I. L. Dalinger, I. A. Vatsadze, T. K. Shkineva, G. P. Popova, S. A. Shevelev, *Mendeleev Commun.* **2010**, *20*, 253–254; b) I. L. Dalinger, I. A. Vatsadze, T. K. Shkineva, G. P. Popova, S. A. Shevelev, Y. V. Nelyubina, *J. Heterocycl. Chem.* **2013**, *50*, 911–924.

[76] I. L. Dalinger, I. A. Vatsadze, T. K. Shkineva, G. P. Popova, S. A. Shevelev, *Synthesis* **2012**, *44*, 2058–2064.

[77] Y. Zhang, Y. Huang, D. A. Parrish, J. M. Shreeve, *J. Mater. Chem.* **2011**, *21*, 6891–6897.

[78] S. Ek, M. Knutsson, N. Latypov, G. Hervé, Characterization of Two Dinitropyrazoles, *11ᵗʰ International Seminar – New Trends in Research of Energetic Materials, Vol. 2*, University of Pardubice, Pardubice, Czech Republic, p. 508–513, **2008**.

[79] X. Zhao, C. Qi, L. Zhang, Y. Wang, S. Li, F. Zhao, S. Pang, *Molecules* **2014**, *19*, 896.

[80] P. F. Pagoria, G. S. Lee, A. R. Mitchell, R. D. Schmidt, *Thermochim. Acta* **2002**, *384*, 187–204.

[81] S. A. Shevelev, I. L. Dalinger, T. K. Shkineva, B. I. Ugrak, V. I. Gulevskaya, M. I. Kanishchev, *Russ. Chem. Bull.* **1993**, *102*, 1063–1068.

[82] P. F. Pagoria, A. R. Mitchell, R. D. Schmidt, R. L. Simpson, F. Garcia, J. Forbes, J. Cutting, R. Lee, R. Swansiger, D. M. Hoffman, Synthesis, Scale-Up and Experimental Testing of LLM-105 (2,6-Diamino-3,5-dinitropyrazine-1-oxide), *Insensitive Munitions and Energetic Materials Technology Symposium*, San Diego, CA, USA, **1998**.

[83] a) P. Pagoria, M. Zhang, A. DeHope, G. Lee, A. Mitchell, "Green" Energetic Materials Synthesis at LLNL, in *15ᵗʰ International Seminar – New Trends in Research of Energetic Materials*, Vol. 1, University of Pardubice, Pardubice, Czech Republic, **2012**, p. 22; b) M. Cameron, B. G. Gowenlock, A. S. F. Boyd, *J. Chem. Soc. Perkin Trans. 2* **1996**, 2271–2274; c) H. P. Patel, J. M. Tedder, *J. Chem. Soc.* **1963**, 4589–4592; d) G. T. Morgan, J. Reilly, *J. Chem. Soc. Trans.* **1914**, *105*, 435–443.

[84] J. Zhang, D. A. Parrish, J. M. Shreeve, *Chem. Asian J.* **2014**, *9*, 2953–2960.

[85] A. G. Stern, J. S. Moran, R. J. Jouet, M. E. Sitzman, P. F. Pagoria, G. S. Lee, *Pat. US 6706889*, The Secretary of the Navy, Washington D.C., USA, **2004**.

[86] a) V. M. Vinogradov, I. L. Dalinger, S. A. Shevelev, *Mendeleev Commun.* **1993**, *3*, 111; b) Y.-N. Li, N. Liu, P.-F. Su, Y.-L. Wang, Z.-X. Ge, H. Li, B.-Z. Wang, *Asian J. Chem.* **2014**, *26*, 7151–7156.

[87] Y. Tamura, J. Minamikawa, K. Sumoto, S. Fujii, M. Ikeda, *J. Org. Chem.* **1973**, *38*, 1239–1241.

Appendix: Underwater Test Results

Expanding highly compressed and heated detonation products causes generation of the overpressure wave which expands outwardly in water. This process for selected explosives was investigated and data collected by pressure sensor are presented in two time scales. First one cover time period in which the primary shock wave is generated that allows calculating shock wave energy (E_{SW}) and shock energy equivalent (E_S). The second time frame covers period of the first bubble pulsation phenomena. Those data is used to determine time interval between the shock-wave pressure peak and the first collapse of the gas bubble (t_b) and subsequently to calculation of the bubble energy (E_{BW}) generated in water and the bubble energy equivalent (E_B).

12.1   Shock wave energy generated in water

The following oscillograms present the primary shock wave for all investigated explosives (a). Additionally, calculated shock wave energies generated in water for investigated explosives are summarized graphically (b).

a. Oscillograms of the primary shock waves, P = f(t), recorded for all investigated explosives (base charges: 0.2, 0.5, 0.7 g)
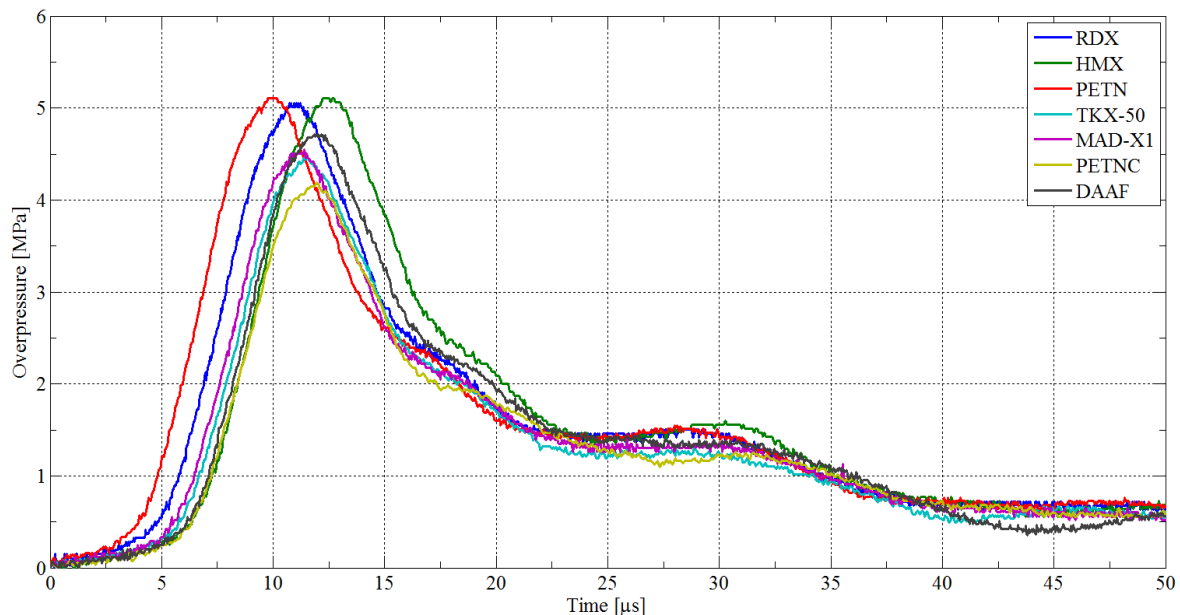
Figure 1. The primary shock wave generated in water by firing detonators filled in with 0.2 g of investigated explosives as a base charge.
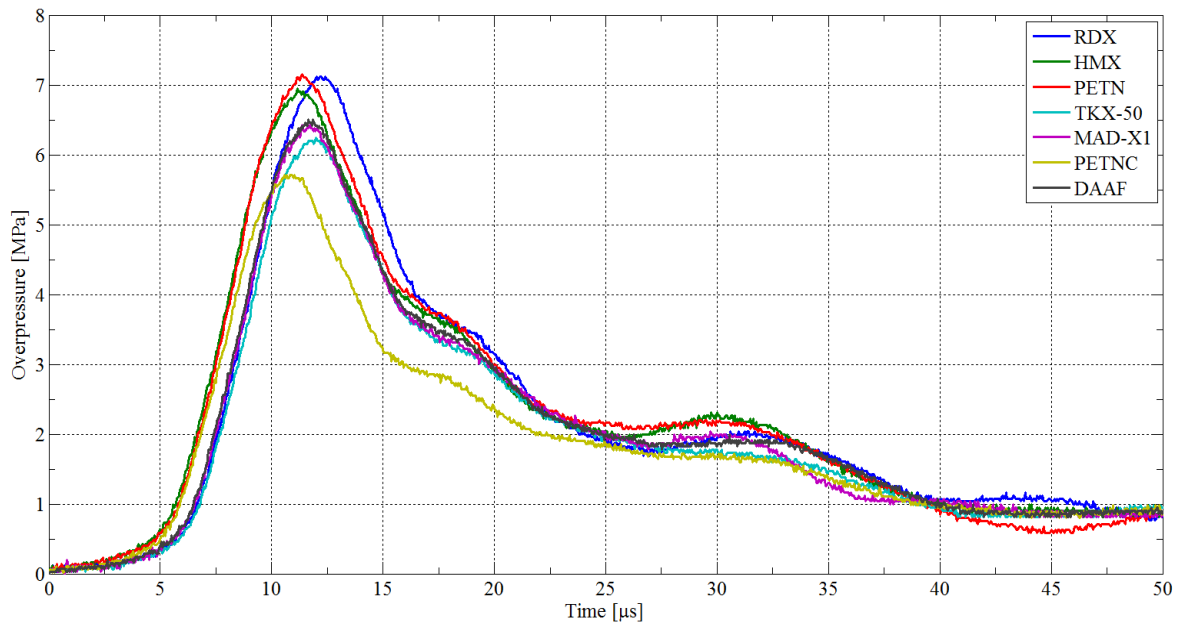
Figure 2. The primary shock wave generated in water by firing detonators filled in with 0.5 g of investigated explosives as a base charge.
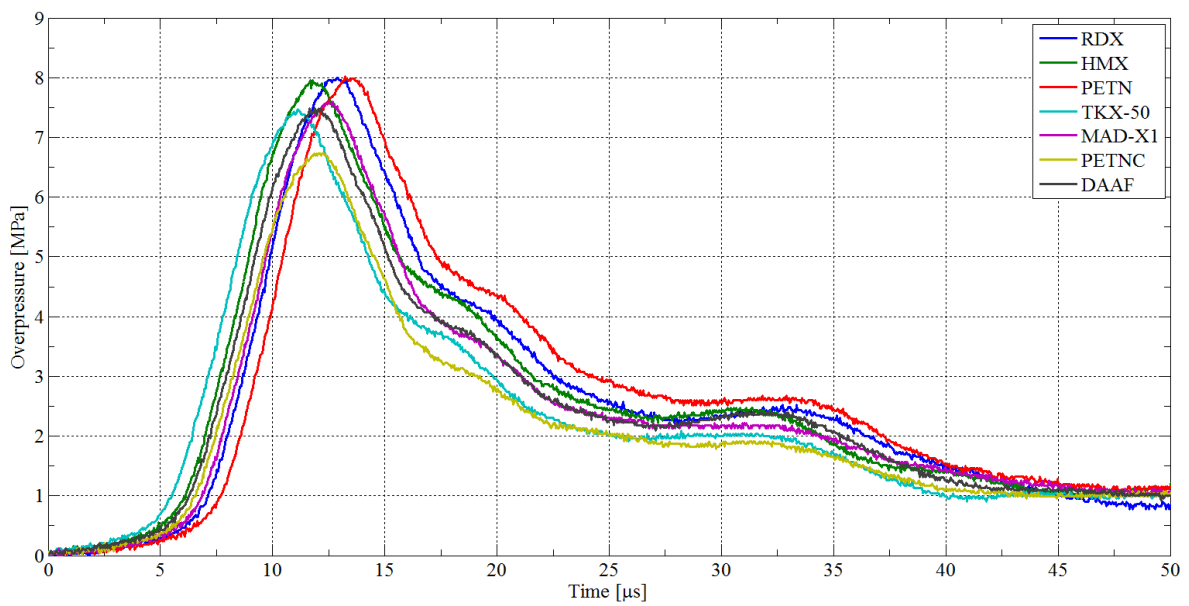
Figure 3. The primary shock wave generated in water by firing detonators filled in with 0.7 g of investigated explosives as a base charge.

b. Graphically comparison of shock wave energy generated in water for investigated explosives (0.2, 0.5, 0.7 g)
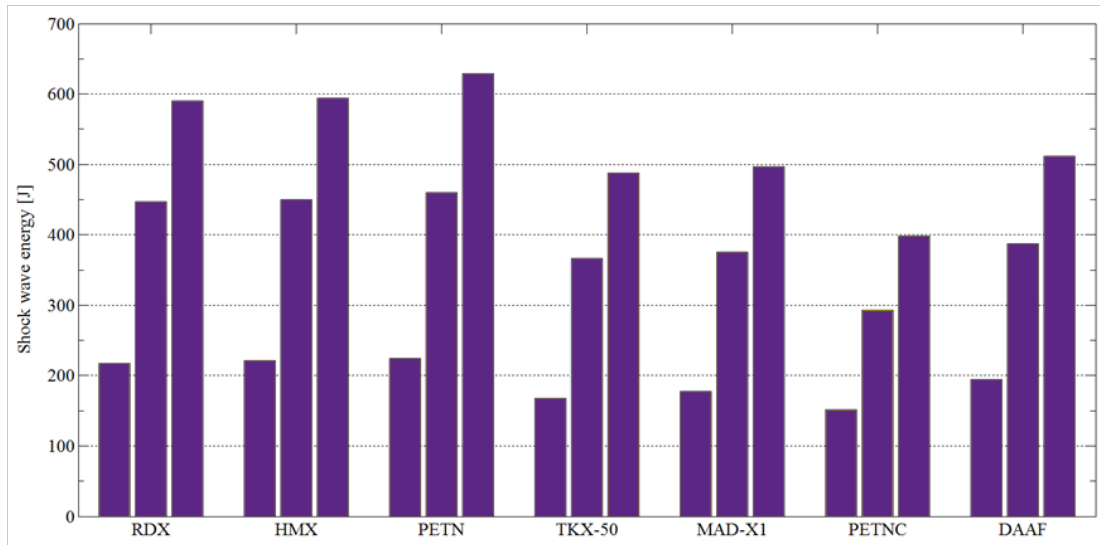
Figure 4. Shock wave energy generated in water for investigated explosives (from left to right side: 0.2, 0.5, 0.7 g).

12.2 Bubble energy generated in water

The following oscillograms present the period of the first bubble pulsation for reference explosives (RDX, HMX, PETN, a) and novel ones (TKX-50, MAD-X1, PETNC, DAAF, b). Furthermore, calculated bubble energies generated in water for investigated explosives are summarized graphically (c).

a. Oscillograms of the period of the first bubble pulsation, P = f(t), recorded for RDX, HMX, PETN (0.2, 0.5, 0.7 g)
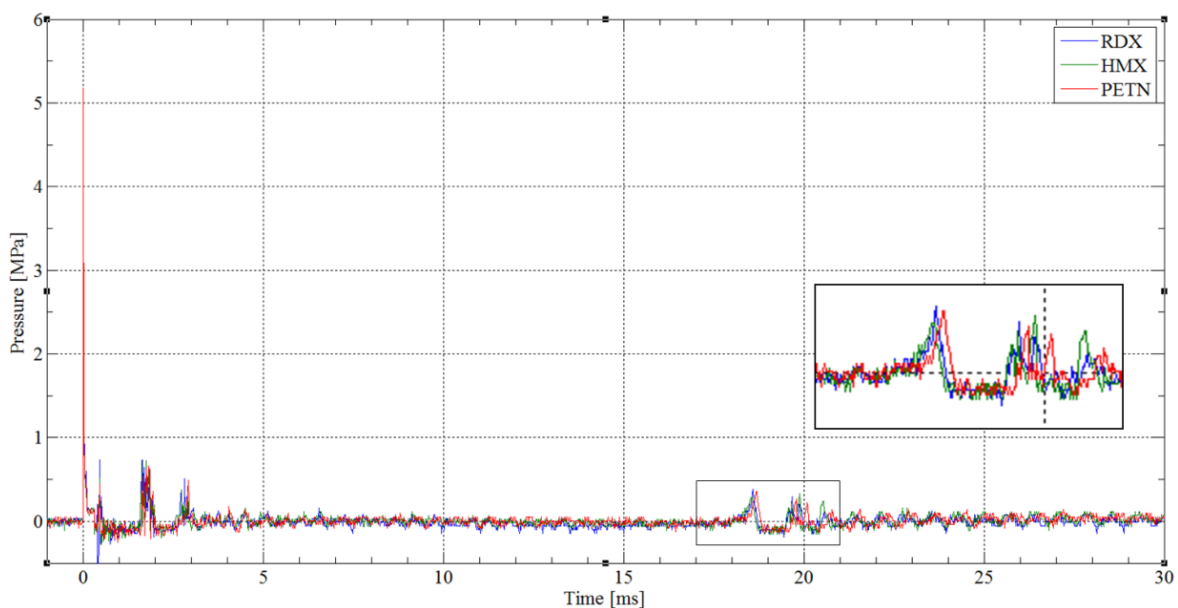
Figure 5. Overpressure generated in water by firing detonators filled in with 0.2 g of investigated explosives as a base charge.
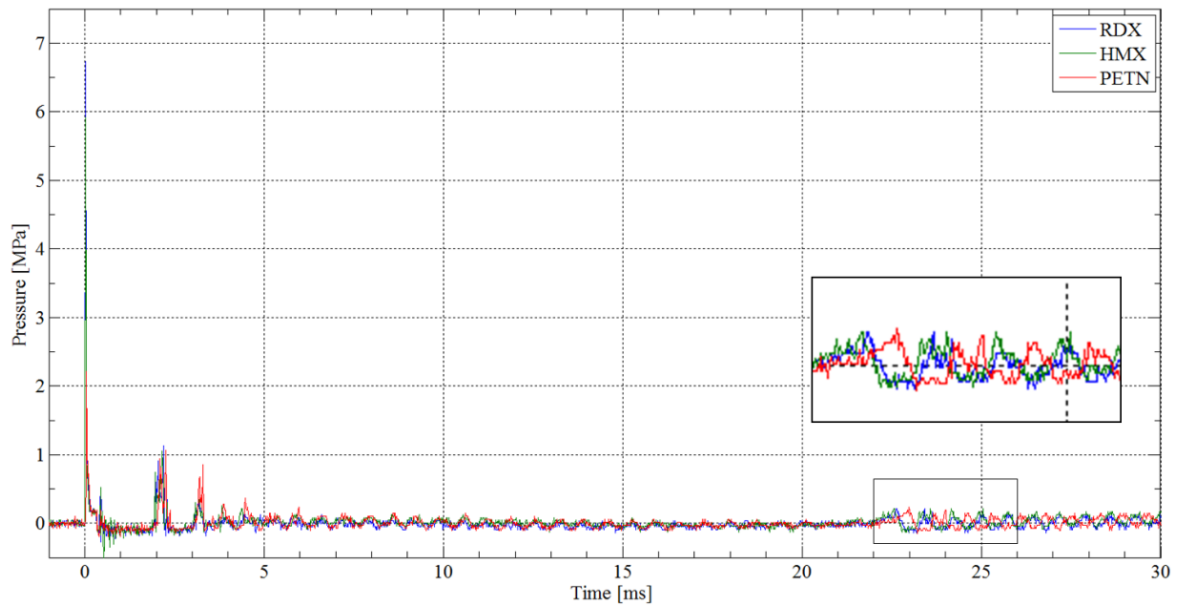
Figure 6. Overpressure generated in water by firing detonators filled in with 0.5 g of investigated explosives as a base charge.
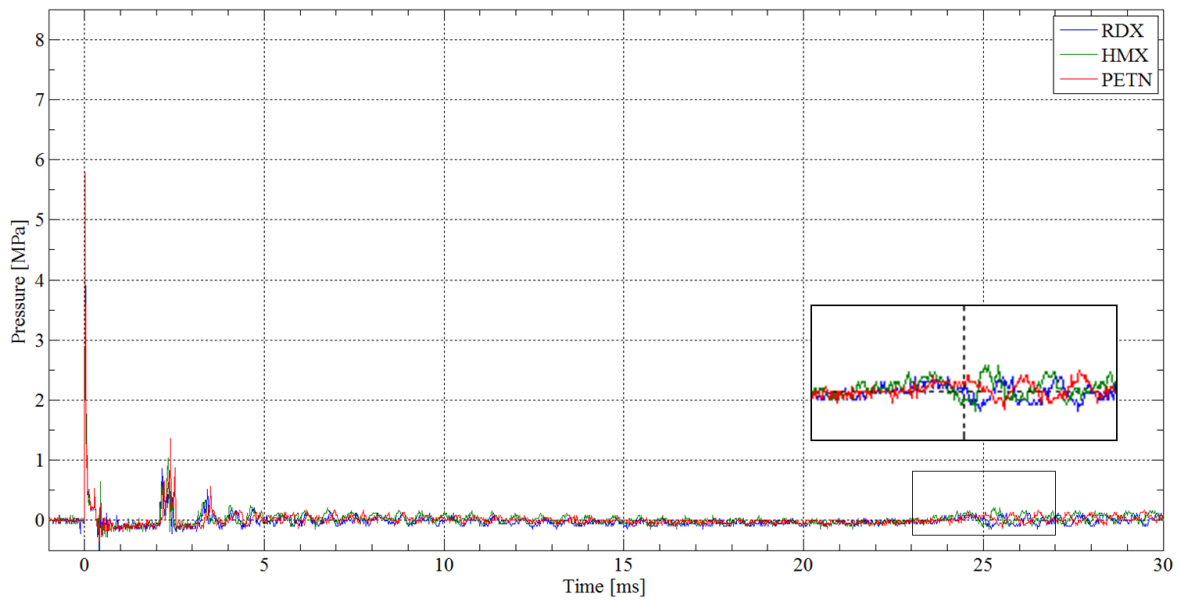
Figure 7. Overpressure generated in water by firing detonators filled in with 0.7 g of investigated explosives as a base charge.

166

b. Oscillograms of the period of the first bubble pulsation, P = f(t), recorded for TKX-50, MAD-X1, PETNC, DAAF (0.2, 0.5, 0.7 g)
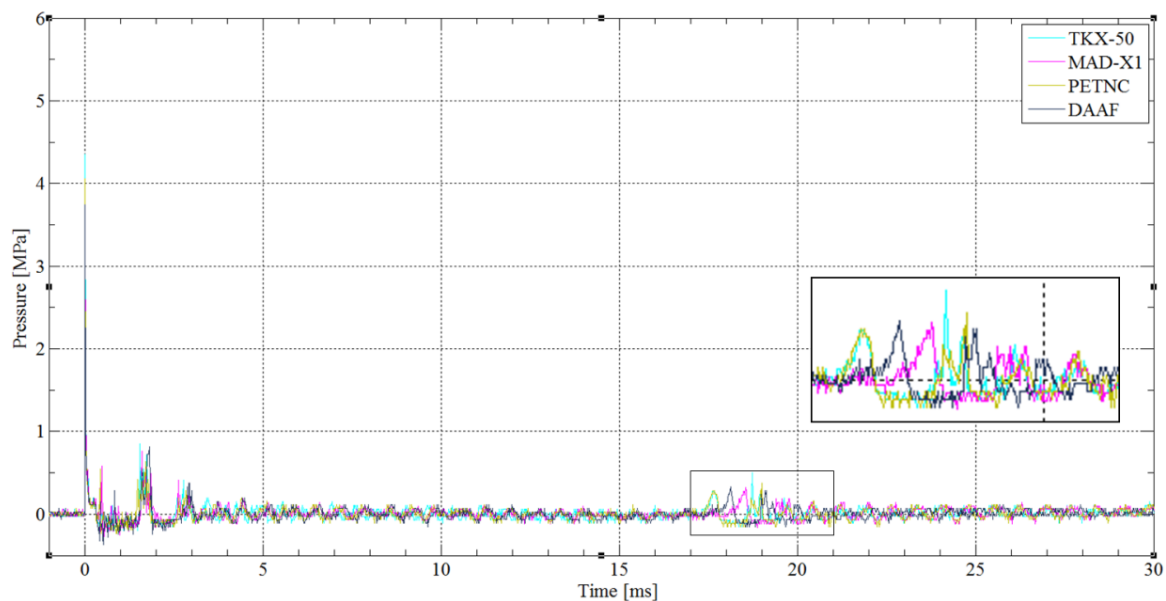
Figure 8. Overpressure generated in water by firing detonators filled in with 0.2 g of investigated explosives as a base charge.
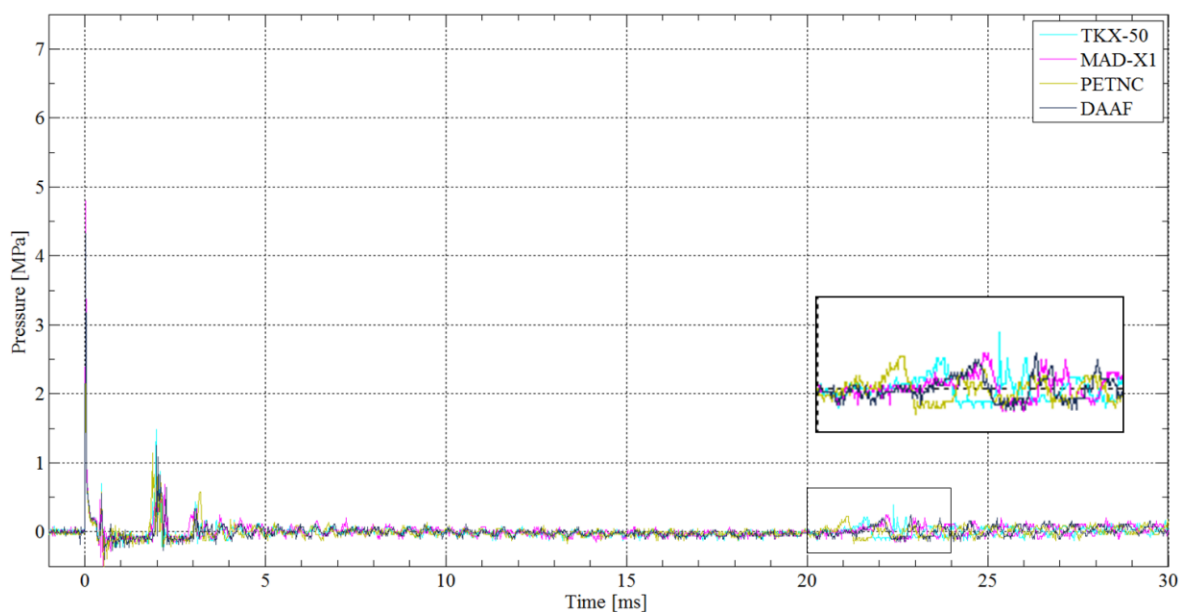
Figure 9. Overpressure generated in water by firing detonators filled in with 0.5 g of investigated explosives as a base charge.
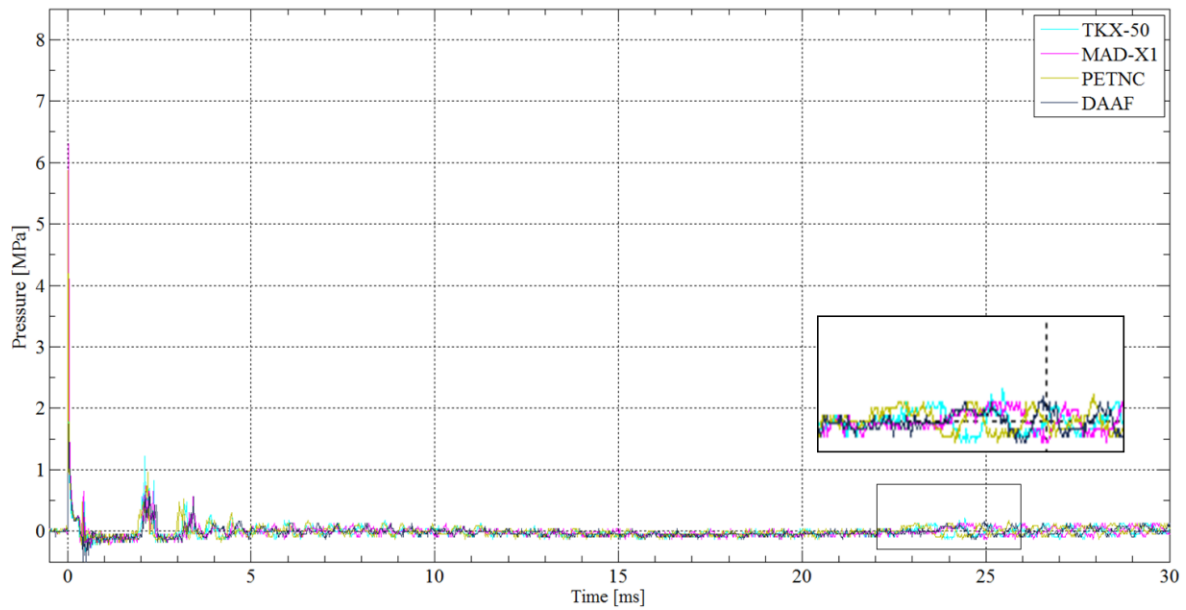
Figure 10. Overpressure generated in water by firing detonators filled in with 0.7 g of investigated explosives as a base charge.

c. Graphically comparison of bubble energy generated in water for investigated explosives (0.2, 0.5, 0.7 g)
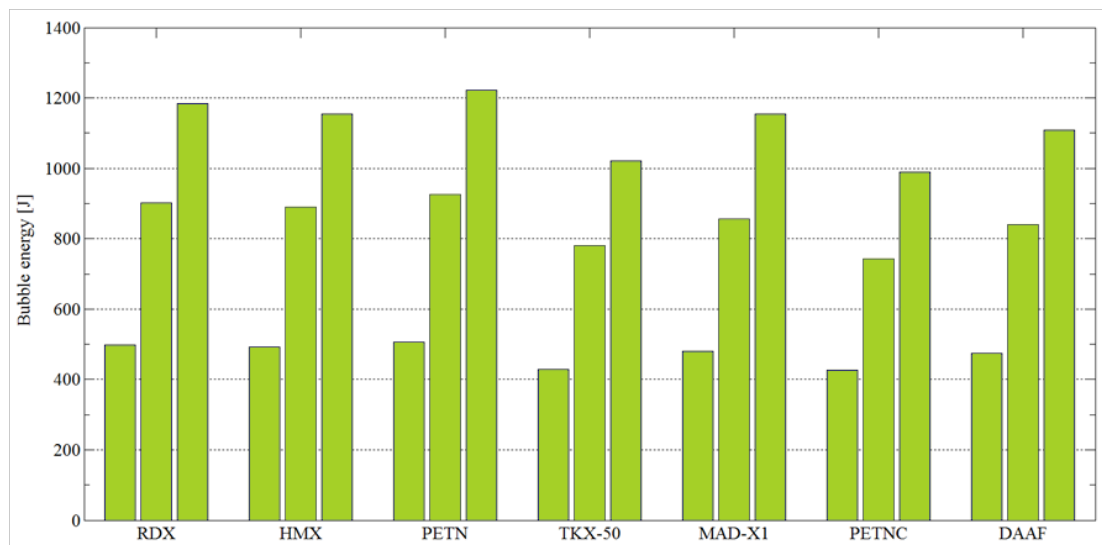
Figure 11. Bubble energy generated in water for investigated explosives (from left to right side: 0.2, 0.5, 0.7 g).

Appendix: General Information

13.1 Materials and Methods

All chemicals and solvents were used as received (Sigma-Aldrich, Fluka, Acros) without further purification unless otherwise stated. Industrially produced explosives were supplied by Chemical Works "NITRO-CHEM" S.A. (RDX, HMX), Nitroerg S.A. (PETN).

13.2 NMR spectroscopy

NMR spectra were recorded using a JEOL Eclipse 270, JEOL EX 400 or a JEOL Eclipse 400 instrument. All spectra were recorded at ambient temperature. The chemical shifts are given in parts per million relative to tetramethylsilane (^{1}H, ^{13}C), nitromethane (^{14}N, ^{15}N), and trichlorofluoromethane (^{19}F).

13.3 Vibrational spectroscopy

Infrared spectra were measured using a Perkin-Elmer Spectrum BX-FTIR spectrometer equipped with a Smiths DuraSamplIR II ATR device. Transmittance values are qualitatively described as "very strong" (vs), "strong" (s), "medium" (m), and "weak" (w).

Raman spectra were recorded using a Bruker MultiRAM FT-Raman instrument fitted with a liquid-nitrogen cooled germanium detector and a Nd:YAG laser ($\lambda = 1064$ nm). The intensities are given as percentages of the most intense peak and are given in parentheses.

13.4 Mass spectrometry and elemental analysis

Low-resolution mass spectra were recorded with a JEOL MStation JMS 700 using either the DEI or FAB technique. The elemental analyses were performed using a Netsch STA 429 simultaneous thermal analyzer.

13.5 Differential thermal analysis and differential scanning calorimetry

Differential thermal analysis (DTA) measurements were performed at a heating rate of 5 °C·min^{-1} with an OZM Research DTA 552-Ex instrument.

Differential Scanning Calorimetry (DSC) was performed using a LINSEIS DSC PT10 calorimeter with approximately 1 mg of substance in covered Al-containers containing a hole (0.1 mm) in the lid for gas release. A heating rate of 5 °·min^{-1} and a nitrogen flow of 5 dm^{3}·h^{-1} were used.

13.6 Sensitivity testing

The impact sensitivity tests were carried out according to STANAG 4489[1] modified instruction[2] using a BAM (Bundesanstalt für Materialforschung) drophammer.[3] The friction sensitivity tests were carried out according to STANAG 4487[4] modified instruction[5] using the BAM friction tester. The classification of the tested compounds is based on the "UN Recommendations on the Transport of Dangerous Goods".[6] Additionally, all compounds were tested for sensitivity towards electrical discharge using the Electric Spark Tester ESD 2010 EN.[7]

13.7 X-Ray diffraction

The single-crystal X-ray diffraction datasets of investigated compounds were collected using an Oxford Xcalibur3 diffractometer with a Spellman generator (voltage 50 kV, current 40 mA), enhance molybdenum $K\alpha$ radiation source ($\lambda = 0.71073$ Å), Oxford Cryosystems Cryostream cooling unit, four circle kappa platform and a Sapphire CCD detector. The data collection and reduction were performed using the CRYSALISPRO software.[8] The structures were solved using SIR-97,[9] refined by full-matrix least-squares on $F2$ with SHELXL-97,[10] and checked with PLATON,[11] which are all integrated into the WINGX software suite.[12] The non-hydrogen atoms were refined anisotropically and the hydrogen atoms were located and freely refined. The finalized CIF files were checked with checkCIF.[13] Intra- and intermolecular contacts were analyzed with MERCURY.[14]

13.8 Heat of formation calculations

All calculations were carried out using the Gaussian G09 (revision C.01) program package.[15] The enthalpies (H), were calculated using the complete basis set (CBS) method of Petersson and coworkers. The CBS models use the known asymptotic convergence of natural orbitals expressions to extrapolate the energy limit for an infinitely large basis set. CBS-4 begins with a HF/3-21G(d) structure optimization and the zero point energy computation. Subsequently, a base energy is computed by applying a larger basis set. A MP2/6-31+G calculation with a CBS extrapolation gives the perturbation-theory corrected energy (takes the electron correlation into account). A MP4(SDQ)/6-31+(d,p) calculation is used to correlate higher order contributions. In this thesis the modified CBS-4M method is applied (M referring to the use of minimal population localization) which is a re-parameterized version of the original CBS-4 method and also includes some additional empirical

corrections.[16] The gas-phase enthalpies ($\Delta_f H°_{(g,M,298K)}$) of the species M were computed according to the atomization energy method (Equation 1).[17]

$$\Delta_f H°_{(g,M,298K)} = H_{(g,M,298K)} - \sum H°_{(g,A_i,298K)} + \sum \Delta_f H°_{(g,A_i,298K)} \left[\frac{J}{mol}\right] \quad (1)$$

The $\Delta_f H°_{(g,A_i,298K)}$ values for the corresponding atoms (A_i) were determined experimentally and have been reported in the literature, whereas the values for $H°_{(g,A_i,298K)}$ were calculated theoretically (Table 1).[18]

Table 1. Literature values for $\Delta_f H°_{(g,A_i,298K)}$ and $H°_{(g,A_i,298K)}$ obtained from theoretical calculations at the CBS-4M level of theory.

Atom	$\Delta_f H°_{(g,A_i,298K)}$ [kcal·mol^{-1}]	$H°_{(g,A_i,298K)}$ [Hartree·atom^{-1}]
H	52.103	−0.500991
C	171.29	−37.786156
N	112.97	−54.522462
O	59.56	−74.991202

Standard molar enthalpies of formation were calculated using $\Delta_f H°_{(g,M,298K)}$ and the standard molar enthalpies of sublimation (estimated using Trouton's rule, Equation 2).[19]

$$\Delta_f H°_M = \Delta_f H°_{(g,M,298K)} - \Delta_{sub} H°_M = \Delta_f H°_{(g,M,298K)} - 188 \cdot T \left[\frac{J}{mol}\right] \quad (2)$$

Where T [K] is either the melting point or the decomposition temperature (if no melting occurs prior to decomposition).

13.9 Detonation parameter calculations

The Chapman-Jouguet (C-J) characteristics, (*i.e.* heat of detonation, $\Delta_E U°$; detonation temperature, T_{C-J}; detonation pressure, p_{C-J}; detonation velocity V_{C-J}) based on the calculated $\Delta_f H°_M$ values, and the theoretical maximum densities were computed in most cases using the EXPLO5 V6.01 thermochemical computer code.[20] Calculations for explosives assume ideal behaviour. Estimation of the detonation parameters is based on the chemical equilibrium steady-state model of detonation. The Becker-Kistiakowsky-Wilson equation of state (BKW EOS) with the following sets of constants: $\alpha = 0.5$, $\beta = 0.38$, $\kappa = 9.4$, and $\Theta = 4120$ for gaseous detonation products and the Murnaghan equation of state for condensed products (compressible solids and liquids) were applied. Calculation of the equilibrium composition of the detonation products used the modified White, Johnson and Dantzig's free energy minimization technique.

The specific energies of explosives (f) were calculated according to the ideal gas equation of state assuming isochoric conditions (Equation 3).

$$f = p_e \cdot V = n \cdot R \cdot T_c \left[\frac{kJ}{kg}\right]$$ (3)

Where p_e is the maximum pressure occurring during the explosion, V is the volume of detonation gases ($m^3 \cdot kg^{-1}$), n is the number of moles of gas formed by the explosion per kilogram of explosive (*Volume of Explosive Gases*), R is the ideal gas constant and T_c is the absolute temperature of the explosion.[20-21]

13.10 Small-Scale Shock Reactivity Test (SSRT)

To evaluate the shock reactivity (*"explosiveness"*) of the investigated compounds, a small-scale shock reactivity test (SSRT) was performed.[22] The SSRT measures the shock reactivity of potentially energetic materials, often below the critical diameter, without requiring a transition to detonation. The test setup combines the advantages of a lead block test[23] and a gap test.[24] The amount m_s of the tested compound was calculated using the following formula: $m_s = V_s \cdot \rho \cdot 0.95$, (where: $V_s = 284$ mm^3). The tested compound was pressed into a perforated steel block. Neither attenuator (between detonator and sample) nor air gap (between sample and aluminum block) were applied. Initiation of the explosive being tested was performed using a commercially available detonator (Orica-DYNADET-C2-0ms). The dent sizes were measured by filling them with powdered SiO_2 and measuring the resulting mass.

13.11 References

[1]   NATO standardization agreement (STANAG) on explosives. *Impact sensitivity tests*. No. 4489, 1st ed., Sept. 17, **1999**.

[2]   WIWEB-Standardarbeitsanweisung 4-5.1.02, Ermittlung der Explosionsgefährlichkeit, hier der Schlagempfindlichkeit mit dem Fallhammer, Nov. 8, **2002**.

[3]   http://www.bam.de

[4]   NATO standardization agreement (STANAG) on explosive. *Friction sensitivity tests*. No. 4487, 1st ed., Aug. 22, **2002**.

[5]   WIWEB-Standardarbeitsanweisung 4-5.1.03, Ermittlung der Explosionsgefährlichkeit oder der Reibempfindlichkeit mit dem Reibeapparat, Nov. 8, **2002**.

[6]   Impact: Insensitive > 40 J, less sensitive ≥ 35 J, sensitive ≥ 4 J, very sensitive ≤ 3 J; friction: Insensitive > 360 N, less sensitive = 360 N, sensitive < 360 N a. > 80 N, very

sensitive ≤ 80 N, extreme sensitive ≤ 10 N; according to the UN recommendations on the transport of dangerous goods. (+) Indicates: not safe for transport.

[7]   http://www.ozm.cz

[8]   *CrysAlisPro* 1.171.37.33, Agilent Technologies, **2014**.

[9]   A. Altomare, M. C. Burla, M. Camalli, G. L. Cascarano, C. Giacovazzo, A. Guagliardi, A. G. G. Moliterni, G. Polidori, R. Spagna, *J. Appl. Crystallogr.* **1999**, *32*, 115−119.

[10]   a) G. M. Sheldrick, *SHELXL-97*, Program for the Refinement of Crystal Structures. University of Göttingen, Germany, **1997**; b) G. M. Sheldrick, *Acta Crystallogr., Sect. A: Found. Adv.* **2008**, *64*, 112−122.

[11]   a) A. L. Spek, *PLATON*, A Multipurpose Crystallographic Tool, Utrecht University, The Netherlands, **1999**; b) A. Spek, *J. Appl. Crystallogr.* **2003**, *36*, 7−13; c) A. Spek, *Acta Crystallogr., Sect. D: Biol. Crystallogr.* **2009**, *65*, 148−155.

[12]   L. Farrugia, *J. Appl. Crystallogr.* **1999**, *32*, 837−838.

[13]   http://checkcif.iucr.org/

[14]   C. F. Macrae, I. J. Bruno, J. A. Chisholm, P. R. Edgington, P. McCabe, E. Pidcock, L. Rodriguez-Monge, R. Taylor, J. van de Streek, P. A. Wood, *J. Appl. Crystallogr.* **2008**, *41*, 466−470.

[15]   *Gaussian 09, Revision C.01*, M. J. Frisch, G. W. Trucks, H. B. Schlegel, G. E. Scuseria, M. A. Robb, J. R. Cheeseman, G. Scalmani, V. Barone, B. Mennucci, G. A. Petersson, H. Nakatsuji, M. Caricato, X. Li, H. P. Hratchian, A. F. Izmaylov, J. Bloino, G. Zheng, J. L. Sonnenberg, M. Hada, M. Ehara, K. Toyota, R. Fukuda, J. Hasegawa, M. Ishida, T. Nakajima, Y. Honda, O. Kitao, H. Nakai, T. Vreven, J. A. Montgomery, Jr., J. E. Peralta, F. Ogliaro, M. Bearpark, J. J. Heyd, E. Brothers, K. N. Kudin, V. N. Staroverov, R. Kobayashi, J. Normand, K. Raghavachari, A. Rendell, J. C. Burant, S. S. Iyengar, J. Tomasi, M. Cossi, N. Rega, J. M. Millam, M. Klene, J. E. Knox, J. B. Cross, V. Bakken, C. Adamo, J. Jaramillo, R. Gomperts, R. E. Stratmann, O. Yazyev, A. J. Austin, R. Cammi, C. Pomelli, J. W. Ochterski, R. L. Martin, K. Morokuma, V. G. Zakrzewski, G. A. Voth, P. Salvador, J. J. Dannenberg, S. Dapprich, A. D. Daniels, Ö. Farkas, J. B. Foresman, J. V. Ortiz, J. Cioslowski, and D. J. Fox, Gaussian, Inc., Wallingford CT, **2009**.

[16]   a) J. W. Ochterski, G. A. Petersson, J. A. Montgomery, *J. Chem. Phys.* **1996**, *104*, 2598−2619; b) J. A. Montgomery, M. J. Frisch, J. W. Ochterski, G. A. Petersson, *J. Chem. Phys.* **2000**, *112*, 6532−6542.

[17] a) L. A. Curtiss, K. Raghavachari, P. C. Redfern, J. A. Pople, J. Chem. Phys. **1997**, *106*, 1063−1079; b) B. M. Rice, S. V. Pai, J. Hare, *Combust. Flame* **1999**, *118*, 445−458; c) E. F. C. Byrd, B. M. Rice, J. Phys. Chem. A **2006**, *110*, 1005−1013.

[18] P. J. Linstrom, W. G. Mallard, *National Institute of Standards and Technology*, Gaithersburg MD, 20899.

[19] a) F. Trouton, *Philos. Mag. (1876-1900)* **1884**, *18*, 54−57; b) M. S. Westwell, M. S. Searle, D. J. Wales, D. H. Williams, *J. Am. Chem. Soc.* **1995**, *117*, 5013−5015.

[20] M. Sućeska, *EXPLO5 Version 6.01 User's Guide*, January **2013**.

[21] a) R. Meyer, J. Köhler, A. Homburg, *Explosives*, 6th edn., Wiley, Weinheim, **2007**, p. 291−292; b) T. M. Klapötke, *Chemistry of High-Energy Materials*, Walter de Gruyter, Berlin, **2015**;

[22] a) H. W. Sandusky, R. H. Granholm, and D.G. Bohl, *IHTR 2701*, Naval Surface Warfare Center, Indian Head Division, MD, USA, 12 August, **2005**; b) J. E. Felts, H. W. Sandusky, R. H. Granholm, *AIP Conf. Proc.* **2009**, *1195*, 233−236.

[23] a) R. Meyer, J. Köhler, A. Homburg, *Explosives*, 6th edn., Wiley, Weinheim, **2007**, p. 196−198.

[24] a) R. Meyer, J. Köhler, A. Homburg, *Explosives*, 6th edn., Wiley, Weinheim, **2007**, p. 145.

List of publications

[1] A. Wojewódka, T. G. Witkowski, *Combust., Explos. Shock Waves (Engl. Transl.)* **2014**, *50*, 362–367.

[2] M. A. Kettner, T. M. Klapötke, T. G. Witkowski, F. von Hundling, *Chem. Eur. J.* **2015**, *21*, 4238–4241.

[3] T. M. Klapötke, T. G. Witkowski, *Propellants, Explos., Pyrotech.* **2015**, *40*, 366–373.

[4] T. M. Klapötke, T. G. Witkowski, Z. Wilk, J. Hadzik, *Propellants, Explos., Pyrotech.* **2016**, *41*, 92–97.

[5] T. M. Klapötke, T. G. Witkowski, *ChemPlusChem* **2016**, *81*, 357–360.

[6] T. M. Klapötke, J. Stierstorfer, M. Weyrauther, T. G. Witkowski, *Chem. Eur. J.* **2016**, 22, 8619–8626.

[7] T. M. Klapötke, T. G. Witkowski, *Propellants, Explos., Pyrotech.* **2016**, *41*, 470–483.

[8] A. Drechsel, T. M. Klapötke, T. G. Witkowski, *J. J. Inorg. Chem.* **2016**, *1*, 008(1–8).

[9] D. Fischer, J. L. Gottfried, T. M. Klapötke, K. Karaghiosoff, J. Stierstorfer, T. G. Witkowski, *Angew. Chem., Int. Ed.* **2016** , *55*, 16132–16135.

[10] T. M. Klapötke, T. G. Witkowski, Z. Wilk, J. Hadzik, *Cent. Eur. J. Energ. Mater.* **2016**, *13*, 821–837.

[11] J. L. Gottfried, T. M. Klapötke, T. G. Witkowski, *Propellants, Explos., Pyrotech.* **2017**, *42*, 353–359.